



HAL
open science

Pyrin inflammasome and familial Mediterranean fever: deciphering the role of B30.2 and CHS in pyrin regulation

Daria Chirita

► **To cite this version:**

Daria Chirita. Pyrin inflammasome and familial Mediterranean fever: deciphering the role of B30.2 and CHS in pyrin regulation. Molecular biology. Université Claude Bernard - Lyon I, 2022. English. NNT: 2022LYO10111 . tel-04329621

HAL Id: tel-04329621

<https://theses.hal.science/tel-04329621v1>

Submitted on 7 Dec 2023

HAL is a multi-disciplinary open access archive for the deposit and dissemination of scientific research documents, whether they are published or not. The documents may come from teaching and research institutions in France or abroad, or from public or private research centers.

L'archive ouverte pluridisciplinaire **HAL**, est destinée au dépôt et à la diffusion de documents scientifiques de niveau recherche, publiés ou non, émanant des établissements d'enseignement et de recherche français ou étrangers, des laboratoires publics ou privés.



**THESE de DOCTORAT DE
L'UNIVERSITE CLAUDE BERNARD LYON 1**

**Ecole Doctorale N° 340
BIOLOGIE MOLÉCULAIRE, INTÉGRATIVE ET CELLULAIRE**

Spécialité de doctorat : Sciences de la vie
Discipline : Immunologie

Soutenue publiquement 22/11/2022, par :

Daria CHIRITA

**L'inflammasome pyrine et la fièvre
Méditerranéenne familiale : le rôle des
domaines B30.2 et CHS dans la
régulation de pyrine**

Devant le jury composé de :

Dr DELON Jérôme
Dr LAFFONT-PRADINES Sophie
Dr BELOT Alexandre
Dr GEORGIN-LAVIALLE Sophie
Dr HUBER Anne-Laure

Chargé de recherche, INSERM
Chargée de recherche, CNRS
PU-PH, UCBL
PU-PH, Sorbonne Université
Chargée de recherche, INSERM

Rapporteur
Rapportrice
Président du jury
Examinatrice
Examinatrice

Dr HENRY Thomas
Dr JAMILLOUX Yvan

Directeur de recherche, INSERM
MCU-PH, UCBL

Directeur de thèse
Co-directeur de thèse /
Membre invité

Université Claude Bernard – LYON 1

Président	M. Frédéric FLEURY
Président du Conseil Académique	M. Hamda BEN HADID
Vice-Président du Conseil d'Administration	M. Didier REVEL
Vice-Présidente de la Commission de Formation	Mme Céline BROCHIER
Vice-Président de la Commission de Recherche	M. Petru MIRONESCU
Directeur Général des Services	M. Pierre ROLLAND

COMPOSANTES SANTE

Département de Formation et Centre de Recherche en Biologie Humaine	Directrice : Mme Anne-Marie SCHOTT
Faculté d'Odontologie	Doyenne : Mme Dominique SEUX
Faculté de Médecine et Maïeutique Lyon Sud - Charles Mérieux	Doyenne : Mme Carole BURILLON
Faculté de Médecine Lyon-Est	Doyen : M. Gilles RODE
Institut des Sciences et Techniques de la Réadaptation (ISTR)	Directeur : M. Xavier PERROT
Institut des Sciences Pharmaceutiques et Biologiques (ISBP)	Directrice : Mme Christine VINCIGUERRA

COMPOSANTES & DEPARTEMENTS DE SCIENCES & TECHNOLOGIE

Département Génie Electrique et des Procédés (GEP)	Directrice : Mme Rosaria FERRIGNO
Département Informatique	Directeur : M. Behzad SHARIAT
Département Mécanique	Directeur M. Marc BUFFAT
Ecole Supérieure de Chimie, Physique, Electronique (CPE Lyon)	Directeur : Gérard PIGNAULT
Institut de Science Financière et d'Assurances (ISFA)	Directeur : M. Nicolas LEBOISNE
Institut National du Professorat et de l'Education	Directeur : M. Pierre CHAREYRON
Institut Universitaire de Technologie de Lyon 1	Directeur : M. Christophe VITON
Observatoire de Lyon	Directrice : Mme Isabelle DANIEL
Polytechnique Lyon	Directeur : Emmanuel PERRIN
UFR Biosciences	Directrice : Mme Kathrin GIESELER
UFR des Sciences et Techniques des Activités Physiques et Sportives (STAPS)	Directeur : M. Yannick VANPOULLE
UFR Faculté des Sciences	Directeur : M. Bruno ANDRIOLETTI

Acknowledgements

Thank you, Thomas, for your guidance, patience, and spearheaded-ness.

Thank you, Yvan for always asking questions we didn't expect.

Thank you to Alex and Sonia, for your valuable advice and opinion on my progress from year to year.

Thank you, Team: all the people who have come and gone in the four years, but in particular to Flora, who was my mentor, a calm and powerful force, to Amandine, without whom the lab would fall apart, to Mira and Gabrielle for endless moral support and all the conversations, to Sarah, Pauline, Manon, Mélissa and Elena, for bringing more life and laughter to our lab routine, to Etienne and Esteban who joined us more recently, but whom I'm glad I met.

Thank you to all those with whom we worked at UCBL: Emilie, Aurore, Karène, Christine and others who I met and worked with during this time. The opportunity to teach regularly for four years was precious to me and I learned a lot from you!

Thank you to my family, my mum and my brother, you support and advice, your perspective and wisdom. I have a very special thought for my dad, who won't see me defend this PhD, but I know he would be so proud.

Thank you, Julien, for always reminding me of the important things, for making me slow down and appreciate the small things, for your care and support.

Table of contents

Acknowledgements	5
Abstract (en)	8
Résumé (fr)	9
List of Abbreviations	10
List of Figures and Tables	12
Introduction	15
1. Inflammasomes	16
1.1 The innate immune sensing of pathogens and danger signals	16
1.2 Inflammasomes	17
1.2.1 Inflammasome sensors	17
1.2.2 Inflammasome adaptor – ASC	17
1.2.3 Inflammasome effector – caspase-1	18
1.3 Pyroptosis – pro-inflammatory cell death	18
2. Pysin structure domain by domain	20
2.1 Pysin structure	20
2.2 PYD	20
2.3 Phosphorylated linker domain	22
2.4 B-Box	23
2.5 Coiled coil	24
2.6 B30.2	25
3. B30.2	26
3.1 SPRY/B30.2 domains and SPRY/B30.2-carrying proteins	26
3.2 B30.2 in pysin	28
4. Pysin inflammasome regulation	34
4.1 Physiological triggers of pysin	34
4.2 Negative regulation of pysin	35
4.3 Pysin inflammasome activation	36
5. Familial Mediterranean Fever (FMF)	39
5.1 FMF: the disease	39
5.2 FMF: diagnosis, treatment, and prognosis	40
5.3 FMF: triggers of attacks	41
6. Other disorders that implicate the pysin inflammasome	43
6.1 PAAND	43
6.2 PAPA	44
6.3 MKD	44
6.4 PFIT	45
6.5 Aberrant CDC42 function and pysin activation	46
7. Steroids and immunity	47
7.1 Steroid hormones	47
7.2 Pro-inflammatory properties of steroids	49
7.3 Anti-inflammatory properties of steroids	52
Results	55
Results. Part 1. <i>Steroid hormone catabolites activate pysin inflammasome through a non-canonical mechanism</i>	56
Results. Part 2. <i>Mutations in the B03.2 and the Central Helical scaffold domains of pysin differentially affect inflammasome activation</i>	107
Additional Results	141
Additional Results. Part 1. <i>Specific mutations in the CHS domain render pysin sensitive to a large spectrum of steroid molecules</i>	143

Additional Results. Part 2. <i>Progesterone abrogates pyrin activation by pregnanolone in a dose-dependent manner</i>	149
Additional Results. Part 3. <i>Specific mutations in the CHS domain render pyrin more sensitive to activation by simvastatin</i>	153
Additional Results. Part 4. <i>Study of the role of interactions between residues within the CHS-B30.2 dimer</i>	159
Additional Results. Part 5. <i>Truncation of the pyrin protein at the G532 residue reveals a spontaneously activated pyrin protein</i>	167
Discussion	173
B30.2 and CHS cooperation	174
Complexity of pyrin regulation by the CHS	175
Cholesterol metabolism sensing by pyrin	177
B30.2 steroid sensing	181
Physiological pertinence of steroid sensing by pyrin	182
Importance of specific residues in pyrin activity	183
Pyrin-associated autoinflammatory diseases (PAAD)	184
Limitations of the model	185
Materials and Methods	187
Bibliography	206
Annexe I	224
Résumé substantiel (fr)	241

Abstract

Pyrin inflammasome is a guard of RhoA activity. Pyrin activation is regulated by two steps: pyrin phosphorylation enacted by RhoA effectors PKN1/2, and a second checkpoint that relies on microtubule dynamics. Mutations in the pyrin encoding *MEFV* gene cause an auto-inflammatory disorder termed Familial Mediterranean fever (FMF). Most FMF-causing mutations cluster in *MEFV* exon 10 encoding the B30.2 domain of pyrin. A chemical screen performed on monocytes stably expressing a constitutively dephosphorylated variant of pyrin, identified novel pyrin activators – steroid hormone derivatives etiocholanolone and pregnanolone. These molecules activate pyrin via a non-canonical mechanism dependent on the B30.2 domain of pyrin and without inhibiting RhoA. This observation suggests that endogenous steroid catabolites could drive autoinflammation. Curiously, progesterone inhibited pyrin activation by pregnanolone in a dose-dependent manner. At the same time pyrin activation by TcdA was independent of B30.2, and B30.2 deletion mimicked a prototypical FMF mutation. Our analysis of the impact of mutations in the central helical scaffold (CHS) domain on pyrin activation by various stimuli revealed that the CHS domain is a second C-terminal regulatory domain of pyrin. Interestingly, specific mutations in the CHS domain, including p.Q426R and p.F479L, render pyrin highly susceptible to activation by steroid hormones and their derivatives, and by simvastatin. Taken together results presented in this manuscript reveal two domains at the C-terminus of pyrin – the CHS and the B30.2 – that regulate pyrin activation in a coupling mechanism, likely mediated by conformational changes. We also identify a novel role for the pyrin inflammasome as a sensor of steroid hormone metabolism.

Key words: pyrin inflammasome, Familial Mediterranean fever, autoinflammatory disease, pyrin regulation, B30.2, steroid sex hormones, cholesterol metabolism.

Résumé

L'inflammasome pyrine est activé en réponse à l'inhibition de RhoA par des pathogènes. La régulation de pyrine se déroule en deux étapes : la phosphorylation de pyrine par les kinases PKN1/2, eux-mêmes des effecteurs de RhoA, et une deuxième étape liée à la dynamique des microtubules. Les mutations du gène *MEFV* qui code pyrine provoquent une maladie auto-inflammatoire – la fièvre Méditerranéenne familiale (FMF). La majorité de mutations associées à la FMF est regroupée au sein de l'exon 10 du gène qui code le domaine B30.2. Un crible chimique effectué sur une lignée de monocytes exprimant une pyrine constitutivement déphosphorylée a identifié de nouveaux activateurs de l'inflammasome pyrine – des dérivés d'hormones stéroïdes : l'étiocolanone et la prégnanolone. Ces molécules activent pyrine par un mécanisme non-canonique dépendant du domaine B30.2 et sans inhibition de RhoA. Ainsi, les catabolites stéroïdes endogènes pourraient être à l'origine d'auto-inflammation. En revanche, la progestérone inhibe l'activation de pyrine par la prégnanolone de manière dose-dépendante. L'activation de pyrine par la toxine bactérienne TcdA est, elle, indépendante du domaine B30.2, et la délétion de ce domaine réplique le phénotype typique de la mutation classique de la FMF (p.M694V). Notre analyse de l'effet des mutations localisées dans le domaine « central helical scaffold » (CHS) sur la réponse de pyrine aux divers stimuli a révélé un deuxième domaine régulateur en C-terminal de pyrine. Des mutations spécifiques, telles que p.Q426R et p.F479L, rendent pyrine particulièrement sensible à l'activation par les hormones stéroïdes et leurs dérivés, ainsi que par la simvastatine. L'ensemble de résultats présenté dans ce manuscrit révèle deux domaines en C-terminal de pyrine – B30.2 et CHS – qui régulent l'activation de l'inflammasome pyrine grâce à un mécanisme de couplage probablement médié par une série de changements conformationnels de la protéine. Nous avons également identifié un nouveau rôle de l'inflammasome pyrine en tant que senseur de métabolisme des hormones stéroïdes.

Mots clés: inflammasome pyrine, fièvre Méditerranéenne familiale, maladie auto-inflammatoire, régulation de pyrine, B30.2, hormones sexuelles stéroïdes, métabolisme du cholestérol.

List of abbreviations

(ds)DNA – (double stranded) deoxyribonucleic acid

AIM2 – absent in melanoma 2 protein

ASC – apoptosis-associated speck-like protein containing a CARD

BTN – butyrophilin

CARD – caspase recruitment domain

CDC42 – Cell division control protein 42 homolog

CDS – coding DNA sequence

CHS – central helical scaffold

DAMPs – damage associated molecular patterns

DNA – deoxyribonucleic acid

ER – endoplasmic reticulum

FMF – familial Mediterranean fever

GGpp – geranylgeranyl pyrophosphate

GSDMD – gasdermin D

GTP – guanosine triphosphate

HAMPs – homeostasis-altering molecular processes

HIDS - hyperimmunoglobulinemia D syndrome

HMPP - hydroxy-3-methyl-but-2-enyl pyrophosphate

ICE - IL-1 β converting enzyme

IFN – interferon

IL-18 – interleukin-18

IL-1 β – interleukin-1 β

IPP – isoprenyl pyrophosphate/diphosphate

iPSC-ML – induced-pluripotent stem cell-derived myeloid cell line

LPS – lipid polysaccharide

MA - mevalonic aciduria

MAPK – mitogen-activated protein kinase

MEFV – MEditerranean FeVer

MHC I – major histocompatibility complex I

MKD – mevalonate kinase-associated disease

MST – microscale thermophoresis

MVK – mevalonate kinase

NINJ1 - nerve injury-induced protein 1

NLRC4 – NLR-family CARD domain-containing protein 4

NLRs – nucleotide-binding domain and leucin-rich repeat containing receptor

PAAD – pyrin associated autoinflammatory disease

PAAND – pyrin associated autoinflammation and neutrophilic dermatosis

PAMPs – pathogen-associated molecular patterns

PAPA – pyogenic arthritits, pyoderma gangrenosum, acne

PFD – pore-forming domain (of GSDMD)

PFIT - Periodic fever, immunodeficiency, and thrombocytopenia

PI – propidium iodide

PKC – protein kinase C

PLD – phosphorylated linker domain

POP – PYD only protein

PSTPIP1 - proline serine threonine phosphatase interacting protein 1

PYD – pyrin domain

RNA – ribonucleic acid

SAA – serum amyloid A

SHR – steroid hormone receptor

TGF – transforming growth factor

TLR – Toll-like receptor

TNF – tumor necrosis factor

TRIM – tripartite motif

VUS – Variants of unknown significance

WDR1 - WD repeat-containing protein 1

β2MG - β2-microglobulin

List of figures and tables

Introduction

Figure 1.1	16	Figure 4.1	34
Figure 2.1	20	Figure 4.2	38
Table 2.1	21	Figure 5.1	39
Figure 2.2	22	Figure 5.2	40
Figure 2.3	24	Table 5.1	41
Figure 2.4	25	Figure 7.1	47
Figure 3.1	26	Figure 7.2	48
Figure 3.2	28	Figure 7.3	50
Figure 3.3	29	Figure 7.4	51
Figure 3.4	31	Figure 7.5	51
Table 3.1	32		

Results

Part 1

Figure 1	77	Figure S3	94
Figure 2	78	Figure S4	96
Figure 3	80	Figure S5	98
Figure 4	82	Figure S6	101
Figure 5	84	Figure S7	102
Figure 6	86	Figure S8	104
Figure 7	88	Figure S9	105
Table S1	91	Figure S10	106
Figure S2	92		

Part 2

Figure 1	123	Figure S1	134
Figure 2	124	Figure S2	135
Figure 3	127	Figure S3	136
Figure 4	128	Table S1	138
Figure 5	130	Table S2	139
Figure 6	132		

Additional results

Figure 1	144	Figure 5	162
Figure 2	150	Table 1	164
Figure 3	154	Figure 6	168
Figure 4	160		

Discussion

Table 1	176	Figure 3	180
Figure 1	177	Figure 4	182
Figure 2	178	Figure 5	186

Methods

Table 1	200	Figure 3	202
Table 2	200	Figure 4	203
Figure 1	201	Figure 5	204
Figure 2	201	Figure 6	205

INTRODUCTION

1. Inflammasomes

The innate immune system is the first barrier that a pathogen encounters during infection. This first line of defence relies on germline-encoded pattern recognition receptors (PRRs) that sense pathogen-associated molecular patterns (PAMPs) such as LPS or flagellin, or other molecules that can be found on the surface or within pathogens. Alternatively, the PRRs can be triggered by damage-associated molecular patterns (DAMPs) such as alarmins, DNA or uric acid that are released in the extracellular space when cells die as a result of infection or cell damage. In the case of PAMP and DAMP, PRRs sense danger through direct binding of a ligand. For example, Toll-Like Receptor 4 (TLR4) binds bacterial LPS and Absent In Melanoma 2 (AIM2) binds cytosolic dsDNA.

1.1 The innate immune sensing of pathogens and danger signals

More recently a new mechanism of indirect pathogen sensing, previously known in plants, has been described in animal cells. In this case, the PRR activation is triggered by an alteration of cellular processes as a result of infection or other abnormal process. Such phenomena became known as homeostasis-altering molecular processes (HAMPs) (Liston and Masters, 2017). HAMP-sensing is the mode of action of the pyrin inflammasome which acts as the guard of RhoA activity.

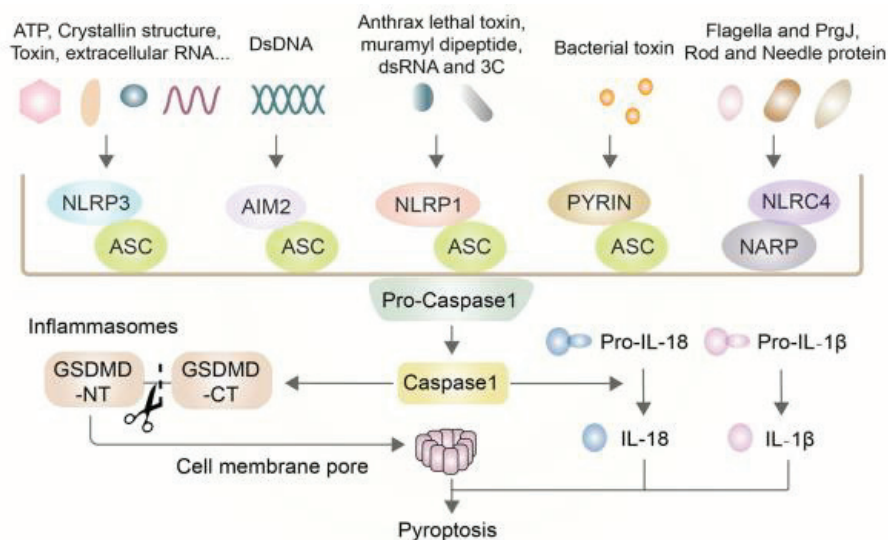


Figure 1.1 Basic mechanisms of canonical inflammasome activation (adapted from (Wei et al., 2022)). Canonical inflammasomes, including NLRP3, AIM2, NLRP1, Pyrin and NLRC4 are composed of PRR, ASC and pro-caspase-1. Activation of the PRR sensor by corresponding stimuli leads to cleavage and activation of caspase-1. Activated caspase-1 can induce the formation of GSDMD-NT, which contributes to the perforation of the cell membrane and enhances the capability of processing IL-1 β and IL-18.

1.2 Inflammasomes

Inflammasomes are large multimeric complexes that oligomerize in the cell cytosol when activated. They were identified in 2002 by Fabio Martinon and colleagues, who described the caspase-activating complex and identified the key protein partners that cooperate to form the inflammasome (Fabio Martinon et al., 2002). Inflammasome activation leads to the activation of caspase-1 and cleavage of the pro-inflammatory cytokines IL-18 and IL-1 β , accompanied by the cleavage of gasdermin D (GSDMD) and the formation of GSDMD pores in the cell membrane. In most cases, as a result, the cell undergoes pyroptosis – a form of rapid pro-inflammatory cell death (**Fig. 1.1**). Therefore, inflammasome activation is a highly potent pro-inflammatory mechanism that is tightly regulated as described later in this manuscript with the example of pyrin inflammasome regulation.

Inflammasomes contain three main components: the sensor, the adaptor and the effector.

1.2.1 Inflammasome sensors

Inflammasome sensors can be triggered into action by a large spectrum of danger signals. It can be specific molecules attributed to pathogens sensed by direct binding, or alterations of the cell homeostasis or the presence of certain molecules outside of the usual compartments. This mechanism of action provides a large flexibility and a great resistance to possible escape techniques that pathogens may develop over time in order to avoid the immune response.

The nucleotide-binding domain and leucine-rich repeat containing receptors (NLRs) are a large family of inflammasome sensors that includes NLRP1, NLRP3 and others. Inflammasome sensors outside of this family also exist, for example, AIM2 or pyrin. The common feature of many of the inflammasome sensors is the presence of the pyrin domain (PYD) which mediates the interaction with the adaptor of the inflammasome - ASC. This presents some notable exceptions like the NAIP/NLRC4 or the NLRP1b inflammasomes which contains the CARD domain and can interact with caspase-1 without an adaptor (Sandstrom et al., 2019, p. 1; Vance, 2015).

1.2.2 Inflammasome adaptor – ASC

Apoptosis-associated speck-like protein containing a caspase recruitment domain (CARD) (ASC) acts as the adaptor within inflammasome complexes. It is a small protein (22 kDa) encoded by the *PYCARD* gene. ASC contains two domains: the PYD and the CARD domains. Both domains of ASC are protein-protein interaction domains that interact with the PYD of the inflammasome sensor on one hand, and the CARD domain of caspase-1 on the other hand. The inflammasome complex nucleates around the

ASC which serves as a platform by forming large structures known as specks. ASC specks are a hallmark of inflammasome activation and can be visualized by immunofluorescence (de Alba, 2019; Srinivasula et al., 2002).

1.2.3 Inflammasome effector – caspase-1

Caspase-1 is a small Cysteine-dependent Aspartate-Specific Protease originally discovered as IL-1 β converting enzyme (ICE). Caspase-1 is produced by the cell in the form of a catalytically inactive zymogen and requires cleavage in order to become activated. Inactive caspase-1 contains a CARD domain that lacks catalytic function, but it is required for caspase-1 to interact with other CARD-containing proteins (such as ASC) during its activation. Caspase-1 undergoes autoproteolysis when it binds the ASC protein within the inflammasome complex, the resulting p33 and p10 peptides form the enzymatically active caspase-1 (Boucher et al., 2018). In this state caspase-1 can cleave and activate pro-IL-1 β and pro-IL-18 which are potent pro-inflammatory cytokines. Also, activated caspase-1 cleaves GSDMD, this cleavage frees the GSDMD-NT, also known as the pore-forming domain (PFD). This PFD then inserts itself into the cell membrane in order to form pores.

Finally, the autoproteolysis of caspase-1 results in a new cleavage and the release of p20 and p10 peptides. It was previously believed that this p20-p10 dimer constitutes the activate form of caspase-1, but more recent studies reveal that in this state, caspase-1 disperses in the cytosol and loses its enzyme activity (Boucher et al., 2018; Martinon et al., 2009; Rathinam and Fitzgerald, 2016).

Other inflammatory caspases and notably caspase-4 can be activated within inflammasomes. Non-caspase-1-inflammasomes are termed non-canonical inflammasomes.

1.3 Pyroptosis – pro-inflammatory cell death

Pyroptosis is a form of inflammatory cell death distinct from other types of programmed cell death. The term “pyroptosis” was first coined in 2001 when it was described in the context of bacterial infection-induced pro-inflammatory cell death in macrophages (Brad T Cookson and Brennan, 2001). Pyroptosis allows the release of activated IL-1 β , IL-18 and certain DAMPs into the extracellular space and thus signal danger to the surrounding cells. Pyroptosis progresses rapidly, with cell swelling, ionic fluxing, mitochondrial depolarization and lysosome leakage (Bergsbaken et al., 2009; de Vasconcelos et al., 2019).

Pyroptosis was first characterized as a caspase-1-dependent process, although several caspases have since been described to mediate pyroptosis (Brad T Cookson and Brennan, 2001; Yu et al., 2021).

Today, GSDMD is recognized to be the pyroptotic effector molecule. Other members of the GSDMD family can also form pores and trigger necrosis although GSDMD is the main cell death executioner downstream of caspase-1.

The cleavage of GSDMD by caspase-1 releases the N-terminal pore forming domain of GSDMD which then forms pores in the cell membrane but also in the membrane of the lysosomes or the mitochondrial membrane (Cao and Kagan, 2022). The final event in pyroptosis is the cell membrane rupture mediated by nerve injury-induced protein 1 (NINJ1) (Kayagaki et al., 2021; Newton et al., 2021). Curiously, GSDMD pore formation is necessary but is not always sufficient for pyroptosis. In cases when the inflammasome activation occurs at a slow enough rate that the cell membrane-repair machinery is able to keep up, the GSDMD pores simply allow the release of mature pro-inflammatory cytokines from the activated cell (Evavold et al., 2018).

2. Pyrin structure domain by domain

2.1 Pyrin structure

The pyrin protein consists of 781 amino acids that yield the molecular weight of 95 kDa. As a member of the TRIM family, pyrin contains some domains typical for this family: the C-terminal B30.2 (also known as PRY/SPRY), the coiled coil, and the B-box domains. Unlike most other TRIM proteins, pyrin lacks an N-terminal RING domain, which is replaced with a PYD domain (Fig.2.1). The phosphorylated linker domain encoded by the exon 2 lacks defined three-dimensional structure but contains some key functional features that are essential for pyrin regulation. Key features and known interactants of pyrin domains are listed in Table 1.

***MEFV* gene**

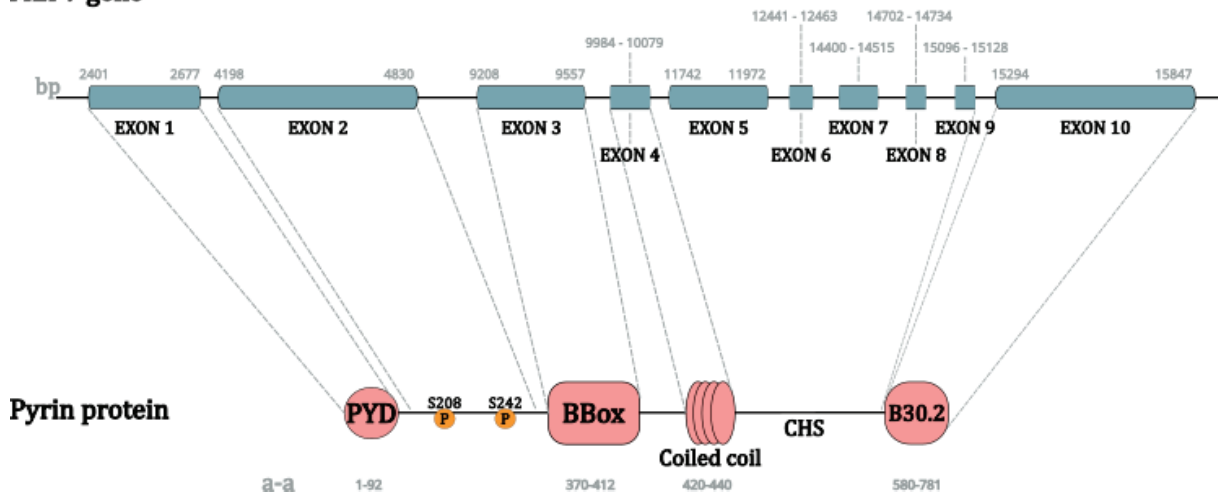


Figure 2.1 Schematic representation of the *MEFV* gene and the pyrin protein that it encodes. The base pair positions corresponding to the start and the end of exons are indicated on the gene. The amino acid positions corresponding to the start and the end of the domains, as well as the names of the domains and some key residues are indicated on the protein. The dotted lines indicate which region of the protein is encoded by which exon.

2.2 PYD

The inflammasome assembly requires protein-protein binding between the sensor protein (pyrin) and the adaptor protein – ASC. This interaction is mediated by the PYD domains of both partners. These are small N-terminal domains of approximately 90 amino acids (92 in pyrin) always located on the N-terminus of the protein. The name PYD comes from “pyrin domain” since it was first identified in the pyrin protein. The three-dimensional structure of a PYD domain with 6 α -helices resembles a Greek key. In all 23 human proteins that carry PYD the hydrophobic core involving five out of six

Domain/Region	Position; length (amino acids)	Interactants	Function	Ref.
PYD	1-92; 92	ASC, own B-box, tubulin	Inflammasome assembly	(Vajjhala et al., 2014; Van Gorp et al., 2016a; J.-W. Yu et al., 2007a)
Phosphorylated linker domain (PLD)		PKN1/2, 14-3-3	Phosphorylation-induced inhibition	(Gao et al., 2016a; Moghaddas et al., 2017a)
B-box	370 – 412; 42	PSTPIP1, own PYD, pyrin	Auto-inhibition, oligomerization	(Shoham et al., 2003a; J.-W. Yu et al., 2007a)
Coiled coil	420 – 440; 20	B30.2, pyrin	Pyrin oligomerization	(Weinert et al., 2015a; J.-W. Yu et al., 2007a)
B30.2	580 – 780; 200	Coiled coil, caspase-1, caspase-5, Siva, β 2MG, yet unidentified ligand	Negative regulation	(Balci-Peynircioglu et al., 2008; Chae et al., 2008a; Papin et al., n.d.; Samukawa et al., 2021; Weinert et al., 2015a)

Table 2.1 List of pyrin domains, their position and length within the protein as well as established interactants and the potential function for that interaction.

helices is conserved; the remaining helix – α 3 – is the most variable and most likely involved in binding specificity (Chu et al., 2015).

The PYD domain is instrumental in interactions that activate the innate immune response, but it is also part of some negative regulation mechanisms. For example, POPs (PYD Only Proteins) consist only of the PYD domain – as is clear from its name – and act as decoy PYD that competes with other proteins for the binding. Interestingly, several such proteins are expressed by human immune cells but they are absent in the mouse proteome (Chu et al., 2015; Khare et al., 2014; Ratsimandresy et al., 2017; Stehlik et al., 2003).

The mechanistics of the inflammasome assembly through PYD-PYD binding is the subject of several studies. Through in vitro binding experiments, Vajjhala and colleagues have identified three regions within pyrin PYD and two regions within the PYD of ASC that participate in the interaction between the two proteins: both of the ASC sites are required to bind to a PYD of pyrin but the pyrin PYD can interact with more than one ASC at a time (**Fig.2.2**) (Vajjhala et al., 2014). Such binding is typical for inflammasome formation which requires an agglomeration of multiple inflammasome components to optimally induce caspase-1 activation. Moreover, the same group found that the same ASC residues are involved in PYD-PYD binding with Pyrin, NLRP3 and POP1, consistent with the idea of regulation by competition (Vajjhala et al., 2012).

Aside from the pyrin PYD binding to ASC, PYD interacts with other domains of the Pyrin protein itself.

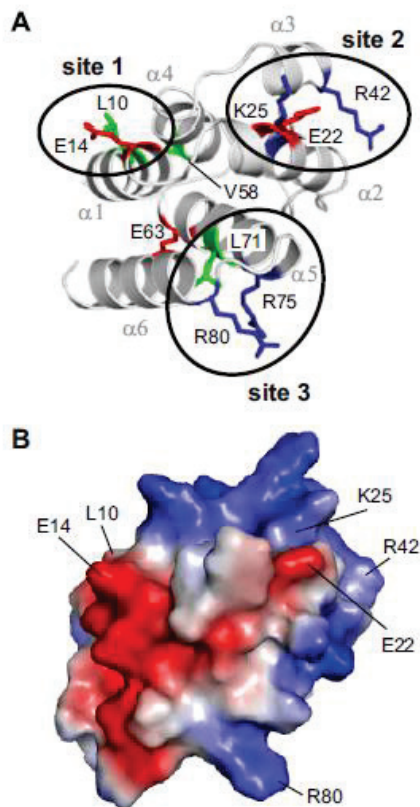


Figure 2.2 Residues important for interaction of pyrin PYD with ASC PYD localize in three clusters: ribbon representation of the pyrin PYD, mutations that affect interaction are highlighted; basic, acidic and hydrophobic residues are coloured blue, red and green respectively (A), surface electrostatic potential of pyrin PYD shown in the same orientation as in A and indicating residues important for interaction (B) (adapted from Vajjhala et al, 2014).

Several studies describe an intramolecular interaction between PYD and B-box of the pyrin protein, that would fold the protein in two – a conformation that possibly results in autoinhibition (Ryan et al., 2010; J.-W. Yu et al., 2007).

Several mutations located in the PYD domain have been described in FMF patients although their pathogenic significance is unclear. On a molecular level, the p.R42W mutation seems to decrease the strength of interaction between ASC and pyrin, but the real physiological impact of the mutations could be minimal since aggregation of multiple molecules involved in the inflammasome could compensate for a diminished strength of a single interaction (Vajjhala et al., 2014; J.-W. Yu et al., 2007). Interestingly, in the PYD domains of other inflammasome proteins, tryptophan (W) is the wild type residue at the equivalent position and evidence suggests that the substitution of arginine (R) for tryptophan (W) in this pyrin variant only contributes to the PYD stability (Vajjhala et al., 2014).

2.3 Phosphorylated linker domain

The second exon of *MEFV* encodes a stretch of approximately 200 amino acids between the PYD domain and the B-box domain with some significant features essential for pyrin regulation. It contains the two key phosphorylation sites that take part in the control of pyrin activation. Originally identified as serine residues S241 and S205 in mice, they are equivalent to the human S242 and S208 (Gao et al., 2016). At steady state pyrin is inhibited by phosphorylation, the linker domain containing phosphorylation sites binds a phospho-dependent chaperone protein from the 14-3-3 family (the mechanism of pyrin activation is presented later in this manuscript). This interaction likely stabilizes the inactive state of the inflammasome. Mutations in this area of pyrin that involve the phosphorylated

residues themselves (p.S242R and p.S208C both identified in FMF patients) or neighbouring residues (e.g. p.E244K), hinder the 14-3-3 binding so the inflammasome activates more easily. This constitutes the pathological mechanism of one of the autoinflammatory diseases associated with pyrin – pyrin-associated autoinflammation with neutrophilic dermatosis (PAAND) (Moghaddas et al., 2017).

2.4 B-Box

The B-box domain of pyrin, located at residues 370 to 412, is a domain exclusive to TRIM proteins. It is often involved in protein-protein interactions and the pyrin B-box appears to interact with several partners. The crystal structure of the pyrin B-box has not been resolved, but it is a type 2 B-box, like in all TRIM proteins containing a single B-box domain, rich in histidine and cysteine residues that ensure zinc binding (Sardiello et al., 2008).

First, an already described intramolecular binding of the pyrin PYD and B-box domains is hypothesised to confer an inhibitory conformation to the protein. Second, B-box likely participates in pyrin oligomerization along with the neighbouring coiled-coil domain (J.-W. Yu et al., 2007). In fact, the role of B-box domain in self-oligomerisation has been established for several other TRIM proteins (Keown and Goldstone, 2016; Sun et al., 2019).

Another interactant for the pyrin B-box was identified thanks to an auto-inflammatory syndrome distinct from FMF. In PAPA syndrome (pyogenic arthritis, pyoderma gangrenosum, acne), mutations in the gene encoding PSTPIP1 (proline serine threonine phosphatase interacting protein 1) lead to an enhanced tyrosine phosphorylation of the latter. Shoham and colleagues revealed that PSTPIP1 binds the B-box domain of pyrin in a phosphorylation-dependent manner. Mutations that increase PSTPIP1 phosphorylation cause a stronger PSTPIP1-pyrin binding and mutations that decrease that phosphorylation, have the opposite effect (Shoham et al., 2003; Waite et al., 2009). The binding of phosphorylated PSTPIP1 to the pyrin B-box leads to inflammasome activation. The model suggested for this activating mechanism is as follows: the pyrin B-box traps the PYD domain at steady state; phosphorylated PSTPIP1 competes with PYD for the B-box, and when the B-box domain interacts with PSTPIP1, the PYD is released and becomes available for inflammasome assembly through ASC binding.

The B-box domain contains several zinc-binding fingers known for their ability to bind nucleotides. Pyrin also contains a b-ZIP domain typically found in transcription factor proteins. It occupies residues 266 to 280, making it adjacent to the B-box in pyrin. There is even evidence that a product of alternative splicing of the *MEFV* gene lacking the exon 2, resides in the nucleus (Papin et al., 2000). Today, the cytosolic subcellular localization of pyrin, as well as its role in cytosolic immunity, is well

established. It remains unclear if these potential nucleotide binding features find utility within the physiological function of pyrin.

Mutations found in the B-box of pyrin are listed as “variant of unknown significance” in the Infevers database: they have been identified in patients with FMF, combined with other mutations, but it is unclear if on their own these mutations are pathogenic. One study in particular looks into the structural impact of two of these variants, p.P369S and p.R408Q. Molecular modelling and a set of in vitro experiments show that it is unlikely that these mutations significantly change the conformation of B-box, or that they impact the interaction with partners like PSTPIP1 or own PYD (**Fig.2.3**). Moreover, these variants do not appear to be spontaneously activated when dephosphorylated, as is the case for typical FMF-causing mutations and patients carrying the p.P369S and the p.R408Q variants exhibit an atypical FMF phenotype and only partially respond to colchicine (Magnotti et al., 2019; Ryan et al., 2010).

2.5 Coiled coil

The coiled coil domain is located between the residues 420 and 440 – it immediately follows the B-box domain and precedes the B30.2 domain of pyrin. This region takes the form of a simple long α -helix, but it may have several important functions.

Like the B-box, the coiled coil domain is characteristic of TRIM proteins. In pyrin, the coiled-coil domain has been shown to mediate the protein self-trimerization (J.-W. Yu et al., 2007); a recent study by Malik and colleagues showed that pyrin presents as a dimer or larger oligomers at steady state (available on bioRxiv; doi: 10.1101/2022.03.23.485108). Additionally, the C-terminal fragment of pyrin containing the coiled coil and B30.2 folds into a complex three-dimensional structure. The resulting dimers, with the coiled coil and the long α -helix that links it to the B30.2 domain serving as the foundation for the

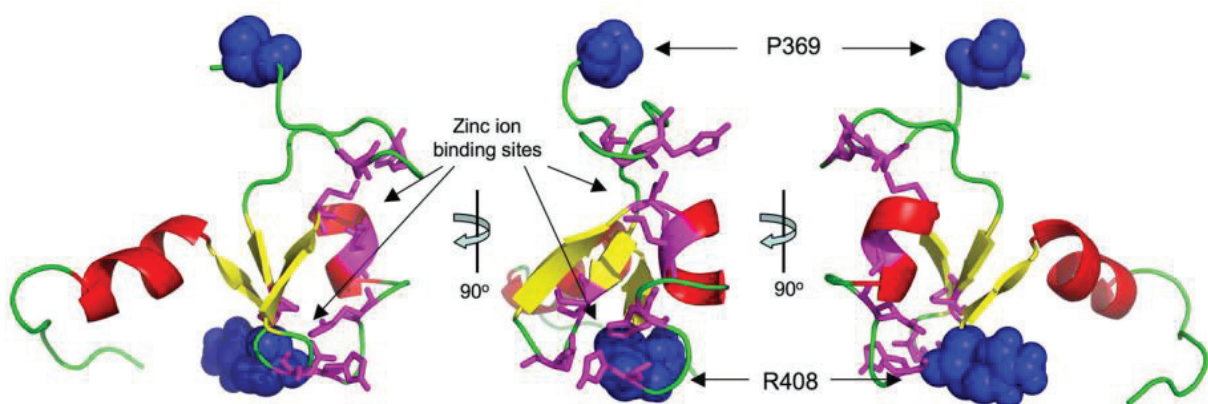


Figure 2.3 Modelling of B-box domain. Substitutions at P369S and R408Q highlighted, neither are predicted to have significant effect on protein conformation (adapted from Ryan et al, 2009).

globular B30.2 domains, could open new possibilities for pyrin intra-molecular interactions and self-oligomerization (**Fig.2.4**). The authors who first described this conformation, suggest a new name for the coiled coil domain based on the fact that it provides support for the B30.2 – the central helical scaffold (CHS) (Weinert et al., 2015). Given that the linker between the CHS and B30.2 is flexible in solution, such dimerization could play a role in B30.2-mediated interaction with a yet unknown ligand.

2.6 B30.2

The most C-terminal domain of the pyrin protein is the B30.2 (PRYSPRY) domain of approximately 200 amino acids that starts at the residue 580 of the full-length protein. The structure, possible functions and putative interactants of this domain are elaborated in the next chapter.

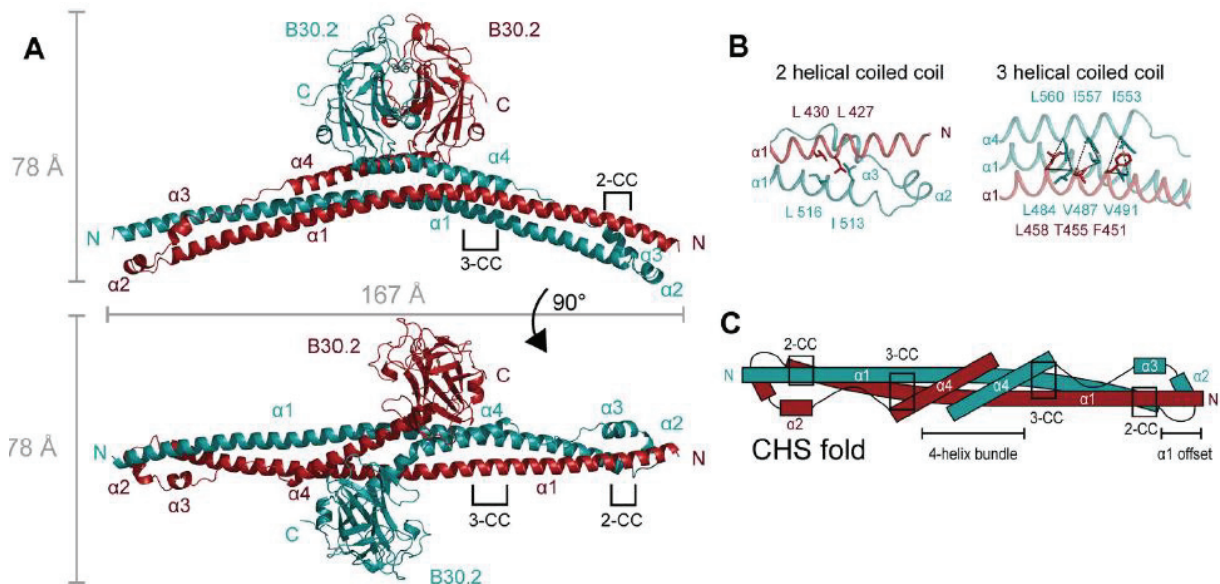


Figure 2.4 Crystal structure of the C-terminal fragment of pyrin containing coiled coil and B30.2. Chains A and B of the dimer are colored in cyan and red, helices of each of the coiled coils are numbered $\alpha 1$ to $\alpha 4$. The dimer is shown from a side and a top view (A), the residues involved in the dimerization are shown (B), topology of the resulting dimer (C) (adapted from Weinert et al, 2015).

3. B30.2

3.1 SPRY/B30.2 domains and SPRY/B30.2-carrying proteins

The terms SPRY and B30.2 are often used interchangeably in literature, but the larger SPRY/B30.2 superfamily can be subdivided into two smaller groups: the SPRY domains of approximately 140 residues, and the PRYSPRY domains – also known as B30.2 domains – which contain an extra N-terminal segment (PRY) of approximately 60 residues (Perfetto et al., 2013).

The SPRY/B30.2 domains are present in many members of the eukaryotic proteome – it is in fact one of the most common folds in higher eukaryotes. There are over 100 SPRY/B30.2-containing proteins in humans – 0.47% of all proteins; 77 in mice – 0.35% of all proteins. They are relatively few in invertebrates with only 0.07% of all fruit fly proteins and 0.05% of all yeast proteins. Indeed, while SPRY domains can be found in proteins across the living species including fungi, plants, bacteria and animals, the B30.2-carrying proteins are only present in vertebrate species indicating its more recent evolutionary history (D’Cruz et al., 2013; Rhodes et al., 2005).

The overall fold of the SPRY/B30.2 domains is relatively conserved and takes the form of a twisted β -sandwich with antiparallel β -sheets (Fig. 3.1).

There are also several conserved peptide signatures that make it possible to establish the evolutionary link between the domains. However, the sequence identity within the family is quite low

(approximately 20%) and only the hydrophobic core around the β -sheets is conserved. The most variable parts of the SPRY/B30.2 domains are the loops that link the β -sheets. A common feature of the SPRY/B30.2 domains is the binding cavity within the SPRY sub-domain (Grütter et al., 2006; Perfetto et al., 2013; Rhodes et al., 2005).

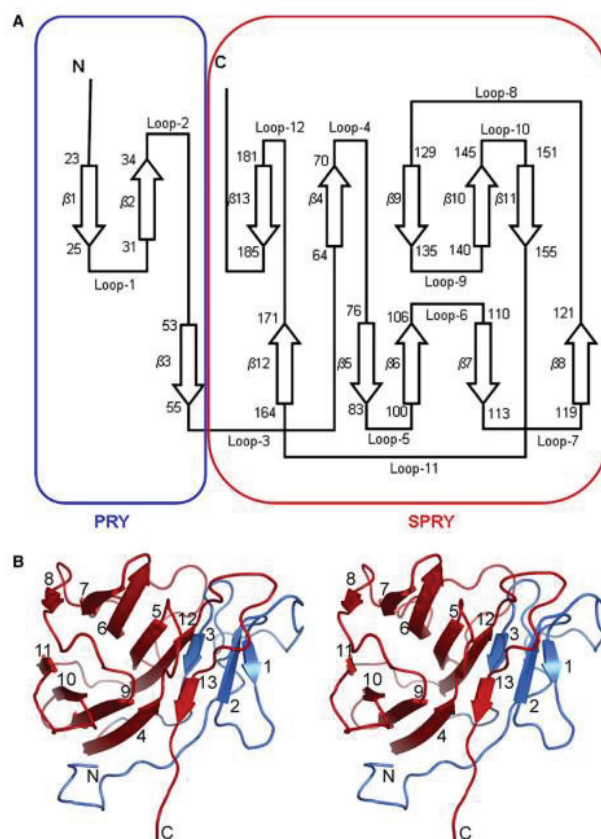


Figure 3.1 PRYSPRY topology cartoon (A) and stereo view of a ribbon representation (B) of the domain with the PRY sub-domain in blue and the SPRY sub-domain in red (adapted from Grütter et al, 2005).

Despite the large number of SPRY/B30.2-carrying proteins expressed in human, for most of them their function, as well as the implication of B30.2 in that function, are poorly understood. In **Table 3.1** I have assembled a list of examples of SPRY/B30.2 domain-carrying proteins, their functions and the putative ligands identified for the SPRY/B30.2 domain.

It is difficult to identify a unique common function for the SPRY/B30.2-carrying proteins. Just over 50% of these proteins in humans belong to the TRIM family and contain a B-box domain and/or a RING domain. Many of them are E3 ligases and it is believed that the SPRY/B30.2 domain may play a role in protein degradation machinery of the cell. Many of them are also involved in innate immune sensing. In fact, several of B30.2-containing proteins are known pathogen recognising receptors (PRR): TRIM5 α , Pypin, BTN3A1 and TRIM25, to name a few.

SPRY/B30.2 typically ensures protein-protein interaction but there are some notable exceptions. Considering that SPRY/B30.2-carrying proteins are involved in a multitude of metabolic cell processes often linked to cell immunity, it is likely that SPRY/B30.2 domains have evolved to serve as a malleable binding platform for ligands of varying nature and size (Perfetto et al., 2013). Here are a few examples of B30.2-containing proteins and their B30.2 ligands that seem to have physiological significance either by binding PAMPs directly or by monitoring the cell homeostasis.

TRIM5 α is an innate immune sensor that plays a key role in restricting retroviral infection. The B30.2 domain of this protein in rhesus macaques efficiently binds HIV-1 capsid and so protects cells from infection. The molecular mechanism of this protection is unclear, and the wild type human TRIM5 α fails to protect us from HIV-1 infection but several variants of TRIM5 α found in humans show a better restriction and, most notably, when its B30.2 is mutated to mirror Rhesus TRIM5 α , the human protein becomes more stable and gains a significant restriction ability against HIV-1. These findings offer therapeutic value to stabilizing human TRIM5 α protein, and they also demonstrate one example of a functionally significant B30.2 -mediated protein-protein interaction (Richardson et al., 2014, p. 5; Stremlau et al., 2005).

Another remarkable example of B30.2 ligand function in human is that of Butyrophilin 3A1 (BTN3A1) – a transmembrane protein with an intracellular B30.2, expressed by antigen-presenting cells. The $\gamma\delta$ T cell subset recognises tumours and infected cells thanks to - among other things - small, phosphorylated phenyl metabolites known as phospho-antigens. Several studies identify B30.2 of BTN3A1 as the binding site for such phospho-antigens as HMBPP or IPP. The binding cavity within B30.2 specifically recognises phospho-antigens inside the cell, this binding leads to a conformational change of B30.2 that goes beyond the molecular surface in the immediate vicinity of the binding pocket. This signal is transduced along the BTN3A1 protein to the cell surface where it is sensed by $\gamma\delta$ T cells (Salim

domain and a C-terminal SPRY sub-domain. In a three-dimensional structure similar to other B30.2 domains, it takes the form of a compact β -barrel (37x35x31 Å) with two anti-parallel six- and seven-stranded β -sheets – this fold resembles a swiss roll, where the two β -sheets lay one on top of the other connected with short helical loops. Additionally, one helix at the most N-terminal end of the domain belonging to the PRY sub-domain is positioned perpendicularly to the seven-stranded β -sheet (**Fig. 3.3**) (Weinert et al., 2009).

Residues involved in the helical loops and several of the β -strands that belong to both the SPRY and the PRY sub-domains form a shallow cavity on the surface of pyrin B30.2. The three-dimensional conformation of this cavity closely resembles that of other B30.2-carrying proteins: TRIM21 or RFPL1. Considering this similarity, it is likely that B30.2 of pyrin, like that of TRIM21 or RFLP1, also has a ligand that remains to be definitively identified. Interestingly, while TRIM21 and RFPL1 ligand binding is ensured by ligand-specific hydrogen bonding within the central cavity, the residues that line the binding cleft of pyrin have been replaced with hydrophobic amino acids. This change would necessarily impact the type of ligand and the types of interactions that would form between the pyrin B30.2 and its putative ligand (Weinert et al., 2009).

There is evidence in the field to support the hypothesis that pyrin B30.2 functionally binds a yet unknown ligand and several studies have aimed to identify it. For example, Chae et al. demonstrated that in THP-1 cells endogenous pyrin co-immunoprecipitates with caspase-1. In a further series of experiments (this time in PT67 cells transfected to express the studied proteins), they elaborated on the nature of this interaction: it is direct (independent from the adaptor protein ASC); it is mediated by the B30.2 domain of pyrin; and it is hindered by the FMF-associated mutations within the domain (Chae et al., 2006). Another study also finds direct interaction between pyrin B30.2 and pro-IL1b but does not observe the negative effect of the B30.2 mutations (Papin et al., 2007).

The major limitation of Chae's study consists in the implemented experimental system where a murine

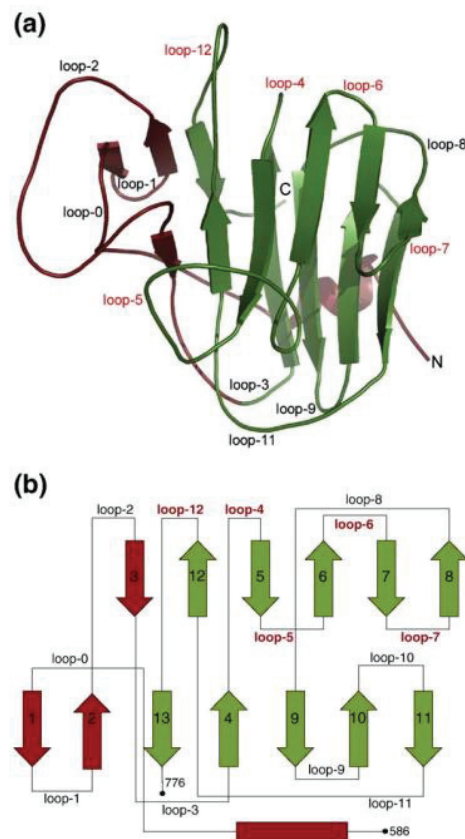


Figure 3.3 Ribbon (A) and topology (B) diagrams of the pyrin B30.2 domain; the PRY sub-domain in red and the SPRY sub-domain in green (adapted from Weinert et al, 2009).

embryonic fibroblast cell line which does not express ASC (PT67) serves as platform to transfect variants of human pyrin and human caspase-1; the cells then apparently spontaneously release IL-1 β 48h post-transfection. Such a model fails to account for known differences in pyrin regulation and function in mice and in humans: endogenous murine pyrin lacks the B30.2 domain and studies show that introducing human wild-type pyrin in mice leads to an auto-inflammatory phenotype (Jae Jin Chae et al., 2000). Moreover, this study predates the definitive identification of Pyrin activity as inflammasome, which puts into question the pertinence of studying its interacting partners in a cell line that lacks ASC.

A recent study identifies β 2-microglobuline (β 2MG) as a novel ligand for the B30.2 of pyrin. β 2MG is a small protein better known for being a part of the MHC-I complex, but it is also enclosed in the granules of neutrophils. β 2MG direct binding to pyrin B30.2 promotes ASC-speck formation within the cell indicative of inflammasome activation (Samukawa et al., 2021). However, the physiological context or mechanism of β 2MG – pyrin interaction is unclear, and the authors do not investigate whether pyrin activation by β 2MG bypasses RhoA inhibition or how it overcomes other checkpoints of pyrin activation.

Interestingly, in a study where the main focus was identifying the crystal structure of pyrin B30.2, the authors report an ethylene glycol molecule lodged inside the binding cavity, but do not pursue a deeper understanding of this interaction (Weinert et al., 2009). Ethylene glycol is a component of the cryoprotectant, and although it could not be the endogenous ligand for B30.2, the finding supports the possibility of a non-peptide binding partner for pyrin B30.2.

It is unclear how this putative interaction between pyrin B30.2 and a putative ligand plays into pyrin function and how it relates to pyrin's activity as a homeostasis-guarding inflammasome. It seems that this interaction is key to regulate pyrin activity, since its disturbance by mutations located in B30.2 leads to the Pyrin inflammasome hyperactivation (Jamilloux et al., 2018).

Analysis of mutations found in FMF patients concludes that mutations associated with the most severe presentation of FMF are, in fact, conservative mutations – meaning that the original amino acid is replaced with one that has similar biochemical properties - located in two highly conserved regions of exon 10 (Moradian et al., 2017). For instance, p.M680I, p.M694V and p.V726A linked with clinically severe FMF are conservative substitutions positioned within these two regions. It is surprising that conservative mutations impact the protein function but there could be an explanation for this.

In fact, most characterized pathogenic or likely pathogenic mutations in the pyrin protein that cause FMF cluster within exon 10 encoding the B30.2 domain. The p.M694V mutation alone is responsible

for 80% of clinical FMF cases. Weinert and colleagues demonstrate that most of these mutations are located either directly inside the cavity, around its edges and within the hydrophobic core or on the opposite side of the central cavity. Molecular modelling *in silico* shows that the two characteristic FMF mutations (p.M694V and p.M680I) would directly impact the interaction stability between pyrin B30.2 and caspase-1 (Arakelov et al., 2018a, 2015). Chae et al. also modelled the putative interaction between B30.2 and caspase-1 and located the same two disease-causing mutations on the interface between the two partners (**Fig. 3.4**).

Curiously, some of the FMF-causing mutations represent a reversal to an ancestral amino acid state: the mutant residues can be found as wild type in Pyrin in other species, particularly in non-human primates. This implies one of two things: either Pyrin binds the same ligand in different species and the mutations qualitatively modulate its binding affinity – this would be similar to the TRIM5a affinity for HIV capsid; or these mutations reflect the change in identity of this ligand or even the change of function for Pyrin in different species (Philip Schaner et al., 2001).

The identity of the ligand for Pyrin B30.2 remains unknown with several of candidates suggested throughout the literature, some more plausible than others. This interaction could be novel, not present in other species, maybe not even in primates, or it could represent a conserved interaction for which the stability is affected by the FMF-causing mutations. Given the diversity presented by the Pyrin protein in mammals and even in primates, it would be important to validate its identity in primary human samples. In any case, all evidence points to the existence of this ligand clearly instrumental to normal Pyrin function and its identification would shed light on much of what remains poorly understood about the Pyrin inflammasome.

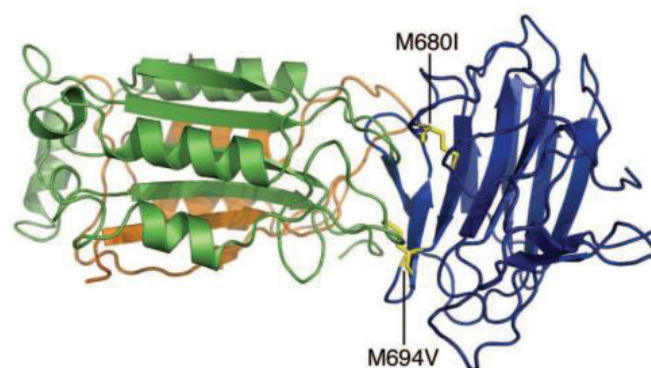


Figure 3.4 An *in silico* generated model for the interaction of pyrin B30.2 domain (blue) and caspase-1 (p10 in brown and p-20 in green); the residues often mutated in FMF – M680 and M694 are located within the putative binding interface (adapted from Chae et al, 2006).

Table 3.1 Unexhaustive list of SPRY/B30.2 containing proteins, their functions and the ligands identified for the SPRY/B30.2 domain.

Protein	SPRY or B30.2	Proposed ligand	Proposed function for interaction with the ligand	Ref.
TRIM5a	B30.2	HIV-1 capsid protein	Defence against retroviral infection, exact mechanism is unclear	(Richardson et al., 2014; Stremmler et al., 2005)
TRIM18/MID1	B30.2	Microtubules	Regulation of cell cycle, exact mechanism is unclear	(Zanchetta and Meroni, 2019)
TRIM20/Pyrin	B30.2	Caspase - 1, IL-1 β , unknown non-peptide ligand	Anti-bacterial immune response, inflammasome activity regulation	(Chae et al., n.d.; Papin et al., n.d.; Weinert et al., 2009)
TRIM21/Ro52	B30.2	IRF3 and IRF7	Regulation of type I IFN ad cytokine production	(Stacey et al., 2012)
TRIM22	B30.2	Unclear, but ensures nuclear localisation of TRIM22	Antiviral response, formation of nuclear bodies	(Sivaramakrishnan et al., 2009)
TRIM25	B30.2	ss- and dsRNA, RIG-1	Antiviral response, activation of RIG-1 and promotion of MAVS degradation	(Choudhury et al., 2017; D'Cruz et al., 2018; Sanchez et al., 2018)
TRIM27	B30.2	NOD2, interferes with RB-mediated gene activation	NOD2 mediated pro-inflammatory responses; Regulation expression of Rb1	(Zurek et al., 2012)

BTN1A1	B30.2	XOS (xanthine oxidoreductase)	Oxidative species generation when expressed in immune cells	(Jeong et al., 2009)
BTN3A1	B30.2	Non-peptidic pyrophosphate antigens	Phospho-antigen-mediated activation of $\gamma\delta$ T cells	(Salim et al., 2017; Sandstrom et al., 2014a)
RFPL1	B30.2	Proteasome-targeted substrates	Regulation of cell cycle, exact mechanism unclear	(Bonnefont et al., 2011)
SPSB1	SPRY	MET (tyrosine kinase domain)	Enhancement of the hepatocyte growth factor-induced Erk-Elk1-SRE pathway	(Wang et al., 2005)
SPSB2	SPRY	iNOS	Negative regulation of iNOS activity	(Kuang et al., 2010)

4. Pysin inflammasome regulation

4.1 Physiological triggers of pyrin

Pyrin is expressed in neutrophils, monocytes and macrophages (Fig. 4.1). This restrictive pattern of expression reflects the role of pyrin in innate immunity and enables it to rapidly respond to infections. Pyrin expression can be up-regulated by LPS, IFN α , IFN γ and TNF, and inhibited by TGF β , IL-4 and IL-10 (Centola et al., 2000; Cornut et al., 2020; Grandemange et al., 2011). In 2014, pyrin was first described as a sensor of bacterial toxins and effectors that inhibit RhoA GTPases. Xu and colleagues demonstrated that pyrin inflammasome activation is triggered by *Clostridium difficile* toxin TcdB. More specifically, TcdB and several other bacterial toxins and effectors (*C. difficile* toxin TcdA, *C. botulinum* toxin C3, *Y. pestis* effectors YopE and YopT, to name a few) target small Rho-GTPases (RhoA, RhoB and RhoC) and inactivate them. Rho inhibition is sensed by the pyrin inflammasome and triggers its activation. Rho-GTPases constantly switch between the two states: Rho-GDP (“off”-state) and Rho-GTP (“on”-state). Pyrin is triggered when the equilibrium between the two states is significantly shifted towards the “off”-state (Park et al., 2016a). Interestingly, the threshold of pyrin activation is lower in FMF: smaller doses of TcdA (and so, lesser RhoA inhibition) triggers pyrin inflammasome activation in monocytes of FMF-patients (Jamilloux et al., 2018).

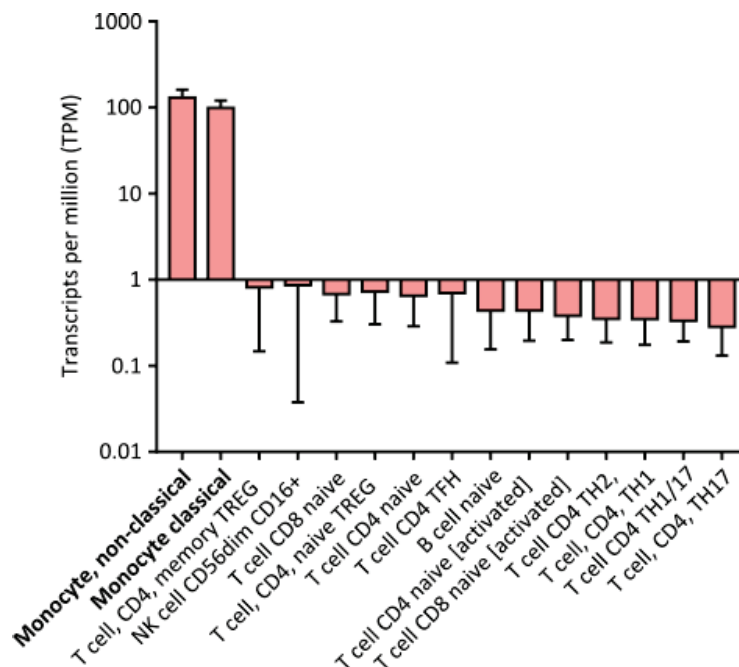


Figure 4.1 Expression level of the MEFV gene in transcripts per million within the cohort of donors studied. Cell types are sorted based on the median expression level within the cohort from highest to lowest. Data extracted from DICE (Database of Immune Cell Expression)

Pyrin does not directly interact with Rho-GTPases. Rather, it senses downstream modifications of the activity of Rho effectors, such as PKN1/2 protein kinases (Malik and Bliska, 2020; Xu et al., 2014). Such indirect sensing of pathogen activity within the cell sets pyrin aside among inflammasome sensors as a guard of cell homeostasis rather than a direct sensor of specific molecules/PAMPs.

In addition to triggers of bacterial origin, several other molecules have been described as pyrin activators. First, bile acid analogues activate pyrin inflammasome and induce both IL-18 secretion and cell death in human cells (Alimov et al., 2019). BAA473 and BAA485 used by Alimov and colleagues are synthetic molecules but similar molecules could be by-products of the microbiome. However, the mechanism of pyrin activation by bile acid analogues is unclear: the question remains whether these molecules inhibit RhoA activity, or act by direct binding to pyrin or in some other fashion. More recently, a small protein β_2 -microglobulin (β_2 MG) has been identified as an activator of the pyrin inflammasome through direct interaction with pyrin, although the physiological context of this interaction remains to be identified (Samukawa et al., 2021).

Pyrin is also activated by several molecules that alter the cell homeostasis. Anisomycin is an antibiotic that hampers protein synthesis by causing ribotoxic stress in the cell, and anisomycin has been described to cause pyrin inflammasome activation (Yu et al., 2013). This phenomenon is mediated by p38 MAPK, a known sensor of stress on a molecular level. Colchicine, an inhibitor of microtubule polymerisation, inhibits pyrin activation by anisomycin which suggests that microtubule dynamics are involved in the mechanism. Additionally, pyrin inflammasome is activated by simvastatin through a mechanism that likely relies on pyrin sensing of RhoA activity (Park et al., 2016).

4.2 Negative regulation of pyrin

Inflammasome activation is a potent pro-inflammatory mechanism and so it is stringently regulated in order to avoid inappropriate immune response. The inhibition of pyrin at steady state is ensured by several regulatory mechanisms. In a study seminal to pyrin inflammasome research, it was demonstrated that pyrin is inhibited by phosphorylation at two sites – S242 and S208 in humans and S241 and S205 in mice (Gao et al., 2016). This phosphorylation is enacted by protein kinase C (PKC) superfamily kinases PKN1 and PKN2, which are themselves effectors of RhoA. Additionally, chaperone protein 14-3-3 binds pyrin when it is phosphorylated, its binding site being pyrin phosphorylation sites S242 and S208C.

To counter pyrin sensing of RhoA inhibition, *Yersinia pestis* has developed a mechanism of immune evasion specifically to prevent pyrin activation. One of its effectors, YopM, hijacks host kinases RSK and PKN1/2, effectors of RhoA, and induces pyrin phosphorylation. This preserves negative regulation of pyrin and allows *Y. pestis* to remain unnoticed by the host immune system, while *Y. pestis* mutant

strain lacking YopM is rapidly detected and eliminated. Curiously, pyrin carrying FMF-associated mutations is less susceptible to YopM inhibition and provides protection against *Y. pestis* infection (LaRock and Cookson, 2012; Park et al., 2020).

Another mechanism of negative regulation of pyrin was suggested by Yu and colleagues who demonstrated that pyrin exists in the cell in the form of a homotrimer, inhibited by the intra-molecular binding of the PYD domain and the B-box domain (J.-W. Yu et al., 2007). The masking of PYD prevents it from interacting with ASC to form the inflammasome complex. This negative control check point is alleviated when proline serine threonine phosphatase-interacting protein 1 (PSTPIP1) binds to pyrin B-box domain which liberates the PYD rendering it available for oligomerisation with ASC. Yet, the physiological role of PSTPIP1 remains unclear.

Pyrin itself is a substrate of caspase-1. The cleavage of pyrin by caspase-1 at the Asp330 residue yields a protein fragment of approximately 50 kDa. According to one study, this cleaved product is translocated to the cell nucleus where it activates the NF- κ B pathway (Chae et al., 2008).

Finally, the B30.2 domain of pyrin may be an auto-inhibitory domain. A significant proportion of FMF-causing mutations and all founder FMF mutations are located in exon 10 of the *MEFV* gene encoding the B30.2 domain of pyrin. These mutations are gain-of-function mutations and lead to pyrin being more easily activated or activated without apparent trigger.

4.3 Pyrin inflammasome activation

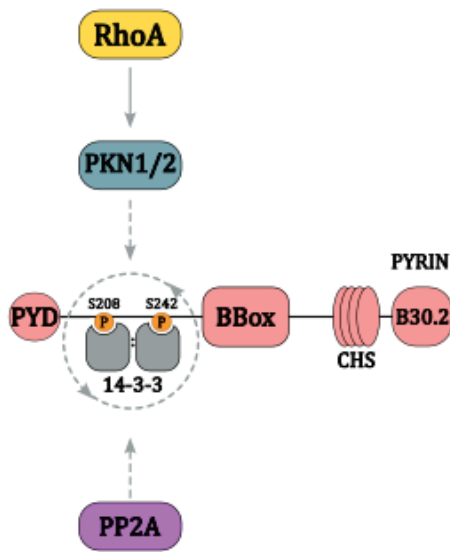
Pyrin dephosphorylation is required for the inflammasome activation. It has long been suspected that pyrin dephosphorylation is an active process. Recently phosphoprotein phosphatase 2A (PP2A) has been identified as the phosphatase implicated in pyrin regulation by the Bliska lab in collaboration with our team (Malik et al., 2022). It likely that the phosphorylation status of pyrin is dynamic.

When RhoA is inhibited, it no longer activates its effectors – PKN1/2 among them. The inhibition of PKN1/2 allows the dynamic equilibrium between phosphorylated and not phosphorylated pyrin to shift towards the dephosphorylated form of pyrin.

Dephosphorylation of pyrin is necessary for its activation but is not sufficient. There is additional regulation of pyrin likely exerted by microtubule dynamics of the cell. This is supported by the fact that microtubule polymerisation-inhibiting drugs prevent pyrin activation downstream of its dephosphorylation. Accordingly, one such drug, colchicine, is the main treatment for FMF (Gao et al., 2016; Goldfinger, 1972; Magnotti et al., 2019; Mansfield et al., 2001). Pyrin inflammasome activation is also dependent on dynein ATPase and dynein adapter HDAC6 (Magupalli et al., 2020). However, other regulatory mechanisms may also be in place (**Fig. 4.2**).

Interestingly, while wild-type pyrin remains inactive when dephosphorylated with a PKC superfamily inhibitor, pyrin carrying FMF-associated mutations activates caspase-1 when dephosphorylated. This indicates that whatever the nature of pyrin regulation other than its phosphorylation, it is abrogated by FMF-associated mutations (Magnotti et al., 2019). Since FMF-associated mutations cluster in the B30.2 domain of pyrin, it is likely that B30.2 is directly implicated in the negative regulation of pyrin.

Pyrin regulation at steady-state



Pyrin activation during infection

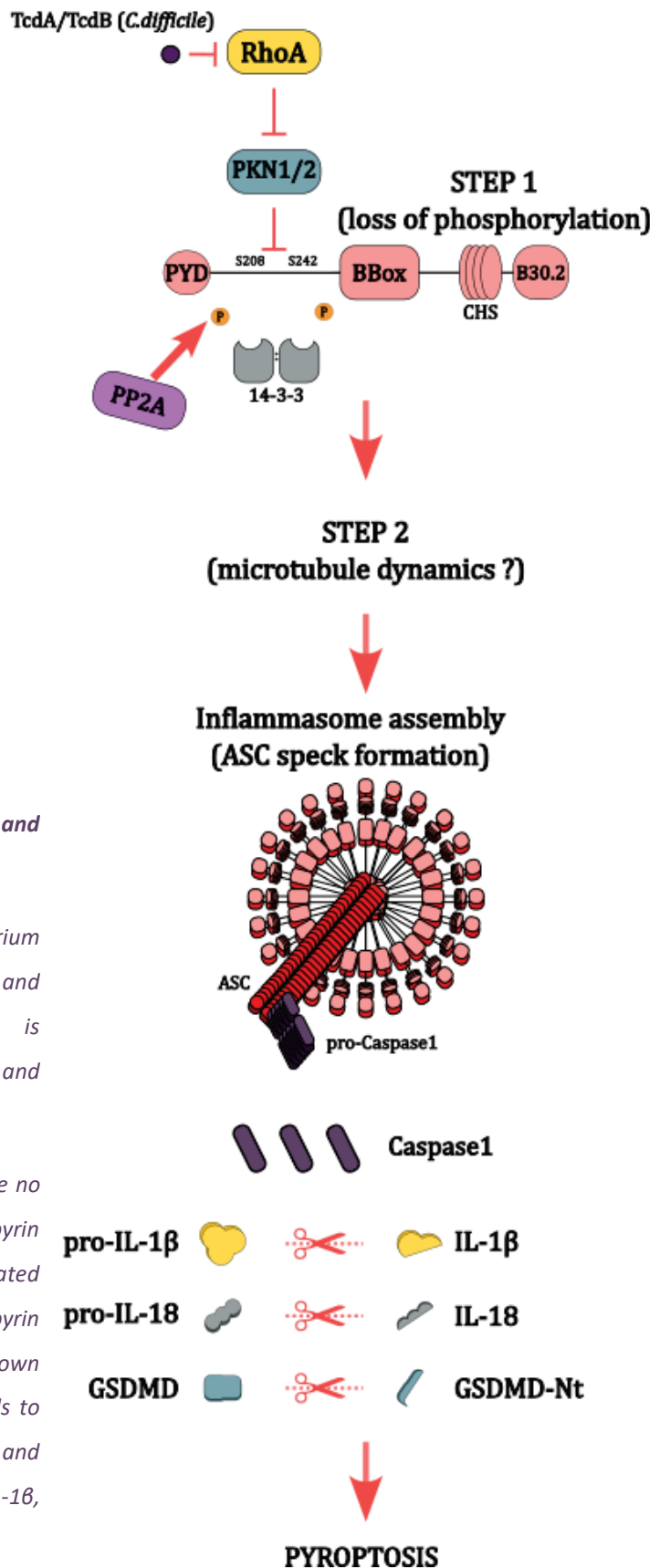


Figure 4.2 Pyrin inflammasome at steady state and pyrin inflammasome activation.

Left panel: at steady state a dynamic equilibrium between pyrin phosphorylation and dephosphorylation is established, as it is phosphorylated by RhoA effectors PKN1/2 and dephosphorylated by PP2A. Pyrin is inhibited.

Right panel: when RhoA is inhibited, PKN1/2 are no longer active. The dynamic equilibrium around pyrin phosphorylation shifts towards dephosphorylated pyrin. Another inhibitory checkpoint maintains pyrin inactivation until it is lifted through an unknown mechanism. Pyrin inflammasome activation leads to oligomerisation of ASC and proteolytic cleavage and activation of caspase-1, cleavage and release of IL-1 β , IL-18 and GSDMD-Nt. This results in pyroptosis.

5. Familial Mediterranean Fever

5.1 Familial Mediterranean Fever: the disease

Familial Mediterranean fever (FMF) is an ancient genetic disease - the pathogenic variants have likely emerged in the human genome more than 1800 years ago (Park et al., 2020). In 1997 missense mutations in the MEditerranean FeVer (*MEFV*) gene were identified as the origin of FMF by two independently working groups (The French FMF Consortium et al., 1997; The International FMF Consortium, 1997). FMF-causing mutations alter the *MEFV*-encoded protein - pyrin - function by lowering its activation threshold (Jamilloux et al., 2018).

Today, FMF is the most common monogenic autoinflammatory disease characterized by bouts of fever and peritonitis experienced by 90% of patients, but also pleuritis accompanied by myalgia and arthralgia (**Fig. 5.1**). Attacks typically last from 12 hours to 3 days and can occur as often as once a week or as rarely as several times a year. The severity of attacks, their frequency, and the quality of life of FMF patients vary depending on the disease-causing mutation (or several mutations), and in some cases on the origin of the patient. It is unclear whether the origin of the patient plays a role due to environmental and life-style factors or simply because different mutations are more prevalent in different populations (Ben-Chetrit and Touitou, 2009). The onset of FMF usually occurs in childhood or adolescence with up to 90% of FMF patients manifesting disease before they reach the age of 20 (Tufan and Lachmann, 2020).

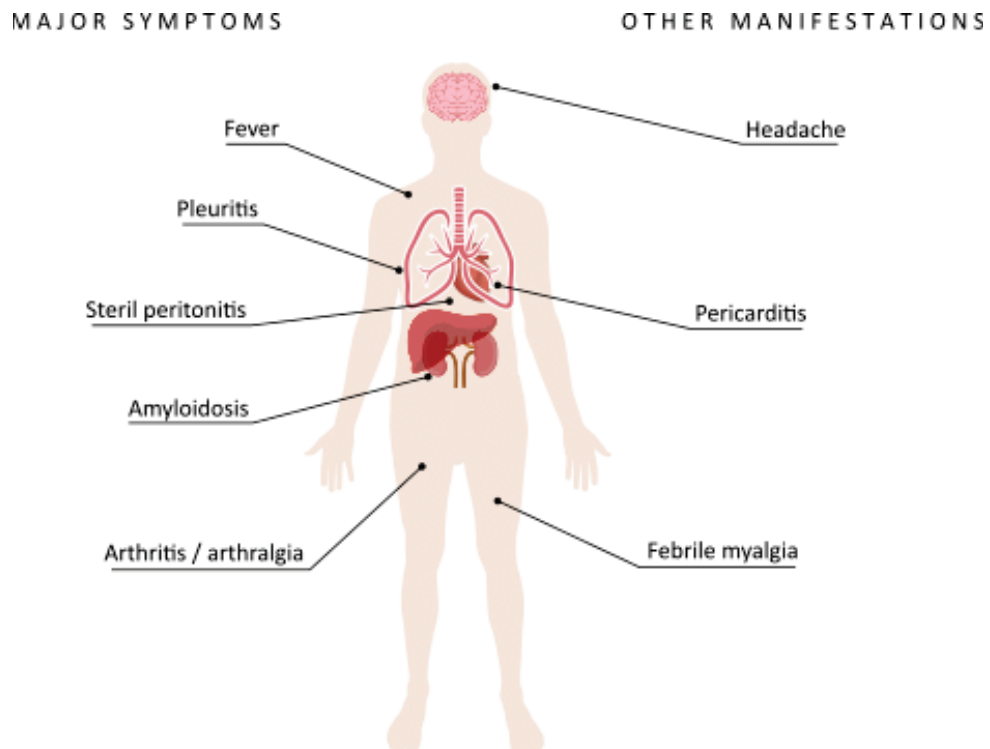


Figure 5.1 Most common clinical manifestations of Familial Mediterranean Fever.

FMF is particularly prevalent in the Mediterranean basin among the non-Ashkenazi Jews, Turks, Armenians and Moroccans, although FMF also occurs in people who are not of Mediterranean origin. The prevalence of FMF is highest in Turkey where it is estimated to be between 1:400 and 1:1000, followed by Armenia (1:500). The carrier rate of a pathogenic *MEFV* variant in these endemic areas can be as high as 1/5 (Ben-Chetrit and Touitou, 2009).

FMF is characterized by autosomal recessive inheritance with the 5 most common mutations being p.M694V, p.M694I, p.M680I, p.V726A located in exon 10 of the *MEFV* gene and p.E148Q located in exon 2. Dominant inheritance of FMF has also been recorded for certain variants such as p.P373L, p.H478Y or p.T557N and p.T557A, or in cases of founder mutations being inherited within complex alleles (Rowczenio et al., 2020). To date, 390 mutations have been identified within the *MEFV* gene in FMF patients and listed in the INFEVERS database. Most of these mutations are variants of unknown significance (VUS), some are characterized as likely benign, and some are (likely) pathogenic. A significant proportion of *MEFV* mutations linked to FMF are located in exons 2 and 10, which suggests that pyrin domains encoded by these exons play an important role in pyrin regulation (Fig. 5.2). It should be noted that not all *MEFV* exons are routinely sequenced in FMF patients, and in 10-20% of patients receiving a clinical diagnosis of FMF, no *MEFV* mutation is detected (Tufan and Lachmann, 2020).

5.2 FMF: diagnosis, treatment and prognosis

In countries where FMF is prevalent, the diagnosis is made on the basis of family history, clinical presentation and response to colchicine (the gold standard treatment for FMF). Genetic confirmation is warranted in cases of atypical presentation or in the absence of Mediterranean origin of the patient. The set of diagnostic criteria for FMF are known as the Tel Hashomer criteria (Table 5.1) and were established in 1997 by Livneh (Livneh et al., 1997).

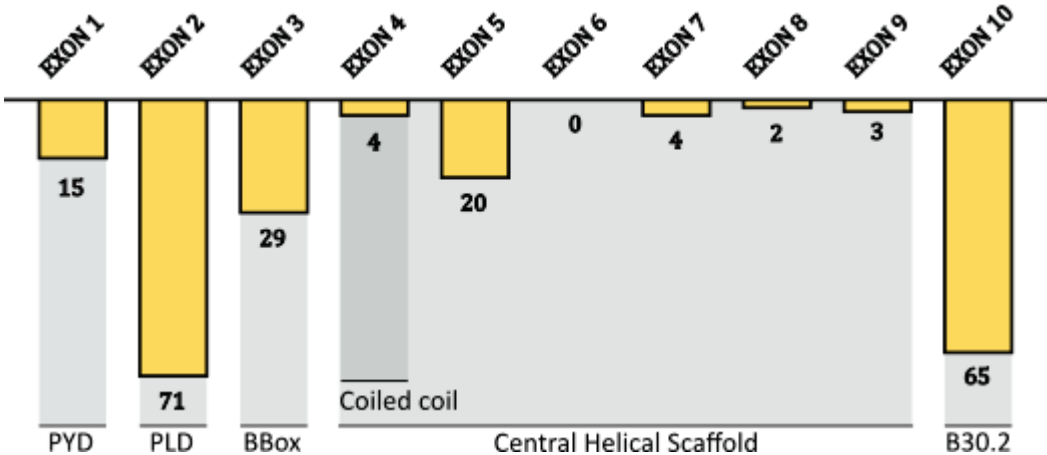


Figure 5.2 Distribution of mutations listed in the Infevers database within the coding region of the *MEFV* gene across exons.

Colchicine was introduced as the routine treatment for FMF in 1972 (Goldfinger, 1972). Colchicine acts by inhibiting microtubule polymerisation, and by inhibiting neutrophil recruitment overall resulting in an anti-inflammatory effect (Dinarelo et al., 1976). In the context of FMF, colchicine is prescribed as a lifetime treatment with daily administration. Colchicine helps manage FMF attacks and, importantly, it prevents the development of AA amyloidosis which is the most serious complication of FMF. Serum amyloid A (SAA) protein normally circulates in the blood in a soluble form but during inflammation its concentration is significantly higher than normal which leads to the formation of insoluble aggregates. AA amyloidosis results from the accumulation of SAA protein aggregates in the kidneys which can lead to the need for renal replacement therapy (dialysis or kidney transplantation) and eventually be fatal. Before the routine introduction of colchicine for FMF, up to 60% of FMF patients in Turkey suffered from amyloidosis (Pras et al., 1982). Today it is a much rarer complication occurring in patients with significantly delayed diagnosis. Side effects from daily colchicine include diarrhea, elevation in transaminases, leukopenia and neuromuscular toxicity. Almost 1/5 of patients are unable to maintain optimal doses of the drug (Tufan and Lachmann, 2020). Some alternative treatments exist for FMF patients who are colchicine-intolerant or -resistant: IL-1 antagonists, most often anakinra or canakinumab.

5.3 FMF: triggers of attacks

Criteria type	Attack
Major criteria	Typical attacks: <ol style="list-style-type: none"> 1. Generalised peritonitis 2. Unilateral pleuritis or pericarditis 3. Monoarthritic or hip, knee or ankle 4. Fever alone 5. Incomplete abdominal attack
Minor criteria	Incomplete attacks involving one or more of the following: <ol style="list-style-type: none"> 1. Pleuritis or pericarditis 2. Monoarthritic or hip, knee or ankle 3. Exertional leg pain 4. Favourable response to colchicine

A diagnosis of FMF is reached if the patient has ≥ 1 major criterion, or ≥ 2 minor criteria. A typical FMF attack is defined as ≥ 3 episodes lasting 12 -72 hours, each of the same type, with fever or 38°C or more. An attack may be considered “*incomplete*” if it differs from the definition of a typical attack in only one or two of the following features: a) temperature less than 38°C , b) attacks duration of 6 hours to 1 week, c) no signs of peritonitis during an abdominal attack, or signs are localised, d) atypical distribution of arthritis. Attacks not fulfilling these specific criteria are not counted towards a diagnosis of FMF. Adapted from **Livneh et al, 1997**.

Table 5.1. Tel Hashomer criteria as adapted from Livneh et al, 1997.

No definitive mechanism has been established to explain the onset of FMF attacks in patients although several studies have investigated the factors that may trigger the disease spells. The triggers most often reported include cold exposure, emotional or physical stress and tiredness. Muscular manifestations (myalgia) accompanying bouts of FMF are associated with physically enduring events such as long travel or long-term standing (Karadag et al., 2013). Physical trauma or infections are sometimes also associated with FMF attacks.

In women, a significant proportion of patients reports that their FMF attacks precede menstruation (33%-53%) and in some women these attacks are exclusively perimenstrual (7%) (Akar et al., 2006; Ben-Chetrit and Ben-Chetrit, 2001; Karadag et al., 2013; Kishida et al., 2020). Notably, women are able to differentiate dysmenorrhea from FMF attacks. The pregnancy experience in women with FMF is varied: some go through a complete symptomatic remission, some see no difference in terms of FMF and some experience more attacks or more severe attacks during pregnancy (Ben-Chetrit and Levy, 2003).

One possible explanation for the menstruation cycle-associated FMF attacks is the effect of oestrogen. Oestrogen can inhibit tubulin assembly using a site similar to that used by colchicine (Chaudoreille et al., 1991). Oestrogen level drops significantly preceding menstruation, possibly leading to a lesser inhibition of microtubule polymerisation and so less efficient control of FMF (Ben-Chetrit and Levy, 2003). That considered, men and women seem to be equally susceptible to FMF and require equal doses of colchicine for disease management. If oestrogen had a protective effect in the context of FMF, women would experience fewer or no FMF attacks after puberty or during the luteal phase of their menstrual cycle when oestrogen reaches its highest level. More studies are required to understand the link between menstrual cycle and FMF manifestations in women.

6. Other disorders that implicate the pyrin inflammasome

FMF might be the most common disease implicating pyrin inflammasome, but it is not the only one. Abnormal pyrin inflammasome activation underlies several other autoinflammatory disorders. Some of these diseases are caused by specific mutations of the *MEFV* gene, like PAAND, others are caused by mutations in other genes, but their pathogenesis is ultimately due to aberrant activation of the pyrin inflammasome. This section contains descriptions of several of such disorders.

6.1 PAAND

Like FMF, pyrin-associated autoinflammation with neutrophilic dermatosis (PAAND) is caused by gain-of-function mutations in the *MEFV* gene. PAAND pathology is due to spontaneous and excessive activation of the pyrin inflammasome. PAAND was first identified in 2016, to this day there is only a handful of known families suffering from PAAND (Masters et al., 2016; Van Nieuwenhove et al., 2021). The distinction between FMF and PAAND comes from several factors.

First, FMF is caused by *MEFV* mutations that mostly cluster within exon 10 (encoding the B30.2 domain of pyrin). PAAND, on the other hand, is caused by *MEFV* mutations within exon 2. On the molecular level, PAAND is caused by the decrease of phosphorylation of pyrin due to mutations that impact phosphorylation sites directly (p.S242R and p.S208C), or due to diminished interaction with the chaperone protein 14-3-3 in the case of the p.E244K mutation, which also leads to spontaneous activation of the pyrin inflammasome.

Until recently, PAAND was described as a dominantly inherited disorder. In 2020, a patient in Japan was diagnosed with PAAND, genetic analysis showed that they carried the p.S242R and p.E148Q mutations, while the patient's mother was an asymptomatic heterozygous carrier of the p.S242R mutation. In addition, PAAND is reported to be an autosomal recessive disease in the case of p.S242G and p.S208T mutations (Vahidnezhad et al., 2021; Van Nieuwenhove et al., 2021). These observations cast doubt over the dominant inheritance of PAAND and suggest that depending on the mutations, PAAND might be an autosomal recessive disease or an autosomal dominant disease with variable penetrance.

FMF and PAAND have somewhat different clinical presentation. While patients with both disorders present with attacks of fever, joint and muscle pain, PAAND attacks are longer (sometimes lasting several weeks), and they are not accompanied by pleuritis or peritonitis (Masters et al., 2016; Moghaddas et al., 2017). Amyloidosis is not typical for PAAND, although at least one such case has been described (Kiyota et al., 2020). Importantly, patients suffering from PAAND develop marked cutaneous manifestations such as sterile neutrophilic dermatosis, acne, and pyoderma gangrenosum.

Currently, there is no consensus on the best strategy for PAAND management, but anti-IL-1 β and anti-TNF treatments are used, colchicine in combination with low dose prednisolone has also been described to help manage PAAND symptoms (Moghaddas et al., 2017; Vahidnezhad et al., 2021; Van Nieuwenhove et al., 2021).

6.2 PAPA

Pyogenic sterile arthritis, pyoderma gangrenosum, and acne (PAPA) syndrome is a dominantly inherited autoinflammatory disease characterized by recurrent inflammatory episodes. Pathogenicity of PAPA syndrome is mediated by granulocytes with neutrophil rich effusions of the joints, cystic acne, and sterile abscesses (Lindor et al., 1997; Wise et al., 2002).

PAPA syndrome is caused by mutations in the proline-serine-threonine phosphatase interacting protein 1 (*PSTPIP1*) gene. *PSTPIP1* is involved in cytoskeletal organization. *PSTPIP1* has also been described to bind the B-Box domain of pyrin, thereby unmasking the PYD domain and inducing pyrin inflammasome activation. PAPA-causing *PSTPIP1* mutations - p.A230T, p.E250Q, and p.E250K – result in increased phosphorylation of *PSTPIP1* which promotes its binding to pyrin and more potent inflammasome activation (Demidowich et al., 2012; Lindwall et al., 2015; Shoham et al., 2003; J.-W. Yu et al., 2007). Therefore, PAPA syndrome is another auto-inflammatory disease mediated by excessive pyrin inflammasome activation, even if the disease-causing mutation does not impact pyrin itself.

PAPA pathology is mediated by high levels of pro-inflammatory cytokines. Although, there is no established standard treatment for this disease, studies describe anakinra targeting IL-1 and infliximab targeting TNF being effective in some patients. Otherwise, corticosteroid or cyclosporine alone or in combination with biological treatments are used to manage symptoms (Demidowich et al., 2012; Dierselhuis et al., 2005; Stichweh et al., 2005).

6.3 MKD

Mevalonate kinase-associated disease (MKD) is a monogenic recessive auto-inflammatory disorder characterized by attacks of fever and articular symptoms such as joint pain and joint swelling accompanied by an increase in pro-inflammatory cytokines, such as IL-1 β , in the serum. Additionally, patients experience abdominal pain, skin lesions and in cases of delayed diagnosis and poor management of symptoms, patients suffering from MKD may develop amyloidosis. MKD episodes last from 4 to 7 days and occur every 4 to 6 weeks, although disease manifestations may vary between patients. Today, MKD is perceived as a spectrum with milder presentations known as hyperimmunoglobulinemia D syndrome (HIDS) and more severe manifestations known as mevalonic aciduria (MA) (Akula et al., 2016; Normand et al., 2009).

The genetic cause of MKD are loss of function mutations of the *mevalonate kinase* gene (MVK). MVK is an enzyme involved in cell metabolism, namely, MVK phosphorylates mevalonic acid, which constitutes an early step in the biosynthesis of isoprenoids. This pathway provides the cell with some important metabolites such as isoprenyl groups and cholesterol (Drenth et al., 1999; Mandey et al., 2006).

The first step on the way to understanding the pathology of MKD was the finding that the increase in IL-1 β was driven by the shortage of geranylgeranyl pyrophosphate (GGpp) in the cell and not by the accumulation of mevalonic acid as was previously believed (Mandey et al., 2006). GGpp is the substrate of a particular post-translational modification known as geranylgeranylation that is required for the membrane targeting and the activity of certain proteins displaying a C-terminal CAAX motif. For instance, RhoA geranylgeranylation is required for its recruitment to the cell membrane which allows its GTPase activity.

Today, MKD is recognized as another disorder that impacts pyrin inflammasome pathway. MVK deficiency in MKD leads to defective geranylgeranylation of RhoA which impedes its recruitment to the cell membrane and, therefore, its activity. RhoA inhibition is then sensed by pyrin and induces inflammasome activation and release of pro-inflammatory cytokines (Park et al., 2016).

Interestingly, while colchicine is an effective treatment for FMF which is also mediated by excessive activation of the pyrin inflammasome, colchicine is ineffective for patients with MKD (Park et al., 2016). Instead, corticosteroids have been used for MKD with good efficacy, also anti-IL-1 β and anti-TNF help manage MKD symptoms with variable success depending on individual responses in patients. Of note, one paper suggests that the lack of protein prenylation in MKD patients monocytes promotes NLRP3 inflammasome rather than pyrin inflammasome activation (Skinner et al., 2019). This controversy remains to be solved but may also explain the poor efficacy of colchicine in these patients.

6.4 PFIT

Periodic fever, immunodeficiency, and thrombocytopenia (PFIT) is an autoinflammatory disease caused by mutations in the actin-interacting WD repeat-containing protein 1-encoding gene (*WDR1*). Patients with PFIT present with episodes of recurrent fever with high serum IL-18, accompanied by high susceptibility to infections and thrombocytopenia (Kile et al., 2007; Rodal et al., 1999; Standing et al., 2017).

In mice, complete deletion of the *WDR1* gene is lethal, but hypermorphic mutations lead to an autoinflammatory condition similar to PFIT. *WDR1* acts in complex with cofilin and together they play an important role in actin filament depolymerization. Mutations in *WDR1* severely impact neutrophil

function and development, and result in high serum IL-18 and significant infiltration of neutrophils in inflammatory lesions (Kile et al., 2007). Several studies describe WDR1 aggregation with pyrin, enhanced by *WDR1* mutations. It is hypothesized that this interaction causes increased activation of the pyrin inflammasome, as evidenced by caspase-1 cleavage and activation, and underlies PFIT pathology (Kim et al., 2015; Standing et al., 2017). Considering that pyrin interacts with actin filaments and that PFIT pathology is mediated by elevated serum IL-18, PFIT is a yet another auto-inflammatory disorder in the pyrin inflammasome pathway (Waite et al., 2009).

Like with other rare auto-inflammatory disorders mentioned before, there is no standard treatment for PFIT. Patients are treated with corticosteroids and anti-inflammatory biologicals with variable efficacy (Standing et al., 2017).

6.5 Aberrant CDC42 function and pyrin activation

Excessive activation of pyrin inflammasome has been implicated in a recently identified neonatal-onset autoinflammation caused by specific variants of cell division control protein 42 homolog (CDC42). Several variants of CDC42 – CDC42^{R186C}, CDC42^{C188Y}, and CDC42^{*192C*24} – lead to severe inflammation characterized by fever, skin rash and elevated inflammatory markers like high IL-18 and IL-1 β in serum (Lam et al., 2019).

The role of aberrant inflammasome activation in pathogenesis of this new syndrome was suspected namely because of high effectiveness of IL-1 β blocking drugs in symptoms management (Gernez et al., 2019). Examination of induced-pluripotent stem cell-derived myeloid cell line (iPS-MLs) established from patients with this syndrome revealed the mechanism behind the disease (Nishitani-Isa et al., 2022). First, iPS-ML derived from one of the patients produced higher levels of IL-18 and IL-1 β in response to TcdA, a physiological pyrin trigger, than to nigericin or flagellin, suggesting an hyperactivation of the pyrin inflammasome.

While the GTPase activity of CDC42^{R186C} is normal, its subcellular localization is altered compared to the WT CDC42: the disease-causing variants of CDC42 are retained in the Golgi apparatus. In fact, retention in the Golgi apparatus is the common feature among the disease-causing variants of CDC42. The anchoring of CDC42 at the Golgi is the result of abnormal CDC42 palmitoylation (Bekhouche et al., 2020). It appears that this irregularity is sensed specifically by the pyrin inflammasome, although the molecular mechanism of the sensing is unclear.

7. Steroids and immunity

Apparently spontaneous pyrin inflammasome activation lies behind FMF attacks in patients. This activation is likely the result of a combination of factors, but the specific triggers of disease spells remain a subject of interest for clinicians and researchers alike. Between a third and a half of women diagnosed with FMF experience peri-menstrual attacks of FMF. This along with results obtained by our group that are presented further in this manuscript leads us to suspect that steroid sex hormones may play a role in pyrin inflammasome regulation and activation.

7.1 Steroid hormones

Steroid hormones are produced from cholesterol in a process of biosynthesis known as steroidogenesis (**Fig. 7.1**). Steroidogenesis can occur within specific organs such as adrenal glands, gonads or the placenta. This is known as glandular steroidogenesis. Additionally, local steroidogenesis (or extra-glandular steroidogenesis) can take place at various sites like the brain, the skin, or the mucosa (**Fig. 7.2**) (Chakraborty et al., 2021).

The two limiting steps of steroidogenesis are the transport of cholesterol into the mitochondria, and conversion of cholesterol into pregnenolone. Pregnenolone is then converted into other steroids either in the mitochondria or in the endoplasmic reticulum (ER). The end-product of steroidogenesis depends on the enzymes expressed and present at the site of steroidogenesis.

Steroid hormones can be divided into five groups: glucocorticoids, mineralocorticoids, androgens, oestrogens and progestogens. The last three are also known as sex hormones or gonadocorticoids. Steroid hormones fulfil a large spectrum of functions in the human body ranging from regulation of metabolism, development of sexual characteristics, salt and water balance in the body, and regulation

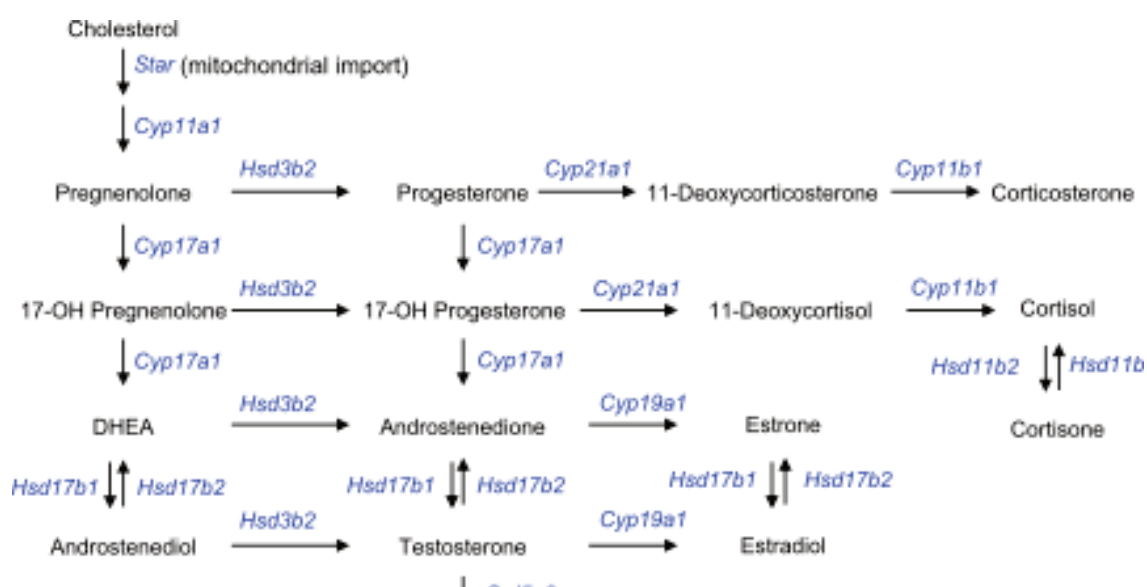


Figure 7.1 Overview of the steroid biosynthesis pathway (adapted from Chakraborty et al, 2021).

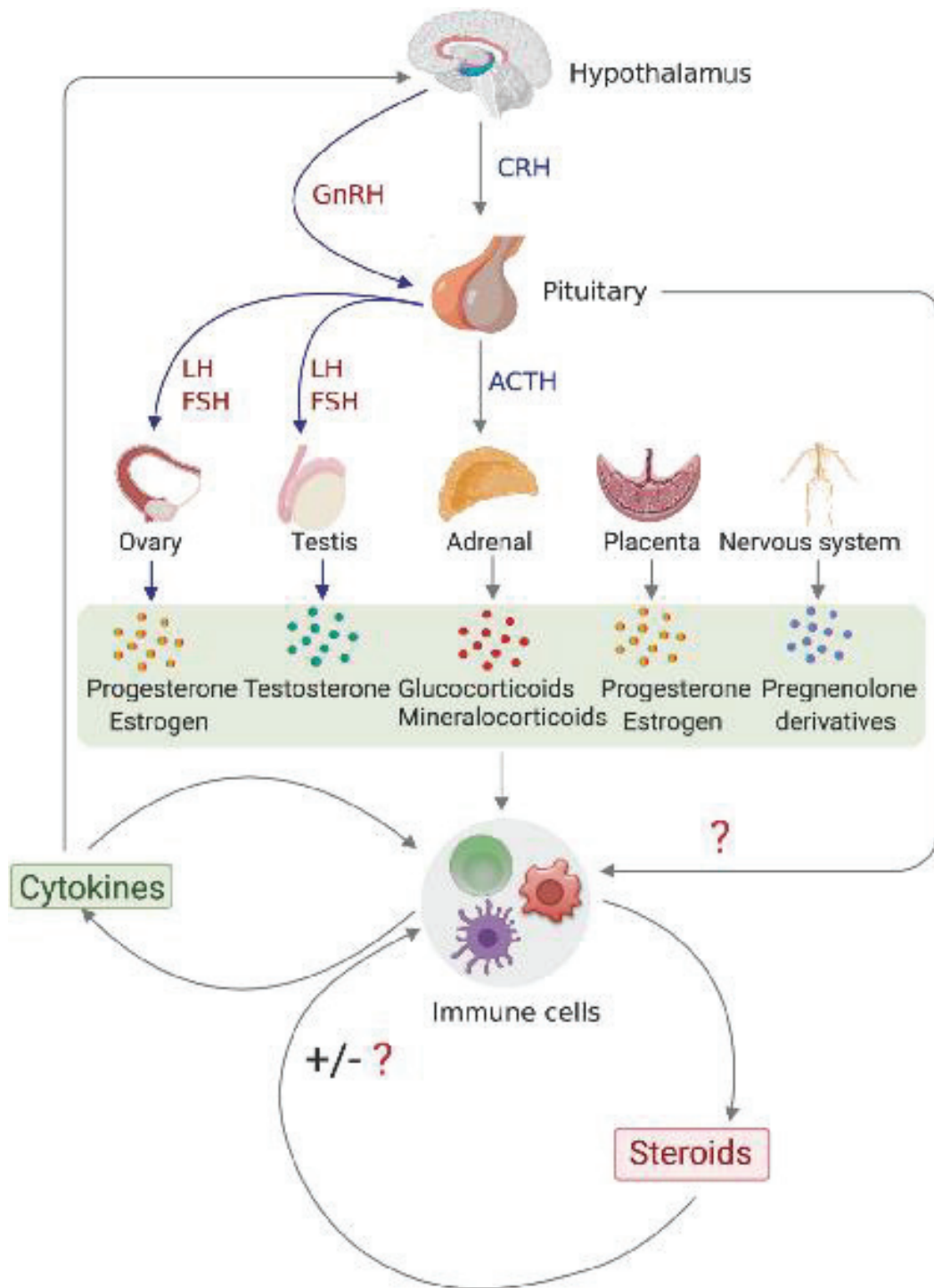


Figure 7.2 Crosstalk between steroid endocrine system and immune system. Glandular steroidogenesis is controlled by the hypothalamus-pituitary-adrenal/gonad/placenta axes. Secreted steroid hormones regulate immune-cell function. Immune cells themselves can also produce steroid hormones (adapted from Chakraborty et al, 2021).

of the immune function and the immune response (Chakraborty et al., 2021; Frye, 2009; Funder et al., 1997).

Steroid hormones trigger transcriptional modifications in target cells by binding to steroid hormone receptors (SHR). SHRs are ligand-activated transcriptional factors expressed in most tissues, which reside either in the cell cytoplasm or the nucleus. Once an SHR binds its ligand, it becomes activated and migrates to the nucleus where it can bind DNA and recruit more coactivators able to remodel chromatin and modulate expression of specific genes (Boonyaratanakornkit and Edwards, 2007; Cato et al., 2002). Transport of the SHR to the nucleus can take 30-60 minutes, therefore genomic action of steroid hormones takes time.

Alternatively, steroid hormones can also produce rapid non-genomic effects. In this case the effect produced by the steroid can be observed within seconds or minutes following steroid treatment and it not affected by RNA inhibition or inhibition of protein synthesis. Non-genomic action of steroids can be mediated by SHRs, but steroids have also been described to transiently interact with membrane associated proteins, protein kinases and membrane ion channels. Among the non-genomic actions of steroids are activation of MAPK pathway, activation of G proteins or adenylyl cyclase, and modulation of intracellular Ca^{2+} (Foradori et al., 2008; Guo et al., 2002).

The effects of steroids on the immune functions are discussed in this chapter.

7.2 Pro-inflammatory properties of steroids

Pro-inflammatory properties of steroid hormones and their derivatives have been known for decades. In 1960 the pyrogenic effects of etiocholanolone (3 α -hydroxyetiocholane-17-one) were first described (Kappas et al., 1960, 1957). Etiocholanolone is a product of testosterone catabolism. Etiocholanolone was the first substance of known chemical structure and physiologic origin to have a consistent pyrogenic effect in humans. Shortly afterwards the same group of researchers have identified pregnanolone (3 α -hydroxy-5 β -pregnan-20-one) as an even more potent pyrogen. Researchers have observed that intra-muscular or intra-venous injection of certain steroid hormone derivatives provoked a rise of body temperature by up to 2°C, while other steroid hormone derivatives caused no such reaction. Of note, the subjects of this study were a small group of adult men and women. The phenomenon was termed “steroid fever” (**Fig. 7.3**) (Bodel and Dillard, 1968; Kappas et al., 1961). The precise mechanism of the pyrogenic effect of steroids is unclear to this day although recent findings published by our group strongly suggest that it involves pyrin inflammasome (Magnotti et al, 2022).

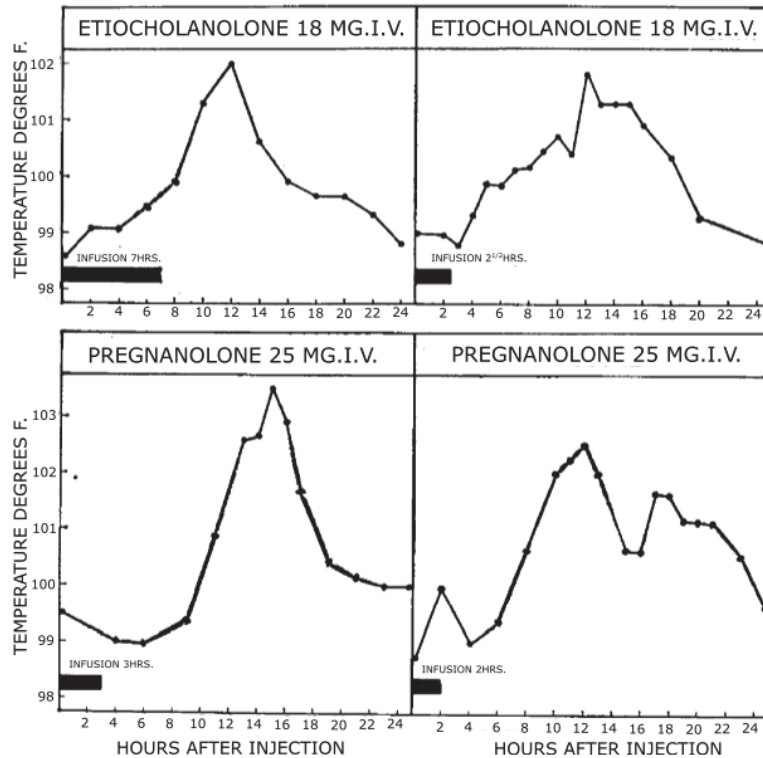


Figure 7.3 Monitoring of rectal temperature following intra-venous administration of etiocholanolone or pregnanolone in human volunteers (adapted from Kappas et al, 1960)

Interestingly, the fever-producing properties of steroid hormone derivatives are species-specific. One study compared the pyrogenic potency of etiocholanolone in New and Old World monkeys. After the injection of etiocholanolone Rhesus monkeys (Old World monkeys) exhibited a rise of roughly 2°C in their rectal temperature. In contrast, Squirrel monkeys (New World monkeys) exhibited no rise in rectal temperature over the 24-hours after injection (Steinetz et al., 1998). Also, no pyrogenic effect of etiocholanolone was observed in rabbits, mice and rats (Bodel and Dillard, 1968; Kappas et al., 1957; Kappas and Ratkovits, 1960; Palmer et al., 1961).

Cyclic fluctuations of several sex hormones in women provide a platform for observation of their effects on other systems within the human body. The rise in basal body temperature during the luteal phase of the menstrual cycle is associated with a rise of progesterone (**Fig. 7.4**) (Baker et al., 2020). This phenomenon is reliable enough that it is routinely used by medical practitioners and women in the private setting to track ovulatory and menstrual cycles. It is of note, that in animals with anovulatory cycles without a periodic rise of progesterone, no rise of basal temperature is observed, although the opposite is not always true (Baker et al., 2020; Chen and Penning, 2014; Dinarello et al., 1976).

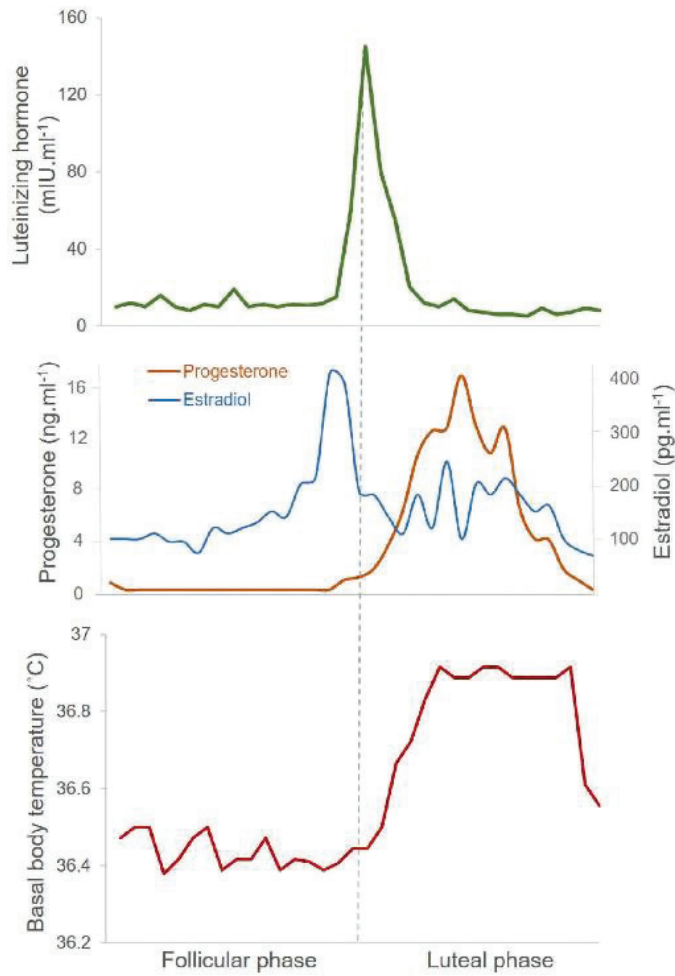


Figure 7.4 Reproductive hormone and basal body temperature changes during an ovulatory menstrual cycle. Data from 10 women with ovulatory menstrual cycles (adapted from Baker et al, 2020).

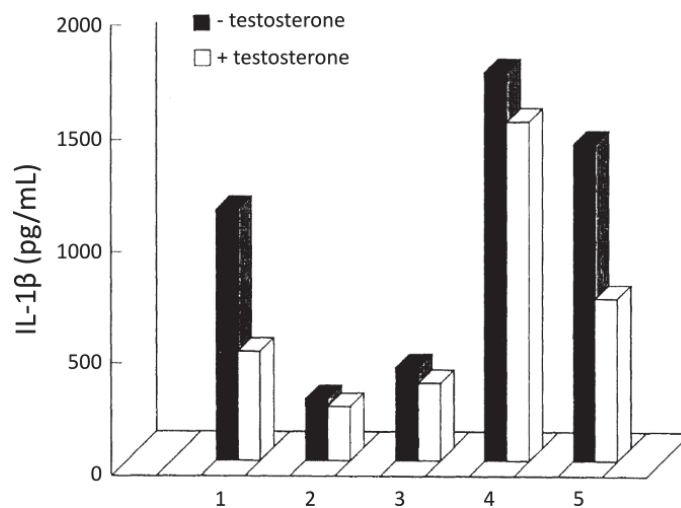


Figure 7.5 Testosterone influence on IL-1 β secretion by synovial human macrophages from 5 RA patients (adapted from Cutolo et al, 1995).

Spontaneous term labour is known as a state of sterile inflammation, characterized by an increase in pro-inflammatory cytokines and a recruitment of immune cells into the cervix and myometrium. This process is thought to be at least partially mediated by inflammasomes, as evidenced by the presence of caspase-1 and IL-1 β in the amniotic fluid in women who experience spontaneous labour at term (Romero et al., 2018). The importance of IL-1 β in labour is also confirmed in mice, although caspase-1 or IL-1 β knock-out mice show no anomaly around labour (Romero et al., 1991). Keeping in mind that a drop in progesterone and a surge in steroid hormone metabolites is a metabolic feature predictive of spontaneous labour, it is tempting to speculate that there could be a link between the two events (Stelzer et al., 2021).

7.3 Anti-inflammatory properties of steroids

Anti-inflammatory properties of glucocorticoids are well-known. Cortisone and prednisolone are glucocorticoids widely used as immunosuppressants for the management of asthma and rheumatoid arthritis, for treatment of allergic reactions, and as mentioned in a previous chapter, for topic inflammatory manifestations such as eczema or pyoderma gangrenosum (Shimba et al., 2021). Glucocorticoid treatment appears to impair the phagocytic activity of macrophages by inhibiting expression of phagocytosis-related genes and renders subjects more susceptible to intracellular bacterial infections such as those with *Mycobacterium tuberculosis* or *Salmonella typhimurium* (Xie et al., 2021). Other mechanisms of glucocorticoid-induced immune suppression could involve inhibition of the NF- κ B pathway, or interference with the MAPK pathway (Ayroldi et al., 2012; Coutinho and Chapman, 2011; Johansson-Haque et al., 2008).

There is also evidence suggesting that sex steroid hormones could have anti-inflammatory properties. Since the 1930's there is recorded evidence that pregnancy, associated with a high level of progesterone in the serum, provides an alleviation of rheumatoid arthritis (RA) symptoms (Cutolo and Straub, 2020). People with a genetic predisposition to produce more androgens, are less susceptible to RA highlighting immunosuppressive properties of androgens (Kim and Kim, 2020; Stark et al., 2015).

On a cellular level, increasing concentrations of progesterone and oestradiol lead to a decrease in IL-1 β secretion by LPS-stimulated macrophages (Polan et al., 1989). In a study of macrophages extracted from the synovial fluid of people suffering from RA, testosterone reduced IL-1 β production by almost a third in all five studied patient samples regardless of their sex (**Fig. 7.5**) (Cutolo et al., 1995).

The effect of steroids on the immune system appears to be dependent on the context, the organ, or the cell type in question. Given that IL-1 β secretion is often modulated (whether up or down) in response to steroid treatment, it is likely that there is a functional link between steroids and the

inflammasomes in humans. It remains to be elucidated whether inflammasomes are involved in steroid sensing or how steroids regulate the inflammasome activation.

RESULTS

Results. Part 1

Context

The first part of the Results section consists of a scientific article accepted for publication in Cell Reports (article in press). A version of it is available on BioRxiv.

Our objective was to better understand the nature of the second step of pyrin regulation. We performed a chemical screen on U937 monocytes with a constitutively activated first step (constitutive dephosphorylation) that revealed novel activators of the pyrin inflammasome. Steroid hormone derivatives – etiocholanolone and pregnanolone – activated pyrin inflammasome in a B30.2-dependent manner and without inhibition of RhoA. Thus, we identified a novel non-canonical mechanism of pyrin activation.

Steroid hormone catabolites activate the pyrin inflammasome through a non-canonical mechanism.

Flora Magnotti¹, Daria Chirita^{1,*}, Sarah Dalmon^{1,*}, Amandine Martin¹, Pauline Bronnec¹, Jeremy Sousa¹, Olivier Helynck², Wonyong Lee³, Daniel L. Kastner³, Jae Jin Chae³, Michael F. McDermott⁴, Alexandre Belot^{1,5,6}, Michel Popoff⁷, Pascal Sève⁸, Sophie Georgin-Lavialle⁹, Hélène Munier-Lehmann², Tu Anh Tran¹⁰, Ellen De Langhe^{11,12,13}, Carine Wouters^{14, 15, 16}, Yvan Jamilloux^{1,6,8, @}, Thomas Henry^{1,@, 17}

¹ CIRI, Centre International de Recherche en Infectiologie, Univ Lyon, Inserm U1111, Université Claude Bernard Lyon 1, CNRS, UMR5308, ENS de Lyon, Univ Lyon, F-69007, LYON, France

² Institut Pasteur, Université de Paris Cité, CNRS UMR3523, Chemistry and Biocatalysis Unit, 75724, Paris Cedex 15, France

³ Inflammatory Disease Section, Metabolic, Cardiovascular and Inflammatory Disease Genomics Branch, National Human Genome Research Institute, Bethesda, MD, USA

⁴ Leeds Institute of Rheumatic and Musculoskeletal Medicine, St James's University Hospital, Leeds, UK

⁵ Department of Pediatric Nephrology, Rheumatology, Dermatology, Reference centre for Rheumatic, AutoImmune and Systemic diseases in children (RAISE), Hôpital Femme Mère Enfant, CHU Lyon, Lyon, France

⁶ LIFE, Lyon Immunopathology Federation, Lyon, France

⁷ Bacterial Toxins, Institut Pasteur, Paris, France.

⁸ Department of Internal Medicine, University Hospital Croix-Rousse, Lyon 1 University, Lyon, France

⁹ Sorbonne University, department of internal medicine, Tenon hospital, DMU 3ID, AP-HP, National reference center for autoinflammatory diseases and inflammatory Amyloidosis (CEREMAIA), INSERM U938, Paris, France

¹⁰ Department of Pediatrics, Carémeau Hospital, CHU Nîmes, Nîmes, France

¹¹ Division of Rheumatology, University Hospitals Leuven, Leuven, Belgium

¹² Laboratory of Tissue Homeostasis and Disease, Department of Development and Regeneration, KU Leuven, Leuven, Belgium

¹³ ERN RITA

¹⁴ KU Leuven - University of Leuven, Department of Microbiology and Immunology, Laboratory of Adaptive Immunology & Immunobiology, Leuven, Belgium

¹⁵ University Hospitals Leuven, Department of Pediatrics, B-3000 Leuven, Belgium

¹⁶ Member of the European Reference Network for Rare Immunodeficiency, Autoinflammatory and Autoimmune Diseases -Project ID No 739543

* These authors contributed equally

¹⁷ Lead contact: Thomas HENRY

@ Senior author; to whom correspondence should be addressed: yvan.jamilloux@inserm.fr or thomas.henry@inserm.fr (+33 (0)4-37-28-23-72)

Abstract

The pyrin inflammasome acts as a guard of RhoA GTPases and is central to immune defences against RhoA-manipulating pathogens. Pyrin activation proceeds in two steps. Yet, the second step is still poorly understood. Using cells constitutively activated for the pyrin step 1, a chemical screen identifies etiocholanolone and pregnanolone, two catabolites of testosterone and progesterone, acting at low concentrations as specific step-2 activators. High concentrations of these metabolites fully and rapidly activate pyrin, in a human-specific, B30.2 domain-dependent manner and without inhibiting RhoA. Mutations in *MEFV*, encoding pyrin, cause two distinct autoinflammatory diseases (PAAND and FMF). Monocytes from PAAND patients, and to a lower extent from FMF patients, display increased responses to these metabolites. This study identifies an unconventional pyrin activation mechanism, indicates that endogenous steroid catabolites can drive autoinflammation, through the pyrin inflammasome, and explains the "steroid fever" described in the late 1950s, upon steroid injection in humans.

Introduction

Inflammasomes are innate immune complexes that contribute to antimicrobial responses (Broz and Monack, 2011) but can also be deleterious in various chronic autoinflammatory conditions (Peckham et al., 2017). Inflammasome activation results in activation of the inflammatory caspase-1, cleavage of the pore forming protein GasderminD (GSDMD) that triggers a fast cell death, termed pyroptosis, and release of the inflammatory cytokines IL-1 β and IL-18. Inflammasome sensors can act as direct pathogen-associated molecular pattern (PAMPs) receptors but have also evolved more general sensing mechanisms allowing them to be activated in response to damage-associated molecular patterns (DAMPs) or to homeostasis-altering molecular processes (HAMPs) (Liston and Masters, 2017). Furthermore, the NLRP3 inflammasome is regulated by several metabolites (Hughes and O'Neill, 2018). Whether metabolites regulate other inflammasome sensors is currently unknown.

Pyrin is an inflammasome sensor acting as a guard of Rho GTPases activity (Xu et al., 2014). Bacterial toxins (e.g. *Clostridioides difficile* toxins A and B (TcdA/B)) or bacterial effectors (e.g. *Yersinia* YopE/T (Chung et al., 2016; Ratner et al., 2016)) inhibit RhoA and trigger pyrin inflammasome activation. Similarly, by disrupting RhoA prenylation, mevalonate kinase deficiency activates pyrin (Akula et al., 2016). RhoA inhibition lifts the dynamic blockage of pyrin. Indeed, at steady state, pyrin is phosphorylated by PKN1/2 on two serine residues (S208 and S242), allowing a phospho-dependent chaperone from the 14-3-3 family to sequester pyrin away from downstream inflammasome molecules. PKN1/2, two kinases from the PKC superfamily, are RhoA effectors that are active in cells with homeostatic levels of RhoA activation. Inhibition of RhoA leads to loss of PKN1/2 activity, dephosphorylation of pyrin and ultimately triggers activation of the pyrin inflammasome (Akula et al., 2016; Gao et al., 2016; Masters et al., 2016; Xu et al., 2014). Yet, pyrin dephosphorylation is not sufficient to trigger the full pyrin inflammasome activation (Magnotti et al., 2019). We have therefore proposed a two-step model for pyrin activation (Fig. 1A). The first step corresponds to pyrin dephosphorylation, while the second step, which remains poorly understood, corresponds to the formation of ASC oligomers and caspase-1 activation. Interestingly, this model is consistent with the observation that colchicine and, other microtubule-depolymerising drugs, block pyrin activation downstream of its dephosphorylation (Gao et al., 2016; Van Gorp et al., 2016).

The two-step model is also supported by the two distinct autoinflammatory diseases associated with mutations in *MEFV*, the gene encoding pyrin (Jamilloux et al., 2018). Indeed, mutations in *MEFV* exon 10, coding the B30.2 domain of pyrin, cause Familial Mediterranean Fever (FMF) and are associated with a constitutively activated step 2 (Magnotti et al., 2019). In contrast, mutations affecting the serine

residues, which are dephosphorylated during step 1 (Hong et al., 2019; Masters et al., 2016), or the neighbouring residues required for the interaction with 14-3-3 proteins (Moghaddas et al., 2017) cause Pyrin-Associated Autoinflammation with Neutrophilic Dermatitis (PAAND).

Despite its importance in health and disease, the mechanism responsible for step 2 is still largely unclear and this study aimed at increasing our knowledge on this specific regulatory mechanism.

Results

A chemical screen identified sex hormone catabolites as pyrin step 2 activators.

To identify molecules that trigger step 2 of the pyrin inflammasome cascade, we used a human monocytic cell line (U937) expressing the PAAND *MEFV* variant (i.e. p.S242R) under the control of a doxycycline-inducible promoter (Magnotti et al., 2019) (Fig. 1B). In these cells, the p.S242R mutation mimics pyrin dephosphorylation resulting in a pyrin protein constitutively activated for step 1. Cells expressing (in the presence of doxycycline) p.S242R *MEFV* were treated with compounds (n=1,199) from the Prestwick® "FDA-approved" Chemical Library (see Methods section and Table S2 for details). At 90 minutes post-addition, cell death was measured by quantifying propidium iodide incorporation. A counter-screen was performed simultaneously in the same conditions but in the absence of doxycycline, (i.e. in the absence of pyrin expression) to retain compounds triggering pyrin-specific cell death. One compound, etiocholanolone (6.9 μ M) was identified as triggering a fast cell death in a doxycycline-dependent manner (Fig. 1C). Etiocholanolone, also termed 3 α -hydroxy 5 β -androstan-17-one, is an endogenous catabolite of the steroid hormone, testosterone (Fig. 1D). Except for medrysone, which was weakly active, none of the other steroids in the Prestwick library triggered pyrin-specific cell death.

The ability of etiocholanolone to trigger cell death in a p.S242R-*MEFV*-dependent manner was validated in an independent set of experiments and demonstrated to be dose-dependent (Fig. 2A). To assess the specificity of etiocholanolone and perform structure-activity relationship studies, a number of hormones and catabolites were then tested. Interestingly, pregnanolone (3 α -hydroxy-5 β -pregnan-20-one), a catabolite of progesterone, triggered p.S242R-*MEFV*-dependent cell death at an even lower concentration than etiocholanolone (Fig. 2A). In contrast, neither testosterone nor progesterone triggered cell death, even at high concentrations (half maximal effective concentration EC₅₀>1000 μ M) and despite similar lipophilic properties as etiocholanolone and pregnanolone (supplemental Fig. S1). Furthermore, both cortisol and its catabolite, tetrahydro-cortisol, were inactive (Fig. 2B), demonstrating the specificity of the pregnanolone and etiocholanolone in triggering this response.

Etiocholanolone and pregnanolone share the same stereochemistry on carbon 3 (3 α) and 5 (5 β) of the sterol. To evaluate the stereospecificity of the response, the two stereoisomers of etiocholanolone were tested for their ability to trigger p.S242R-*MEFV*-dependent cell death. 3 β -hydroxy-5 β -androstano-17-one (3 β 5 β) and androsterone, (i.e. 3 α -hydroxy 5 α -androstano-17-one, (3 α 5 α)), displayed EC50 greater than 1000 μ M (Fig. 2C and supplemental Fig. S1), indicating that the response is stereospecific.

Furthermore, experiments with pregnanolone derivatives demonstrated that sulfation, a modification associated with steroid inactivation and excretion (Schiffer et al., 2019) leads to a complete loss of activity (Fig. 2D). All the modifications tested on the sterol ring or the terminal carbon or ketone (supplemental Fig. S1) decreased the pyrin-specific cytotoxicity. In particular, hydroxylation on C17 fully abolished the cell death, thereby explaining the absence of activity of the cortisol catabolite (Fig. 2D, E). Overall, these structure-function analyses demonstrated that etiocholanolone and pregnanolone are highly specific compounds that trigger S242R-pyrin-mediated cell death.

To validate this result in primary human monocytes, we used the PKC superfamily inhibitor, UCN-01, which inhibits PKN1/2 and dephosphorylates pyrin, thus recapitulating the effect of the p.S242R mutation. As previously described (Magnotti et al., 2020, 2019), UCN-01 alone does not trigger pyroptosis in primary human monocytes from healthy donors. Similarly, neither etiocholanolone (12 μ M) nor pregnanolone (6 μ M) alone were cytotoxic, even after long incubation times (Supplemental Fig. S2A). Yet, the combination of UCN-01 and either of these two steroid catabolites triggered a very fast cell death (Fig. 2F, G) and IL-1 β release (Fig. 2H). These results thus strongly suggest that, in primary monocytes, steroid catabolites activate pyrin step 2 and trigger activation of the pyrin inflammasome and pyroptosis, in the presence of the step 1 activator, UCN-01.

High concentrations of steroid catabolites trigger full activation of the pyrin inflammasome in the absence of a step 1 activator.

Interestingly, while at low concentration (<12 μ M) steroid catabolites required activation of step 1, through either genetic (p.S242R) or chemical (UCN-01) means, we noticed that, at high concentrations, both etiocholanolone (Fig. 3A) and pregnanolone (Fig. 3B) triggered death of U937 cells expressing WT *MEFV*. High doses of pregnanolone (50 μ M) or etiocholanolone (100 μ M) triggered pyrin dephosphorylation to a similar extent as TcdA or UCN-01 while low doses of steroid catabolites did not (Fig. 3C). Calyculin A, a phosphatase inhibitor, was recently shown to inhibit pyrin inflammasome in response to bacterial toxins and infections (Malik et al., 2022a). Similarly, Calyculin A blocked etiocholanolone and pregnanolone-mediated cell death and IL-1 β release in healthy donor monocytes and U937 cells expressing pyrin (Supplemental Fig. S2B-D). In addition, high doses of steroid catabolites triggered ASC oligomerization as revealed by cross-linking experiments and Western blot analysis (Fig.

3D). Low doses of etiocholanolone or pregnanolone did not unless combined with UCN-01. These results suggested that, at high doses, these molecules can trigger both step 1 (i.e. pyrin dephosphorylation) and step 2 to promote ASC oligomerization and inflammasome activation. Accordingly, primary human monocytes exposed to high doses of steroid catabolites (50-100 μ M) underwent a fast cell death (Fig. 3E, F) and released IL-1 β (Fig. 3G). LPS priming was not required for etiocholanolone or pregnanolone-induced monocyte death (Fig. 3E-F) but was used to induce proIL-1 β expression whenever inflammasome activation was monitored by quantifying IL-1 β release by ELISA. Primary neutrophils, treated with steroid catabolites, also underwent a rapid cell death (supplemental Fig. S3A). In contrast, steroid catabolites did not demonstrate substantial cytotoxicity towards lymphocytes (supplemental Fig. S3B) in agreement with the lack of *MEFV* expression in these cells (supplemental Fig. S3C). Etiocholanolone or pregnanolone addition triggered processing and release of caspase-1, IL-1 β and GSDMD (Fig. 3H). In agreement with the greater potency of pregnanolone compared to etiocholanolone to trigger IL-1 β release (Fig. 3G), pregnanolone treatment led to higher caspase-1 and GSDMD cleavage than etiocholanolone treatment did. Furthermore, pre-treatment with the caspase-1 inhibitor, VX765, fully abolished IL-1 β release by primary human monocytes (supplemental Fig. S3D). Finally, Casp1^{KO} and GSDMD^{KO} U937 expressing WT pyrin were fully resistant to steroid catabolites-mediated cell death (Fig. 3I) and did not release substantial amounts of IL-1 β (Fig. 3J). Altogether, these experiments demonstrated that steroid catabolites specifically triggered pyrin dephosphorylation, ASC oligomerization, inflammasome activation, caspase-1-dependent, GSDMD-dependent pyroptosis and IL-1 β release. This response was independent of NLRP3 (supplemental Fig. S3E).

Steroid catabolites differ from the prototypical activator TcdA and trigger pyrin activation in a B30.2-dependent manner and in the absence of RhoA inhibition.

Activation of the pyrin inflammasome in response to RhoA-inhibiting toxins depends on microtubule network integrity and is inhibited by microtubule-depolymerising drugs (e.g. colchicine or nocodazole) (Gao et al., 2016; Van Gorp et al., 2016). Similarly, colchicine and nocodazole inhibited pyroptosis induced by steroid catabolites in primary human monocytes (Fig. 4A, B). Colchicine also reduced IL-1 β release in response to etiocholanolone and pregnanolone (Fig. 4C) while it had no detectable action on NLRP3-dependent pyroptosis. Interestingly, the observed inhibition was only partial in most donors (Fig. 4B, 4C) and was lost at higher doses of pregnanolone (supplemental Fig. S4A). These results suggest that these high steroid catabolite concentrations can overcome the microtubule integrity requirement to activate the pyrin inflammasome in monocytes.

Current knowledge places the activation of the pyrin inflammasome downstream of RhoA GTPases inhibition (Akula et al., 2016; Xu et al., 2014). Yet, we observed no decrease in RhoA activity after etiocholanolone, a result that contrasted with the robust RhoA inhibition observed upon TcdA treatment (Fig. 4D, supplemental Fig. S4B). This observation suggests that steroid catabolites activate pyrin by a mechanism distinct from the one triggered by TcdA. Accordingly, low doses of steroid catabolites synergized with suboptimal doses of TcdA to promote cell death (Fig. S4C-D) and IL-18 release (Fig. S4E).

We then investigated the pyrin domains required for steroid catabolite-mediated pyroptosis and IL-1 β release. Pyrin proteins lacking either the pyrin (PYD) domain, the exon 2-encoded phosphorylated linker (PLD), the B-box (BBox), the coiled-coil (CC) or the B30.2 domains were stably expressed in U937 cells (Supplemental Fig. S4F). The resulting cell lines were treated with pregnanolone, etiocholanolone or TcdA. While the B30.2 domain was dispensable for TcdA-mediated response, steroid catabolites did not trigger release of IL-1 β in absence of the B30.2 domain (Fig. 4E). Conversely, in absence of the phosphorylated linker domain, steroid catabolites triggered IL-1 β release, further strengthening the evidence that the activation mechanism is primarily independent of step 1. The PYD, B-Box and coiled-coil domains were required for both steroid catabolites and TcdA responses. Furthermore, all the different cell lines responded similarly to NLRP3 stimulation by LPS + nigericin.

The difference in the B30.2 dependence was further validated by comparing pyrin serine 242 dephosphorylation after treatment with TcdA or steroid catabolites. Indeed, TcdA and UCN-01 triggered the dephosphorylation of both WT and Δ B30.2 pyrin proteins while etiocholanolone and pregnanolone only triggered pyrin dephosphorylation in the presence of the B30.2 domain (Fig. 4F). These experiments indicated that pyrin dephosphorylation happened in a B30.2-dependent manner specifically after addition of steroid catabolites.

Although the exact molecular mechanisms remain to be deciphered, these experiments revealed an activation mechanism that strongly differs from the one triggered by RhoA-inhibiting toxins. Indeed, pyrin activation by steroid catabolites is initiated in a B30.2-dependent manner, takes place in the absence of RhoA inhibition and does not require the phosphorylated linker domain, which includes the two serine residues required to launch TcdA/B-mediated pyrin responses (Gao et al., 2016).

The response to steroid catabolites is specific to human pyrin.

Mouse pyrin does not contain a B30.2 domain (J. J. Chae et al., 2000) but is a functional protein triggering inflammasome activation in response to RhoA-inhibiting toxins (Xu et al., 2014). In addition, the B30.2 domain is highly polymorphic in primates (P. Schaner et al., 2001). Since we observed a total

dependence on the B30.2 domain for the response to steroid catabolites, we assessed whether pyrin proteins from other species could promote responsiveness to steroid catabolites. Etiocholanolone and pregnanolone did not trigger pyroptosis in U937 cells expressing either mouse or macaque pyrin (Fig. 5A, B and supplemental Fig. S5A-B) while these cells underwent cell death in response to TcdA (Fig. 5C). These results were further confirmed by quantifying IL-1 β secretion (Fig. 5D). The unresponsiveness of the murine pyrin inflammasome to etiocholanolone and pregnanolone was further validated in primary murine macrophages (Fig. 5E).

To test whether the lack of response of murine macrophages to steroid catabolites was intrinsic to the pyrin protein or linked to a more general defect, we expressed human pyrin in the murine macrophage cell line, J774 (Supplemental Fig. S5B). The expression of human pyrin was sufficient to recapitulate the responses seen in human cells (Fig. 5F, 5H). The response to NLRP3 stimulation was independent of human pyrin expression (Fig. 5G, H) while, as expected, TNF levels were not impacted by human pyrin expression (Fig. 5I). In order to map the species specificity in regards to pyrin domains, chimeric mouse-human *MEFV* constructs were generated and expressed in U937 cells (Fig. 5J and Supplemental Fig. S5C). Inclusion of the murine PYD domain did not impair the response to steroid catabolites while inclusion of both murine PYD and phosphorylated linker domain (PLD) reduced but did not abolish the response to steroid catabolites (Fig. 5K, Supplemental Fig. S5D). The response to *C. difficile* toxins was not affected in either of the two chimera (Fig. 5K). Chimeras with larger murine N-terminal pyrin were not functional, possibly due to low expression level (Supplemental Fig. S5C). Altogether, these results demonstrate that the response to steroid catabolites is human-specific and that this species specificity is conferred, in an intrinsic manner, by the pyrin C-terminal domains.

Monocytes from FMF patients display a moderate increase in the response to steroid catabolites compared to HD.

We then investigated whether FMF-associated mutations in *MEFV* exon 10 (altering the B30.2 domain) had an impact on the response of the pyrin inflammasome to steroid catabolites. U937 cells expressing three clearly pathogenic *MEFV* variants (Touitou, 2001) were exposed to etiocholanolone and pregnanolone (Fig. 6A and supplemental Fig. S6A). While p.M680I and p.M694V mutations decreased these EC50 (reaching statistical significance for p.M680I in the case of pregnanolone), the less severe p.V726A mutation (Cekin et al., 2017), significantly increased the EC50 of both etiocholanolone and pregnanolone. We then evaluated the steroid catabolites response of primary monocytes from FMF patients presenting at least one p.M680I or p.M694V mutation. A trend towards a faster and stronger cell death response was observed in response to steroid catabolites in monocytes from FMF patients compared to HD (Fig. 6B, C). No difference was observed in response to NLRP3 inflammasome

engagement (Fig. 6B, C) while, as previously described (Magnotti et al., 2020, 2019), UCN-01-mediated pyroptosis was specifically observed in monocytes from FMF patients (Fig. 6B, C).

FMF monocytes released on average 4.5-fold and 1.6-fold more IL-1 β than HD monocytes in response to low or high concentrations of pregnanolone, respectively (Fig. 6D). In response to 100 μ M etiocholanolone, monocytes from FMF patients released significantly more IL-1 β than HD's monocytes ($p=0.015$). The difference in IL-1 β concentrations were much stronger in response to UCN-01 (19.9-fold increase, $p<0.001$) while no difference was observed upon NLRP3 stimulation. Altogether, these results suggest that FMF patients display a moderate increase in steroid catabolite-induced inflammasome responses that could contribute to inflammatory flares and be dependent on the *MEFV* genotype.

The pyrin inflammasome in FMF patients is mostly controlled at the step1 level (pyrin dephosphorylation) (Magnotti et al., 2019) likely explaining why the response to steroid catabolites (acting primarily on the step 2) is not drastically affected by FMF-associated *MEFV* mutations. We then decided to investigate the effects of steroid catabolites on cells from PAAND patients, in which the pyrin inflammasome step1 is constitutively activated leading to a pyrin inflammasome controlled mostly at the step2.

Monocytes from PAAND patients respond to low concentrations of steroid catabolites in the absence of step 1 activator.

To assess the impact of PAAND-associated *MEFV* mutations on the response to steroid catabolites, we generated U937 cells expressing either of three reported PAAND mutations (p.S208C, p.S242R, p.E244K-supplemental Fig. S7A). Contrary to WT or p.M694V-expressing cell lines, all PAAND cell lines died quickly in response to low concentrations of pregnanolone or etiocholanolone (Fig. 7A, B). UCN-01 synergized with the low concentrations of steroid catabolites in p.S208C-expressing cells whereas it had no additional effect in p.S242R or p.E244K-expressing cells. Phosphorylation of serine residue 242 and interaction of 14-3-3 chaperone with the neighbouring residues may thus be more important to maintain pyrin inactive than phosphorylation of serine residue 208. This hypothesis is consistent with the fact that p.S242R and p.E244K mutations promote disease in a dominant manner while p.S208C does so in a recessive manner (Hong et al., 2019; Masters et al., 2016; Moghaddas et al., 2017).

We then investigated four distinct exon 2-encoded *MEFV* mutations identified in patients, and that have been either assigned as "variant of unknown significance" (p.E148Q, p.G250A) or likely pathogenic (p.E167D, p.T267I) and associated with a clinical FMF-like phenotype. Interestingly, one mutation (p.G250A), absent from Gnomad, gave a partial response to low doses of steroid catabolites

suggesting it may affect pyrin step1 and be a pathogenic PAAND-like mutation. None of the other three mutations gave cellular phenotypes differing from WT pyrin-expressing cells (Fig. S7B-C) suggesting that they correspond either to *MEFV* benign polymorphisms or to FMF-like mutations (which was not tested here).

We then assessed pyroptosis and IL-1 β release in primary monocytes from PAAND patients from two independent families with heterozygous p.S242R mutation. At low concentration, pregnanolone and etiocholanolone triggered cell death (Fig. 7C, D), IL-1 β release (Fig. 7D, E) and ASC specks formation (Fig. 7F, G). In contrast, none of these responses were observed in monocytes from HD. No differences were observed upon stimulation with TcdB or UCN-01 (in the presence or absence of low concentrations of steroid catabolites) (Fig. 7C-E, G). High concentrations of pregnanolone or etiocholanolone also triggered higher IL-1 β release in PAAND patients' monocytes compared to HD monocytes (Fig. 7E) possibly due to a faster and stronger inflammasome response (Fig. 7 D, supplemental Fig. S7D).

These results thus demonstrate that PAAND patients' monocytes strongly respond to low doses of steroid catabolites suggesting that these molecules could contribute to inflammation in these patients and also to the distinct clinical features observed in PAAND and FMF patients.

Discussion

The identification of steroid catabolites as molecules triggering pyrin step 2 provides insights into pyrin activation mechanisms. First, it confirms that the two steps can be activated independently. Indeed, low doses of sex steroid catabolites do not impact pyrin phosphorylation but the same doses trigger inflammasome activation in the presence of pyrin variants impaired for phosphorylation. Furthermore, the step 2 is dependent on the B30.2 domain, and independent of the phosphorylated linker domain, while the inverse applies to TcdA-mediated pyrin activation. Finally, a coupling mechanism likely exists between two steps since high doses of steroid catabolites trigger the full activation of pyrin. This coupling mechanism might be mediated by pyrin conformation changes affecting the phosphorylation/dephosphorylation balance mediated by PKN1/2 and by the calyculin A-sensitive phosphatase(s) (Malik et al., 2022). Alternatively, high doses of steroid catabolites might affect the activity of PKN1/2 or of the pyrin phosphatase(s). Of note, in this particular setting, what we initially termed "second step" is likely to be upstream of pyrin dephosphorylation.

In contrast to the TcdA/B responses, the response to steroid catabolites is human-specific. In mice, the lack of B30.2 domain partly explains the absence of response. Yet, we did not observe any response in bone-marrow derived macrophages from knock-in mice presenting the murine pyrin protein fused to

the human B30.2 domain (Chae et al., 2011; Park et al., 2020) (Supplemental Fig. S5E). The resulting chimeric pyrin does not include the human coiled-coil domain likely explaining the lack of response of these cells. Indeed, the coiled-coil domain is required for steroid catabolite-mediated pyrin activation and is highly divergent between murine and human pyrin proteins (Supplemental Fig. S5A). Surprisingly, the expression of *Macaca fascicularis* pyrin did not confer responsiveness to steroid catabolites either, despite the presence of similar coiled-coil and B30.2 domains. *MEFV* has been subjected to a strong evolutionary pressure in primates (P. Schaner et al., 2001), possibly explaining the difference in steroid catabolites responsiveness between *M. fascicularis* and *Homo sapiens*.

Sex hormones are known to regulate immune responses and their variations during menstrual cycle and pregnancy correlate with profound modifications in local and systemic immune responses (Beagley and Gockel, 2003; Stelzer et al., 2021; Regan et al., 2013). Particularly, IL-1 β and IL-18 levels fluctuate during menstrual cycle and pregnancy (Azlan et al., 2020; Cannon and Dinarello, 1985; Romero et al., 2018). Since pregnanolone sensitizes cells to low doses of the bacterial toxin TcdA (Fig. S4C-E), the increase in pregnanolone may lower pyrin inflammasome threshold towards the end of pregnancy and during menstruation. To our knowledge, plasma etiocholanolone/ pregnanolone levels never reach micromolar concentrations (pregnanolone plasma level can reach up to 70 nM during pregnancy (Deligiannidis et al., 2016; Hill et al., 2007)) so it is unlikely that physiological steroid catabolites concentrations could fully activate the pyrin inflammasome in the absence of a synergistic signal or pathogenic *MEFV* mutations. Interestingly, flares in women with FMF are frequently associated with menstruation (Akar et al., 2006; Duzgun et al., 2006; Kishida et al., 2020), which correspond to the peak of progesterone catabolism. While this correlation is appealing, demonstrating the pathophysiological role of pregnanolone (and/or etiocholanolone) remains challenging, especially due to the current lack of animal models and the complexity of the metabolome changes during menstrual cycles and pregnancy (Stelzer et al., 2021).

Progesterone and testosterone were completely inactive with regards to pyrin inflammasome activation. Similarly, all the modifications tested on the etiocholanolone or the pregnanolone backbones decreased inflammasome responses. We thus believe that human pyrin has specifically evolved in humans to sense these catabolites. Interestingly, Alimov and colleagues identified a synthetic molecule, BAA473, that shares the same steroid backbone and the same stereochemistry as etiocholanolone and pregnanolone and activates pyrin. In contrast to the molecules identified here, which are endogenous molecules, the relevance of BAA473 remains to be established although, theoretically, BAA473 could be generated from the secondary bile acid, deoxycholic acid (Alimov et al., 2019). BAA473-mediated pyrin inflammasome activation likely proceeds through an identical mechanism as steroid catabolites.

In addition to being sex hormones catabolites, pregnanolone and etiocholanolone are also neurosteroids that can be generated de novo in the central nervous system (Yilmaz et al., 2019). Neurosteroids levels vary greatly, depending on the specific physiological situations, and can reach submicromolar to micromolar concentrations (Hosie et al., 2006). Particularly, pregnanolone levels increase during psychological stress (Park et al., 2017; Ströhle et al., 2002), a condition known to promote flares in FMF patients (Kishida et al., 2020b). Whether etiocholanolone or pregnanolone could locally reach high enough concentrations to prime or activate the WT pyrin inflammasome in a particular neurological environment (and contribute to neuroinflammation) is unclear at the moment. Interestingly, we observed that at least one *MEFV* mutation (p.P373L) confers responsiveness to nanomolar concentrations of steroid catabolites (Fig. S6B) indicating that physiological concentrations can modulate pyrin inflammasome activation. All other neurosteroids tested (pregnenolone and pregnenolone sulfate) were inactive, and we could not identify receptors upstream of the pyrin inflammasome to explain the pyroptotic effect of pregnanolone and or etiocholanolone. The pyrin B30.2 domain contains a hydrophobic pocket that has been hypothesized to bind a ligand. Similarly, the butyrophilin 3A1 B30.2 domain displays a pocket that accommodates microbial-derived phosphoantigens resulting in the activation of gamma delta T cells (Sandstrom et al., 2014). It is thus tempting to speculate that pregnanolone and etiocholanolone could directly bind the pyrin B30.2 domain to activate the inflammasome. This speculation is supported by the impact of some B30.2-affecting mutations (e.g. V726A) which decreased the efficacy of steroid catabolites to activate the pyrin inflammasome (Fig. 6A).

Importantly, experiments performed in the late 50s have demonstrated the fast and potent pyrogenic activity of steroids of endogenous origin, including etiocholanolone and pregnanolone upon injection in human volunteers (KAPPAS et al., 1960, 1957). These historical experiments thus validate these steroid catabolites as potent in vivo inflammation inducers and our results strongly suggest that activation of the pyrin inflammasome was at the origin of this enigmatic "Steroid fever" (KAPPAS et al., 1961).

Limitations of the study

The requirement for the B30.2 domain and the lack of observed RhoA inhibition suggest that steroid catabolites activate pyrin by an unconventional mechanism. This conclusion is based on negative data (lack of observed RhoA inhibition) and chimeric or truncated pyrin variants for which it is difficult to exclude non-specific impact on the overall protein structure and function. We speculate that the pyrin B30.2 may directly bind steroid catabolites to promote pyrin activation step 2 although so far, we did not manage to demonstrate this interaction.

While the "steroid fever" experiments indicate that these molecules can trigger inflammation upon injection in humans and could be used as proinflammatory mediators, we were unable to test whether physiological steroid catabolites concentrations can locally prime or fully activate the WT pyrin inflammasome. At the moment, most of the experiments were performed with steroid catabolites concentrations \approx 100-fold higher than those found in serum. Novel animal models and/or clinical studies are needed to investigate the links between pyrin inflammasome and steroid hormones catabolism at key life stages in females and males.

ACKNOWLEDGMENTS.

We warmly thank the patients and their family for their involvement in this project. This work was performed in the framework of the Centre National de Référence RAISE. We acknowledge the contribution of SFR Biosciences (UMS3444/CNRS, US8/Inserm, ENS de Lyon, UCBL) Platim, cytometry and PBES facilities. We acknowledge the contributions of the CELPHEDIA Infrastructure (<http://www.celphedia.eu/>), especially the centre AniRA in Lyon. We acknowledge the contribution of the Etablissement Français du Sang Auvergne - Rhône-Alpes, Mathieu Gerfaud-Valentin, Emmanuelle Weber, Agnès Duquesne, Marine Fouillet-Desjonquères (Lyon university hospital), Marion Delplanque (Tenon Hospital) for patient recruitment. We thank Pr Etienne Merlin (CHU Clermont-Ferrand), Emmanuel Lemichez (Pasteur institute, Paris), TH team and ImmunAID members for advice and stimulating discussions. Funding: This work is supported by an ANR grant (FMFgeneToDiag). This project has received funding from the European Union's Horizon 2020 research and innovation programme under grant agreement No 779295. TH team is supported by The Fondation pour la Recherche Médicale (FRM EQU202103012640). DC is supported by a fellowship from The Fondation pour la Recherche Médicale (FDT202106012874).

Author contributions

Conceptualization: FM, YJ, TH, MFMcD. Investigation: FM, DC, SD, AM, PB, JS, OH, WL. Resources: DK, JJC, AB, MP, PS, SGL, TAT, EDL, CW, YJ. Supervision: TH, JJC. Funding Acquisition: YJ, TH. Project administration: YJ, CW, MFMcD. Methodology: HML. Writing-original draft: FM, TH. Writing -review and editing: all authors.

Declaration of interests

The authors declare no competing interests.

STAR Methods

RESOURCE AVAILABILITY:

Lead contact

Further information and requests for resources and reagents should be directed to the lead contact, Thomas Henry (thomas.henry@inserm.fr).

Materials availability

The WT, p.M694V (FMF), p.S08C/S242R (PAAND) pyrin-encoding plasmids have been previously deposited to Addgene (ID 134702, 703, 706). Other point mutants plasmids are available upon request to the lead contact. All unique/sable reagents generated in this study are available from the lead contact without restriction.

Data and code availability

- Raw data (full Western blot images and Raw data) have been deposited at Mendeley and are publicly available as of the date of publication. DOI is listed in the key resources table.
- This paper does not report original code
- Any additional information required to reanalyze the data reported in this paper is available from the lead contact upon request.

EXPERIMENTAL MODEL AND SUBJECT DETAILS:

Human subjects:

The study was approved by the French Comité de Protection des Personnes SUD-EST IV (CPP,#L16-189), Ile de France IV (CPP, #2018/95) and by the French Comité Consultatif sur le Traitement de l'Information en matière de Recherche dans le domaine de la Santé (CCTIRS, #16.864) and the Leuven/Onderzoek Ethic committee (#S58600). The authors observed a strict accordance to the Helsinki Declaration guidelines. HD blood was provided by the Etablissement Français du Sang in the framework of the convention #14-1820. Informed consent was obtained from all healthy donors and patients.

All FMF patients fulfilled the Tel Hashomer criteria for FMF, had at least one mutation in the *MEFV* gene and are listed in Supplemental Table S2. PAAND patients all bear heterozygous p.S242R mutation. Three patients have been previously reported (Van Nieuwenhove et al., 2021b) while three patients (1 adult 2 children) were identified by Pr. Tran (CHU Nîmes). The potential carriage of *MEFV* mutations in HD was not assessed. Blood samples from HD were drawn on the same day as patients.

The age and sex of patients are provided in Supplemental Table S2. The number of patients in each experiment is reported in the corresponding figure panels.

Cell lines:

The human myeloid cell line U937 (ATCC #CRL-1593.2) was grown in RPMI 1640 medium with glutaMAX-I supplemented with 10% (vol/vol) FCS, 100 IU/mL penicillin, 100 µg/mL streptomycin (ThermoFischer Scientific) at 37 °C . U937 cell line was derived in 1974 from malignant cells obtained from the pleural effusion of a 37-year-old, White, male patient with histiocytic lymphoma. U937 cells were obtained from CelluloNet-BRC, SFR Bioscience, tested mycoplasma-free. The cell line has not been authenticated.

293T cell line (ATCC #CRL-3216) is an epithelial-like cell line that was isolated from the kidney of a female fetus. 293T cells were grown in DMEM medium with glutaMAX-I supplemented with 10% (vol/vol) FCS at 37 °C. 293T cells were obtained from Anira-vectorology platform, SFR Bioscience, tested mycoplasma-free. The cell line has not been authenticated.

Primary cells:

Bone-marrow progenitors from the femurs and tibias from female 6-12 weeks-old C57BL6/J (Charles River) or *MEFV*^{M694VKI} (Chae et al., 2011) mice were obtained in the framework of the ethical approval ENS_2012_061 (CECCAPP, Lyon, France). Mice were maintained in the PBES animal facility by trained staff with daily monitoring of animal behaviour and husbandry conditions in agreement with the French laws ("Décret n 2013-118 du 1er février 2013 relatif à la protection des animaux utilisés à des fins scientifiques"). Cages contained enrichment and bedding material. Water and food was given ad libitum. Progenitors were differentiated into bone-marrow derived macrophages (BMDMs) during 6 days in DMEM medium with glutaMAX-I supplemented with 10% (vol/vol) FCS and 10% M-CSF-containing supernatant at 37 °C. Progenitors were seeded in non-tissue culture treated petri dishes and following differentiation were lifted in PBS without calcium and magnesium using cell scrapers (Sarstedt).

Human monocytes, neutrophils, lymphocytes: Blood was drawn in heparin-coated tubes and kept at room temperature overnight. The age and sex of patients is provided in Supplemental table S2, the age and sex of healthy donors was not available due to full anonymization of donors from the EFS blood bank. Monocytes were isolated as previously reported (Magnotti et al., 2019). Briefly, peripheral blood mononuclear cells (PBMCs) and neutrophils were isolated by density-gradient centrifugation. Monocytes were further isolated by magnetic positive selection using CD14 MicroBeads (Miltenyi Biotec) following manufacturer's instructions. Lymphocytes were recovered from the negative fraction

of monocytes isolation. Neutrophils were separated from red blood cells (RBCs) using Dextran (Sigma, #31392), residual RBCs were lysed with ice cold bi-distilled water and contaminating CD14⁺ monocytes were excluded using CD14 MicroBeads. Live cells were enumerated by flow cytometry (BD Accuri C6 Flow Cytometer®). All human cells were grown in RPMI 1640 medium with glutaMAX-I supplemented with 10% (vol/vol) FCS, 100 IU/mL penicillin, 100 µg/mL streptomycin (ThermoFischer Scientific) at 37 °C in the presence of 5% CO₂.

METHOD DETAILS

Compound library and reagents. The Prestwick® Chemical Library (Prestwick Chemical, Illkirch, France) amounts to a total of 1,199 compounds arrayed in fifteen 96-well plates. This 2013 version of the library contains mostly US Food and Drug Administration (FDA)-approved drugs. All the compounds were stored in DMSO at -20°C. Mother plates 1-14 were at a concentration of 2 mg/mL, which corresponds to 6.32 ± 2.8 mM, and the last one at a concentration of 10 mM. All the compounds and their final concentrations are listed in Table S1. Etiocholanolone (3 α -hydroxy-5 β -androstane-17-one, #R278572), Testosterone (#86500), Androsterone (3 α -hydroxy-5 α -androstane-17-one, #31579), 3 β -hydroxy-5 β -androstane-17-one (R213691), Progesterone (#P8783), Pregnanolone (5-beta-pregnan-3 α -ol, 20-one, #P8129), cortisol (#C-106), UCN-01 (#U6508), Doxycycline (#D9891) were from Sigma. Pregnanolone (5-beta-pregnan-3 α -ol, 20-one, #P8150-000), 11-one: (5-beta-pregnan-3 α -ol-11, 20-dione, #P7850-000), 11 α OH: (5 β -pregnan-3 α , 11 α -diol-20-one, #P6400-00), 11 β OH: (5- β -pregnan-3- α , 11 β -diol-20-one, #P6420-000), Hemisuccinate: (5- β -pregnan-3- α , 21-diol-20-one, 21 hemisuccinate, #P6944-000), 21OH: (5- β -pregnan-3- α , 21-diol-20-one, #P6920-000), 17OH (5- β -pregnan-3- α , 17 diol-20-one, #P6570-000), 20H (5- β -pregnan-3- α -ol, #P7800-000), Sulphate (5 β -pregnan-3 α -ol-20-one sulphate, sodium salt, #P8168-000) were from Steraloids. Tetrahydrocortisol (#T293370) was from Toronto Research Chemicals. LPS-EB Ultrapure (#tlrl-3pelps), Nigericin (#tlrl-nig) were from Invivogen. TcdB was from Abcam (#ab124001). TcdA was purified from *Clostridium difficile* VPI10463 strain, as previously described (Popoff, 1987; von Eichel-Streiber et al., 1987).

Chemical library screening. All robotic steps were performed on a Tecan Freedom EVO platform. Compounds from the Prestwick Chemical Library® were evaluated at a 1:1,000 or 1:2,000 dilution of the original stock for plates 1-14 and plate 15, respectively (see Table S1). 1 µL of DMSO solutions was spiked into dry well of F-bottom clear cell culture treated 96-wells plates (Greiner Bio One), with columns 1 and 12 devoted to controls and used to calculate the Z'-factor. U937 cells expressing p.S242R MEFV were treated or not (counterscreen) with doxycycline (1 µg/mL) for 16 h, centrifuged and seeded at 10⁵ cells per well (100µL final volume) in RPMI 1640 without phenol red, 10% FCS, 1mM HEPES, 1% PSA, 1mM Glutamine, in the presence of propidium iodide at 5 µg/ml. Following 90 min of

incubation at 37°C, fluorescence intensity (excitation wavelength at 535 nm and emission wavelength at 635 nm) corresponding to propidium iodide incorporation was measured on a microplate reader (Infinite M1000, Tecan). The average Z' value was 0.67 ± 0.12 , indicating a robust and reliable assay. Mean fluorescence + 3SD was retained as a threshold. Compounds triggering cell death only in the presence of doxycycline were considered as pyrin-specific and defined as hits.

Genetic manipulation. *Casp1*^{KO} and *GSDMD*^{KO} cell lines, U937 cell lines expressing WT, p.S208C, p.S242R, p.M694V, p.M680I under the control of a doxycycline-inducible promoter, have been previously described (Lagrange et al., 2018; Magnotti et al., 2019c). p.[V726A], p.[E244K], ΔPYD, ΔPLD, ΔB-Box, ΔCoiled-coil, ΔB30.2 *MEFV* were generated by mutagenesis of the pENTR1A-3xFlag *MEFV* using primers presented in supplemental table S3, pfu ultra II Fusion high fidelity polymerase (Agilent) followed by digestion of the parental plasmid using Dpn1 restriction enzyme. The resulting plasmids were validated by sequencing and the mutated *MEFV* constructs were transferred into the GFP-expressing plasmid pINDUCER21 (Meerbrey et al., 2011) under the control of a doxycycline-inducible promoter using LR recombinase (Invitrogen). Lentiviral particles were produced in 293T cells using pMD2.G and psPAX2 (from Didier Trono, Addgene plasmids #12259 and #12260), and pINDUCER-21 plasmids. U937 cells were transduced by spinoculation and selected at day 4 post-transduction based on GFP expression on an Aria cell sorter and maintained polyclonal. Pyrin expression was induced by treatment with doxycycline ($1 \mu\text{g}\cdot\text{mL}^{-1}$) for 16 h before stimulation. All parental cell lines were tested for mycoplasma contamination.

Inflammasome activation

For cytokine quantification, primary monocytes were seeded in 96-well plates at 5×10^3 cells/well, in RPMI 1640, GlutaMAX medium (ThermoFisher) supplemented with 10% foetal calf serum (Lonza) and incubated for 3 hours in the presence of LPS (10 ng/ml, Invivogen). Primary monocytes were then treated for 1 h 30 with nigericin (5 μM , Invivogen); UCN-01 (12.5 μM , Sigma), TcdB (125 ng/ml, Abcam) or steroid catabolites at the indicated concentrations. When indicated, monocytes were treated with colchicine (1 μM , Sigma), nocodazole (5 μM , Sigma), VX-765 (25 μM , Invivogen), MCC950 (10 μM , Adipogen AG-CR1-3615) or Calyculin A (Sigma, 208851) 30 minutes before addition of steroid catabolites, UCN-01, TcdB or Nigericin. Following the incubation, cells were centrifuged, and supernatants were collected.

To assess cytokine release, 8×10^4 U937 cells per well of a 96 wells plate were exposed to $100 \text{ ng}\cdot\text{mL}^{-1}$ of phorbol 12-myristate 13-acetate (PMA; InvivoGen) for 48 h and primed with LPS at 50 ng/ml for 3

h. When applicable, nigericin was used at 50 $\mu\text{g}\cdot\text{mL}^{-1}$. Supernatant was collected at 3 h post treatment. Levels of IL-1 β , IL-18 or TNF in cell supernatants were quantified by ELISA (R&D Systems). The number of replicates and independent experiments are listed in the corresponding figure legends.

ASC specks Immunofluorescence

Monocytes were fixed with paraformaldehyde 2% for 20 min before spreading onto poly-lysine adhesion slides (Thermo Scientific™) using the Cytospin3 (Shandon) 5 min at 450 rpm. Following permeabilization with Triton X100 (0.1% in PBS), cells were stained using anti-ASC (Santa Cruz, sc22514R, 4 $\mu\text{g}\cdot\text{mL}^{-1}$), Alexa594-goat anti rabbit antibodies (Invitrogen, A-110088, 10 $\mu\text{g}\cdot\text{mL}^{-1}$) and DAPI (100 $\text{ng}\cdot\text{mL}^{-1}$). ASC specks were visualized on the Zeiss LSM800 confocal microscope. Quantification was performed on 10 fields per sample.

Real time cell death and EC50 calculation. For real time cell death assays, monocytes and U937 cells were seeded at 2 or 5 x 10⁴ per well of a black 96 well plate (Costar, Corning), respectively, in the presence of propidium iodide (PI, Sigma) at 5 $\mu\text{g}/\text{ml}$. Three technical replicates per conditions were done. Real time PI incorporation was measured every 5 to 15 min immediately post-stimuli addition on a fluorimeter (Tecan) using the following wavelengths: excitation 535 nm (bandwidth 15 nm); emission 635 nm (bandwidth 15 nm) (C. L. Case and Roy, 2011; Pierini et al., 2012). Cell death was normalized using PI incorporation in cells treated with triton X100 for 15 min (=100% cell death) and PI incorporation at each time point in untreated cells (0% cell death). As a further correction, the first time point of the kinetics was set to 0. The areas under the curve were computed using the trapezoid rule (Prism 6; GraphPad). To calculate the EC50 (Half maximal effective concentration), the normalized cell death at 3 h post-compound addition was used. To compare different cell lines, butyrate (1mM) was added for 16 h (in the meantime as doxycycline) to revert transgene silencing (Chen et al., 1997). The different concentrations were log-transformed, and a non-linear regression was applied using the Log (agonist) vs. normalized response-variable slope model (Prism 6; GraphPad). The least squares (ordinary) fitting method was applied.

RhoA activity

RhoA activity was determined by G-LISA (Cytoskeleton) following manufacturer's instructions.

Crosslinking, immunoprecipitation, Immunoblot

Cells were lysed in 25mM Tris HCl, 150mM NaCl, 1mM EDTA and 0.1% NP-40 buffer containing Mini Protease Inhibitor Mixture (Roche) and sodium fluoride (Sigma) by a quick freezing and thawing step. Flag-Pyrin was immuno-precipitated using anti Flag M2 affinity gel (Sigma). ASC was cross-linked in the

insoluble pellet using DSS (Disuccinimidyl suberate, ThermoFisher #21655) 2 mM (1 h at 37°C). Proteins were separated by SDS/PAGE on precast 4-15% acrylamide gels (Bio-rad) and transferred to TransBlot® Turbo™ Midi-size PVDF membranes (Bio-rad). Antibodies used were mouse monoclonal anti-FLAG® (Sigma-Aldrich, clone M2; 1:1,000 dilution), anti-Pyrin (Adipogen, AL196, 1: 1,000 dilution), anti-phospho S242 Pyrin (Abcam, ab200420; 1:1,000 dilution)(Gao et al., 2016c), anti-human Caspase-1 (Santa Cruz, sc515, 1: 1,000 dilution), anti-human GSGMD (sigma, HPA044487, 1: 1,000 dilution), anti-human IL-1 β (Cell signalling, #12703, 1: 1,000 dilution), anti-ASC (Santa Cruz, sc22514R, 1:1,000 dilution). Cell lysates were reprobbed with a mouse monoclonal antibody anti- β -actin (clone C4, Millipore; 1:5,000 dilution).

QUANTIFICATION AND STATISTICAL ANALYSIS.

Normality was verified using D'Agostino & Person omnibus normality test, Shapiro-Wilk normality test or Kolmogorov-Smirnov test with Dallal-Wilkinson-Lille for P value if the number of values was too small for the former test. Gaussian distribution was assumed for technical triplicates. Unmatched normalized values were analysed by Ordinary one-way ANOVA with Sidak's multiple comparisons test. When normality could not be verified, matched values were analysed by the Friedman test, with Dunn's correction or using Sidak's multiple comparisons test. Normal matched values were analysed with RM one-way ANOVA, with the Greenhouse-Geisser correction and Dunnett correction for multiple comparisons. Unmatched values, for which normality could not be verified, were analysed using Kruskal-Wallis analysis with Dunn's correction. Effect of treatment was analysed by Wilcoxon matched-pairs signed rank tests. Prism 7 (GraphPad) was used for statistical analyses. The statistical analyses and parameters for each experiments are listed in the corresponding figure legends.

Figures and legends

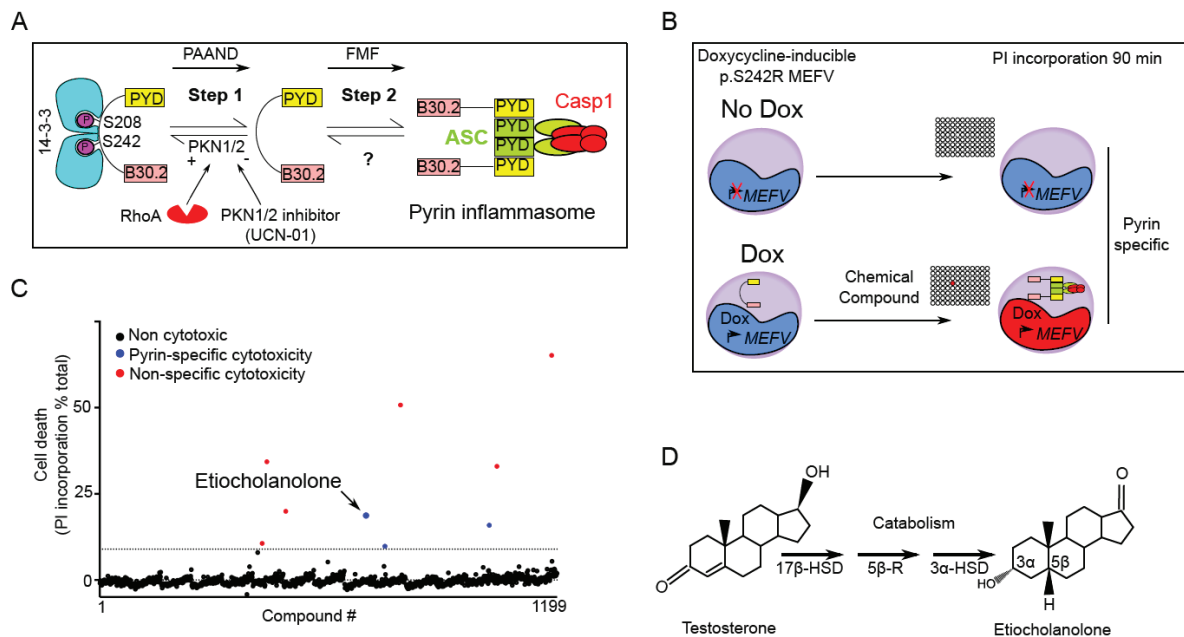


Figure 1: a chemical screen identifies etiocholanolone, a testosterone catabolite, as a pyrin inflammasome step 2 activator.

(A) Model for pyrin two step activation mechanism. Step 1 is due to dephosphorylation of pyrin and loss of 14-3-3 binding and is constitutive in PAAND patient. Step 2 is uncharacterized but is upstream of ASC speck formation and is constitutive in FMF patients. (B) Chemical screen overview: cells expressing (Dox: doxycycline) or not (No Dox) p.S242R MEFV were exposed to individual chemical compounds. 90 min post-exposure, cell death was monitored using propidium iodide (PI). Compounds driving cell death independently of pyrin (i.e. in the absence of doxycycline) were excluded. (C) Screen results are shown, each dot represents the cell death value of cells exposed to one chemical compound. The dotted line represents the mean + 3 SD. Red dots represent non-specific hits (killing cells irrespective of the presence or the absence of Dox) while blue dots represent specific hits displaying cytotoxicity only upon pyrin expression. Etiocholanolone (Etio, 6.9 μ M) is highlighted. Each chemical compound was screened once in the presence and in the absence of doxycycline. The value shown corresponds to normalized cell death value of a single well. (D) Structure of progesterone and its catabolite etiocholanolone are shown. The stereochemistry of carbon 3 and 5 is indicated. 17 β -HSD: 17 β -hydroxy-steroid dehydrogenase, 5 β -R: 5 β -reductase, 3 α -HSD: 3 α -hydroxy-steroid dehydrogenase.

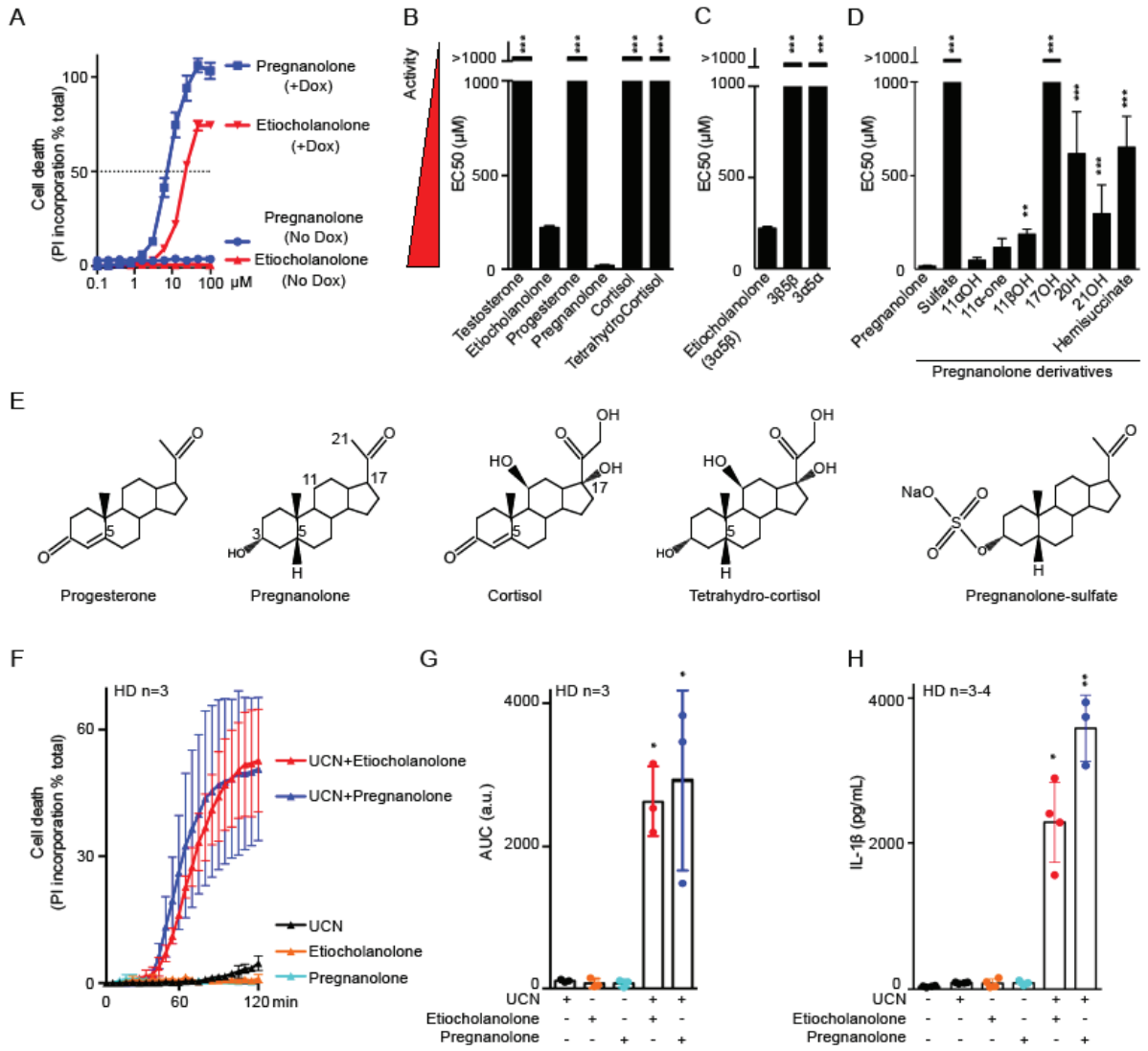
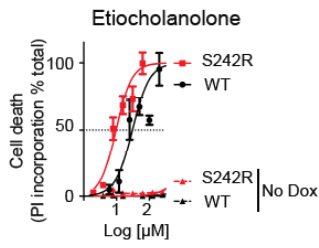


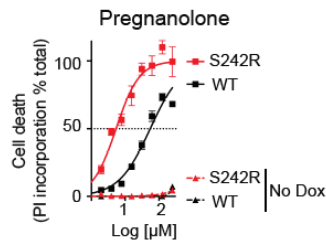
Figure 2: Pregnanolone and etiocholanolone specifically triggers pyrin inflammasome step 2.

(A) Pregnanolone (blue) and etiocholanolone (red) were added at different concentrations on cells expressing (in the presence of doxycycline, DOX+) or not (No Dox) p.S242R *MEFV*. Cell death was determined at 3 h post-addition. The concentration triggering 50% cell death (horizontal dotted line) determined the EC50 (Half maximal effective concentration which is inversely correlated to the activity of the tested molecule). (B) Structure activity of various steroid hormones, their catabolites, (C) of etiocholanolone (also known as 3 α -hydroxy 5 β -androstan-17-one (3 α , 5 β)) and its two stereoisomers 3 β -hydroxy-5 β -androstan-17-one (3 β , 5 β) and androsterone (3 α , 5 α), (D) of pregnanolone and molecules closely related. EC50 were calculated as in A. (E) Structures of selected compounds. All compounds can be found in supplemental Fig. S1. (F) Primary monocytes from healthy donors (HD, n=3) were pre-treated with pregnanolone (6 μ M) or etiocholanolone (12 μ M) for 1 h followed by addition of the PKC superfamily inhibitor, UCN-01. Cell death was monitored every 5 min for 2 h. (G) The Area Under the Curve (AUC) was computed for each HD. (H) Primary monocytes from healthy donors (HD, n=3-4) were treated with LPS for 2 h, then pre-treated with pregnanolone (6 μ M) or etiocholanolone (12 μ M) for 1 h followed by UCN-01 addition. IL-1 β concentration in the supernatant was quantified at 3 h post-UCN-01 addition. One experiment representative of three (A) or two (B-D) independent experiment is shown. Mean and SEM of triplicates are shown. Sulphate: 5 β -pregnan-3 α -ol-20-one sulphate; 11 α OH: 5 β -pregnan-3 α , 11 α -diol-20-one; 11-one: 5-beta-pregnan-3 α -ol-11, 20-dione; 11 β OH: 5- β -pregnan-3- α , 11 β -diol-20-one; 17OH: 5- β -pregnan-3- α , 17 diol-20-one; 20H: 5- β -pregnan-3- α -ol; 21OH: 5- β -pregnan-3- α , 21-diol-20-one; Hemisuccinate: 5- β -pregnan-3- α , 21-diol-20-one 21 hemisuccinate. (B, C, D) One-way ANOVA with Dunn's correction was applied. ***:p<0.001; **p=0.007. (F) each point corresponds to the mean +/- SEM of 3 HD values, each one being the mean of a triplicate. (G) Each point corresponds to the mean AUC of kinetics of one HD performed in triplicate, the bar represents the mean +/- SEM of 3HD. AUC are expressed as arbitrary units (a.u.). Friedman test with Dunn's correction for multiple analysis was performed in comparison to untreated cells. *: p=0.023 (Etio + UCN); p=0.011 (Pregna + UCN). (H) Each point corresponds to the mean IL-1 β concentration of 1 HD calculated from a triplicate, the bar represents the mean +/- SEM of 3-4 HD. Kruskal-Wallis test with Dunn's correction for multiple analysis was performed in comparison to LPS-treated cells. *:p=0.011; **p=0.002.

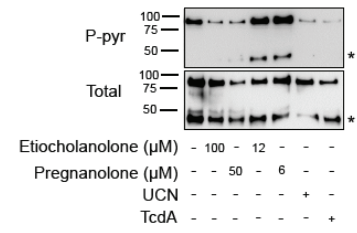
A



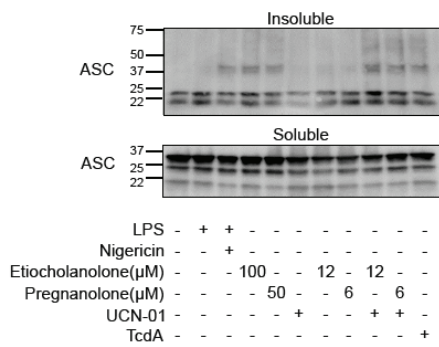
B



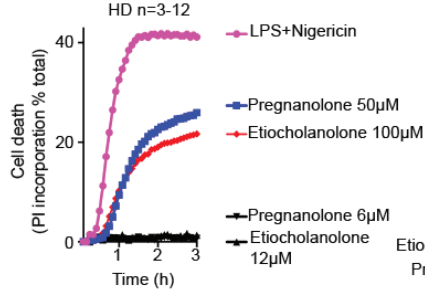
C



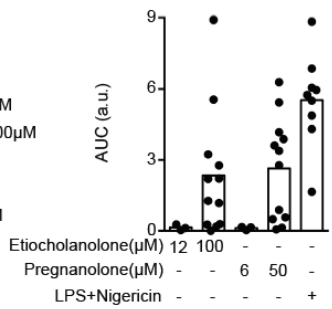
D



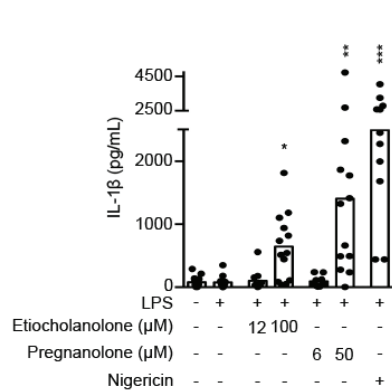
E



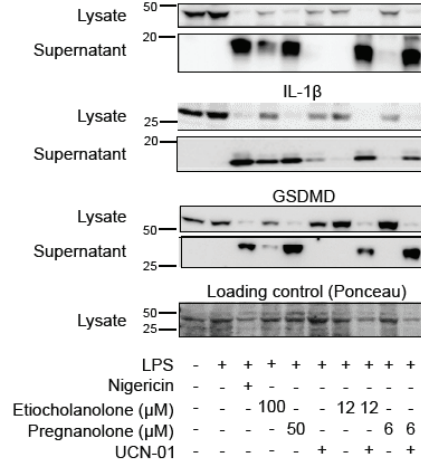
F



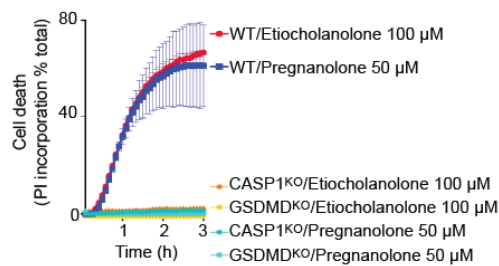
G



H



I



J

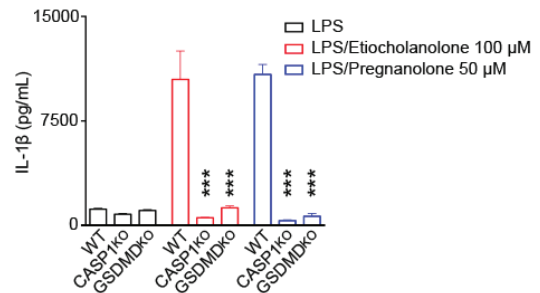


Figure 3: High concentrations of etiocholanolone and pregnanolone trigger full activation of pyrin inflammasome.

(A, B) U937 cells expressing (plain lines) or not (No Dox, dotted lines) p.S242R (red) or WT (black) *MEFV* were treated with various concentration of etiocholanolone (A) or pregnanolone (B). Cell death was determined at 3 h post-addition. (C) 3xFlag-WT pyrin from U937 cells treated with the indicated stimuli at the indicated concentrations was immunoprecipitated. Ser242 phosphorylation (P-pyr) and total pyrin levels were monitored by Western blot. "*" indicates a cleaved form of pyrin. (D) ASC immunoblot from U937 cells expressing WT *MEFV*. Cells were treated with the indicated molecules. ASC oligomers in the insoluble fraction were treated with DSS (2 mM) cross linker after lysis. ASC monomers in the soluble fraction is shown. "*" and "***" correspond to the size of ASC dimer and trimer, respectively. (E) Monocytes from healthy donors (n=3-12) were treated with low (black) or high concentrations of etiocholanolone (red) and pregnanolone (blue) or with LPS + Nigericin (Magenta). Propidium iodide incorporation (PI) was monitored every 5 min for 3 h. (F) The corresponding Area Under the Curve (AUC) for each donor are shown. (G) Monocytes were primed with LPS for 3 h and exposed to the indicated stimuli at the indicated concentration. IL-1 β concentration in the supernatant was quantified at 3 h post-addition. (H) Monocytes from one HD were primed or not with LPS for 3 h before addition of the indicated stimuli. Caspase-1, IL-1 β and GSDMD processing were analysed by Western blot in the cell lysate and supernatant at 3 h post stimuli addition. (I) *MEFV*-expressing U937 monocytes or (J) PMA-differentiated U937 macrophages WT or knock-out for *CASP1* or *GSDMD* as indicated were treated with doxycycline during 16 h. (I) Propidium iodide (PI) incorporation was monitored every 5 min for 3 h post stimuli addition. (J) Cells were primed with LPS for 3 h before addition of the indicated stimuli. IL-1 β concentration in the supernatant was quantified at 3 h post-addition. One experiment representative of three (A-C) to two (H-I) independent experiment is shown. Mean and SEM of triplicates are shown. (A-B) Non-linear regression curve computed using least squares fit method is shown. (G) Kruskal-Wallis test with Dunn's multiple comparisons tests was performed to compare the different treatments to the LPS treatment. *: p=0.026; **: p=0.0011; ***: p<0.001. (J) One-way ANOVA analysis with Sidak's multiple comparisons test was performed to compared WT U937 to *CASP1*^{KO} or *GSDMD*^{KO} cells. ***:p<0.001.

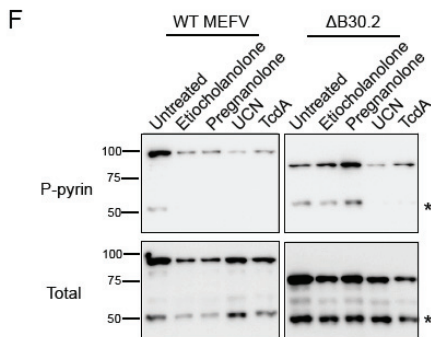
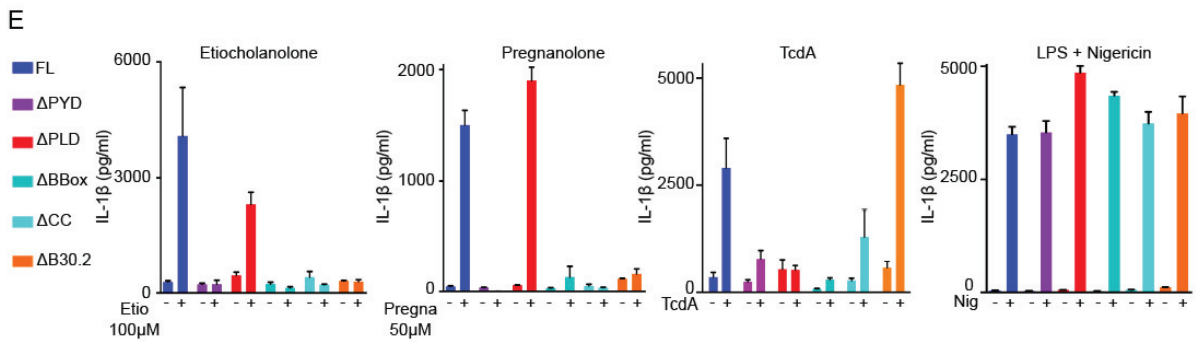
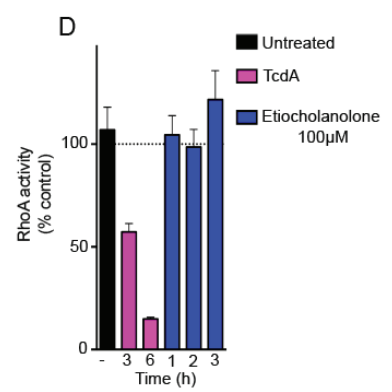
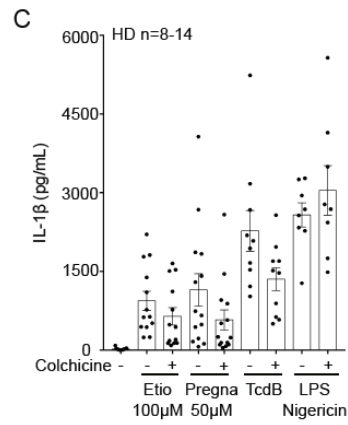
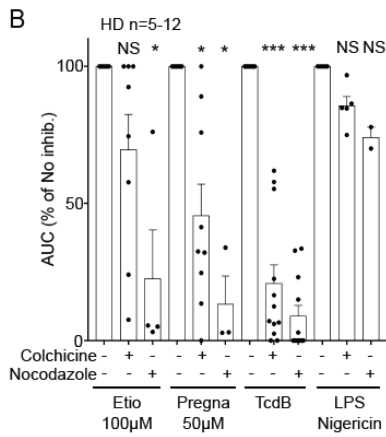
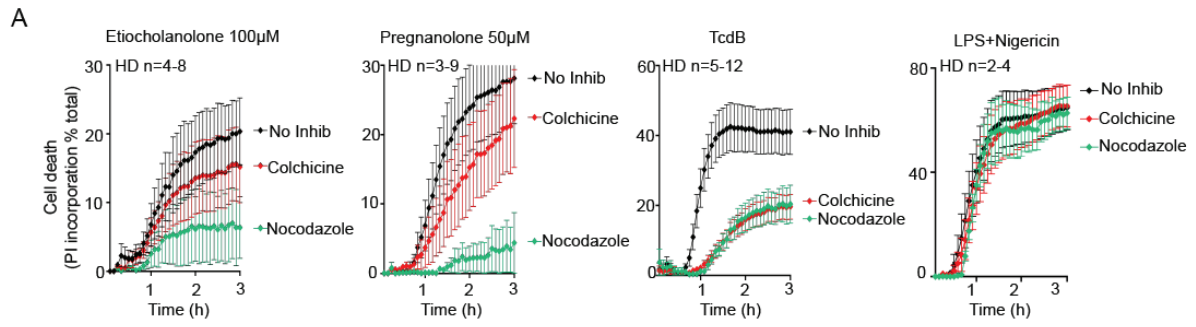


Figure 4: Pyrin inflammasome activation proceeds differently following TcdA/B and steroid catabolites addition.

(A) Monocytes from HD (n=2-12) were treated with colchicine or nocodazole and 30 min later with the indicated stimuli. Propidium iodide incorporation was monitored every 5 min for 3 h. (B) The Area Under the Curve (AUC) are shown. For each HD, the AUC values in the presence of inhibitors were normalized to the AUC value obtained in the absence of inhibitor. (C) Monocytes from HD (n=8-14) were treated with colchicine and 30 min later with the indicated stimuli. IL-1 β concentration in the supernatant was quantified at 3 h post-addition. (D) RhoA activity was determined by G-LISA at different time post-treatment in the lysate of U937 cells. The activity of the different treatments at the indicated time is presented in supplemental Fig. S4B. (E) Doxycycline-induced, PMA-differentiated U937 macrophages expressing *MEFV* Full-length (FL), deleted of the pyrin (Δ PYD), of the phosphorylated linker (Δ PLD), of the BBox (Δ Bbox), of the Coiled-coil (Δ CC) or the B30.2 (Δ B30.2) domains were treated LPS for 3 h and then with the indicated stimuli. IL-1 β concentration in the supernatant was quantified at 3 h post-addition. (F) Doxycycline-induced, U937 monocytes expressing WT or Δ B30.2 *MEFV* were treated with the indicated stimuli for 90 min. Pyrin S242 phosphorylation was assessed by Western blot analysis following immunoprecipitation. "*" indicates a cleaved form of pyrin. (A-E) Mean and SEM are shown. (B-C) each dot represents the value for one HD. (D-E) One experiment with technical triplicates representative of two (D) to three (E) independent experiments is shown. (B-C) Wilcoxon matched-pairs signed rank tests were performed to compare values with or without colchicine/nocodazole. Two-tailed p-values: (B) **p=0.0078; ***p<0.001 (C) ***p<0.001, **p=0.002 (D) Ordinary one way ANOVA with Holm-Sidak's correction for multiple tests was performed. *p=0.015, ***p<0.001. (E) Ordinary one way ANOVA with Sidak's correction for multiple tests was performed. *p=0.011, *** p<0.001.

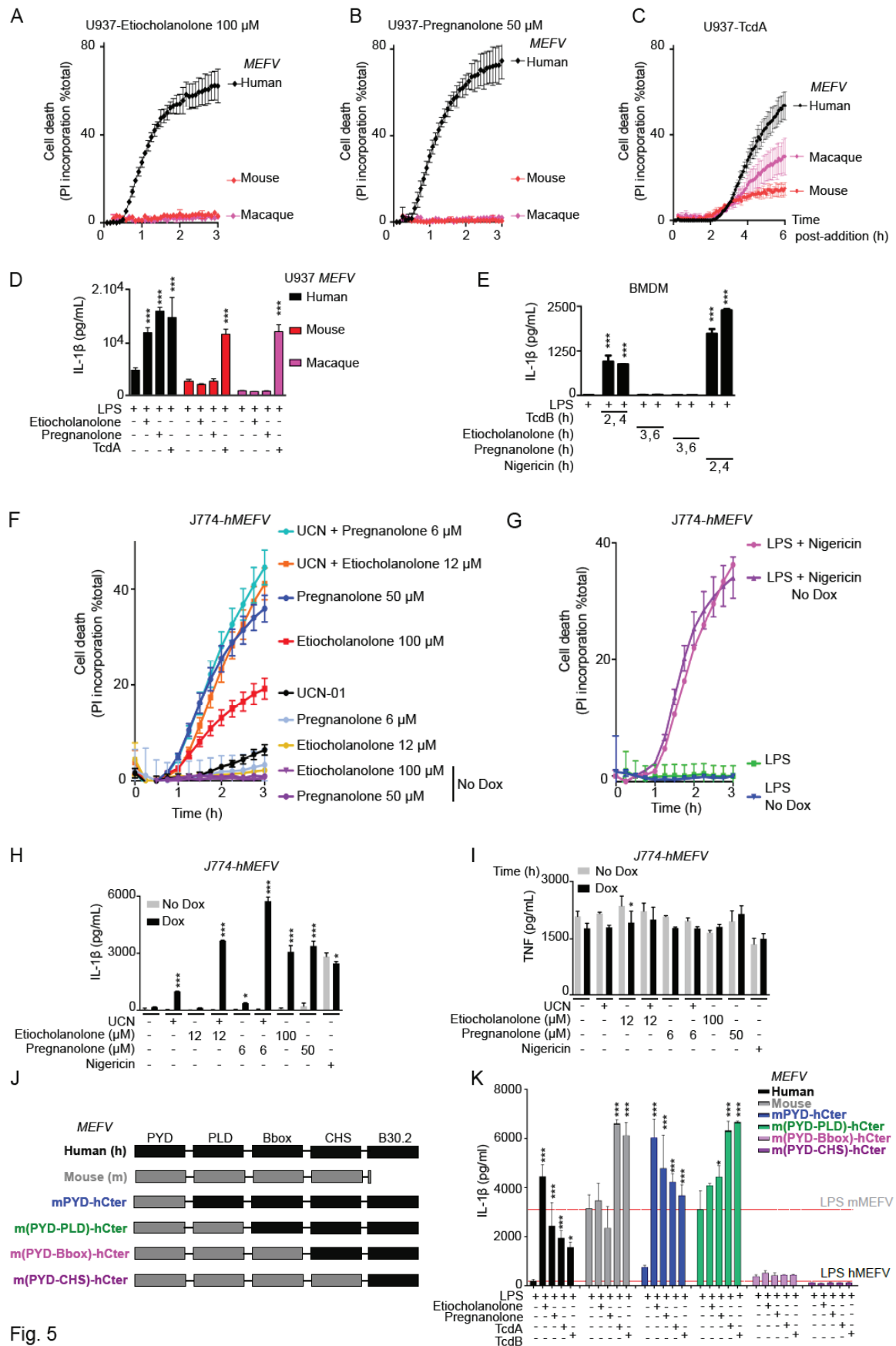


Fig. 5

Figure 5: The human specificity of the response to steroid catabolites is intrinsic to the pyrin protein.

(A-C) Doxycycline-induced U937 monocytes or (D, K) PMA-differentiated U937 macrophages expressing human (black), mouse (red), *macaca fascicularis* (magenta) or the indicated chimeric (J, K) *MEFV* were treated with the indicated stimuli. (A-C) Propidium iodide (PI) incorporation was monitored every 5 min for 3 to 6 h. (D, K) IL-1 β concentration in the supernatant was quantified at 3 h (Etiocolanolone, Pregnanolone) or 6 h (TcdA, TcdB) post-addition. (E) WT bone-marrow derived macrophages (BMDM) were primed for 16 h with LPS (100 ng/ml) and treated with TcdB (10 ng/ml), etiocholanolone (100 μ M), pregnanolone (50 μ M), or nigericin (10 μ g/mL). IL-1 β concentration in the supernatant was quantified at the indicated time point post-compound addition. (F-I) J774 macrophages expressing or not (No Dox) human *MEFV* were treated with the indicated stimuli. (F-G) Propidium iodide (PI) incorporation was monitored every 5 min for 3 h. (H-I) Cells were primed for 3h with LPS before stimuli addition. (H) IL-1 β and (I) TNF concentrations in the supernatant were quantified at 3 h post-addition. (K) The dotted lines indicate the basal value in LPS-treated U937 cells expressing human *MEFV* or murine *MEFV*. (A-I, K) one experiment representative of three independent experiments with mean and SEM of biological triplicates is shown. (D-E, H-I, K) One-way ANOVA with Sidak's test was used, ***: $p < 0.001$, (H) *: $p = 0.214$; (I) *: $p = 0.0304$; (K) from left to right: *: $p = 0.0123$, $p = 0.0159$.

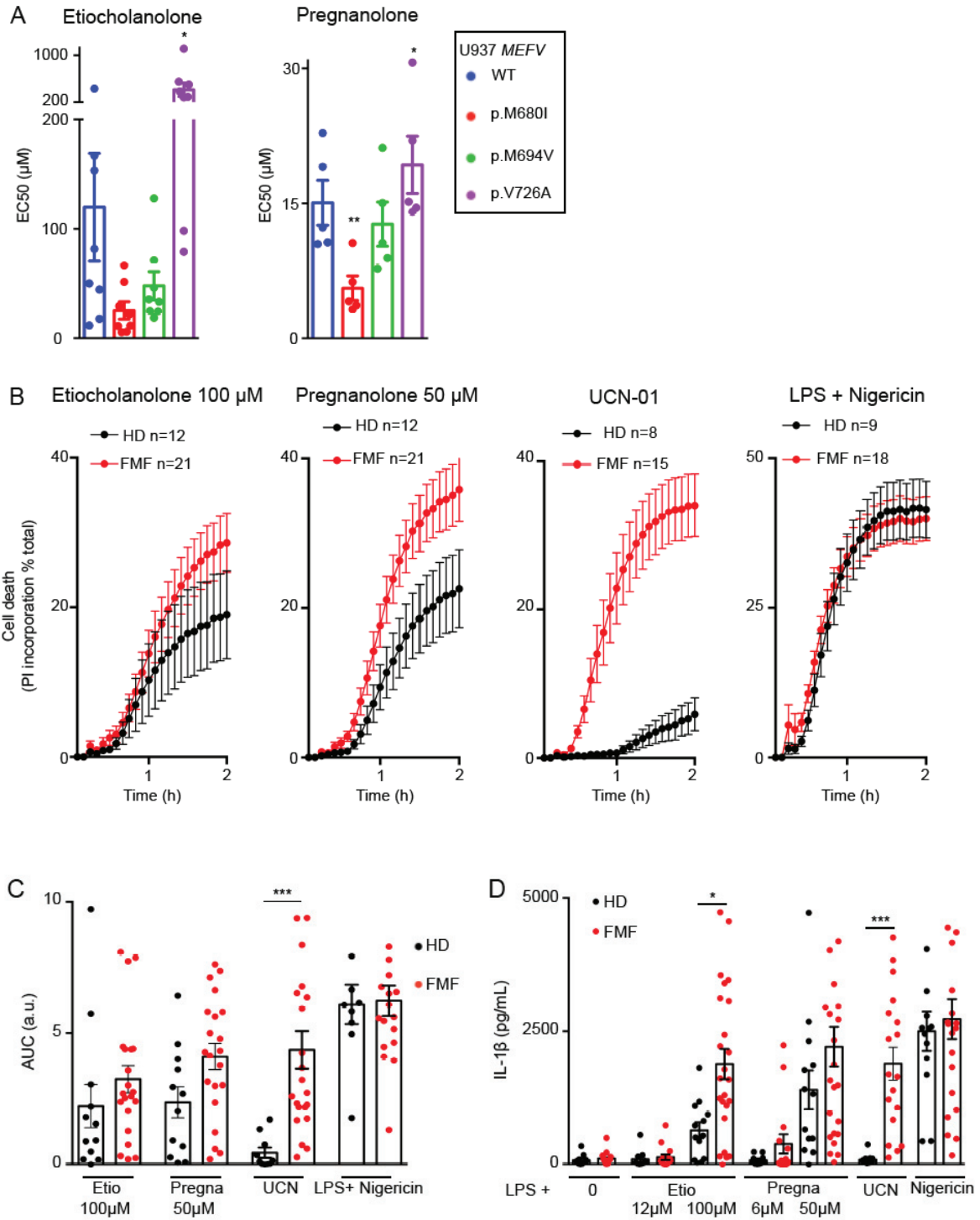


Figure 6: Monocytes from FMF patients display a moderately increased response to steroid catabolites compared to HD.

(A) U937 expressing the indicated *MEFV* variant were exposed to the indicated steroid catabolite and the EC50 was determined at 3 h post-addition. (B) monocytes from HD (n=8-12) or FMF patients (n=15-21) were treated with the indicated stimuli. Propidium iodide (PI) incorporation was monitored every 5 min for 2 h. (C) The corresponding area under the curve (AUC) are shown. (D) IL-1 β concentrations were determined at 3 h post addition of the indicated molecules. (A) Mean and SEM of five to eight independent experiments are shown. Each dot represents the mean value of a triplicate from one experiment. RM one-way ANOVA with Dunnet's multiple comparisons test was performed. Etio *: p=0.018; Pregna *: p=0.033 **: p=0.0042. (B) Mean and SEM of 8 to 21 individuals are show as indicated, each one corresponding to the average of a biological triplicate. (C) Each dot corresponds to the mean AUC of one individual performed in triplicates, the bar represents the mean of 8 to 21 individuals. (D) Each dot corresponds to the mean IL-1 β concentrations of one individual performed in triplicates, the bar represents the mean of 8 to 21 individuals. (C-D) One-way Anova with Sidak's multiple comparison test was applied; *p=0.015; ***p<0.001.

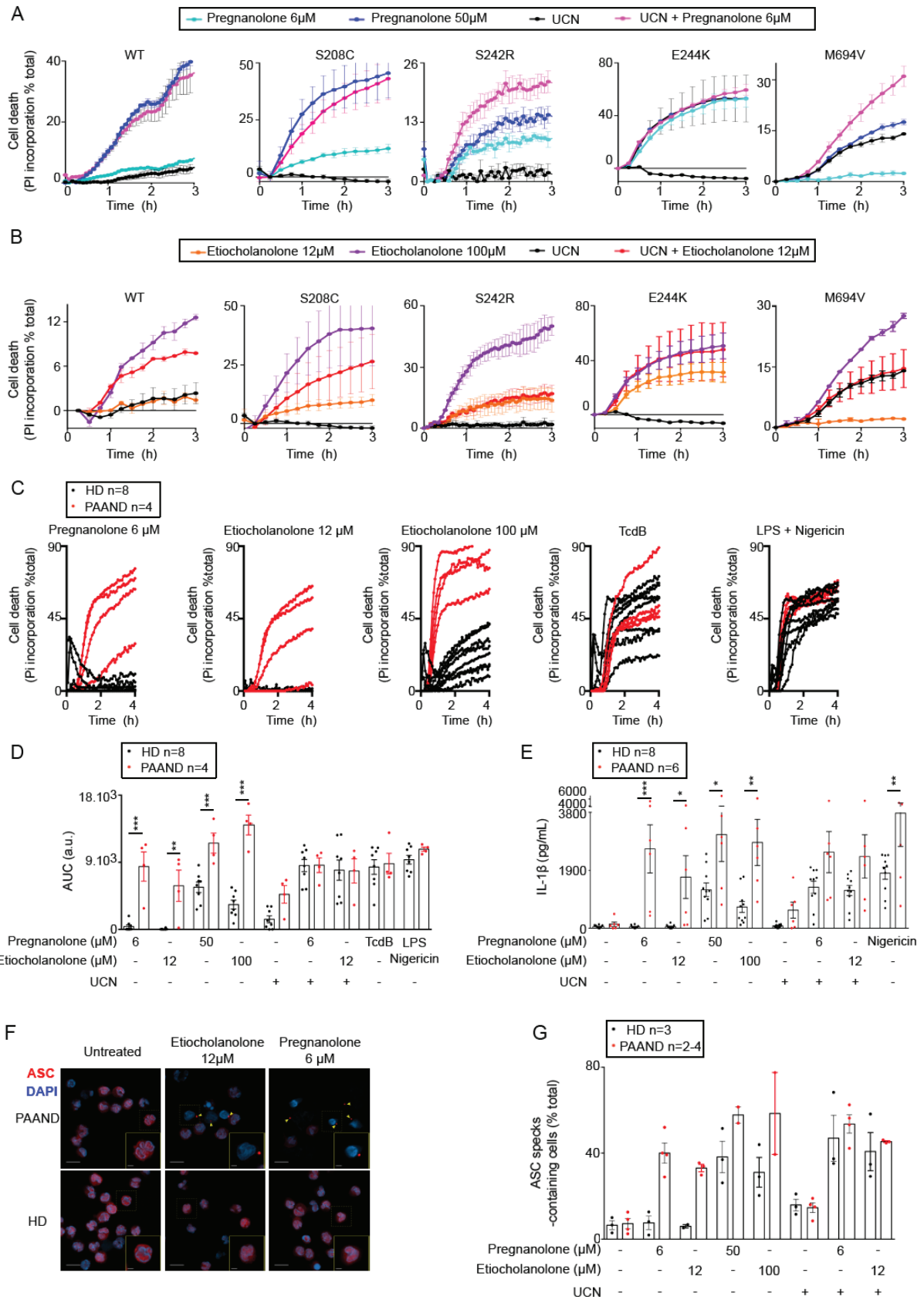


Figure 7: PAAND mutations confer hyper-responsiveness to steroid catabolites.

(A-B) U937 cell lines expressing WT or the indicated PAAND MEFV variant were treated with the indicated stimuli. Propidium iodide (PI) incorporation was monitored every 15 min for 3 h. (C-G) monocytes from PAAND patient(s) (red, n=4-6) or HD (black, n=8) were treated with the indicated stimuli. (C) Propidium iodide (PI) incorporation was monitored every 15 min for 4 h. (D) The corresponding area under the curve (AUC) are shown. (E) IL-1 β concentrations were determined in the cell supernatant after 3 h of LPS treatment followed by 1 h 30 of the indicated treatment. (F-G) ASC speck formation (indicated by yellow arrows) were monitored by immunofluorescence at 90 min post treatment. (F) Representative images are shown. The scale bars correspond to 10 and 2.5 μ M, in the main pictures and insets, respectively. (G) Quantification is shown. (A-B) One experiment representative of three independent experiments is shown. (A-B) Mean and SEM or (C) mean of triplicates are shown. (D, E) Each dot represents the mean of a triplicate for one individual. The bar represents the mean \pm SEM. One way ANOVA with Sidak's correction for multiple test was performed. (D) **: p=0.0011; ***: p<0.001; a.u.: arbitrary units. (E) Etio 12 μ M *:p=0.043; Pregna 50 μ M *:p=0.016; Etio 100 μ M **:p=0.0026; LPS Nig **:p=0.0064; ***: p=0.0001. (G) Kruskal-Wallis test with Dunn's multiple comparison was performed. Each dot corresponds to the percentage of ASC specks based on more than 100 cells counted per condition. Each dot represents the value for one individual. The bar represents the mean \pm SEM.

Name	Structure	LogP	Name	Structure	LogP
Etiocholanolone (3 α -hydroxy 5 β -androstan-17one)		4.2	5 β -Pregnan-3 α ,11 α -diol -20-one		
Pregnanolone (3 α -hydroxy 5 β -Pregnan-20one)		4.8	5 β -Pregnan-3 α ,11 β -diol -20-one		
Testosterone		4.1	3 α -hydroxy 5 β -Pregnan-11,20-dione		
Progesterone		4.7	5 β -Pregnan-3 α , 17diol-20-one		
Cortisol		2.6	5 β -Pregnan-3 α -ol		
Tetrahydro-cortisol		2.8	5 β -Pregnan-3 α ,21-diol-20-one		
Pregnanolone-sulfate		5.8	5 β -Pregnan-3 α ,21-diol-20-one 21-hemisuccinate		
3 β -hydroxy 5 β -androstan-17one			Androsterone		4.2

Table S1: Compounds present in the Prestwick library ("FDA-approved" 2013 version) and final concentration used in the screen (related to figure 1).

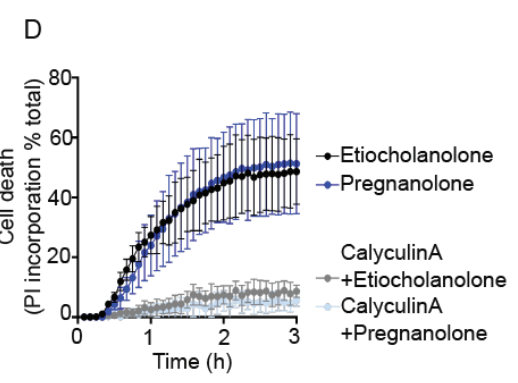
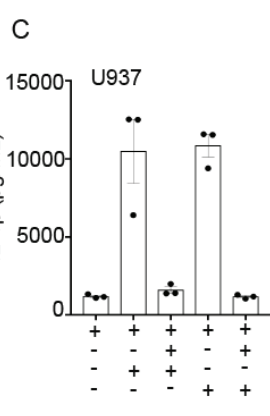
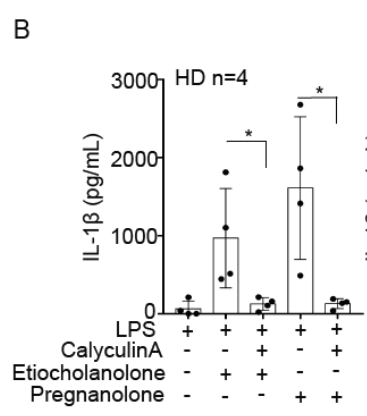
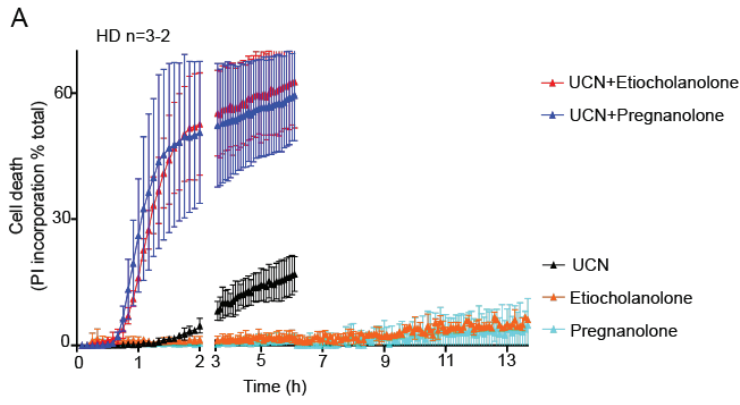


Figure S2: Long treatment with low concentrations of steroid catabolites do not trigger human monocyte death and Calyculin A blocks etiocholanolone and pregnanolone- mediated pyrin activation.

(A) Primary monocytes from healthy donors (HD, n=3-2) were pre-treated with pregnanolone (6 μ M) or etiocholanolone (12 μ M) for 1 h followed by addition of UCN-01. Cell death was monitored every 5 min for 6-13 h. UCN-01 alone triggers delayed apoptosis while low concentrations of steroid catabolites are inactive in the absence of UCN-01. (B) Primary monocytes from healthy donors (HD, n=4) were primed 3 h with LPS (10 ng/ml), pre-treated with Calyculin A (40 nM) for 30 minutes and treated with etiocholanolone (100 μ M) or pregnanolone (50 μ M). IL-1 β concentrations were determined in the cell supernatant 1 h 30 after the final treatment. (C) Doxycycline- induced, PMA-differentiated U937 macrophages expressing WT pyrin were primed 3 h with LPS (50 ng/ml), pre-treated with Calyculin A (40 nM) for 30 minutes and treated with etiocholanolone (100 μ M) or pregnanolone (50 μ M). IL-1 β concentrations were determined in the cell supernatant 3 h after the final treatment. (D) U937 cells expressing WT pyrin (in the presence of doxycycline) were pre-treated with Calyculin A (40 nM) for 30 minutes and treated with etiocholanolone (100 μ M) or pregnanolone (50 μ M). Cell death was monitored by following propidium iodide incorporation every 5 min for 3 h.

Data information: (B) each dot represents the value for one HD. Ordinary one way ANOVA with Holm-Sidak's multiple comparison test was performed. * $p < 0.005$. (C-D) One experiment with technical triplicates representative of three independent experiments is shown.

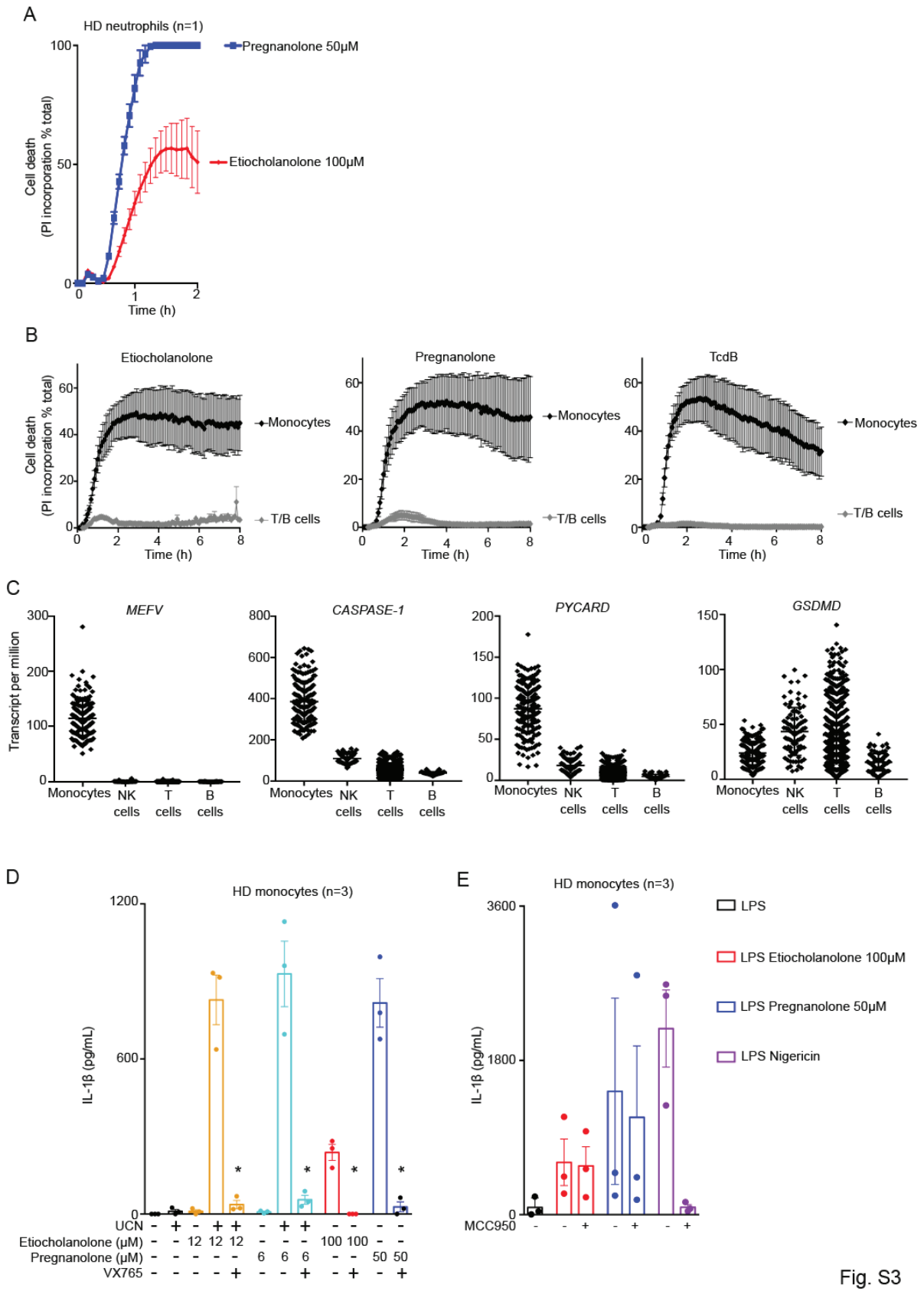
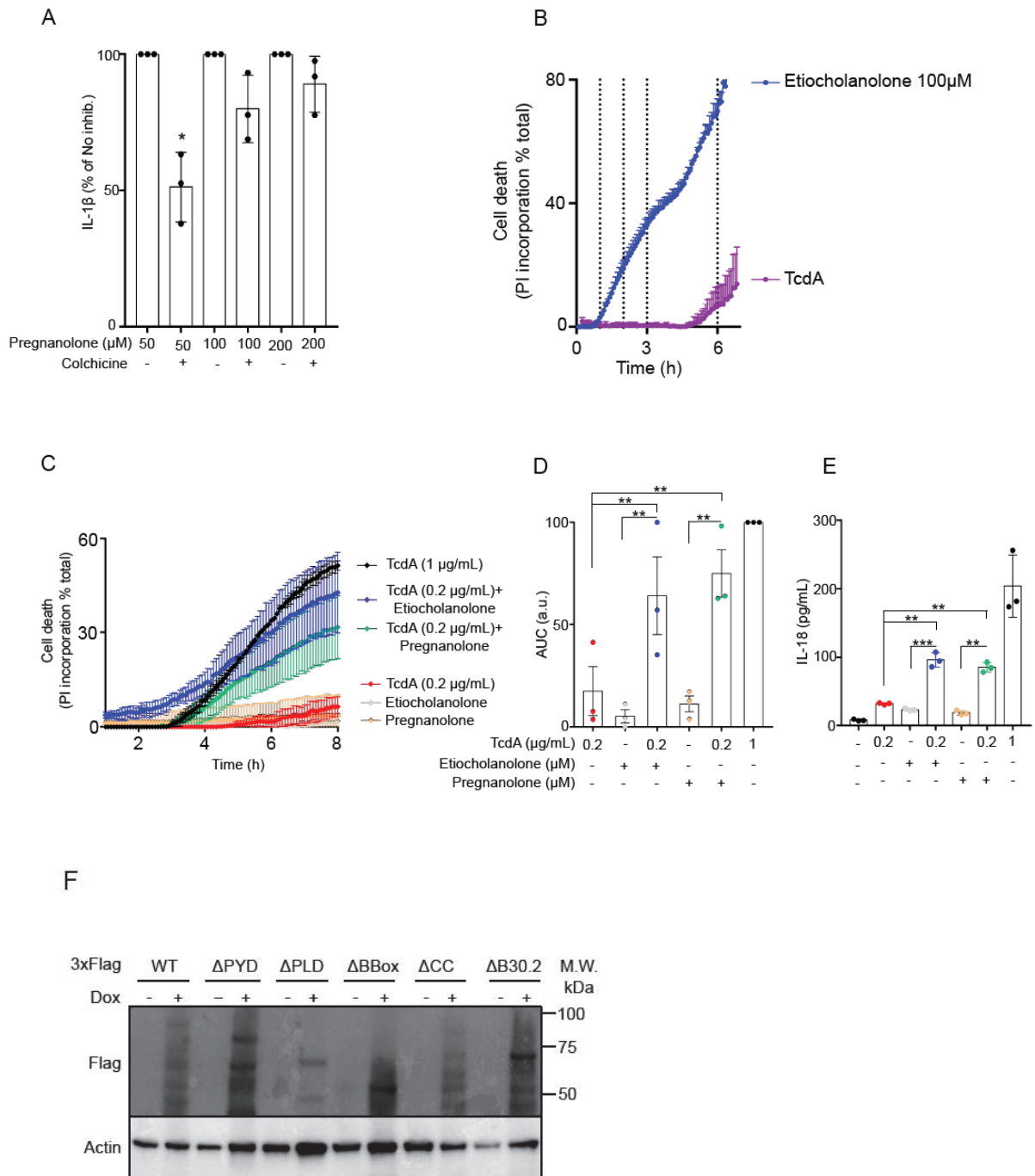


Fig. S3

Figure S3: The response to steroid catabolites is conserved in neutrophils but not in lymphocytes and is caspase-1-dependent, and NLRP3-independent in monocytes.

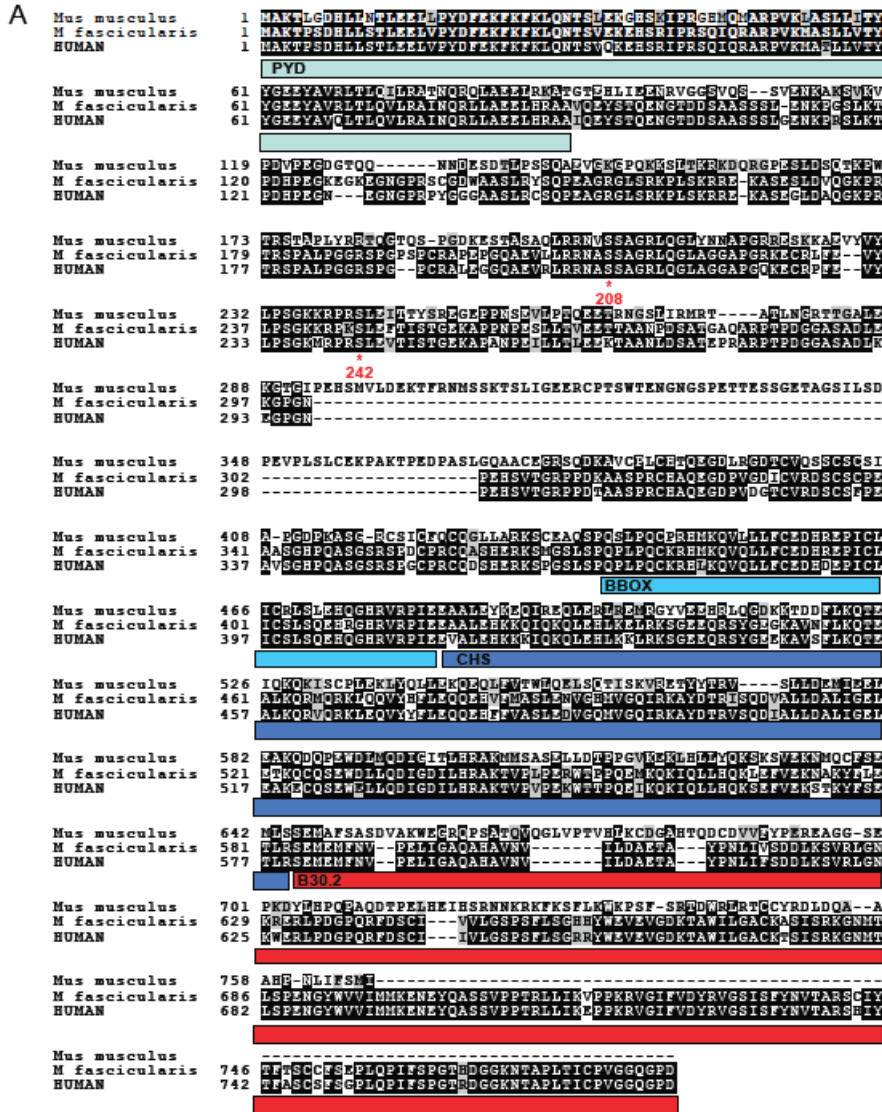
(A) Propidium iodide incorporation in neutrophils from one HD treated with pregnanolone or etiocholanolone was monitored every 5 min for 2 h. (B) Primary monocytes and lymphocytes from healthy donors (n=3) were treated with etiocholanolone (100 μ M), pregnanolone (50 μ M) or TcdB (125 ng/ml). Cell death was monitored every 5 min for 8 h. (C) *MEFV*, *CASPASE-1*, *PYCARD*, *GSDMD* gene expression levels in monocytes, NK cells and lymphocytes as determined by RNAseq. (D) HD monocytes (n=3) were treated with LPS for 2 h 30 followed by addition or not of (B) the caspase-1 inhibitor VX-765, (E) the NLRP3 inhibitor (MCC950) and 30 min later of the indicated molecules. IL-1 β concentrations were determined in the cell supernatant 1 h 30 after the final treatment.

Data information: (A) One experiment representative of two independent experiments is shown. Mean and SEM of a technical triplicates are shown. Cell death was normalized using untreated neutrophils (0%) and Triton X100-treated neutrophils (100%). (B) each dot represents the mean of three healthy donors values each one from a technical triplicate. SEM is shown. (C) Each dot represents one RNAseq value from one healthy donor extracted from the database of Immune Cell Expression: <https://dice-database.org/>. (D-E): Each dot represents the value of one HD (mean of a triplicate). The bar represents the mean \pm SEM of 3 HD values. Matched one-way ANOVA with Sidak's multiple comparisons test was performed to compare untreated vs. VX-765-treated samples. *: p<0.05.



Supplemental Fig. S4: Increasing pregnanolone doses overcome colchicine inhibition and low concentrations of catabolites synergize with low TcdA doses for pyrin inflammasome activation.

(A) Monocytes from HD (n=3) were treated with colchicine and 30 min later with Pregnanolone (50-100-200 μ M). IL-1 β concentration in the supernatant was quantified at 3 h post-addition. Values obtained in the presence of inhibitors were normalized to the value obtained without the inhibitor. (B) U937 cells expressing WT pyrin (in the presence of doxycycline) were treated with etiocholanolone or TcdA. Cell death was monitored by following propidium iodide incorporation every 5 min for 7 h. The dotted vertical lines indicate the time points at which U937 cells were collected in a parallel experiment to assess RhoA inhibition (see Fig. 4D; 1, 2, 3 h for etiocholanolone and 3, 6 h for TcdA treatment). (C-D) U937 cells expressing WT pyrin (in the presence of doxycycline) were pre-treated with etiocholanolone or pregnanolone for 1h and treated with TcdA at the indicated concentrations. Cell death was monitored by following propidium iodide incorporation every 5 min for 8 h. (D) The Area Under the Curve (AUC) was computed for 3 different experiments. (E) Doxycycline-induced, U937 monocytes expressing WT pyrin were treated as in (C-D). IL-18 concentration in the supernatant was quantified at 6 h post-treatment. (F) U937 cell lines expressing the indicated 3xFlag-MEFV variants were analysed by Western blot in the presence or absence of doxycycline (Dox). Actin was used as a loading control.



Supplemental Fig. S5: Alignment of human, mouse and *macaca fascicularis* pyrin proteins and validation of cell lines with ectopic expression of human, mouse, macaque or chimeric pyrin.

(A) The PYD, the two critical serine residues, the B-Box, Central Helical scaffold (CHS) and B-30.2 domains are shown. (B-C) Western blot analysis of U937 (left panel) or J774 (right panel) cells expressing 3xFlag-pyrin from the indicated species or the indicated chimeric proteins. Cells were treated or not with doxycycline (DOX) and cell lysates were analysed with anti-Flag (top panel) or anti-actin (bottom panel) antibodies. (D) U937 cell lines expressing the indicated chimera were treated with Etiocholanolone (100 μ M). Propidium iodide (PI) incorporation was monitored every 5 min for 12 h.

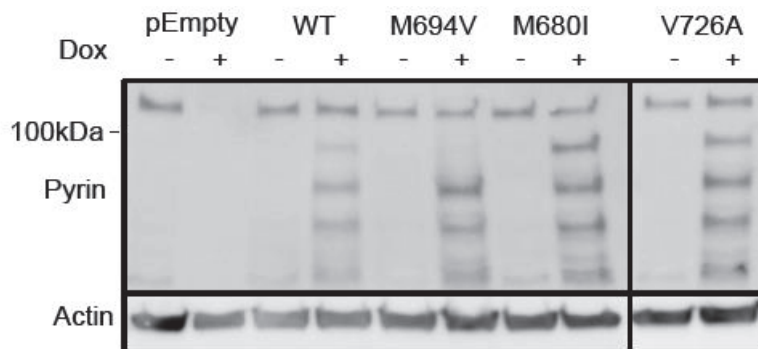
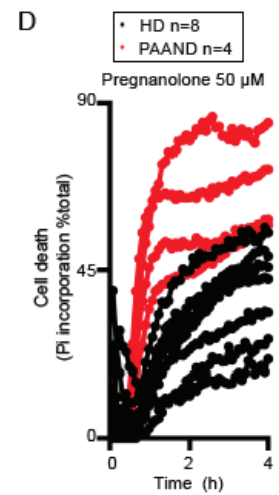
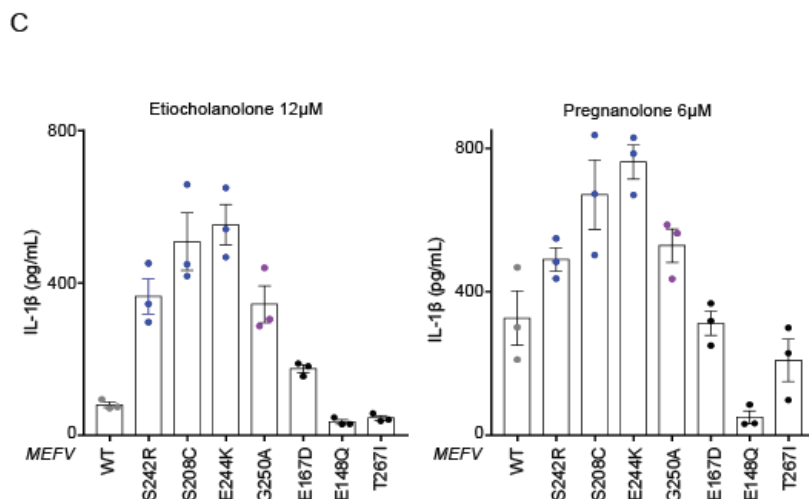
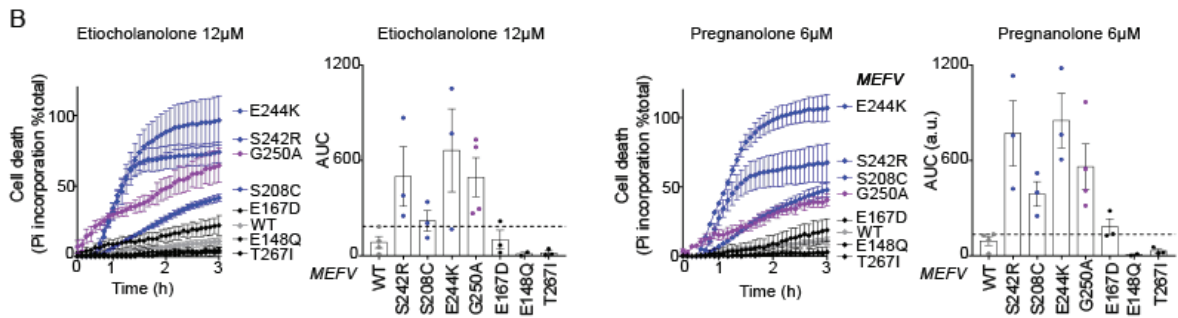
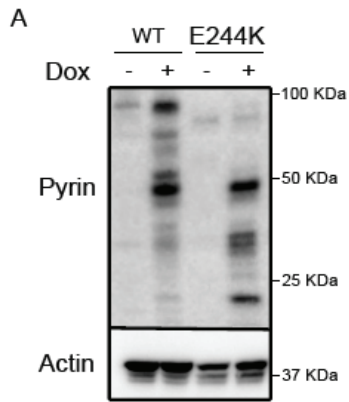


Fig. S6

Supplemental Fig. S6: Western blot analysis of U937 cell expressing p.V726A pyrin.

U937 cell lines expressing the indicated pyrin variants were treated or not with doxycycline (Dox) and cell lysates were analysed with anti-pyrin (top panel) or anti-actin (bottom panel) antibodies. Cell lines expressing WT, M694V and M680I pyrin variants have been previously characterized.



Supplemental Fig. S7: PAAND patients monocytes present a strong increase in steroid catabolites responses compared to HD. (A) Western blot analysis of U937 cell expressing p.E244K pyrin variant. U937 cell lines expressing the indicated pyrin protein were treated or not with doxycycline (Dox) and cell lysates were analysed with anti-Pyrin (top panel) or anti-actin (bottom panel) antibodies. Cell lines expressing WT, S208C and S242R pyrin variants have been previously characterized ¹¹. (B) U937 cells expressing *MEFV* exon 2 variants of unknown significance or WT *MEFV* were treated with low doses of etiocholanolone or pregnanolone. Cell death was monitored every 5 min for 3 h. The Area Under the Curve (AUC) was computed for 3-4 different experiments. (C) Doxycycline-induced, PMA-differentiated U937 macrophages expressing *MEFV* exon 2 variants of unknown significance or WT *MEFV*, were primed with LPS during 3 h and treated with low doses of etiocholanolone or pregnanolone. IL-1 β concentration in the supernatant was quantified at 3 h post-treatment. (D) Monocytes from PAAND patients (red, n=4) or HD (black, n=8) were treated with pregnanolone (50 μ M). Cell death/propidium iodide incorporation was monitored in real time every 15 min for 4 h. Each dot corresponds to the average of a triplicate for one individual.

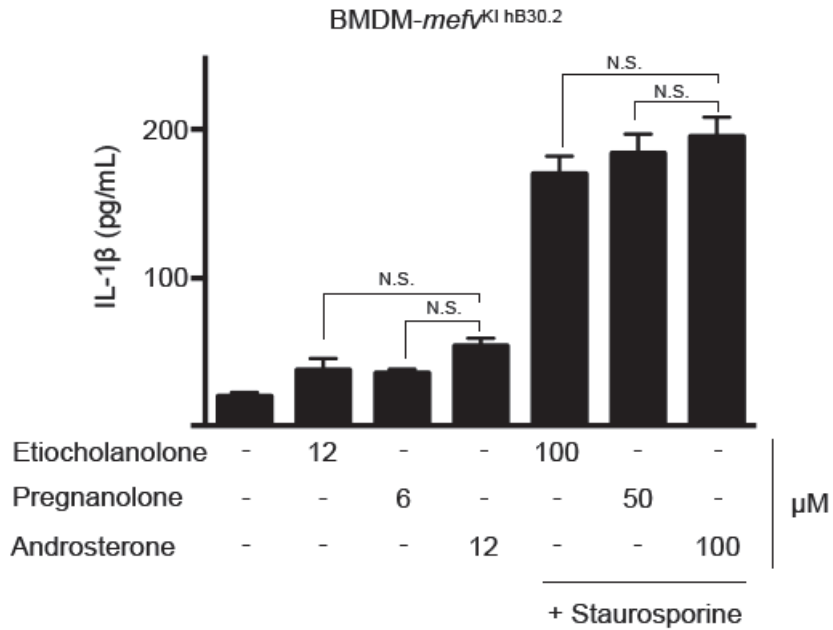


Fig. S8

Supplemental Fig. S8: Bone marrow derived macrophages (BMDM) from human B30.2 knock-in mice do not respond to steroid catabolites.

BMDM from *mefv*^{KI} hB30.2p.M694V mice harbouring human B30.2 domain in fusion with murine pyrin protein were treated with the indicated steroid molecules for 1 h followed by addition (or not) of staurosporine (1 μ M) for 3 h. IL-1 β concentrations were determined in the cell supernatant 4 h after steroid addition. Androsterone (Andro) was used as a negative control based on Fig. 2C results. Etiocholanolone and pregnanolone treatment did not differ from androsterone treatment in the presence or absence of the PKC superfamily inhibitor, staurosporine, used here to trigger pyrin step 1. One way ANOVA with Sidak's multiple comparisons test was performed. N.S.: not significant

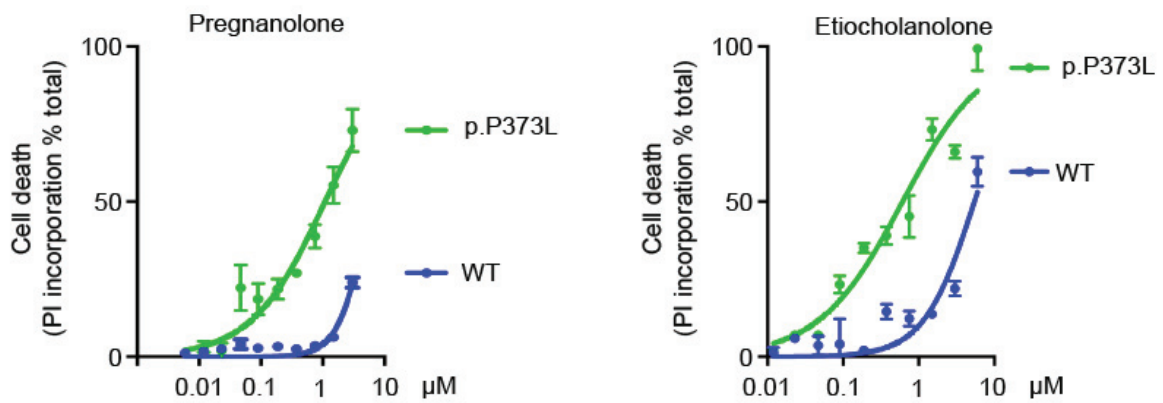
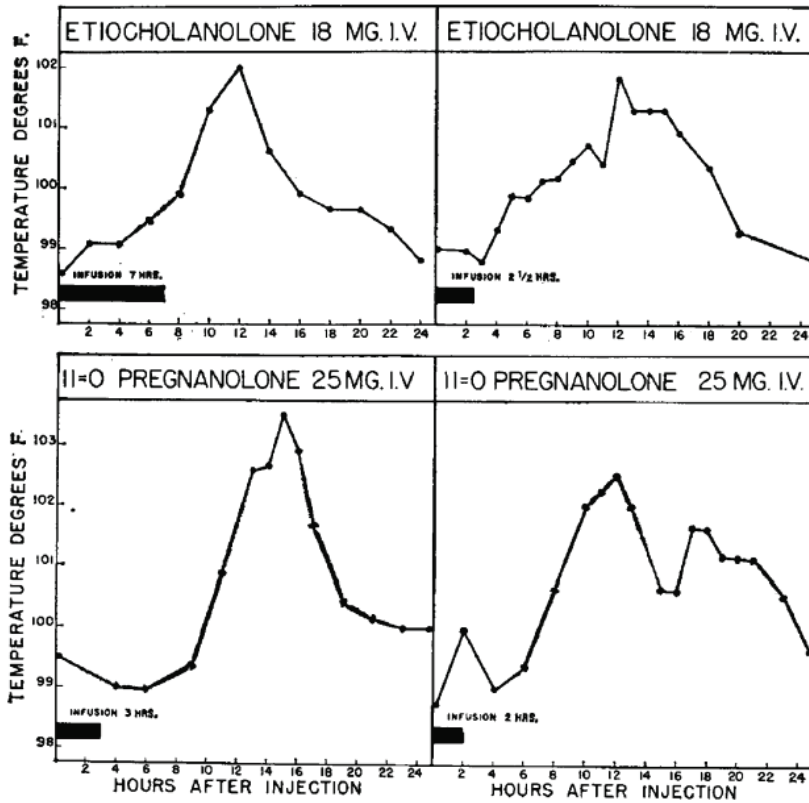


Fig. S9

Supplemental Fig. S9: p.P373L *MEFV* variant confers responsiveness to nanomolar concentrations of steroid catabolites.

U937 cells expressing the indicated *MEFV* variant (green p.P373L; blue WT) were treated with doxycycline for 16 h followed by addition of pregnanolone or etiocholanolone at various concentrations. Cell death was measured at 3 h post-addition.

Data information: One experiment representative of three independent experiment is shown. Mean and SEM of triplicates are shown. Non-linear regression curve computed using least squares fit method is shown.



Supplemental Fig. S10: Etiocholanolone and pregnanolone trigger steroid fever in humans.

Figure from ⁴³. Historical evidence that intravenous injection of etiocholanolone (top panel) or pregnanolone (bottom panel) trigger fever in humans. Results from 4 individuals healthy volunteers are shown.

Results. Part 2

Context

The second part of the Results section consists of a scientific article ready for submission, the targeted journal is Cell Death and Differentiation.

Work on this article was performed in parallel with the article presented in Part 1, the two articles are complementary. Here, we focused on establishing the role of B30.2 as a negative regulator of pyrin inflammasome – a role long suspected but never before clearly demonstrated. We further investigated the role of another pyrin domain, the CHS, to discover that it also plays an important part in pyrin regulation. Additionally, we further characterized pyrin sensing of steroid hormone catabolites.

Mutations in the B30.2 and the Central Helical scaffold domains of pyrin differentially affect inflammasome activation

Daria Chirita¹, Flora Magnotti¹, Pauline Bronnec¹, Sarah Dalmon¹, Amandine Martin¹, Mathieu Gerfaud-Valentin², Pascal Sève², Alexandre Belot^{1,3,4}, Agnes Duquesne⁴, Irene Lemelle⁴, Anne Contis⁵, Gaetane Nocturne⁶, Sophie Georgin-Lavialle⁷, Guilaine Boursier⁸, Isabelle Touitou⁸, Yvan Jamilloux^{1,2,3}, Thomas Henry^{1,@}

¹ CIRI, Centre International de Recherche en Infectiologie, Univ Lyon, Inserm U1111, Université Claude Bernard Lyon 1, CNRS, UMR5308, ENS de Lyon, Univ Lyon, F-69007, LYON, France^[1]_{SEP}

² Department of Internal Medicine, University Hospital Croix-Rousse, Lyon 1 University, Lyon, France

³ LIFE, Lyon Immunopathology Federation, Lyon, France

⁴ Department of Pediatric Nephrology, Rheumatology, Dermatology, Reference centre for Rheumatic, AutoImmune and Systemic diseases in children (RAISE), Hôpital Femme Mère Enfant, CHU Lyon, Lyon, France

⁵ Department of Internal Medicine, Saint André Hospital, CHU Bordeaux, Bordeaux, France.

⁶ Department of Rheumatology, Assistance Publique Hôpitaux de Paris, Hôpital Bicêtre, National Reference Center for Rare Systemic Autoimmune Diseases, Le Kremlin-Bicêtre, France

⁷ Sorbonne University, department of internal medicine, Tenon hospital, DMU 3ID, AP-HP, National reference center for autoinflammatory diseases and inflammatory Amyloidosis (CEREMAIA), INSERM U938, Paris, France

⁸ Department of Medical Genetics, Rare Diseases and Personalized Medicine, Rare and Autoinflammatory Diseases Unit CHU Montpellier, Reference Center for Autoinflammatory Diseases and Amyloidosis (Ceremaia), Montpellier, France

Abstract

Familial Mediterranean Fever (FMF) is the most common monogenic autoinflammatory disorder. FMF is caused by mutations in the *MEFV* gene, encoding pyrin, an inflammasome sensor. The best characterized pathogenic mutations associated with FMF cluster in exon 10 although mutations have been described along the whole *MEFV* coding sequence. Exon 10 encodes the B30.2 domain of the pyrin protein, but the function of this human-specific domain remains unclear. Pyrin is an inflammasome sensor detecting RhoA GTPase inhibition following exposure to bacterial toxins such as TcdA. Here, we demonstrate that B30.2 is dispensable for pyrin inflammasome activation in response to this toxin. Deletion of B30.2 domain mimics the most typical FMF-associated mutation and confers spontaneous inflammasome activation in response to pyrin dephosphorylation. Our results indicate that the B30.2 domain is a negative regulator of the pyrin inflammasome that acts independently from and downstream of pyrin dephosphorylation and independently of caspase-1. Additionally, we identify the central helical scaffold of pyrin, which lies immediately upstream of the B30.2 domain as a second regulatory domain. Mutations affecting the CHS domain mimic pathogenic mutations in the B30.2 domain and leave pyrin inflammasome activation under the sole control of the dephosphorylation. In addition, specific mutations in the CHS domain strongly increase the cell susceptibility to steroid catabolites, recently described to activate pyrin, in both a cell line model and in monocytes from genotype-selected FMF patients. Taken together, our work reveals the existence of two distinct regulatory regions at the C-terminus of the pyrin protein, that act in a distinct manner to regulate positively or negatively inflammasome activation. Furthermore, our results indicate that different mutations in pyrin regulatory domains have different functional impacts on the pyrin inflammasome which could account for the different subsets of pyrin-associated autoinflammatory diseases.

Introduction

Inflammasomes are multiprotein platforms assembled in the cytosol upon sensing of microbial infections, danger signals, or alteration of the cell homeostasis (F. Martinon et al., 2002). Inflammasome activation leads to activation of the pro-inflammatory caspase-1, release of IL-1 β and IL-18. In most cases, inflammasome activation leads to a fast cell death, termed pyroptosis which results from caspase-1-mediated cleavage of the pore-forming protein, gasdermin D. Inflammasomes participate in the innate immune defenses (Broz and Monack, 2011). Yet, inflammasomes are also involved in deleterious inflammatory processes. Particularly, mutations in genes encoding various inflammasome sensors are responsible for rare autoinflammatory diseases (Manthiram et al., 2017).

Pyrin is an inflammasome sensor acting as a guard of RhoA GTPases activity. Various bacterial toxins (such as *Clostridioides difficile* toxin A, TcdA) or effectors inhibit RhoA and trigger pyrin activation. The mechanisms linking RhoA inhibition to pyrin activation have been partly solved (Magnotti et al., 2019; Masters et al., 2016; Park et al., 2016). At steady state, RhoA activates its effectors including PKN1 and PKN2, two kinases that phosphorylate pyrin on two serine residues (S208 and S242). Phosphorylated pyrin interacts with 14-3-3 chaperone proteins that sequester pyrin away from the inflammasome adaptor, ASC (Gao et al., 2016; Jeru et al., 2005; Van Gorp et al., 2016). Inhibition of RhoA and the ensuing deactivation of PKN1/2 leads to the PP2A-mediated dephosphorylation of pyrin (Malik et al., 2022). Yet, this is not sufficient to trigger pyrin inflammasome activation. Another poorly understood mechanism controls pyrin inflammasome activation downstream of pyrin dephosphorylation in a microtubule-dependent manner (Gao et al., 2016; Magnotti et al., 2019; Van Gorp et al., 2016). In addition to RhoA inhibition, we and others recently identified steroid metabolites/analogues that can activate pyrin in a B30.2-dependent manner (Alimov et al., 2019; Magnotti et al., 2021).

Mutations in *MEFV*, the gene encoding pyrin, cause two autoinflammatory diseases, familial Mediterranean fever (FMF) and pyrin-associated autoinflammation with neutrophilic dermatosis (PAAND) (“A candidate gene for familial Mediterranean fever. The French FMF Consortium,” 1997; Jamilloux et al., 2018; Masters et al., 2016; The International FMF Consortium, 1997). PAAND are caused by mutations affecting the phosphorylated serine or neighboring residues involved in the interaction with 14-3-3 proteins (Masters et al., 2016; Moghaddas et al., 2017). The link between genotype and phenotype in FMF is more complex and less understood (Touitou, 2001). The prototypical FMF disease is a recessive disease due to bi-allelic mutations in *MEFV* exon 10, encoding pyrin B30.2 domain with the most frequent pathogenic mutation being p.M694V. FMF-associated *MEFV* mutations deregulate the pyrin inflammasome in monocytes by lifting the requirement for an intact microtubule network (Shiba et al., 2019; Van Gorp et al., 2016), by invalidating pyrin regulatory

mechanism 2 and leaving its activation under the sole control of its dephosphorylation (Magnotti et al., 2019). These mutations result in pyrin inflammasome demonstrating a lower threshold of activation to specific pyrin agonists (Jamilloux et al., 2018) and higher responses to LPS exposure (Omenetti et al., 2014). Beside *MEFV* exon 10 mutations, a number of patients with a clinical diagnosis of FMF have *MEFV* mutations affecting other exons (Touitou, 2001). In addition, a number of these mutations results in FMF diseases with a dominant inheritance pattern (Aldea et al., 2004; Rowczenio et al., 2020). Most of these mutations are of unknown significance due to their rare frequency in the human population and due to lack of knowledge on the role of affected domain in pyrin regulation.

Here, we studied the role of the two C-terminal domains of pyrin in inflammasome activation in response to diverse stimuli to increase our knowledge on the regulatory mechanisms controlling pyrin inflammasome activation and the impact of FMF-associated mutations.

Results

B30.2 domain is dispensable for pyrin activation in response to TcdA

Pyrin is a multidomain protein containing a PYD domain, a linker domain containing the two critical phosphorylation residues and encoded by exon 2, a B-box domain, a central helical scaffold and a B30.2 domain. The role of each domain in pyrin inflammasome activation is still unclear. To answer this question, we used the human monocytic cell line, U937 and generated cell lines stably expressing doxycycline-inducible pyrin variants that lack one of the domains (Fig.1A). U937 cells stably expressing the classical FMF-associated *MEFV* variant p.M694V were also included as a control. The obtained monocytes were first stimulated with *C. difficile* toxin A (TcdA) and IL-18 release was monitored as an inflammasome readout (Fig. 1B). Cells expressing the pyrin variant lacking the B30.2 domain (Δ B30.2) responded to TcdA and secreted similar or even slightly higher IL-18 levels than cells expressing WT pyrin. In contrast, all the other domain deletions strongly decreased (coiled-coil domain deletion) or abolished IL-18 secretion in response to TcdA. Cells expressing p.M694V pyrin secreted higher level of IL-18 than cells expressing WT pyrin in agreement with the hyper-reactivity of primary monocytes from FMF patients to clostridial toxins (Honda et al., 2021; Jamilloux et al., 2018). Undifferentiated U937 cells are deficient for IL-1 β production. U937 cells were thus differentiated into macrophages using PMA and LPS was used to induce proIL-1 β expression. Similarly, PMA-differentiated U937 macrophages expressing Δ B30.2 pyrin variant released high levels of IL-1 β (Fig. 1C) while all the other cell lines expressing deletion mutants led to minimal IL-1 β secretion. No major differences in IL-18 or IL-1 β secretion were observed following treatment with the NLRP3-specific stimulus LPS + nigericin (Fig.1 D-E), indicating that the pyrin exon 2-encoded phosphorylated linker domain, the B-box and the

coiled-coil domains are specifically required for inflammasome cytokines secretion in response to the pyrin-specific stimulus TcdA. These results indicated that the B30.2 domain is dispensable for pyrin activation in response to TcdA.

Deletion of the B30.2 domain suppresses pyrin regulatory step 2.

We have previously demonstrated that FMF-associated p.M694V/I or p.M680I mutations lead to the loss of a regulatory mechanism and to the exclusive control of the pyrin inflammasome by phosphorylation/dephosphorylation (Magnotti et al., 2019). This defect can be functionally evidenced by treating cells with a PKC superfamily inhibitor UCN-01, that inhibits PKN1 and PKN2, leading to pyrin dephosphorylation (Magnotti et al., 2019). Interestingly, Δ B30.2 pyrin expressing cells released high levels of IL-18 in response to UCN-01. As expected, cells expressing WT pyrin did not release IL-18 in contrast to cells expressing p.M694V variant (Fig. 2A). Similarly, upon differentiation into macrophages and treatment with UCN-01, only cells expressing p.M694V or Δ B30.2 *MEFV* variants led to a markedly greater secretion of IL-1 β than WT pyrin-expressing cells (Fig. 2B). These results suggest that deletion of the B30.2 domain abolishes the second pyrin regulatory mechanism to leave pyrin activation under the sole control of pyrin dephosphorylation.

To confirm this phenotype genetically without relying on a chemical inhibitor, we generated a U937 cell line invalidated for step 1 inhibitory mechanism (p.S08C/S242R phospho-null mutations) on a Δ B30.2 background. The phospho-null mutations combined with the p.M694V mutation (p.S208C/S242R/M694V) yield to a constitutively activated pyrin inflammasome (Magnotti et al., 2019). The corresponding cell line was used as a positive control. Importantly, doxycycline-mediated induction of p.S208C/S242R/ Δ B30.2 pyrin variant was sufficient to trigger cell death indicating that this protein is constitutively activated (Fig. 2C, D). Due to the high doxycycline-induced cell death, these cell lines barely responded to UCN-01 stimulation in contrast to p.M694V or Δ B30.2 single mutants (Fig. 2C, E). Similarly, induction of the p.S208C/S242R/ Δ B30.2 pyrin protein led to potent IL-18 secretion in the absence of any additional stimulus (Fig. 2F). These results indicate that deletion of the B30.2 domain fully invalidated pyrin regulatory mechanism 2 and, when combined with mutations invalidating pyrin regulatory mechanism 1, led to constitutive activation of this pyrin variant. Taken together these results demonstrate that the B30.2 domain of pyrin acts as a negative regulator of pyrin activation following TcdA treatment, UCN-01-mediated dephosphorylation or genetic invalidation of phosphorylation sites.

The B30.2 domain-mediated regulation acts downstream of pyrin dephosphorylation, upstream of ASC speck formation and, independently from caspase-1.

The above results suggest that pyrin B30.2 domain-mediated regulation acts on pyrin regulatory mechanism 2 and not on the first regulatory mechanism associated with pyrin phosphorylation/dephosphorylation. Since the impact of FMF-associated, B30.2-affecting point mutations on phosphorylation is unclear (Gao et al., 2016; Magnotti et al., 2021; Park et al., 2016; Van Gorp et al., 2016), we investigated the impact of B30.2 deletion on pyrin dephosphorylation. Although at steady state, the Δ B30.2 pyrin protein was expressed at higher level than WT or p.M694V protein variants (possibly reflecting a greater stability), B30.2 deletion had no impact on UCN-01-mediated pyrin dephosphorylation (Fig. 3A-B). The B30.2-mediated regulation thus likely occurs downstream of pyrin dephosphorylation.

To further map the B30.2-mediated regulation along the pyrin inflammasome activation process, we monitored ASC speck formation following UCN-01 treatment. As expected, and in line with the results presented above, UCN-01-mediated pyrin dephosphorylation was sufficient to trigger ASC speck formation in cells expressing p.M694V or Δ B30.2 pyrin variants (Fig 3, C-D). Cells expressing WT pyrin did not display any increase in ASC speck formation in the presence of UCN-01 (i.e. upon pyrin dephosphorylation). These results thus indicate that the B30.2-mediated regulation takes place downstream of pyrin dephosphorylation but upstream of ASC speck formation.

The B30.2 domain has been shown to interact with caspase-1 leading to the hypothesis that the B30.2 domain could regulate pyrin inflammasome through caspase-1 inhibition (Arakelov et al., 2018; Chae et al., 2006, p. 2; Fayez et al., 2022). The above results demonstrate that the B30.2 domain regulate pyrin activation upstream of ASC speck formation suggesting that it may act independently of caspase-1. To validate this finding, we transduced the various pyrin mutants in caspase-1-deficient cells and quantified ASC speck formation in response to UCN-01 (Fig. 3C). ASC speck formation was slightly higher in these cells likely due to the lack of caspase-1-mediated pyroptosis. Yet, in the absence of caspase-1, UCN-01 increased ASC speck formation in Δ B30.2 pyrin-expressing cells but not in WT pyrin-expressing cells clearly indicating that B30.2 negatively regulates pyrin inflammasome activation downstream of the dephosphorylation, upstream of ASC speck formation and independently of caspase-1. Since p.M694V mimics B30.2 deletion for all the above assays, these results suggest that the p.M694V mutation fully abolishes the negative regulatory function of this domain. This exon 10-encoded mutation may thus be classified as a loss-of-function mutation with regard to the functionality of the B30.2 domain (loss of the negative regulation) and thus a as gain of function in term of the full protein.

Mutations in the Central Helical Scaffold phenocopy B30.2 pathogenic mutations in terms of UCN-01-mediated responses.

Structural data on the C-terminal part of the pyrin protein indicates that the B30.2 domain interacts with another domain, termed the central helical scaffold which is made of coiled-coil α helices. This 272 amino acid-long domain (from 414 to 586), encoded by *MEFV* exons 3-8, has a function largely unknown and mutations affecting this domain mostly result in *MEFV* variants of unknown significance (Milhavel et al., 2008).

We thus generated five distinct U937 cell lines expressing *MEFV* variants of unknown significance identified in patients. These variants (p.Q426R; p.H478Y; p.F479L; p.E552D; p.L559F) present mutations in various section of the CHS domain (Fig. 4A). All these constructs were expressed under a doxycycline-inducible promoter. Addition of doxycycline induced all these variants (Supplemental Fig. S2A) but did not trigger substantial cell death indicating that the corresponding proteins are not constitutively activated. We then assessed the impact of each of this variant on TcdA-triggered responses. Cells expressing the dominant p.H478Y variant behaved like cells expressing p.M694V variant and underwent cell death significantly faster than WT *MEFV*-expressing cells (Fig. 4B-C). A similar trend, although not statistically different from WT was observed for cells expressing p.Q426R, p.F479L and p.L559F. Cells expressing p.E552D *MEFV* variant had a milder and more variable phenotype than all the other cell lines. LPS + nigericin-mediated cell death was similar in all the cell lines (with some kinetics difference potentially linked to a cross-talk between pyrin and NLRP3 inflammasomes (Omenetti et al., 2014)) (Supplemental Fig. S2B-D). IL-1 β quantification led to the same conclusions with TcdA-mediated responses statistically greater in cells expressing p.H478Y and p.M694V *MEFV* variants (Fig. 4D). Thus, in agreement with Honda and colleagues (Honda et al., 2021), we observed that different mutations within *MEFV*, including p.M694V, lead to different level of enhancement of TcdA-triggered responses. This suggests that different CHS-targeting mutations may cause different level of deregulation of the pyrin inflammasome.

To confirm this, we switched to UCN-01, which better discriminates whether the variants behave like the prototypical p.M694V variant (Honda et al., 2021; Magnotti et al., 2020, 2019). Three of these variants-expressing cell lines (p.Q426R, p.H478Y and p.F479L) responded to UCN-01 and underwent a rapid cell death, previously characterized as a pyroptotic cell death (Fig. 4E-F). This inflammasome response was confirmed by quantifying IL-18 secretion (Fig. 4G). Cell lines expressing p.E552D and p.L559F did not display any major phenotype in term of UCN-01-mediated cell death although IL-18 dosage (a more sensitive technique) suggests that these two mutations may partially deregulate pyrin inflammasome (Fig. 4G). To genetically strengthen these findings, the 5 CHS mutations were combined to p.S208C/p.S242R mutations. These results (Fig. 4H-J) confirmed the major phenotype of p.Q426R, p.H478Y (and as expected p.M694V). p.F479L, p.E552D and p.L559F also caused substantial

deregulation of the pyrin inflammasome responses when combined to p.S208C/p.S242R mutations although it was not statistically significant in all the assays.

Overall, these results indicate that specific CHS-affecting mutations mimic pathogenic FMF mutations affecting the B30.2 domain (e.g. p.M694V) and activate the pyrin inflammasome following dephosphorylation. Based on these cellular phenotypes, they should thus be qualified as pathogenic mutations. Interestingly, these assays clearly indicate that the different mutations have different quantitative impact on the pyrin inflammasome mirroring the clinical FMF presentations that rank from mild to severe (Touitou, 2001).

Distinct mutations in the CHS domain render pyrin highly susceptible to low doses of steroid catabolites.

We recently identified that the pyrin inflammasome can be activated by pregnanolone and etiocholanolone, two catabolites from the steroid hormones, progesterone and testosterone. This response is dependent on the B30.2 and on the CHS domains (Magnotti et al., 2021). We thus wondered whether the identified pathogenic mutations also affected the response to steroid catabolites. U937 cell lines expressing the different *MEFV* variants were thus treated with increasing concentrations of pregnanolone, and the concentration required to trigger 50% cell death (EC50) was determined. Strikingly, two mutations, p.Q426R and p.F479L, decreased pregnanolone EC50 by >50-fold (Fig. 5A). Indeed, 2 μ M of pregnanolone killed 50% of p.F479L or p.Q426R-expressing cells (EC50 = 1.9 \pm 2.6 μ M; n=5 and EC50 = 2.1 \pm 3.6 μ M; n=6, respectively), while EC50 for WT *MEFV*-expressing cells was 110 \pm 27 μ M; (n=7) (Fig. 5B). Similar differences were observed in response to etiocholanolone although not as drastic potentially due to the lower ability of etiocholanolone to activate the pyrin inflammasome. As previously described (Magnotti et al., 2021), cells expressing p.M694V did not demonstrate a substantial reduction in EC50. Surprisingly, cells expressing p.H478Y variant were largely resistant to etiocholanolone and to a lower extent to pregnanolone. These results suggest that mutations affecting the CHS have divergent effect on the steroid catabolites response.

To get insights into the molecular mechanism, we investigated pyrin S242 phosphorylation at steady state and upon exposure to low (6 μ M) or high (50 μ M) doses of pregnanolone. In contrast to the high doses, low doses of pregnanolone do not promote WT pyrin dephosphorylation (Magnotti et al., 2021). No major differences were seen in terms of steady state phosphorylation levels in the different cell lines (Fig. 5C). Yet, low doses of pregnanolone significantly triggered dephosphorylation of pyrin in cells expressing p.Q426R or p.F479L *MEFV* variants (Fig. 5C). In agreement with the high doses required to

trigger pyrin activation, pyrin dephosphorylation was only observed at 50 μ M in the other cell lines. Similarly, UCN-01 triggered dephosphorylation in all the cell lines.

Altogether, these data indicate that distinct CHS mutations trigger distinct pyrin inflammasome deregulation. While we failed to observe any strong phenotype for p.E552D and p.L559F, three mutations (p.Q426R, p.H478Y, p.F479L) behaved as the prototypical FMF exon 10 mutation p.M694V and rendered the pyrin inflammasome controlled only by dephosphorylation. Interestingly, only two of these (p.Q426R and p.F479L) had a further deregulation of pyrin inflammasome responses with a heightened sensitivity to steroid catabolites.

Primary human monocytes from patients presenting the p.F479L mutation demonstrate pyrin inflammasome response to low doses of steroid catabolites.

p.Q426R and p.F479L are rare to very rare mutations (Supplementary Fig. S3A). Six compound heterozygous FMF patients from three independent families with p.F479L-p.E167D/p.V726A mutations were identified in three recruiting centers. The p.E167D mutation co-segregates with the p.F479L mutation in a complex allele (Supplementary Fig. S3B). U937 cells expressing p.E167D *MEFV* variant showed similar phenotypes as WT *MEFV*-expressing cells (Supplementary Fig. S3C-P) suggesting that this variant is likely a benign polymorphism and does not affect in a substantial way WT or p.F479L pyrin responses. p.V726A variant is usually associated with incomplete penetrance or milder forms of the disease (Touitou, 2001). Yet, all the patients displayed typical FMF disease (Supplementary table 1) strongly suggesting that, in agreement with the above results and with previous studies (Honda et al., 2021; Magnotti et al., 2020), the p.F479L *MEFV* variant is pathogenic. Indeed, primary monocytes from patients presenting the p.F479L-p.E167D/p.V726A genotype responded to UCN-01 by secreting IL-1 β (Fig. 6B). As expected, monocytes from healthy donors did not demonstrate substantial production of IL-1 β in response to UCN-01 while their pyrin inflammasome could be triggered by TcdB (Fig. 6A). We then investigated whether primary monocytes from these patients responded to low doses of the steroid catabolites pregnanolone and etiocholanolone (6 μ M and 12 μ M, respectively). As observed with U937 cells, primary monocytes bearing the p.F479L mutation released IL-1 β in response to low doses of pregnanolone and etiocholanolone (Fig. 6C, 6D) while monocytes from HD did not. A large difference in IL-1 β secretion between monocytes from HD and patient bearing the p.F479L was also seen at higher doses of steroid catabolites (50 and 100 μ M) although at these doses, inflammasome activation was observed in primary monocytes from HD (Fig 6C, D). Similar results were observed when investigating primary monocytes cell death in real time (Fig. 6E-M). Indeed, primary monocytes from p.F479L expressing patients died in response to low doses of pregnanolone and etiocholanolone (Fig. 6F, I, M) in contrast to monocytes from HD. At higher doses

of steroid catabolites, cell death was more extensive in primary monocytes from p.F479L-expressing patients than in monocytes from HD (Fig. 6E, H). As observed with IL-1 β secretion (Fig. 6C, 6D), these differences were largely ablated in the presence of both steroid catabolites and UCN-01 suggesting that the p.F479L mutation may affect a coupling mechanism between low doses of steroid catabolites and dephosphorylation.

Altogether, these results validate in primary patients bearing the p.F479L mutation that particular FMF mutations render pyrin inflammasome sensitive to low doses of steroid catabolites.

Discussion

In contrast to other inflammasome sensors such as NLRP3 (Bauernfeind et al., 2009; Py et al., 2013, p. 3; Stutz et al., 2017), the regulation of pyrin is still largely unknown. Phosphorylation of two key serine residues is central to the activation mechanism (Gao et al., 2016; Masters et al., 2016). The microtubule network is also key to pyrin inflammasome activation (Gao et al., 2016; Magupalli et al., 2020, p. 6; Mansfield et al., 2001; Van Gorp et al., 2016; J. W. Yu et al., 2007) although the mechanisms are still unclear. The roles of pyrin domains in the pyrin regulation are still largely unknown. The B30.2 domain has long been hypothesized to negatively regulate human pyrin. Yet, the experimental evidence sustaining this negative regulation are sparse. Furthermore, the proposed mechanisms vary from interaction with NLRP3 to mediate autophagy-mediated degradation (Kimura et al., 2015) to direct interaction with caspase-1 or IL-1 β to directly regulate these inflammasome mediators (Arakelov et al., 2018; Chae et al., 2006; Papin et al., 2007; Weinert et al., 2015). Here, we clearly demonstrate that the B30.2 domain is dispensable for pyrin inflammasome response in response to TcdA. This result is fully in line with results obtained in mice in which pyrin is naturally devoid of the B30.2 domain (Xu et al., 2014) and with recent data obtained in U937 cells infected with *Y. pestis* (Park et al., 2020). Not only, the B30.2 domain is dispensable, but our data show that deletion of this domain renders the activation of the pyrin inflammasome under the sole regulation of the dephosphorylation of the serine residues 208 and 242. This observation thus suggests that the B30.2 domain negatively control pyrin inflammasome activation downstream of the dephosphorylation. Importantly, we were able to observe the B30.2-mediated regulation when investigating ASC speck formation in *CASP1*^{KO} cells. Altogether these results demonstrate that the B30.2 regulate pyrin inflammasome activation downstream of the dephosphorylation and upstream of ASC speck formation hence regulating the step 2 of pyrin inflammasome cascade.

Surprisingly, in response to TcdA, we did not observe higher IL-1 β or IL-18 responses in Δ B30.2-*MEFV*-expressing cells compared to WT *MEFV*-expressing cells while p.M694V *MEFV*-expressing cells showed

higher responses. Thus, while the B30.2 deletion mimics p.M694V mutation in terms of loss of step 2 regulation, the B30.2 domain may also, at least when mutated in position p.M694V, positively regulate inflammasome activation.

The B30.2 domain sits onto a flexible coiled-coil domain that has been termed the Central Helical Scaffold (CHS). In the butyrophilin BTN3A1 protein that displays a similar domain sequence, the coiled-coil domain is implicated in the signal transduction following binding of a small ligand in the BTN3A1 B30.2 cavity. We thus made the hypothesis that the pyrin CHS domain may act together with the B30.2 domain to regulate pyrin inflammasome activation. In agreement with this hypothesis, several mutations along the CHS domains mimic p.M694V mutations and renders the pyrin inflammasome activation under the sole control of the dephosphorylation. In WT pyrin, we hypothesize that the CHS domain may transduce a negative signal initiated by the B30.2 domain. In this model, pyrin activation would be negatively regulated by these two C-terminal domains acting together to control pyrin step 2. More molecular characterization of pyrin protein and its conformational changes remain to be performed to assess the validity of this model.

While most of the research on pyrin has focused on the B30.2 domain, our results indicate that the CHS domain is a central regulator of pyrin inflammasome. Furthermore, this study and others (Aldea et al., 2004; Honda et al., 2021) demonstrate that various mutations in the CHS are pathogenic and validate that *MEFV* mutations outside exon 10 (i.e. affecting other domains than the B30.2 domain) can cause FMF. These results thus highlight the need to sequence the whole *MEFV* gene to genetically validate (or not) a clinical diagnosis of FMF.

Of particular interest, different mutations within the CHS domain have different impact on the functionality of the pyrin inflammasome in response to steroid catabolites. Particularly, two mutations (p.Q426R and p.F479L) decrease by a ≈ 100 -fold the sensitivity of cells expressing pyrin to pregnanolone. Interestingly, these two mutations maps to amino-acids at the interface between two to three distinct alpha helices from two different CHS molecules within the CHS-B30.2 dimer (Weinert et al., 2015). Modifications of the CHS conformation may allow to switch the B30.2 domain from a closed to an open state (Weinert et al., 2015) and the two identified mutations may thus lock or facilitate this switch.

We were not able to obtain neither primary cells nor clinical information from the single patient bearing the p.Q426R mutation described so far (Milhavet et al., 2008). In contrast, we recruited 6 patients from three independent families bearing the p.F479L mutation. All these patients were i) presenting a complex p.E167D/p.F479L allele 2) compound heterozygotes with p.V726A as the second

mutation. Of note the p.V726A mutation is usually associated with mild form of FMF (Touitou, 2001). The practitioners following these patients did not report any inflammatory flares related to life events potentially associated with an increase in steroid sex hormones catabolism (puberty, pregnancy...). Yet, for 5 out of 6 patients, arthralgia/ osteoarticular manifestations were mentioned, a clinical feature previously reported in 43% of pediatric patients with two high penetrance *MEFV* mutations (p.M680I, p. M694I, p.M694V) (Federici et al., 2012). Whether a steroid catabolite may be responsible for this clinical manifestation is unclear.

Altogether, this study demonstrates that in the C-terminus of pyrin, the B30.2 and the CHS domains regulate pyrin activation in particular by negatively regulating the step 2. *MEFV* mutations affecting the serine residues or the B30.2 domain lead to two different diseases (PAAND and FMF). Here, we identified that different mutations affecting the CHS domain differentially affect the pyrin inflammasome response and potentially the clinical presentation of the patients. Thus, our study strengthens the concept of a spectrum of *MEFV* mutations, affecting differently the regulation mechanisms of the pyrin protein and leading to various Pyrin-Associated Autoinflammatory Diseases (Boursier et al., 2019) with varying degrees of severity.

Materials and Methods

Mutagenesis and cell line generation

U937 cell lines expressing the different *MEFV* variants were generated as described in Magnotti et al, 2019. Briefly, *MEFV* variants were generated by site-directed mutagenesis using the QuickChange II Site-Directed Mutagenesis Kit (Agilent) or the Q5 Site-Directed Mutagenesis Kit (NEB) with primers listed in the Supplementary table 2. The variants were cloned into the GFP-expressing lentiviral vector pINDUCER21 under a doxycycline-inducible promoter through a 3xFlag derivative of pENTR1A vector (Invitrogen). The resulting plasmids were used to produce lentiviruses in HEK293 cells. The human myeloid cell line U937 (CelluloNet, Lyon, France) was transduced with the obtained lentiviruses. Transduced cells sorted based on GFP expression on an Aria cell sorter. U937 cells were maintained in RPMI 1640 medium with glutaMAX_I supplemented with 10% FCS, 1% HEPES, 1% Sodium Pyruvate, 2mM L-glutamate, 1% PSA. *CASP1*^{KO} cell lines were generated using the CRISPR/Cas9 method as previously described by our group.

Cytokine detection and cell death assay

For real time cell death analysis, U937 cells were seeded at 5×10^4 cells per well in a black 96-well plate (Costar, Corning) and treated with doxycycline (1 μ g/ml) overnight. Then, the cells were stimulated

with relevant compounds, propidium iodide (PI) (5µg/ml final) was added to all wells and a readout was immediately performed every 5 or 15 minutes for 3 – 16 hours on a thermostatic fluorimeter (Tecan) with excitation wavelength of 535 nm (bandwidth 15 nm) and emission wavelength 635 nm (bandwidth 15 nm). The obtained results were normalized with the use of PI incorporation in cells treated with Triton-X 1% as 100% cell death.

To assess IL-18 secretion, U937 cells were seeded at 2×10^5 cells per well of a 96-well plate and treated with doxycycline (1µg/ml) overnight. The appropriate inflammasome stimuli were added and the cells were incubated at 37°C with 5% CO₂ for 3 hours. The supernatant was collected and the concentration in IL-18 was determined by ELISA with anti-human IL-18 antibody (4µg/ml, #D044-3, MBL, Woburn, MA, USA) as capture antibody and anti-human IL-18 antibody coupled with biotin (20 ng/ml, #D045-6, MBL) as detection antibody.

To assess IL-1β secretion U937 cells were seeded at 5×10^4 cells per well of a 96-well plate and treated with 100 ng/ml of phorbol 12-myristate 12-acetate (PMA, Invitrogen) for 3 hours, then washed and incubated with 1 µg/ml doxycycline overnight. The appropriate inflammasome stimuli were added and the cells were incubated at 37°C with 5% CO₂ for 3 hours. The supernatant was collected and the concentration in IL-1β was determined by ELISA (R&D Systems).

In each of these experiments three technical replicates were performed. The inflammasome stimuli used were: UCN-01 at 12,5 µM without priming, TcdA at 1µg/ml without priming and Nigericin at 50 µg/ml following 3 hours priming with LPS 1 µg/ml.

HEK293t cell transfection, immunoprecipitation and immunoblot analysis

To examine pyrin phosphorylation, U937 cells were seeded 3×10^6 per condition in a 6-well plate and incubated with doxycycline (1 µg/ml) overnight at 37°C with 5% CO₂. The cells were then either treated or not with Carfilizomib 100 ng/ml for 30 minutes, then UCN-01 12.5µM for 15 minutes.

To examine pyrin interaction with PKN1, HEK 293t cells were seeded 5×10^5 cells per condition in 12-well plates, transient transfection was performed with Lipofectamine 2000 Transfection Reagent (Invitrogen) and 500 ng of plasmid DNA: pINDUCER21 plasmids containing the MEFV gene and/or plasmids containing the PKN1 gene with V5 tag (a kind gift of JJ Chae, NIH, USA). 24 hours after transfection, the cells were incubated with doxycycline (1µg/ml) overnight and collected 40 hours post-transfection.

Once collected, the cells were washed in cold PBS and lysed in Tris HCl pH 7.0 25 mM, NaCl 150 mM, EDTA 1 mM, Igepal CA-630 (NP40) 0.1% supplemented with Sodium fluoride (phosphatase inhibitor, Sigma, S7920) at 10mM and, cOmplete™ EDTA-free Protease Inhibitor Cocktail (Roche 05056489001). Flag-pyrin was immunoprecipitated with BSA-saturated Anti-FLAG® M2 Magnetic Beads (Sigma, M8823) for 2 hours at 4°C. Proteins were separated by SDS-PAGE on precast 4-15% acrylamide gels (Bio-Rad) and then transferred to Transblot Turbo Midi-size PVDF membranes (Bio-Rad). For immunoblotting the following antibodies were used: mouse anti-Flag (Sigma Aldrich, clone M2, 1:1000), rabbit anti-Pyrin (Adipogen, AL196, 1:1000), rabbit anti-phosphoS241 Pyrin (Abcam, ab200420, 1:1000), mouse anti-V5 tag (Invitrogen, 37-7500, 1:1000), mouse anti-βActin (Sigma Aldrich, clone C4, MAB1501, 1:5000) and anti-mouse IgG (Promega, W4021, 1:3000) and anti-rabbit IgG (Sigma, A0545, 1:3000).

Immunofluorescence

To quantify ASC specks, U937 cells were seeded 2×10^5 per condition in a 96-well V-bottom plate and incubated with or without doxycycline (1µg/ml) overnight. Then the cells were additionally treated or not with UCN-01 12,5µM for 25 minutes, washed with PBS, and fixed with 2% paraformaldehyde (15 minutes at 37°C). The cells were washed once in PBS and transferred onto glass slides with cytospin, then permeabilized with Triton-X100 0.1% in PBS. The samples were stained with anti-ASC (Santa Cruz, sc22514R, 4µg/ml) for 1 hour at room temperature, then with donkey anti-rabbit Alexa Fluor 594 (Life Technologies, A21207, 10 µg/ml), followed by DAPI (100 ng/ml). Coverslips were mounted using mowiol.

Figures and legends

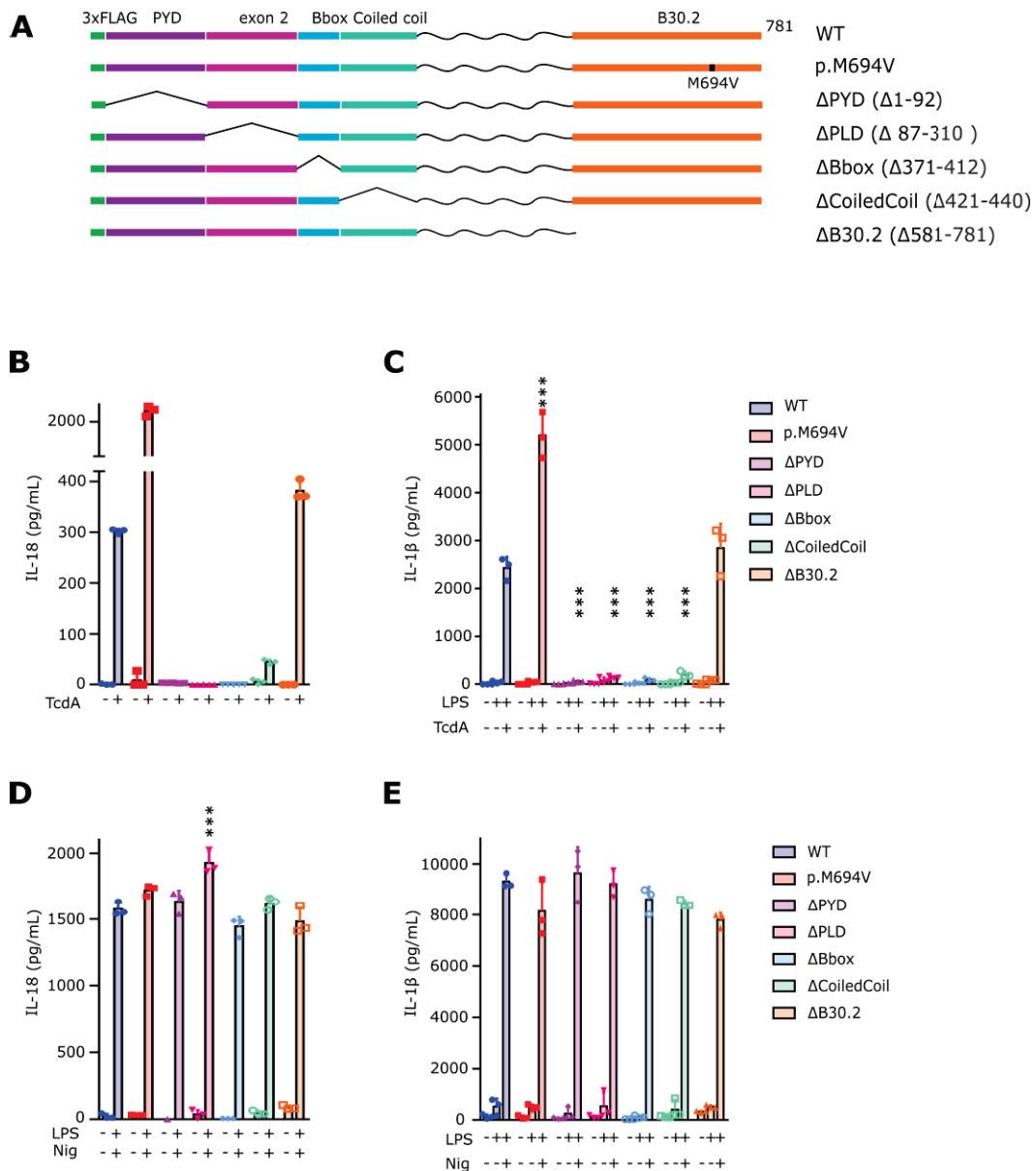


Figure 1. B30.2 is dispensable for TcdA-mediated pyrin activation. (A) Schematic representation of pyrin variants. U937 monocytes (B, D) or macrophages (C, E) incubated with doxycycline to induce expression of the indicated pyrin variants, were treated with TcdA for 6 h (B-C) or with LPS for 3 h followed by Nigericin for 3 hours (D-E). The concentration of IL-18 (B, D) and IL-1β (C, E) in the supernatant was determined by ELISA.

Data information: Data from one experiment representative of three independent experiments. Mean, SD of triplicates and individual data points are shown. (B) Kruskal-Wallis and Dunn's multiple comparisons tests and (C-E) ordinary one-way ANOVA and Dunnett's multiple comparisons tests were performed to compare U937 cells expressing WT pyrin to the other cell lines. (C) ***: $p < 0.001$, (D) ***: $p < 0.001$.

Figure 2. Deletion of the B30.2 domain suppresses pyrin regulation step 2. (A-B) U937 monocytes (A) or macrophages (B) incubated with doxycycline to induce pyrin expression were treated with UCN-01 for 3 h. IL-18 (A) and IL-1 β (B) concentration was determined in the supernatant by ELISA. (C) Cell death kinetics upon doxycycline addition followed by UCN-01 treatment were determined in U937 monocytes expressing the indicated pyrin variants. PI incorporation/fluorescence was monitored every 15 min for the indicated time. (D-E) Areas Under the Curve (AUC) corresponding to the above kinetics are shown. (F) U937 monocytes were treated with doxycycline for 16 h followed by UCN-01 addition for 2 h, IL-18 concentration in the supernatant was measured by ELISA.

Data information: Data from one experiment representative of three independent experiments. Mean, SD of triplicates and individual data points are shown. (D) a.u.: arbitrary units. (A-B) Kruskal-Wallis and Dunn's multiple comparisons tests and (E-F) ordinary one-way ANOVA and Dunnett's multiple comparisons tests were performed to compare U937 cells expressing WT pyrin to the other cell lines. (D) *: p=0.0232; **: p=0.0038; (E) ** (left to right): p=0.0076, 0.0014 ; ***: p<0.001 ; (F) *** : p<0.001.

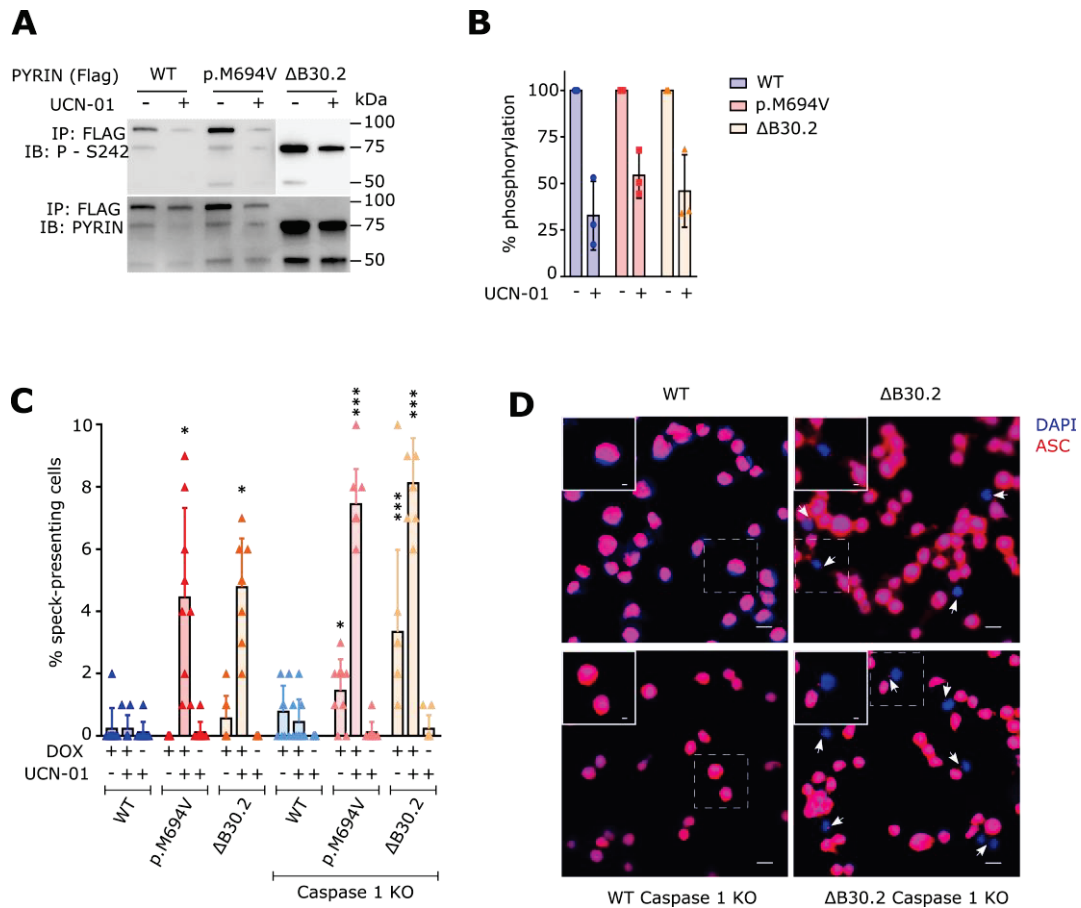


Figure 3. The B30.2-mediated regulation acts downstream of dephosphorylation, and independently of Caspase-1. (A-B) Doxycycline-induced U937 monocytes expressing pyrin WT, p.M694V or pyrin deleted from the B30.2 domain were treated with UCN-01 for 15 minutes. (A) Pyrin phosphorylation at the S242 site was assessed by Western blot following immunoprecipitation and (B) quantified by densitometry. (C-D) U937 monocytes WT or *Caspase-1* knock-out (KO) were treated with doxycycline for 15 hours and/or with UCN-01 for 25 minutes. ASC speck formation (indicated with white arrows) was monitored by immunofluorescence. Quantification (C) and representative images (D) are shown.

Data information: (A, C) Data from one experiment representative of three independent experiments. (B) Values from individual experiments, mean and SD from three independent experiments are represented. Pyrin S242 phosphorylation was quantified using ImageJ software and reported as percentage of the untreated condition of the corresponding cell line. Each point represents the densitometry quantification from one experiment. (C) Values from individual experiments, mean and SD from three independent experiments are represented. Each dot corresponds to the percentage of ASC specks found in approximately 100 cells counted per condition. Kruskal-Wallis and Dunn's multiple comparisons tests were performed. * (left to right): $p=0.0306, 0.0351, 0.0494$; ***: $p<0.001$. (D) Scale bars: $10\mu\text{m}$ and $2,5\mu\text{m}$ in the main figures and insets, respectively.

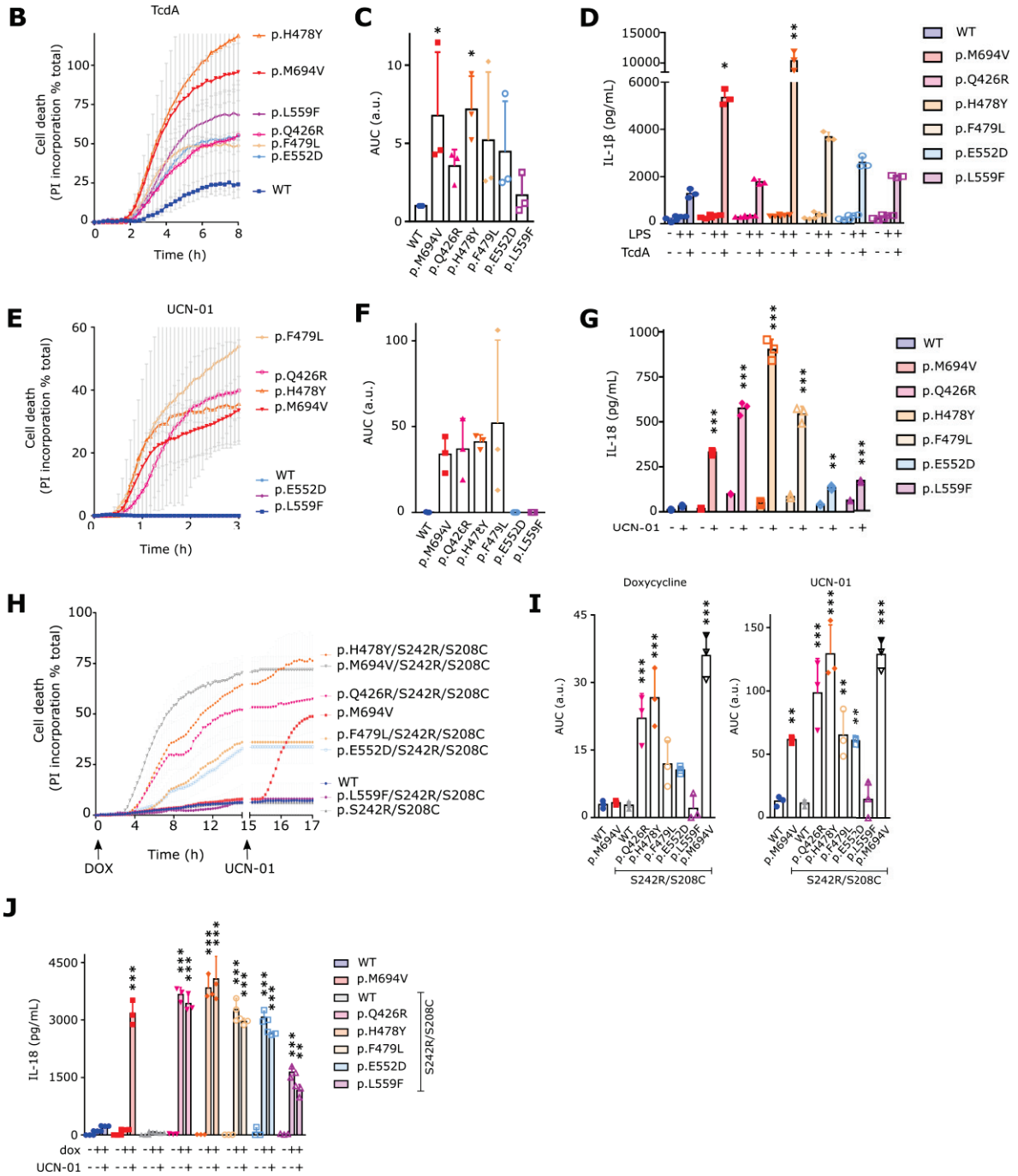
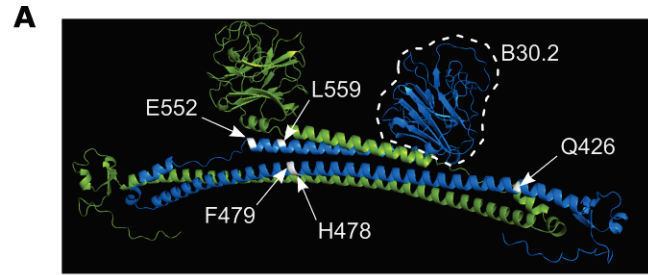


Figure 4. Mutations in the Central Helical Scaffold (CHS) domain phenocopy the classical FMF-associated B30.2 mutation - p.M694V - in terms of UCN-01 and TcdA-mediated responses. (A-C, F-H) U937 monocytes or (D-E) macrophages incubated with doxycycline to induce expression of the indicated variants, were treated with (A-B, D) TcdA for 6 h, or (C, E) LPS for 3 h followed by Nigericin for 3 h, or (F-H) UCN-01 for 3 h. (A, C, F) Cell death kinetics was monitored through PI incorporation/fluorescence every 5 minutes over the indicated time. (B, G) Areas Under the Curve (AUC) corresponding to the kinetics are shown. (D-E) IL-1 β or (H) IL-18 concentration in the supernatant was determined by ELISA. (I-K) U937 monocytes were treated doxycycline for 16 h followed by UCN-01 for 2 h. (I) PI incorporation/fluorescence was monitored every 15 minutes for the indicated time, (J) corresponding AUC are shown. (K) IL-18 concentration in the supernatant was determined by ELISA.

Data information: Data from one experiment representative of three independent experiments. Mean and SD of triplicates and individual data points are shown. (B, G) a.u.: arbitrary units. (D) Kruskal-Wallis and Dunn's multiple comparisons tests or (B, E, H, J-K) ordinary one-way ANOVA and Dunnett's multiple comparisons tests were performed to compare U937 cells expressing WT pyrin to those expressing other variants. (B) *: p=0.0127; **: p=0.0035 ; (D) *: p= 0.0184 ; **: p=0.0023 ; (E) ***: p<0.001 ; (H) **: p=0.0054 ; ***: p<0.001 ; (J) ** (left to right): p=0.0055, 0.0029, 0.0061 ; ***: p<0.001 ; (K) **: p=0.0026 ; ***: p<0.001.

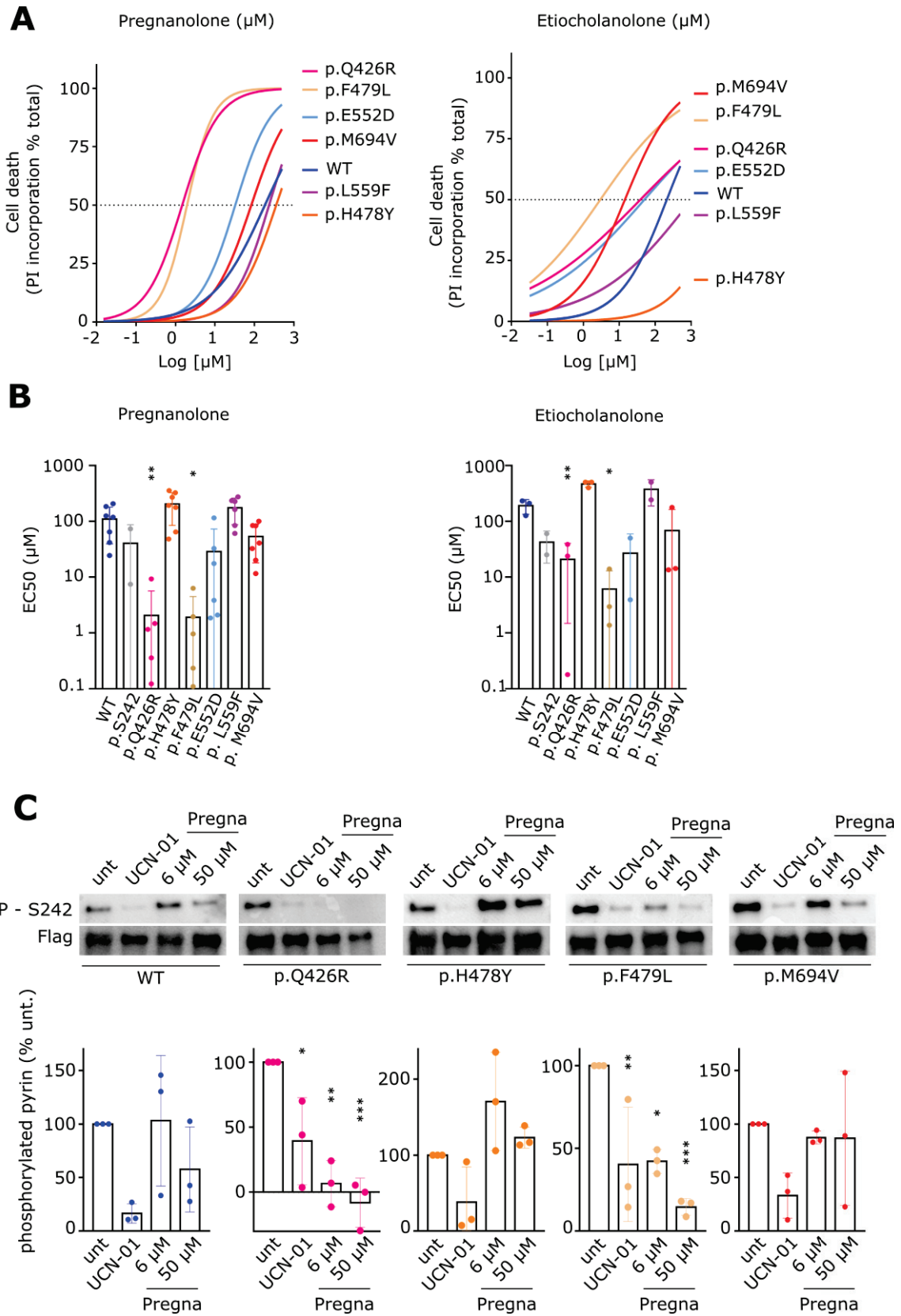


Figure 5. Specific mutations in the CHS domain render pyrin highly sensitive to steroid catabolites. U937 monocytes incubated with doxycycline to induce expression of the indicated pyrin variants, were treated (A-B) with decreasing doses of pregnanolone or etiocholanolone or (C) with UCN-01 for 15 minutes or with VX765 for 30 minutes followed by pregnanolone at the indicated dose for 30 minutes. (A) Cell death levels were measured at 3 h post-treatment in response to varying concentrations of pregnanolone (left panel) or etiocholanolone (right panel). (B) EC50 was determined 3 h post-treatment. (C) Pyrin phosphorylation at the S242 site was assessed by Western blot following immunoprecipitation and quantified by densitometry.

Data information: (A) Data from one experiment representative of three independent experiments. The curve was obtained by an ordinary (Least squares) fit using the log (agonist) vs. normalized response-variable slope model. (B) EC values were obtained from the above analysis using best-fit values. Each point represents the mean EC50 calculated from one biological triplicate. The bars represent the mean and SD of 3 to 7 independent experiments. Kruskal-Wallis and Dunn's multiple comparisons tests for the panel on the left and ordinary one-way ANOVA and Dunnett's multiple comparisons tests for the panel on the right were performed. (C-Top panel) Images from one experiment representative of three independent experiments are shown. (Bottom panel): Each point represents the densitometry quantification (normalized to the untreated sample) from one experiment. The bars represent the mean and SD of 3 independent experiments. (B-C) Ordinary one-way ANOVA and Dunnett's multiple comparisons tests were performed. (B) * (left to right): $p=0.0168, 0.0405$; ** (left to right): $p=0.0078, 0.0022$. (C) * (left to right): $p=0.0198, 0.0104$; ** (left to right): $p=0.0017, 0.0088$; ***: $p<0.001$.

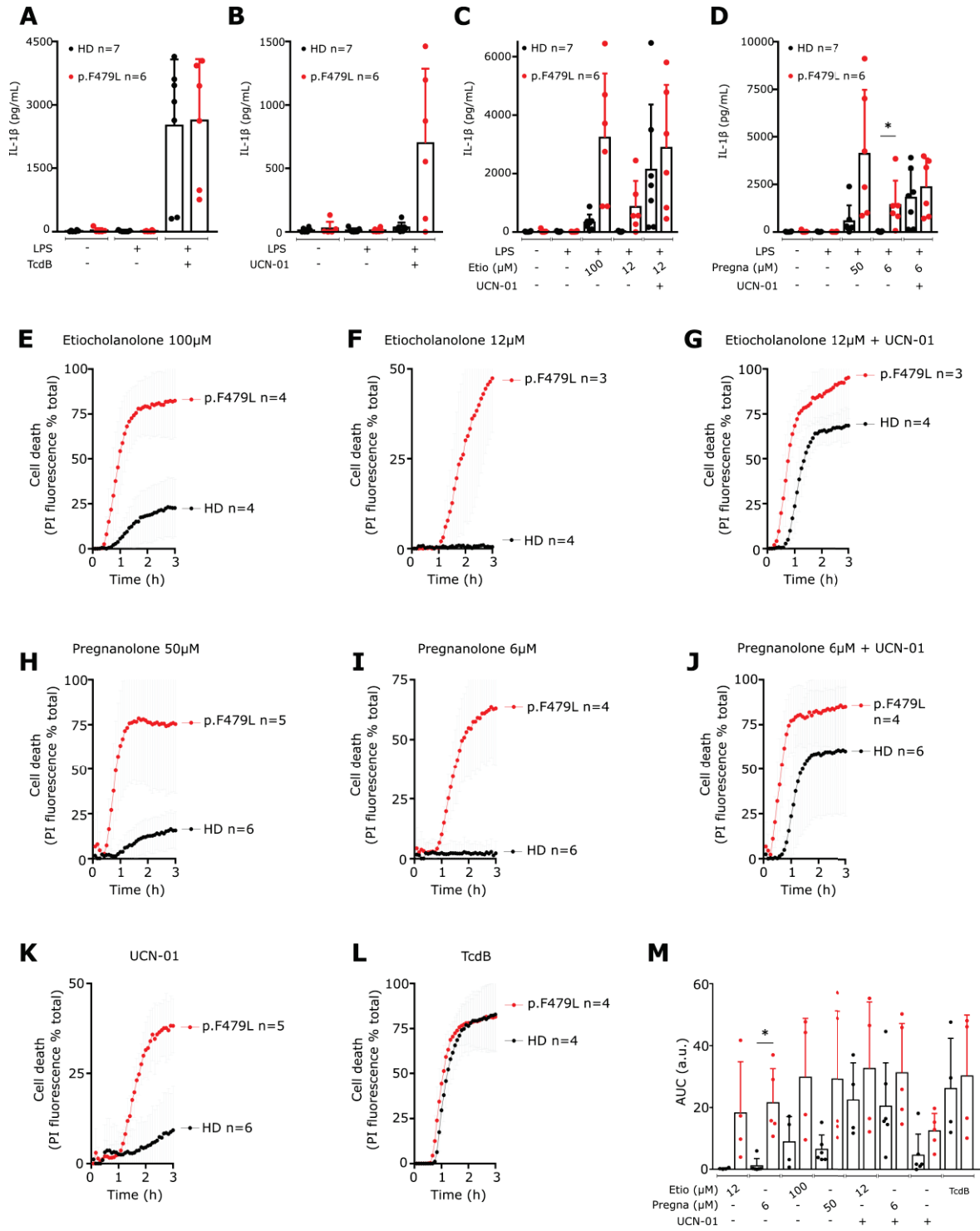


Figure 6. Primary human monocytes from patients presenting the p.F479L mutation demonstrated pyrin inflammasome response to low doses of steroid catabolites. Monocytes from healthy donors (HD) or FMF patients carrying the p.F479L mutation (see table S1 for full genotype) were treated with indicated stimuli. (A-D) IL-1 β concentrations in the supernatant collected after 3 h of treatment were determined by ELISA. (E-L) PI incorporation/fluorescence was monitored every 5 minutes for 3 h, (M) corresponding AUC are shown.

Data information: Mean and SD of triplicates and individual data points are shown for the indicated number of HD and p.F479L patients, each corresponding to the average of a biological triplicate. (M) a.u.: arbitrary units. Kruskal-Wallis and Dunn's multiple comparisons tests were performed to compare the HD to the p.F479L patients. (D) *: $p=0.0265$; (M) * : $p=0.0284$

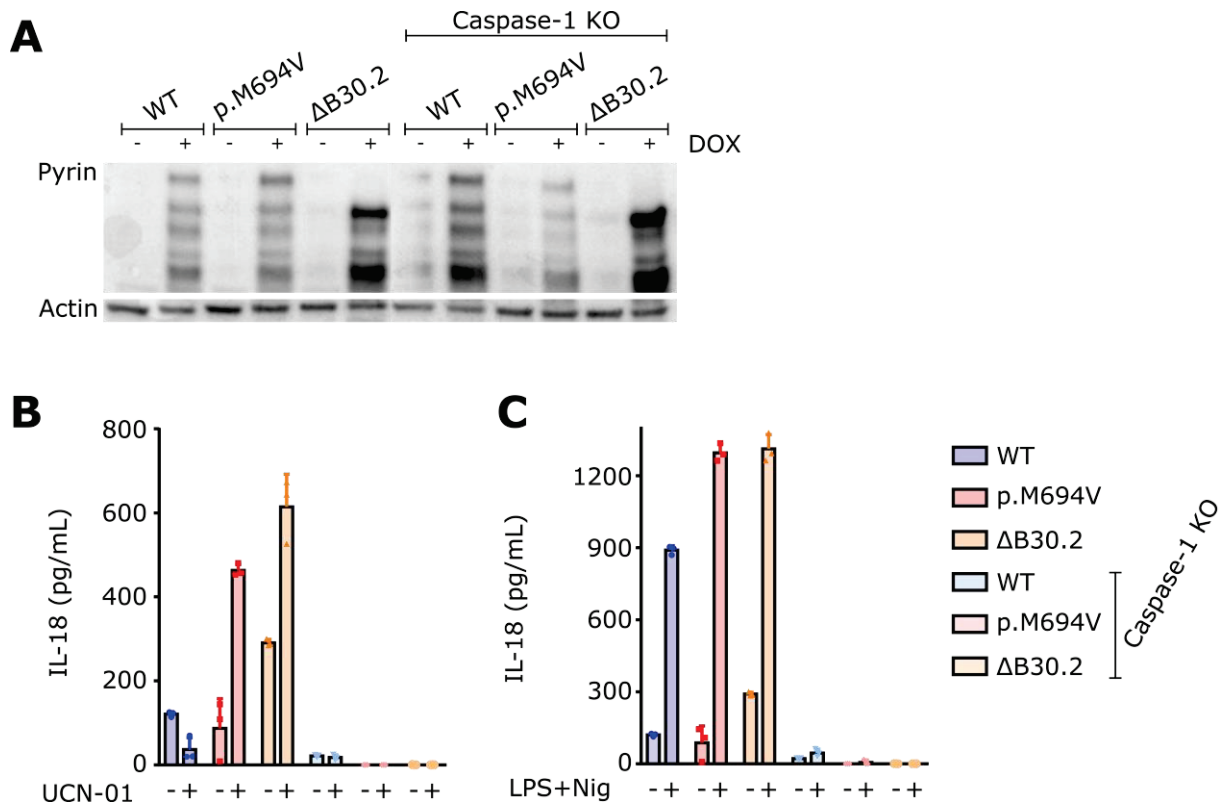


Figure S1 Expression of pyrin in U937 caspase-1 KO monocytes and IL-18 secretion in response to UCN-01 and nigericin. U937 monocytes knocked-out or not for caspase-1 expressing the indicated pyrin variants under the control of a doxycycline-inducible promoter were generated. (A) Pyrin expression was verified by Western blot. The monocytes were treated with (B) UCN-01 and (C) Nigericin, IL-18 concentration was measured in the supernatant with ELISA.

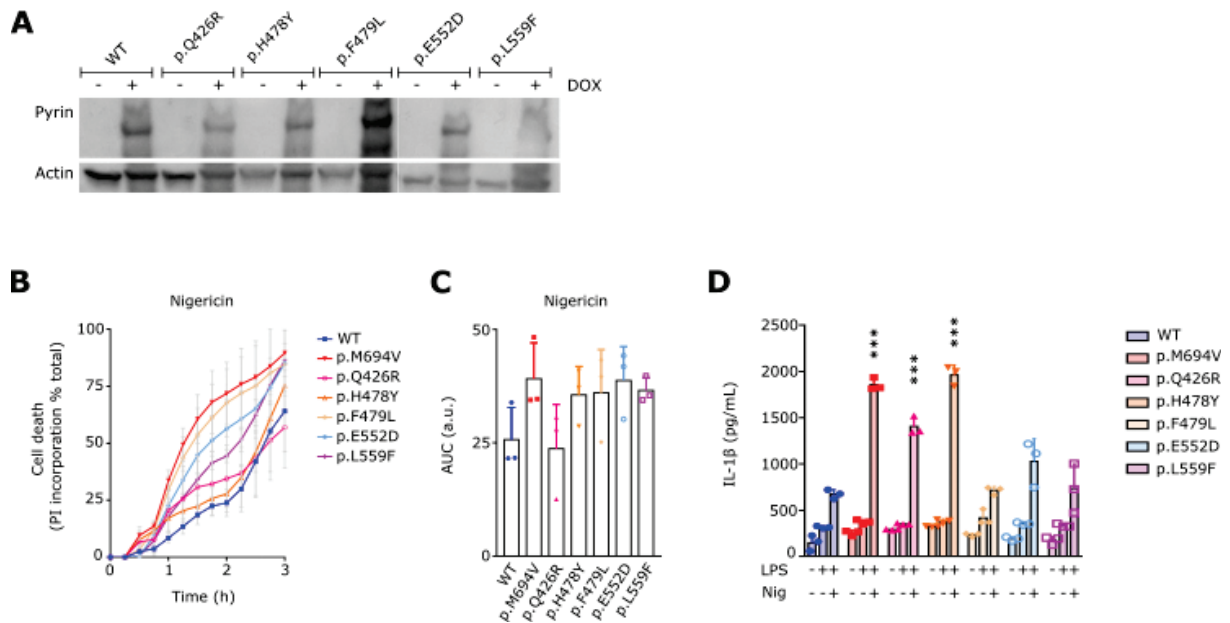
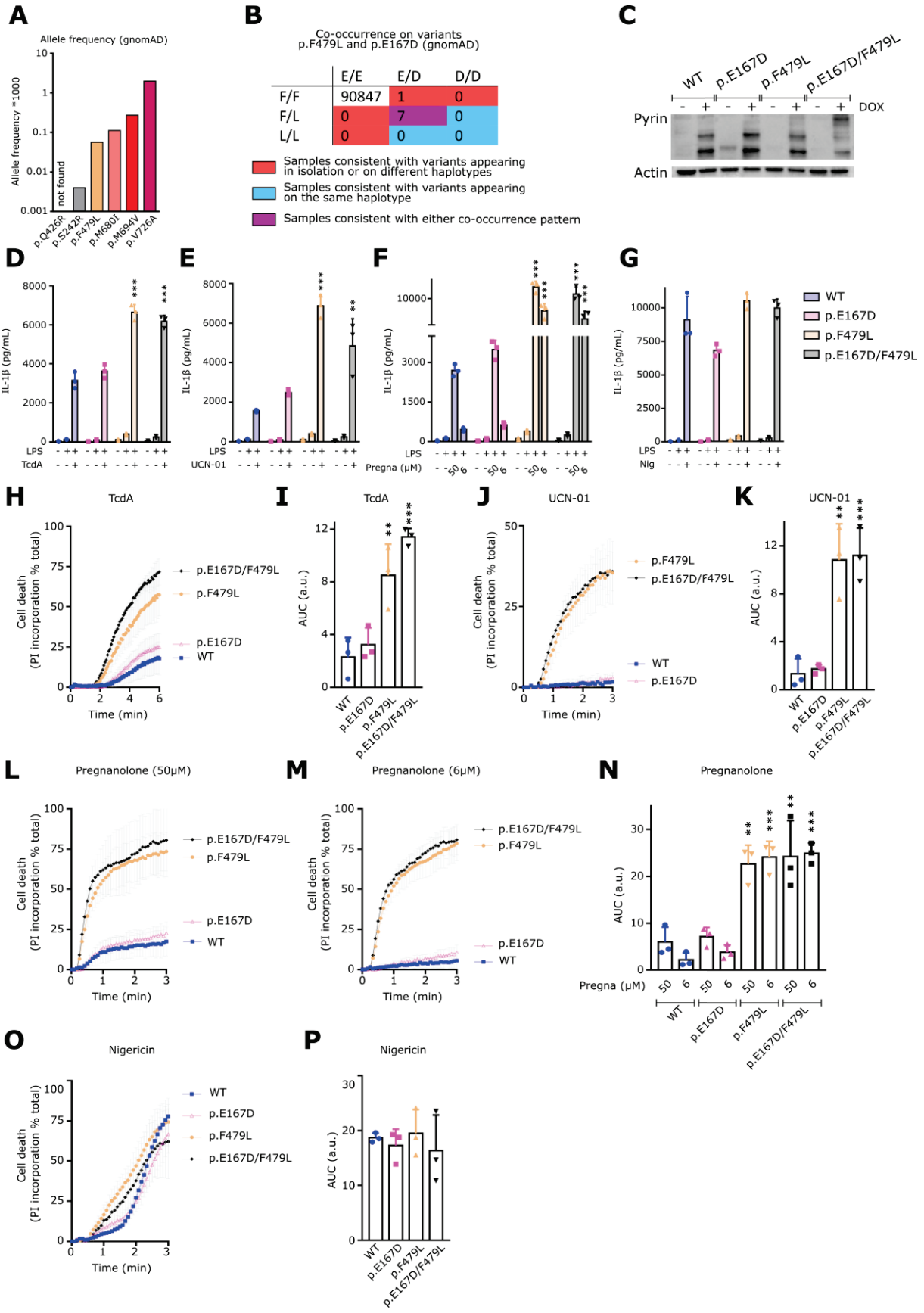


Figure S2. Expression of pyrin mutated in the CHS domain and the impact of the CHS mutations on NLRP3 activation. U937 monocytes expressing the indicated pyrin variants under the control of a doxycycline-inducible promoter were generated. (A) Pyrin expression was verified by Western blot. The indicated cell lines were treated with LPS for 3 h, then with Nigericin. (B) Cell death kinetics were monitored through PI/fluorescence every 5 minutes over the indicated time, (C) corresponding AUC are shown. (D) IL-1 β concentration in the supernatant was measured with ELISA.

Data information: Data from one experiment of three independent experiments. Mean and SD of triplicates and individual data points are shown. a.u.: arbitrary units. (C) Kruskal-Wallis and Dunn's multiple comparisons tests or (D) ordinary one-way ANOVA and Dunnett's multiple comparisons tests were performed to compare U937 cells expressing WT pyrin to those expressing other variants. (D) ***: $p < 0.001$



Supplementary figure 3. p.F479L variant drives the hyper-inflammatory phenotype in cells expressing pyrin with the double mutation p.E167D/F479L. (A) Frequency of co-occurrence of p.E167D and p.F479L mutations according to the Genome Aggregation Database (gnomAD). The data is shown only for the p.F479L variant 16-3297166-G-C (c.1437C>G, rs104895083) (B) Frequency of co-occurrence of p.E167D and p.F479L pyrin variants according to gnomAD (C) U937 monocytes expressing the indicated pyrin variants under the control of a doxycycline-inducible promoter were generated. These cell lines were treated as indicated. (D-G) IL-1 β concentration in the supernatant was determined by ELISA. (H, J, L-M, O) Cell death kinetics were monitored through PI incorporation/fluorescence every 5 minutes over the indicated time, (I, K, N, P) corresponding AUC are shown.

Data information: Data from one experiment representative of three independent experiments. Mean and SD of triplicates and individual data points are shown. (I, K, N, P) a.u.: arbitrary units. (D-F, I, K, N, P) Ordinary one-way ANOVA and Dunnett's multiple comparisons tests or (G) Kruskal-Wallis and Dunn's multiple comparisons tests were performed to compare U937 cells expressing WT pyrin to those expressing other variants. (D) ***: p<0.001; (E) **: p=0.0018; ***: p<0.001; (F) ***: p<0.001; (I) **: p=0.0033; ***: p<0.001; (K) **: p=0.0011; ***: p<0.001; (N) ** (left to right): p=0.0064, 0.0038; ***: p<0.001

Patient	Sex	Mutation	Age	Age onset	Colchicine treatment	Symptoms
P1	F	E167D, F479L	35	-	-	-
P2	F	E167D, F479L	41	10	1 mg / day	3-day episodes of abdominal pain with arthralgia
P3	M	E167D, F479L, V726A	67	24	1 mg / day	Skin rash, abdominal pain (hard stomach), joint pain, total hip replacement, occasional fatigue, or physical weakness
P4	F	E167D, F479L, V726A	11	2.5	0.5 mg/day	Variable proteinuria and some leukorrhea, aseptic long-lasting osteoarticular manifestations, regress with colchicine, no biological inflammatory syndrome
P5	M	E167D, F479L, V726A	10	2	0.5 mg/day	Occasional aseptic osteoarticular manifestations, regress spontaneously or with colchicine, no biological inflammatory syndrome
P6	M	E167D, F479L, V726A	7	2.5	0.5 mg/day	Occasional aseptic osteoarticular manifestations, regress spontaneously or with colchicine, persistent cervical adenopathy, biological inflammatory syndrome

Supplementary table 1. Clinical profiles of patients with the p.F479L MEFV mutation. (Related to figure 6)

Supplementary Table 2. Primers used for *MEFV* mutagenesis.

Site-directed mutagenesis primers	
M694V - WT	5'-GGTACTCATTTCCTTCATCATTATCACCACCCAGTAG-3'
	5'-CTACTGGGTGGTGATAATGATGAAGGAAAATGAGTACC-3'
WT – Δ1-92	5' – GAATATTCCACACAAGAAAACGGCACAGATG – 3'
	5' – CGCGGCCGCAAGCTTGTC – 3'
WT - dExon2	5' – GAAGGCCACCAGACACGG – 3'
	5' – CCTGAATGGCTGCCCTGT – 3'
WT – Δ371-412	5' – GGGGCTTAGGCTTCCCGGGCGAGGAGGTCGCCCTGGAACA – 3'
	5' – GCCCGGGAAGCCTAAGCCCCTGTTCCAGGGCGACCTCCTC – 3'
WT – Δ421-440	5' – CGATCCTATGGGGAGGAG – 3'
	5' – CTTGTGTTCCAGGGCGAC – 3'
WT – S580X	5' – GAACATTTCCATTTCTTAACGCAGGGTTTCTGAGAAGTAC – 3'
	5' – GTACTTCTCAGAAACCCTGCGTTAAGAAATGGAAATGTTCAA – 3'
WT - S242R	5'- GAAATGGTGACCTCAAGTCTTCTAGGTGCGCATCTT-3'
	5'- AAGATGCGACCTAGAAGACTTGAGGTCACCATTT-3'
WT - S208C	5'- CCCC GCGGAGCAGGCGTTTCTGC-3'
	5'- GCAGAAACGCCTGCTCCGCGGGG-3'
WT – Q426R	5' – AAGAAGAAAATTCAGAAGCGGCTGGAGCATCTGAAGAAG - 3'
	5' - CTTCTTCAGATGCTCCAGCCGCTTCTGAATTTTCTTCTT - 3'
WT – H478Y	5' - CCTGGAGCAGCAAGAGTATTTCTTTGTGGCCTC - 3'
	5' - GAGGCCACAAAGAAATACTCTTGCTGCTCCAGG - 3'
WT – F479L	5' - GAGCAGCAAGAGCATTGTTTGTGGCCTCACTGG - 3'
	5' - CCAGTGAGGCCACAAACAATGCTCTTGCTGCTC - 3'
WT – E552D	5' - GTGGACCACTCCTCAAGACATAAAAACAAAAGATCCAAC - 3'
	5' - GTTGGATCTTTGTTTTATGTCTTGAGGAGTGGTCCAC - 3'
WT – L559F	5' - CCTCAAGAGATAAAAACAAAAGATCCAATTCCTCCACCAGAAG - 3'
	5' - CTTCTGGTGGAGGAATTGGATCTTTGTTTTATCTCTTGAGG - 3'
WT – E167D	5' - GTCCAGGCCGTCGAGGCCTTCTCT - 3'
	5' - AGAGAGAAGGCCTCGGACGGCCTGGAC - 3'

ADDITIONAL RESULTS

This section contains some additional results that were not included in the articles presented in the previous section. Some of the presented figures contain results that were out of the scope of presented articles, preliminary results that will serve as basis for future publications, others require additional complementary experiments to establish a clear mechanism.

Nonetheless, we consider them important for a fuller understanding of pyrin inflammasome and its regulatory mechanisms.

Part 1.

Specific mutations in the CHS domain render pyrin sensitive to a large spectrum of steroid molecules.

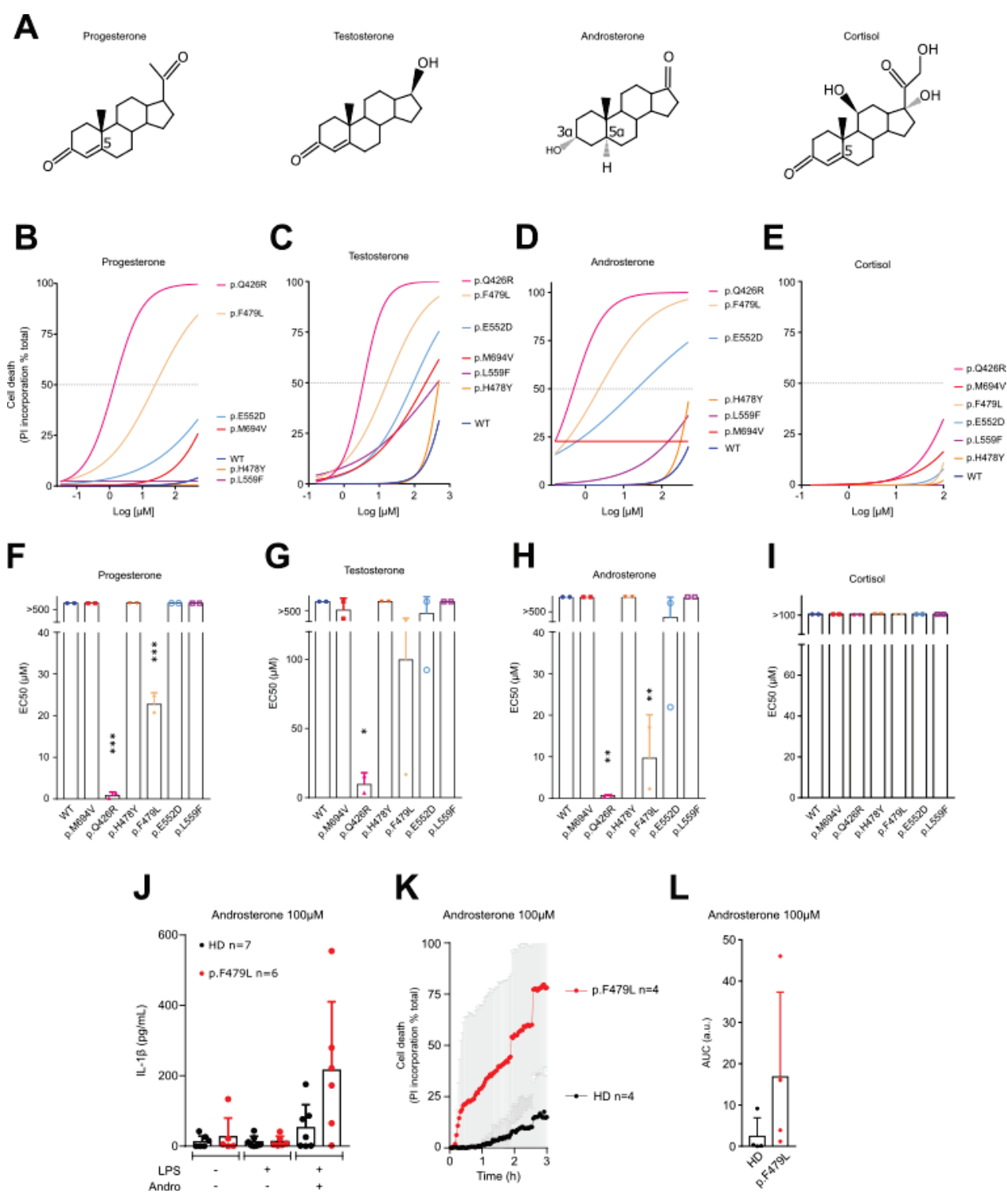


Figure 1. Specific mutations in the CHS domain render pyrin sensitive to a large spectrum of steroid molecules. (A) Structure of the steroid molecules used in this set of experiments. U937 monocytes were incubated with doxycycline to induce expression of the indicated pyrin variants, then treated with decreasing doses of progesterone, testosterone, androsterone or cortisol. (B-E) Cell death levels were measured by PI incorporation/fluorescence at 3 h post-treatment in response to (B) progesterone, (C) testosterone, (D) androsterone or (E) cortisol. (F-I) Corresponding EC50 was calculated. Monocytes from healthy donors (HD) or FMF patients carrying the p.F479L mutation were treated with androsterone 100 μ M. (J) IL-1 β concentrations in the supernatant collected after 3 h of treatment was determined with ELISA. (K) Cell death kinetics were monitored through PI incorporation/fluorescence every 5 minutes for 3 h. (L) Corresponding AUC are shown.

Data information: (B-E) Data from one experiment representative of two independent experiments. The curve was obtained by an ordinary (Least squares) fit using the log (agonist) vs. normalized response-variable slope model. (F-I) EC50 values were obtained from the above analysis using best-fit values. Each point represents the mean EC50 calculated from one biological triplicate. The bars represent the mean and SD of two independent experiments. (F-I) Ordinary one-way ANOVA and Dunnett's multiple comparisons tests was performed. (J-K) Mean and SD of triplicates and individual data points are shown for the indicated number of HD and p.F479L patients, each corresponding to the mean of a biological triplicate. (L) a.u. : arbitrary units. (F) ***: $p < 0.001$, (G) *: $p = 0.0417$, (H) ** (left to right): $p = 0.0090$; $p = 0.0099$.

Introduction

Steroid catabolites etiocholanolone and pregnanolone are non-canonical activators of the pyrin inflammasome. Results presented earlier in this manuscript suggest that steroid sensing by pyrin relies on the specific stereochemistry of the steroid. Namely, stereoisomers of etiocholanolone and pregnanolone with a different stereochemistry on carbon 3 and carbon 5 could not activate pyrin inflammasome. However, following our observation that the p.Q426R and the p.F479L FMF-associated variants of pyrin exhibit a significantly higher sensitivity to etiocholanolone and pregnanolone than WT pyrin, we wondered whether these mutations located in the CHS domain of pyrin could also impact the specificity of pyrin response to steroid molecules.

For this experiment we selected progesterone and testosterone, from which pregnanolone and etiocholanolone are generated, androsterone, a stereoisomer of etiocholanolone with altered stereochemistry on carbon 5 (5α), and cortisol (Fig. 1A).

Results

U937 monocytes expressing pyrin variants with FMF-associated mutations located in the CHS domain were treated with decreasing doses of progesterone, testosterone, androsterone and cortisol. Cell death kinetics were monitored and EC₅₀ value (the concentration of steroid required to trigger 50% cell death) for each of the cell lines and each of the molecules was calculated. As previously demonstrated, WT pyrin and pyrin with the prototypical FMF-associated mutation p.M694V were activated by very high concentrations or not at all activated by these steroid molecules. No PI incorporation was observed in WT pyrin-expressing cells treated with as much as 500 μ M of progesterone, testosterone, androsterone or 100 μ M of cortisol.

In stark contrast, sex steroid hormones progesterone, testosterone and androsterone triggered cell death in U937 monocytes expressing pyrin variants p.Q426R and p.F479L (Fig. 1B-D). The associated EC₅₀ value was drastically reduced for these three molecules compared to monocytes expressing WT pyrin. Androsterone was the most potent activator of p.Q426R and p.F479L variants of pyrin with mean EC₅₀ as low as 0.63 μ M and 9.6 μ M respectively, followed by progesterone with mean EC₅₀ of 0.83 μ M and 22.7 μ M and testosterone with mean EC₅₀ of 9.5 μ M and 99.5 μ M (Fig. 1F-H). Like with pregnanolone and etiocholanolone, the p.Q426R variant was more sensitive to steroid hormones than the p.F479L variant.

Interestingly, sex steroid hormones used in this experiment did not trigger cell death in U937 monocytes expressing the p.H478Y variant. This mirrors the low sensitivity of this pyrin CHS variant to etiocholanolone and pregnanolone and highlights the finesse of steroid sensing by pyrin.

Another steroid hormone, cortisol, did not trigger pyrin-dependent inflammasome activation in any of the examined U937 cell lines even at 100 μ M (Fig. 1E, I).

In order to validate our findings in primary monocytes, we exposed primary monocytes from FMF patients (n=4-6) with the p.F479L mutation to 100 μ M of androsterone. We measured IL-1 β secretion and cell death triggered by this treatment. Monocytes from patients with p.F479L mutation secreted IL-1 β when treated with androsterone, while monocytes from HD did not (Fig. 1J). Also, androsterone triggered rapid cell death in monocytes from patients bearing the p.F479L mutation, and not in monocytes from HD (Fig. 1K-L). Although the difference between these responses was not statistically significant, the trend is clear, and it confirms our observations in U937 monocytes.

Discussion

Results presented in this section reveal that mutations in the CHS domain of pyrin not only significantly lower its activation threshold by the steroid catabolites etiocholanolone and pregnanolone, but also widen the spectrum of steroids that are able to trigger pyrin inflammasome activation. While WT pyrin appears to be activated exclusively by steroids with specific stereochemistry on carbon 3 (3 α) and 5 (5 β), pyrin variants p.Q426R and p.F479L are also triggered by androsterone (3 α 5 α), progesterone and testosterone. Cortisol did not induce pyrin inflammasome activation in monocytes expressing pyrin variants with mutations in the CHS domain, indicating that even when the CHS domain is modified, there is some specificity to the response produced by steroid molecules regarding pyrin inflammasome activation. Interestingly, as presented in additional results, part 2, in cells expressing WT pyrin, progesterone can inhibit pregnanolone-mediated pyrin activation.

This could mean one of several things. First, variants of pyrin with mutation in the CHS domain could be able to sense and be activated by a larger number of steroid molecules than the WT pyrin. Alternatively, these variants could be less sensitive than WT pyrin to the specific stereochemistry of the steroids. In this scenario both WT pyrin and pyrin variants with mutations in the CHS domain could be capable of sensing a wider range of steroid molecules, but the WT pyrin is only activated by molecules with specific stereochemistry.

At the same time, monocytes expressing the p.H478Y variant of pyrin did not exhibit cell death when exposed to steroid hormones even at high concentrations. This highlights the importance of distinct pyrin residues for steroid molecule sensing.

We favored the following model: WT pyrin might bind pregnanolone and etiocholanolone via the direct binding of these metabolites to the B30.2 domain. This binding triggers a conformational change of the B30.2 which is transduced to the phosphorylation sites by the CHS domain. Specific mutations in

the CHS (e.g. p.Q426R and p.F479L) may favor signal transduction and thus promote pyrin activation with lower doses of pregnanolone and etiocholanolone. The mutated CHS domain may even be able to transduce the signal generated by the fixation of molecules (e.g. progesterone) otherwise inactive. In contrast p.H478Y mutation may decrease the signal transduction and thus limit the sensitivity of pyrin to steroid molecules. This model is discussed in more detail later in this manuscript (c.f. Discussion).

Part 2.

Progesterone abrogates pyrin activation by pregnanolone in a dose-dependent manner.

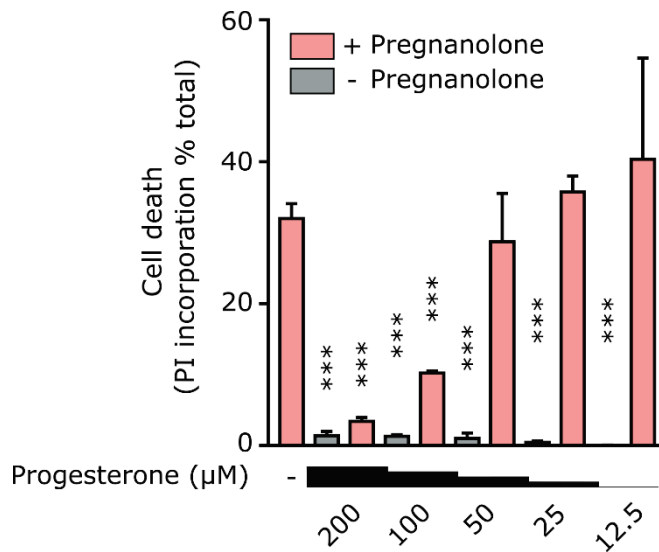


Figure 2. Progesterone abrogates pyrin activation by pregnanolone in a dose-dependent manner.

U937 monocytes expressing WT pyrin were incubated with pregnanolone 50 µM alone, progesterone at a dose ranging from 200 µM to 12.5 µM alone, or pre-incubated for 15 minutes with progesterone at a dose ranging from 200 µM to 12.5 µM, then treated with pregnanolone 50 µM. Cell death kinetics were monitored by PI incorporation/fluorescence at 3h minutes post-pregnanolone addition.

Data information: Preliminary results of one experiment (performed by Amandine Martin) are represented. Mean, SD of duplicates and individual data points are shown. Ordinary one-way ANOVA and Dunnett's multiple comparisons tests were performed to compare U937 cells treated with pregnanolone 50 µM alone with the other treatments. ***: p<0.001

Introduction

Steroid hormone catabolites such as pregnanolone and etiocholanolone, catabolites of progesterone and testosterone respectively, are non-canonical activators of the pyrin inflammasome (Magnotti et al., 2021). At the same time, progesterone and testosterone do not activate WT pyrin. Initially, our results led us to believe that pyrin was not able to sense steroids such as progesterone and testosterone, and that the sensing of steroids by pyrin was dependent on the specific stereochemical structure present in pregnanolone and etiocholanolone but absent in progesterone and testosterone. However, the results presented in the previous section (Additional results, part 1) have demonstrated that certain variants of pyrin associated with FMF that carry mutations in the CHS region, are able to sense a wider spectrum of steroid molecules, including progesterone and testosterone.

Therefore, we wanted to investigate whether WT pyrin was able to sense progesterone without triggering pyrin activation, and whether that sensing was dependent on the same site as sensing of pregnanolone.

Results

U937 monocytes expressing WT pyrin can be activated by a high dose of pregnanolone (50 μ M). To determine whether progesterone was also sensed by WT pyrin, like it is sensed by pyrin variants with mutations in the CHS domain, we treated these monocytes with progesterone alone at concentrations ranging from 200 μ M to 12.5 μ M, or we incubated WT pyrin-expressing monocytes with progesterone for 15 minutes, then treated them with 50 μ M of pregnanolone.

As previously demonstrated, pregnanolone at 50 μ M triggered pyrin inflammasome activation in monocytes that express WT pyrin. Progesterone alone, even at 200 μ M, did not, as evidenced by the lack of PI incorporation following treatment (Fig. 2). Interestingly, when monocytes were preincubated with progesterone in excess as compared to pregnanolone added 15 minutes later, progesterone appeared to inhibit pyrin activation by pregnanolone. For instance, when monocytes were pre-incubated with progesterone 200 μ M prior to pregnanolone treatment, this pre-treatment reduced cell death by 10-fold compared to pregnanolone alone. As for pre-incubation with 100 μ M of progesterone, it reduced activation by pregnanolone by 3-fold compared to pregnanolone alone. Finally, when progesterone and pregnanolone concentrations were equal or the concentration of pregnanolone greater than that of progesterone, progesterone was no longer able to counter pyrin activation by pregnanolone.

Discussion

The discovery of steroid-sensing by pyrin is very recent, and the mechanism of this sensing remains to be elucidated. Also, it is unclear what is the physiological role of pyrin activation by steroid hormone catabolites, or whether the sensing is mediated by direct binding.

Results presented in this section suggest that progesterone inhibits pyrin inflammasome activation by pregnanolone. Considering that pyrin activation by pregnanolone is B30.2-dependent (Magnotti et al., 2021), it is likely that progesterone interferes with the capacity of B30.2 to sense pregnanolone.

The B30.2 domain of pyrin contains a pocket that could serve as a ligand-binding site in a manner analogous to that described for other B30.2 containing proteins such as BTN3A1 (Sandstrom et al., 2014). On the basis of *in silico* and secondary *in vitro* evidence, our team has previously speculated that steroid hormone catabolites (e.g. pregnanolone) could bind pyrin B30.2 directly. Here, the inhibition of pregnanolone-induced activation of pyrin inflammasome by progesterone in a dose-dependent manner suggests, that the two molecules compete for the same binding site. At equal concentrations of progesterone and pregnanolone, progesterone no longer counters pyrin activation by pregnanolone, which suggests that the affinity of pyrin is greater for pregnanolone than for progesterone. Unfortunately, we are currently missing the experimental system to assess biochemically the direct binding of steroid molecules to pyrin B30.2 and the associated association/dissociation constant.

As discussed earlier in this manuscript progesterone and other sex steroid molecules have anti-inflammatory properties. Progesterone in particular inhibits IL-1 β secretion by LPS-treated macrophages (Polan et al., 1989). It would be interesting to determine whether progesterone actively inhibits pyrin activation until it is replaced by an activator ligand (pregnanolone) and possibly in other physiological situations of pyrin activation. For this, we would like to test if progesterone is able to counter pyrin activation by other stimuli such as TcdA or simvastatin. Additionally, we would like to investigate if the same competing relationship in terms of pyrin activation would be true of testosterone and etiocholanolone.

Part 3.

Specific mutations in the CHS domain render pyrin more sensitive to activation by simvastatin.

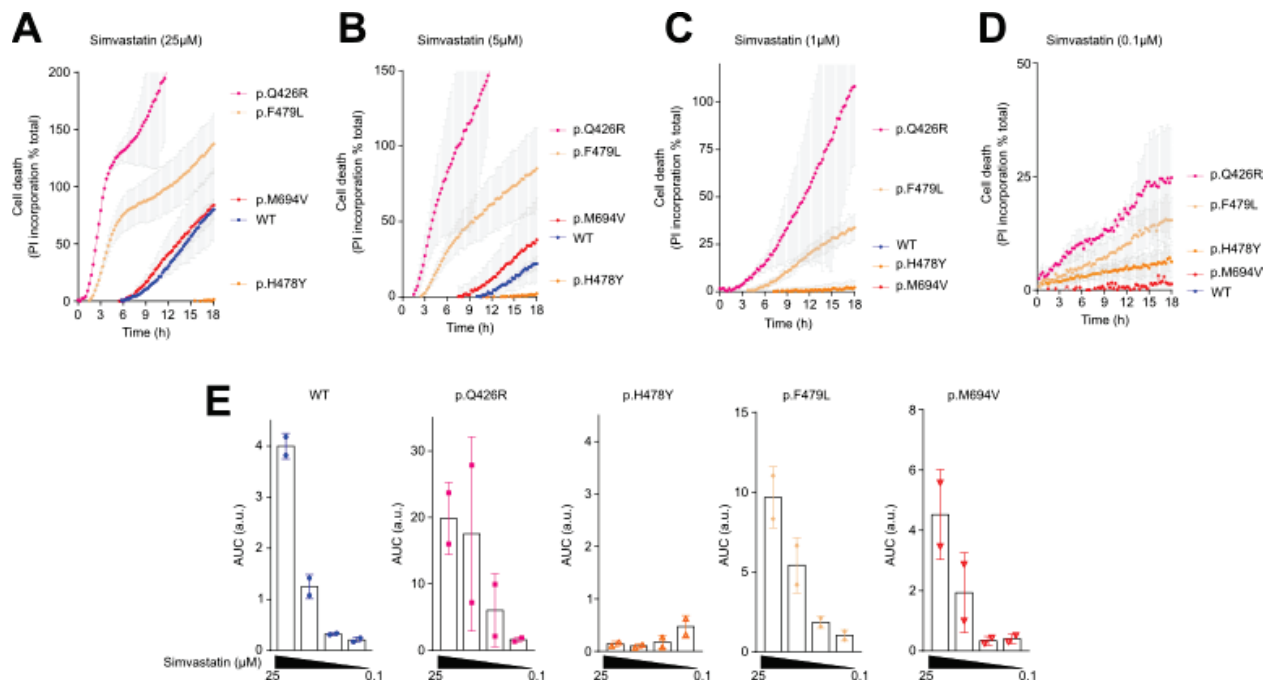


Figure 3. Specific mutations in the CHS domain render pyrin more sensitive to activation by simvastatin. U937 monocytes incubated with doxycycline to induce expression of the indicated pyrin variants were treated with decreasing doses of simvastatin ranging from 25 μM to 0.1 μM. (A-D) Cell death kinetics were monitored through PI incorporation every 20 minutes for 18 h, (E) corresponding AUC are shown. Please note that the scale is different in each graph to visualize the dose response effect.

Data information: Preliminary results of one experiment (performed by Pauline Bronnec) are represented. Mean, SD of duplicates and individual data points are shown. (E) a.u.: arbitrary units. No statistical analysis could be performed due to lack of statistical power.

Introduction

Simvastatin belongs to a large and widely used group of medications called statins. Statins are HMG-CoA reductase inhibitors with cholesterol-lowering properties with a good safety profile often prescribed to people with a high risk of cardio-vascular disease (Alenghat and Davis, 2019; Reamy and Viera, 2022). On a molecular level, statins inhibit cholesterol synthesis by intervening in the mevalonate kinase pathway described in more detail earlier in this manuscript. Additionally, simvastatin activates the pyrin inflammasome, although it is unclear what mechanism mediates this activation (Park et al., 2016). Considering the diverging effects pyrin mutations in the CHS domain have on its response to various stimuli, we wondered how these mutations would affect pyrin activation by simvastatin.

Results

U937 cell lines expressing variants of the *MEFV* gene with mutations in the CHS domain were treated with doxycycline to induce pyrin expression, then treated with decreasing concentrations of simvastatin ranging from 25 μ M to 0.1 μ M. When treated with 25 μ M and 5 μ M of simvastatin cells expressing WT pyrin and pyrin carrying the prototypical FMF mutations p.M694V exhibited doxycycline-dependent cell death 6-8 hours after treatment (Fig. 3A-B). No cell death was induced in these cell lines by lower doses of simvastatin (Fig. 3C-D). Simvastatin did not induce cell death in U937 cells that were not pre-incubated with doxycycline (data not shown), confirming that the observed phenotypes are pyrin-dependent.

In stark contrast to the WT pyrin, simvastatin induced much more rapid cell death in cells expressing certain but not all pyrin variants with mutations in the CHS domain. U937 monocytes expressing the p.Q426R and p.F479L pyrin variants reached 50% cell death in less than 4 hours when treated with 25 μ M simvastatin (Fig. 3A). Smaller doses of simvastatin used in this experiment were still able to induce cell death in cell lines expressing the p.Q426R and the p.F479L pyrin variants, which was not the case for the WT and the p.M694V pyrin (Fig. 3C-D). In addition to a more rapid response to simvastatin by the p.Q426R and the p.F479L variants of pyrin, the intensity of pyrin activation in these variants was also potentiated, as evidenced by a largely increased areas under the curve (Fig. 3E). Therefore, p.Q426R and p.F479L mutations in the CHS domain of pyrin increase pyrin sensitivity to simvastatin. The observed phenotype is somewhat stronger for the U937 cells expressing p.Q426R pyrin variant, although replicate experiments are required to confirm this.

Curiously, the other pyrin variant mutated in the CHS domain included in this experiment, p.H478Y, did not respond to even the highest doses of simvastatin used (Fig. 3E, middle panel). Interestingly,

the high sensitivity of p.Q426R and p.F479L and the low sensitivity of p.H478Y to simvastatin mirrors the sensitivity of these variants to pregnanolone (see discussion).

Discussion

The understanding of pyrin activation by simvastatin is limited. As mentioned before, simvastatin inhibits HMG-CoA reductase in the mevalonate kinase pathway, which inhibits the synthesis of geranylgeranyl pyrophosphate (GGpp) (Drenth et al., 1999; Mandey et al., 2006). GGpp is a substrate of geranylgeranylation of RhoA – a post-translational modification necessary for its localisation at the membrane. Addition of GGpp to pyrin-expressing cells at the same time as simvastatin, counters inflammasome activation (Park et al., 2016). Based on this finding, it has been believed until now that pyrin activation by simvastatin is triggered because of RhoA inhibition due to the lack of RhoA geranylgeranylation. If this is true, then the mechanism involved would be similar to that triggered by TcdA which also causes a break down in RhoA post-translational modification.

The results presented in this section challenge the assumption that pyrin activation by simvastatin and by TcdA follow the same pathway. The prototypical FMF p.M694V pyrin variant has a lower activation threshold by TcdA which results in earlier and stronger activation of this variant by TcdA compared to the WT pyrin (Jamilloux et al., 2018). In contrast, the p.M694V variant and the WT pyrin respond similarly to simvastatin treatment for all the concentrations tested in our experiment both in terms of the time of response and the level of cell death induced.

An additional difference between pyrin response to TcdA and to simvastatin comes from pyrin variants with mutations in the CHS domain. CHS variants p.Q426R, p.H478Y and p.F479L variants undergo rapid cell death with kinetics similar to the p.M694V in response to TcdA. However, when treated with simvastatin the p.Q426R and p.F479L variants undergo much faster cell death than the p.M694V or the WT pyrin, and the response of the p.H478Y pyrin variants is very limited.

The strong pyrin activation for the p.Q426R and the p.F479L variants and the almost complete lack of activation for the p.H478Y variant observed here in response to simvastatin is the same pattern as the one we observed in response to steroid hormones and their catabolites. Therefore, we believe that the mechanism triggered by simvastatin that results in pyrin activation is at least partially shared with that triggered by steroid hormones catabolites. Yet, GGpp which inhibits simvastatin-mediated pyrin inflammasome activation does not affect pregnanolone responses. Due to common chemical structures between cholesterol and pregnanolone/etiocholanolone, it is tempting to speculate that simvastatin could generate an endogenous cholesterol catabolite that could activate the pyrin inflammasome in a similar way as pregnanolone or etiocholanolone. Alternatively, since simvastatin is reducing cholesterol anabolism, it could decrease the concentration an endogenous steroid molecule

that might inhibit pyrin at steady state and that could be possibly displaced by addition of pregnanolone or etiocholanolone. These speculations remain to be tested experimentally.

Part 4.

Study of the role of interactions between residues within the CHS-B30.2 dimer.

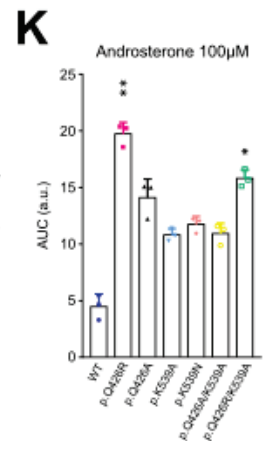
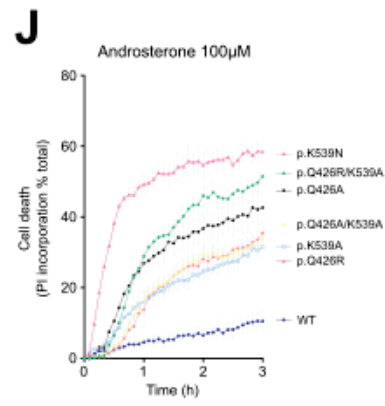
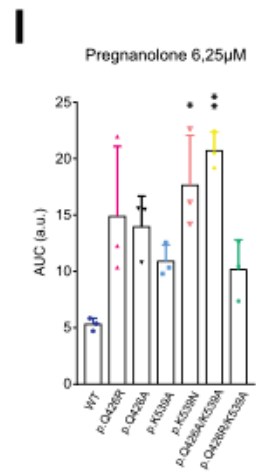
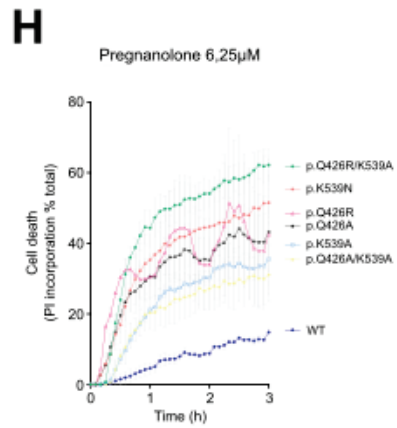
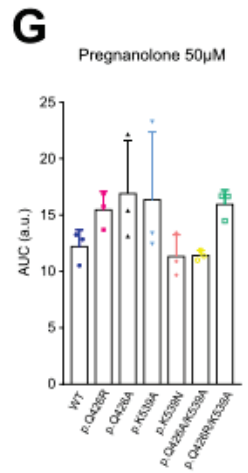
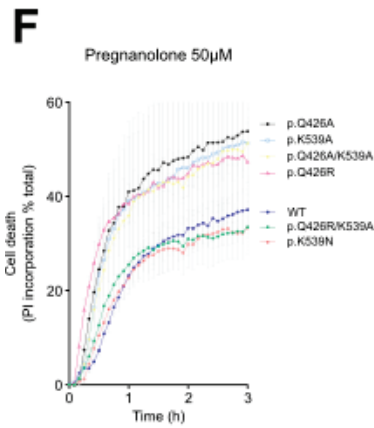
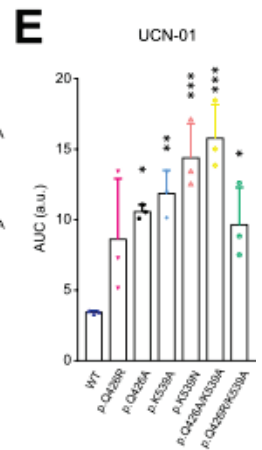
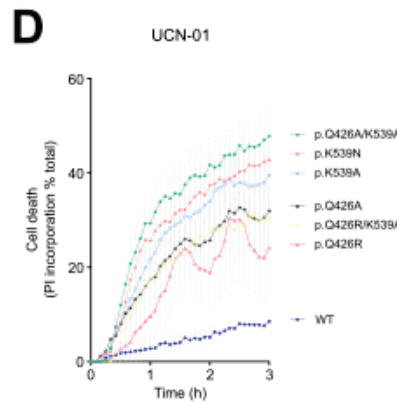
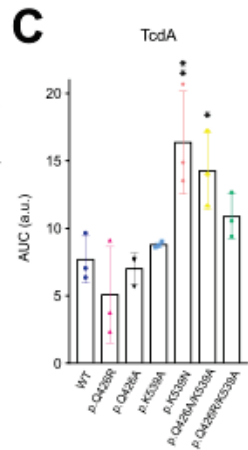
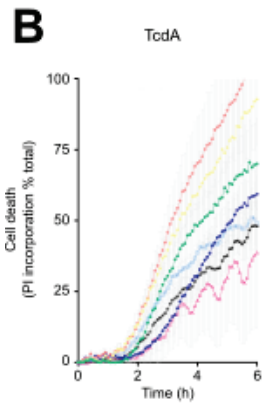
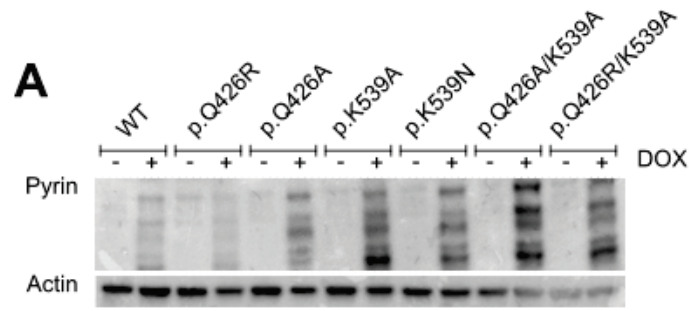


Figure 4. Mutations of the Lys539 residue (facing the Gln426 residue) significantly impact pyrin inflammasome function. U937 monocytes were incubated with doxycycline to induce expression of the indicated pyrin variants, (A) pyrin expression was verified by Western blot. Monocytes were treated with (B-C) TcdA for 6h, (D-E) UCN-01 for 3h, (F-I) pregnanolone at the indicated concentration for 3h, or (J-K) androsterone for 3h. (B, D, F, H J) Cell death kinetics were monitored through PI incorporation/fluorescence every 5 to 15 minutes over the indicated time, ((C, E, G, I, K) corresponding AUC are shown.

Data information: Data from one experiment representative of three independent experiments. Mean, SD of triplicates and individual data points are shown. (C, E, G, I, K) a.u.; arbitrary units. (C, E, G) Ordinary one-way ANOVA and Dunnett's multiple comparisons tests and (I, K) Kruskal-Wallis and Dunn's multiple comparisons tests were performed to compare U937 cells expressing WT pyrin to the other cell lines. (C) *: p=0.0249, **: p=0.0034, (E) * (left to right): p=0.0123, p=0.0303, **: p=0.0035, ***: p<0.001, (I) *: p=0.0228, **: p=0.0076, (K) *: p=0.0184, **: p=0.0023.

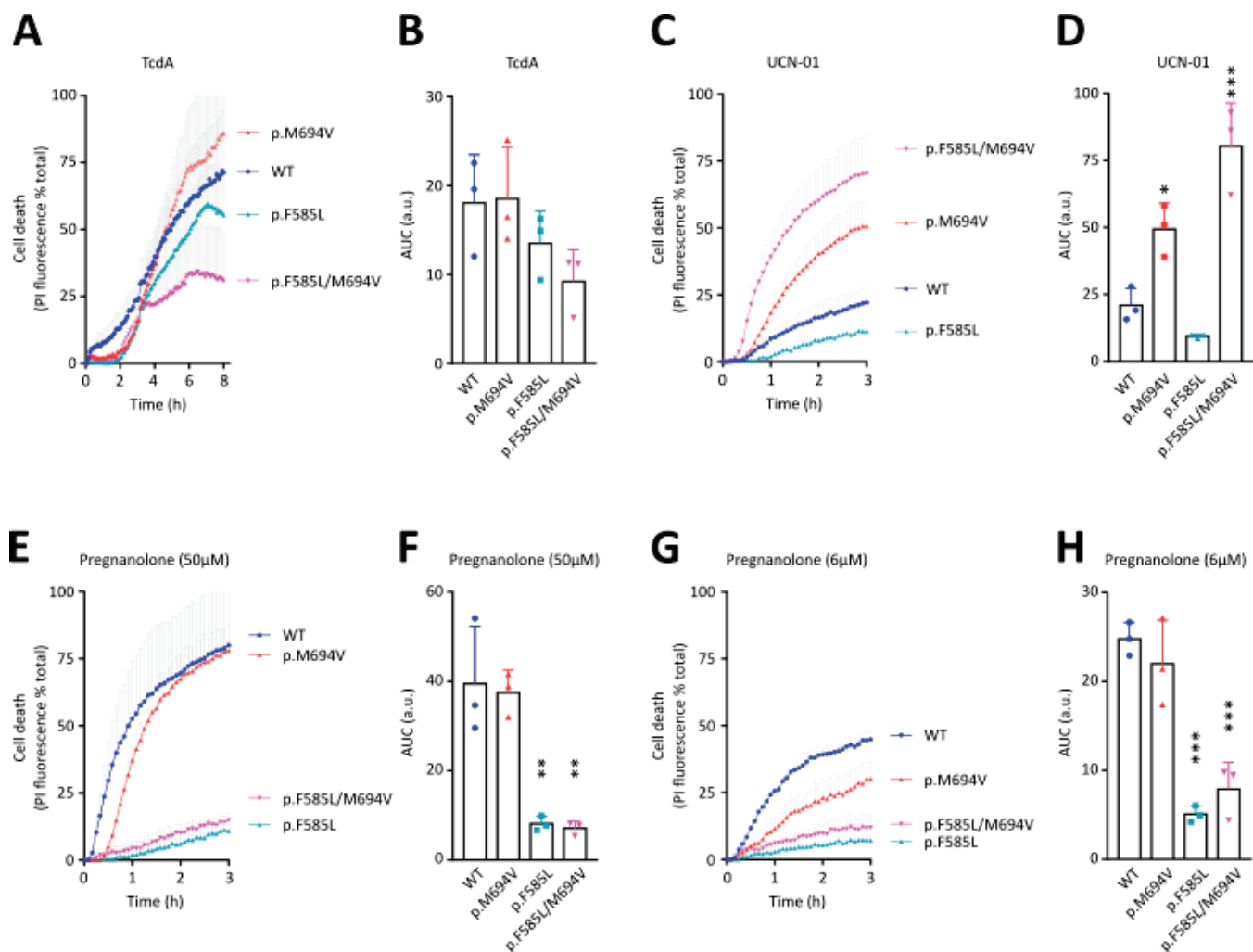


Figure 5. The Phe585 residue (facing the Phe479 residue) of pyrin is crucial for its response to steroid hormone catabolites. U937 monocytes incubated with doxycycline to induce expression of the indicated pyrin variants, were treated with (A-B) TcdA for 8h, or (C-D) UCN-01 for 3h, or (E-H) pregnanolone at the indicated concentration for 3 h. (A, C, E, G) Cell death kinetics were monitored through PI incorporation/fluorescence every 5 to 15 minutes over the indicated time, (B, D, F, H) corresponding AUC are shown.

Data information: Data form one experiment representative of two independent experiments. Mean, SD of triplicates and individual data points are shown. (B, D, F, H) a.u.: arbitrary units. (B, D, F, H) Ordinary one-way ANOVA and Dunnett's multiple comparisons tests were performed to compare U037 cells expressing WT pyrin to the other cell lines. (D) *: $p=0.02$, ***: $p<0.001$; (F) (left to right) **: $p=0.0016$, $p=0.0013$; (H) ***: $p<0.001$.

Introduction

The effect of mutations identified in the *MEFV* gene varies greatly depending on their location, co-occurrence with other mutations and, likely, other environmental factors. The variety of MEFV-associated phenotypes is evident in patients with pyrin-associated autoinflammatory diseases (PAADs), but also *in vivo* in cell line models. For PAADs the prediction of disease penetrance and severity remains difficult, largely because the details of the mechanisms governing pyrin inflammasome regulation and activation require a better understanding (Accetturo et al., 2020; Solak et al., 2008). However, it is clear that pyrin structure is sensitive to change, and that phenotypes resulting from *MEFV* mutations can go from potentially gain-of-function to loss-of-function in a span of a single amino acid position.

In this section we concentrated our attention on two variants of pyrin with mutations in the CHS domain that have been reported to cause FMF-like disease, and that demonstrated a particular phenotype in our U937 cell line model – p.Q426R and p.F479L. A close inspection of the crystal structure of the C-terminal fragment of pyrin containing the CHS domain and the B30.2 domain revealed that each of the two residues Gln426 and Phe479 are located in close proximity or interact with another residue on the interface within the CHS-B30.2 dimer (Weinert et al., 2015). Gln426 of one monomer is in close proximity to the Lys539 residue of the other monomer within the CHS-B30.2 dimer. Similarly, Phe479 residue of one monomer interacts with Phe585 residue of the other monomer within the CHS-B30.2 dimer.

We hypothesized that the distinct phenotypes of p.Q426R and p.F479L pyrin variants could originate from a disturbance of these interactions. To test this hypothesis, we created U937 monocytes that stably expressed p.Q426A, p.K539A, p.K539N, p.Q426A/K539A, p.Q426R/K539A, p.F585L and p.F585L/M694V, and tested their response to various stimuli targeting pyrin inflammasome.

Results

Gln426 and Lys539

In p.Q426R the nonpolar glutamine is replaced by a positively charged arginine. Considering that lysine in position 539, is also a positively charged amino acid, and it finds itself directly in front of the 426 residue, the glutamine to arginine substitution would result in two positively charged amino acids coming close to one another. This could lead to significant change in the conformation of the CHS-B30.2 dimer.

We created U937 monocytic cell lines stably expressing pyrin variants where we replaced Gln426 and/or Lys539 with alanine, a small nonpolar amino acid. Interestingly, one mutation of *MEFV* that impacts Lys539 residue – p.K539N – has been reported, although it was found in a healthy control

subject (Ueda et al., 2016). We decided to include this variant in our experiment. Additionally, we created cell lines that expressed double mutants p.Q426A/K539A and p.Q426R/K539A. Doxycycline-induced pyrin expression in each of these cell lines was verified (Fig. 4A).

Substitutions of Gln426 by alanine or arginine did not significantly impact pyrin-dependent cell death triggered by TcdA suggesting that the charge of the residue in position 426 has no major effect on pyrin inflammasome activation in response to TcdA. The same was true for the p.K539A variant, but not for p.K539N. Monocytes expressing p.K539N pyrin variant showed significantly more cell death than cells expressing WT pyrin ($p=0.0249$) (Fig. 4B-C). TcdA also triggered more cell death in both of the double mutants with substitutions on residues 426 and 539, although the difference was only statistically significant for the p.Q426A/K539A variant (Fig. 4B-C).

Pyrin dephosphorylation with the PKC inhibitor UCN-01 triggered rapid cell death in all variants with mutations at the 426 and 539 residues (Fig. 4D-E). Since UCN-01 triggers pyrin activation only in pathogenic pyrin variants, this result indicates that the 539 is an important residue for pyrin inflammasome regulation. A low dose of pregnanolone (6 μ M), that is not sufficient to trigger rapid pyroptosis in cells expressing WT pyrin, activated pyrin inflammasome mutated at residues 426 and 539 (Fig. 4H-I). Additionally, mutations of residues 426 and 539 of pyrin increased the ability of pyrin inflammasome to be activated by androsterone, although the area under the curve was significantly increased only for the p.Q526R and the p.Q426R/K539A variants ($p=0.0184$ and $p=0.0023$ respectively) (Fig. 4J-K). The high concentration of pregnanolone, known to activate WT pyrin, triggered similar cell death kinetics in all the pyrin variant-expressing cell lines (Fig. 4F-G). Altogether these results indicated that by focusing on the residue interacting with Q426, we identified another pyrin residue which mutation strongly impact pyrin inflammasome regulation (Table 1). Since the phenotypes triggered by Q426A/R and K539A are similar, these suggest that these two residues participate in the same regulatory pathway. Yet, the experiments designed to test the role of the charge and the possible

Pyrin variant		Pyrin activation by:			
		TcdA	UCN-01	Pregnanolone	Androsterone
WT	Q ⁻ - K ⁺	+	-	+	-
p.Q426R	R ⁺ → K ⁺	+	+	++	+
p.K539A	Q ⁻ - A	+	++	++	+
p.Q246R/K539A	R ⁺ - A	+	+	+	+
p.Q246A/K539A	A ⁻ - A	++	++	++	+

Table 1 Summary table recapitulating phenotypes of U937 monocytes expressing pyrin variants with mutations of the Gln426 and Lys539.

repulsion between the residue 426 and the residue 539 (both being charged positively when Q426 is mutated in Q426R) were not conclusive since Q426A triggers the same phenotype as Q426R and K539A does not complement the Q426R mutation.

Phe479 and Phe585

The benzene ring of phenylalanine in position 479 in the CHS of one monomer interacts with the benzene ring of phenylalanine in position 585 of the B30.2 of the other monomer within the CHS-B30.2 dimer. In p.F479L the phenylalanine is substituted for a non-aromatic leucine. This mutation may weaken the interaction between residues 479 of one monomer and 585 of the other monomer within the dimer.

We created U937 monocytic cell line stable expressing the p.F585L variant of pyrin, where Phe585 was substituted for a leucine like in the p.F479L variant. Additionally, we created a cell line that expressed the double mutant p.F585/M694V, p.M694V being the prototypical FMF-associated mutation.

Bacterial toxin TcdA triggered pyrin inflammasome activation in the p.F585L variant comparable to that in the WT pyrin (Fig. 5A-B). UCN-01 did not trigger a response any different from that of the WT pyrin, or from the p.M694V variant for the double p.F585L/M694V mutant suggesting that the p.F585L mutation did not invalidate pyrin regulation downstream of its dephosphorylation (Fig. 5C-D).

However, p.F585L mutation significantly affected pyrin activation by pregnanolone. When treated with a high (50 μ M) (Fig. 5E-F) or a low (6 μ M) (Fig. 5G-H) concentration of pregnanolone, neither U937 monocytes expressing the p.F585L nor cells expressing the p.F585L/M694V pyrin variant exhibited rapid cell death associated with pyrin inflammasome activation, indicating that this mutation triggers a loss-of-function phenotype in regards to pregnanolone-mediated pyrin activation.

Discussion

Here, we attempted to elucidate the role of interactions between specific amino acids within the CHS-B30.2 dimer. We targeted residues that are implicated in a significant reduction in pyrin threshold activation both after dephosphorylation or by steroid hormone catabolites.

Our findings strongly suggest that Gln426 and Lys539 are implicated in maintenance of the step 2 in pyrin regulation, the checkpoint downstream of pyrin dephosphorylation of which the nature is unclear. Both Gln426 and Lys539 appear to be implicated to pyrin activation by steroid catabolites, because the substitutions we examined increased pyrin activation by pregnanolone and androsterone.

The Phe585 residue did not appear to be involved pyrin regulation downstream of its phosphorylation like its counterpart Phe479. Importantly, though, Phe585 is implicated in pyrin sensing of

pregnanolone since the p.F585L mutation completely abolished pyrin activation by this molecule. This result underlies the importance of this residue in the pregnanolone response and suggest that the interaction between Phe585 (in the B30.2 domain) and Phe479 (in the CHS domain) may be important to transduce the activating signal to the phosphorylation site.

Taken together, these results are difficult to interpret. The genetic approach we implemented here does not provide a lot of information about the exact changes in the three-dimensional structure of the protein that are caused by amino acid substitutions. Also, it is unclear if the differences we observe between the WT pyrin and pyrin mutated at Lys539 or Phe585 are truly due to the conformational change we intended to create. Further study of the three-dimensional conformation of the CHS-B30.2 dimer of pyrin, and more information about pyrin activation after dephosphorylation, would help our understanding of the phenotypes observed.

Part 5.

Truncation of the pyrin protein at the G532 residue reveals a spontaneously activated pyrin protein.

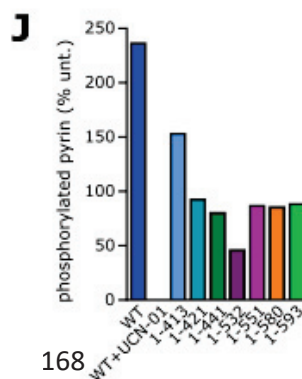
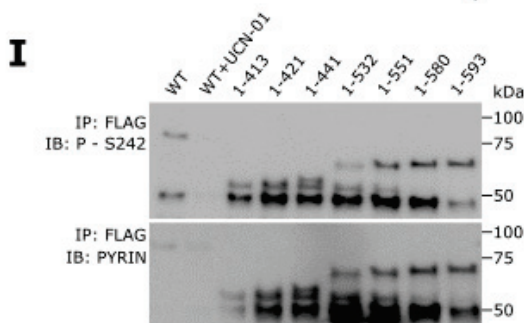
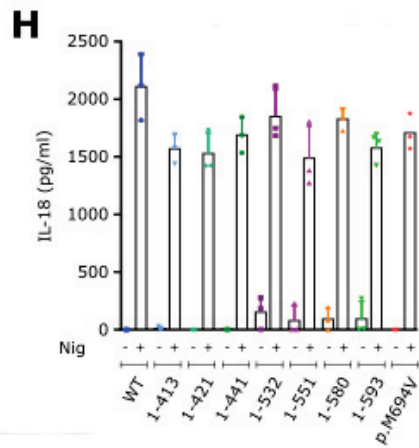
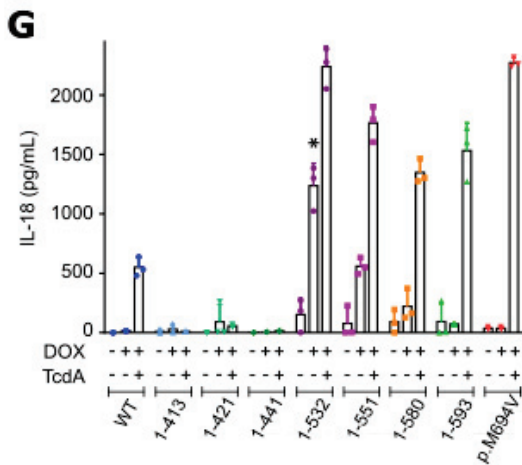
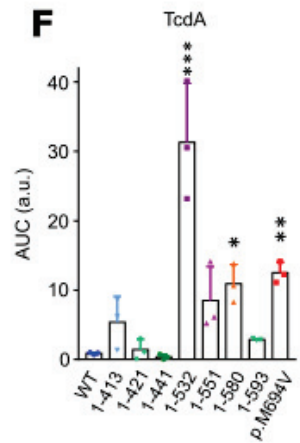
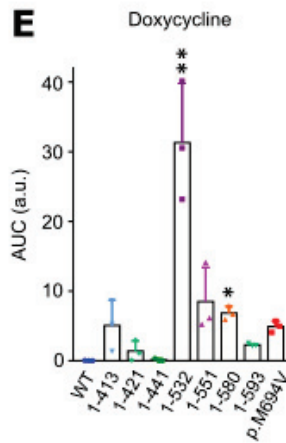
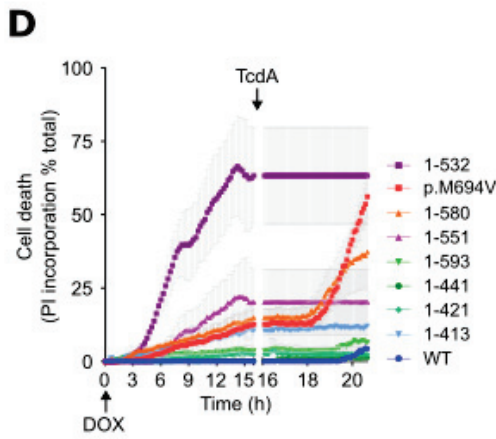
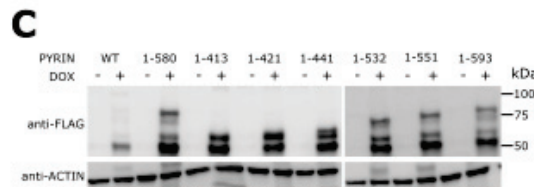
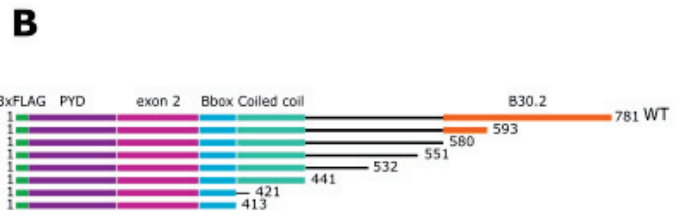
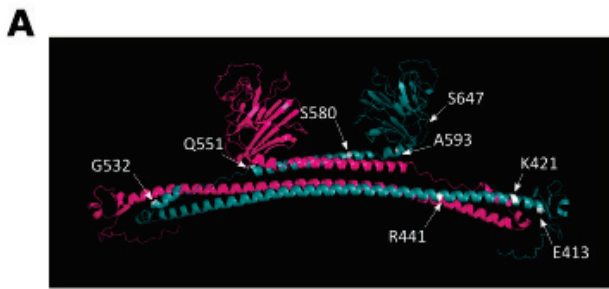


Figure 6. Truncation of the pyrin protein at the G532 residue reveals a spontaneously activated pyrin protein. (A) Truncation sites (white) within the structure of the CHS and the B30.2 domains of pyrin, (B) linear view of the truncated proteins. (C) The expression of truncated variants in U937 cells was verified by Western blot. U937 monocytes were treated with doxycycline for 16 hours, then with TcdA for 6 hours. (D) Cell death kinetics were monitored by PI incorporation/fluorescence every 15 minutes over 16 hours, then every 5 minutes for 6 hours, (E-F) corresponding AUC are shown. IL-18 concentration in the supernatant was measured by ELISA (G) after 16 hours of doxycycline and 6 hours of TcdA, (H) and after LPS for 3 hours + Nigericin for 3 hours. (I) Pyrin phosphorylation at the S242 site was assessed by Western blot following immunoprecipitation and (J) quantified by densitometry.

Data information: Data from one experiment representative of three independent experiments. Mean, SD of triplicates and individual data points are shown. (E, G) Kruskal-Wallis and Dunn's multiple comparison tests and (F) ordinary one-way ANOVA and Dunnett's multiple comparisons tests were performed to compare U937 cells expressing WT pyrin to the other cell lines. (E) **: $p=0.0025$; *: $p=0.0438$, (F) ***: $p<0.001$, **: $p=0.0073$, *: $p=0.0221$, (G) *: $p=0.0486$

Introduction

Our results presented in the main manuscript revealed that the B30.2 domain of pyrin encoded by the 200 residues at the C-terminus of the protein are dispensable for pyrin activation by TcdA. In the light of this finding, we wanted to determine the minimal region of the pyrin protein necessary for its response to physiological triggers such as TcdA. For this purpose, we generated U937 monocyte cell lines that express truncated pyrin variants under the control of a doxycycline inducible promoter. The truncation sites were selected on the basis of the crystal structure of pyrin CHS-B30.2 region (Fig. 6A-B) (Weinert et al., 2015).

Results

First, we looked at cell death kinetics following pyrin expression induction by doxycycline. We discovered that expression of the 1-532 truncated pyrin variant resulted in rapid spontaneous cell death consistent with pyroptosis, while shorter truncated variants remained inactive when expressed (Fig. 6D). Spontaneous cell death was not substantially observed for longer truncated variants (Fig. 6E). This unique property of the 1-532 truncated variant was confirmed by significantly elevated IL-18 secretion induced by doxycycline alone compared to the WT pyrin. IL-18 was much less or not present in U937 monocytes that expressed other truncated variants of pyrin (Fig. 6G).

TcdA induced pyroptosis in U937 monocytes expressing the 1-580 truncated variant (equivalent to Δ B30.2), and in U937 monocytes expressing p.M694V variant, confirming results previously obtained by our group (Fig. 6F). Additionally, TcdA triggered IL-18 secretion in monocytes expressing truncated variants of pyrin longer than 532 residues (Fig. 6G), indicating that residues 1-441 are not sufficient to provide a functional pyrin protein. Nigericin induced similar IL-18 secretion in all tested cell lines (Fig. 6H).

Based on this set of results we were able to conclude that the 1-532 region constitutes the minimal region of the pyrin protein necessary for TcdA-mediated pyrin activation.

We wanted to further investigate spontaneous pyrin inflammasome activation in cells expressing the 1-532 truncated variant. Pyrin inhibition at steady state is ensured by its phosphorylation by kinases PKN1/2 at S242 and S208 sites (Gao et al., 2016b; Park et al., 2016a). We investigated phosphorylation of pyrin truncated variants at the S242 site at steady state. As expected, we observed lower phosphorylation of the 1-532 truncated variant compared to the WT pyrin or the other truncated variants (Fig. 6I-J), consistent with the loss of inhibition at steady state.

Discussion

The minimal necessary region of pyrin has not been previously established. Here, we reveal that the 1-441 region of pyrin is not sufficient for pyrin activity as an inflammasome sensor since the 1-441 truncated variant of pyrin was unable to trigger pyrin inflammasome activation when U937 were exposed to TcdA. Additionally, we show that the 1-532 region of pyrin was sufficient to trigger the inflammasome formation, although this truncated variant apparently lacks the inhibitory mechanisms that prevent spontaneous pyrin activation. In line with this, we found that the 1-532 truncated variant of pyrin was markedly less phosphorylated than the WT pyrin or the other truncated variants, indicating that this truncation invalidated negative regulation of pyrin at steady state.

Results provided in this section demonstrate that the CHS domain of pyrin is required for its activity. The 1-441 truncated pyrin protein completely lacks the CHS domain and the B30.2 domain, this truncation completely abrogated TcdA sensing by pyrin. At the same time, the 1-532 truncated pyrin variant induced spontaneous inflammasome activation, suggesting that the 532-781 region of pyrin negatively regulates pyrin activation.

Curiously, caspase-1 cleaves pyrin protein at the Asp330 residue. The resulting N-terminal fragment has been described to translocate to the nucleus and activate the NF- κ B signaling pathway (Chae et al., 2008). Interestingly, the inflammasome NLRP1 acts as a protease sensor and is activated by various microbial proteases (Planès et al., 2022; Xu et al., 2019). Similarly, our findings open the possibility of pyrin acting as a decoy for another protease. Indeed, cleavage at the 532 site or a site close by it could yield a spontaneously activated sensor. It would thus be interesting to screen pyrin against a library of proteases of pathogenic or even endogenous origin to attempt to identify such an enzyme.

Together with other results presented in this manuscript, this supports our hypothesis that the B30.2 and the CHS domain of pyrin cooperate to provide negative regulation of the pyrin inflammasome. Indeed, several FMF-associated mutations located in the CHS domain have been described as dominant, suggesting that the negative regulation of pyrin by B30.2 requires the CHS domain (Aldea et al., 2004; Rowczenio et al., 2020).

DISCUSSION

Little is known about mechanisms regulating pyrin inflammasome activation. Pyrin was rather recently recognized as an inflammasome sensor, and while its regulation by phosphorylation was described soon afterwards, further mechanism of pyrin activation is still unclear (Gao et al., 2016; Xu et al., 2014). Our work brings more insight into pyrin regulation.

B30.2 and CHS cooperation

Given the gain-of-function profile of FMF-causing mutations and their clustering in the B30.2 domain, it has long been suspected that the B30.2 domain negatively regulates pyrin inflammasome. The results provided in this manuscript demonstrate negative regulation of pyrin by the B30.2 domain for the first time. Also, it appears that negative regulation of pyrin is more intricate than a simple phosphorylation and inhibition by B30.2.

Specific mutations in the Central Helical Scaffold (CHS) domain, like p.H478Y, result in dominant FMF-like disease in patients (Aldea et al., 2004). Other mutations in this domain are pathogenic but recessive, like p.F479L. At the same time, some of these mutations significantly heighten pyrin sensitivity to some (e.g. steroid hormone catabolites, simvastatin), but not all (e.g. UCN-01, TcdA) activating signals *in vitro*. Our findings bring attention to the previously unsuspected role of CHS in pyrin regulation.

Pyrin response to steroid hormone catabolites is, on the one hand, B30.2-dependent and, on the other hand, modulated by mutation in the CHS region. B30.2 and CHS appear to act together in a coupling mechanism, where an activating signal (or an alleviation of an inhibitory signal) perceived by the B30.2 domain and transduced along the CHS domain, likely through a series of conformational changes, toward the phosphorylated linker domain (PLD), triggers pyrin dephosphorylation. This cooperation can be seen in the way pyrin is activated by steroid catabolites. While small doses of pregnanolone and etiocholanolone are not sufficient to dephosphorylate pyrin and hence to completely activate it, they do lift pyrin inhibition mediated by the B30.2 domain (step 2) since in this setting, inflammasome activation can be triggered by pyrin dephosphorylation by a PKC superfamily inhibitor (Magnotti et al., 2021).

Additionally, our discovery of this mode of pyrin activation demonstrates that pyrin regulation by phosphorylation and pyrin regulation by the step 2 (mediated by B30.2 and CHS, according to our results), are not completely independent. Pyrin is activated when cells are treated with pregnanolone or etiocholanolone alone at a high concentration. This potentially means that a strong activation of the regulatory step 2 can overcome and trigger the regulatory step1 (phosphorylation), suggesting that there is a mechanistic link between the two checkpoints. Similarly, TcdA/B toxins, known to dephosphorylate

pyrin can fully activate pyrin (step 1 and 2) suggesting that TcdA/B are able to activate step 2 directly or by strongly engaging step 1, that these toxins could trigger a coupling mechanism between step1 and step2.

In fact, such cooperation has already been described in a different CHS- and B30.2-containing protein. Butyrophilin 3A1 (BTN3A1) is a membrane protein expressed by antigen-presenting cells. Binding of specific phosphoantigens to the intracellular B30.2 domain of BTN3A1 induces conformational changes in the B30.2 domain and beyond this domain itself. A series of such conformational changes that involve the CHS leads to the BTN3A1 dimerizing with another butyrophilin, BTN2A1, and transducing a signal from the inside of the cell to the outside. This complex on the surface of the antigen-presenting cell interacts with the $\gamma\delta$ T cell receptor and activates $\gamma\delta$ T cells (Rigau et al., 2020; Yang et al., 2019). Interestingly, the binding pocket of the BTN3A1 protein is hydrophilic (allowing it to accommodate phosphoantigens) while the corresponding groove in pyrin B30.2 domain is hydrophobic which has implications for the type of interaction between the B30.2 and its ligand.

Complexity of pyrin regulation by the CHS

The diversity of phenotypes exhibited by pyrin variants with mutations on different residues of the CHS sheds light on the complexity of pyrin regulation by this region. This complexity is best illustrated by the contrast between phenotypes of the p.F479L mutant and the p.H478Y mutant expressed in our U937 monocyte model (**Table 1**). It should be noted that the p.F479L variant is not unique, our results reveal the existence of at least one other mutation, p.Q426R, with a similar profile.

While both TcdA and UCN-01 trigger pyrin inflammasome activation in both the p.F479L and the p.H478Y variants similarly to the classical FMF p.M694V variant, there are important distinctions in the behaviour of these variants.

First, p.F479L variant is hypersensitive to steroid hormone catabolites, activated by a dose of pregnanolone that is up to 50 times smaller comparing to the WT protein. Additionally, p.F479L pyrin is activated by a larger spectrum of steroid hormones and their catabolites. In contrast, p.H478Y is less sensitive to pregnanolone or etiocholanolone than the WT pyrin, and little activation of p.H478Y is induced by other steroid hormones like progesterone or androsterone (**Table 1**).

The other important distinction to examine, is the difference in response of these two variants following treatment with simvastatin. Simvastatin inhibits HMG-CoA reductase implicated in the mevalonate kinase

pathway. Blocking mevalonate kinase pathway prevents geranylgeranylation of RhoA and inhibits its activity. At the same time, simvastatin activates pyrin inflammasome (Park et al., 2016). Our findings demonstrate that CHS mutations of pyrin differentially impact its ability to be activated by simvastatin in a pattern reminiscent of their effect on pyrin activation by steroid catabolites: the p.F479L variant is rapidly and potently activated by simvastatin at doses even lower, than those that activate the WT pyrin, while the p.H478Y variant is not at all activated by simvastatin (**Table 1**).

This difference in response to simvastatin is surprising considering that both the p.F479L and the p.H478Y variants are activated by TcdA. Until now, it was thought that simvastatin-induced activation of pyrin, like its activation by TcdA, is due to the inhibition of RhoA because of a break down in the post-translational modifications of RhoA. Mevalonate kinase pathway inhibited by simvastatin is the source of geranylgeranyl pyrophosphate (GGpp) – a substrate used for geranylgeranylation of proteins like RhoA. GGpp complementation abolishes pyrin activation by simvastatin, supporting this hypothesis (**Fig. 1**) (Park et al., 2016). If pyrin activation by TcdA and simvastatin involves the same mechanism of RhoA inhibition sensing, then what could be behind such a drastic difference in the response of the different variants to simvastatin (while they respond similarly to TcdA)?

Actually, there could be an alternative mechanism of pyrin activation by simvastatin distinct from pyrin activation by TcdA. The mevalonate kinase pathway also produces cholesterol in the cell. Therefore, simvastatin deprives the cell of GGpp and cholesterol at the same time. Cholesterol being the substrate of steroidogenesis, its deficiency could alter steroid metabolism in the cell. Considering the differential sensitivity of p.F479L pyrin and p.H478Y pyrin to steroid hormones and their catabolites brought to light by our results, it is tempting to speculate that pyrin activation by simvastatin is based at least in part on

		Pyrin variant:			
Treatment:	p.F479L	p.H478Y	WT	p.M694V	
TcdA	++	+++	+	+++	
UCN-01	+++	+++	-	+++	
Pregnanolone	+++	+	+	+	
Etiocholanolone	+++	+	+	+	
Progesterone	++	-	-	-	
Simvastatin	+++	-	+	+	
Nigericin	+	+	+	+	

Table 1 Comparison of phenotypes exhibited by pyrin variants with mutations in the CHS domain – p.F479L and p.H478Y, WT pyrin and the prototypical FMF mutation p.M694V, in response to various stimuli.

its sensing of cholesterol metabolism – a role that has not been previously assigned to the pyrin inflammasome (Fig. 1).

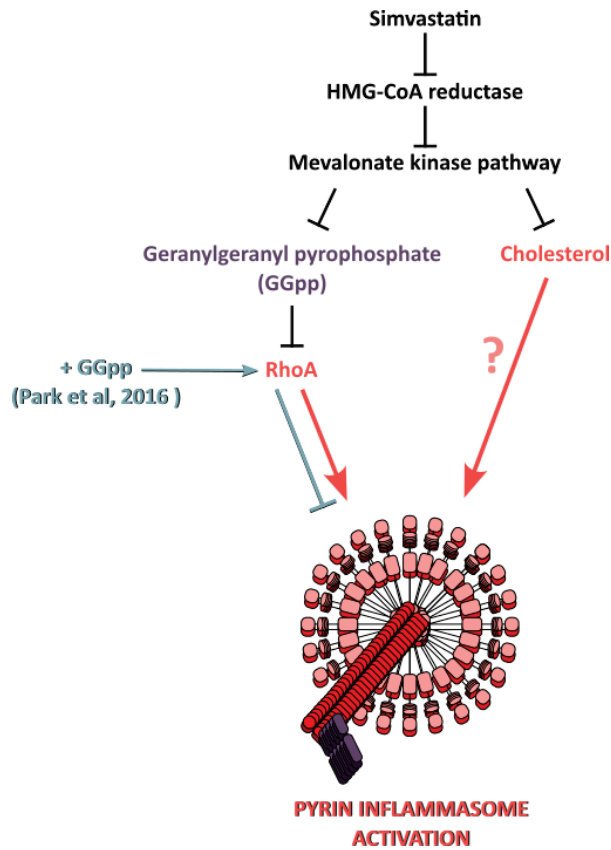


Figure 1. Pyrin inflammasome activation by simvastatin. Simvastatin targets HMG-CoA reductase, an enzyme implicated in the mevalonate kinase pathway. Its inhibition results in the inhibition of geranylgeranyl pyrophosphate (GGpp) synthesis and of cholesterol synthesis. Complementation with GGpp prevents pyrin activation by simvastatin, as demonstrated by Park and colleagues. Our results strongly suggest that pyrin activation by simvastatin is at least partially mediated by pyrin sensing cholesterol metabolism.

Cholesterol metabolism sensing by pyrin

Mevalonate kinase pathway provides the cell with cholesterol as well as other important metabolites. Steroidogenesis uses cholesterol to transform it into other steroid molecules such as glucocorticoids and steroid sex hormones. Simvastatin inhibits the mevalonate kinase pathway, and limits cholesterol synthesis in the cell (Fig. 2) (Tang, 2022). Statins inhibit synthesis of steroid molecules both *in vitro* and on the scale of an entire organism (Stamerra et al., 2021).

Results provided in this manuscript lead us to believe that pyrin senses various steroids and their derivatives with varying affinity and varying effects on the pyrin inflammasome. For example, it appears that both progesterone and pregnanolone impact pyrin activation (Additional results, Fig. 2). Progesterone has either a neutral or an inhibitory effect on the pyrin inflammasome and likely has a weaker affinity to pyrin if the binding is direct. On the other hand, pregnanolone can activate pyrin and is sensed with a higher affinity, because it is able to activate the pyrin inflammasome as soon as its concentration is equal to that of progesterone (Additional results, Fig. 2).

We hypothesize that pyrin activation by simvastatin is at least partially due to pyrin-mediated sensing of cholesterol metabolism imbalance induced by the statin treatment. We propose a model where pyrin

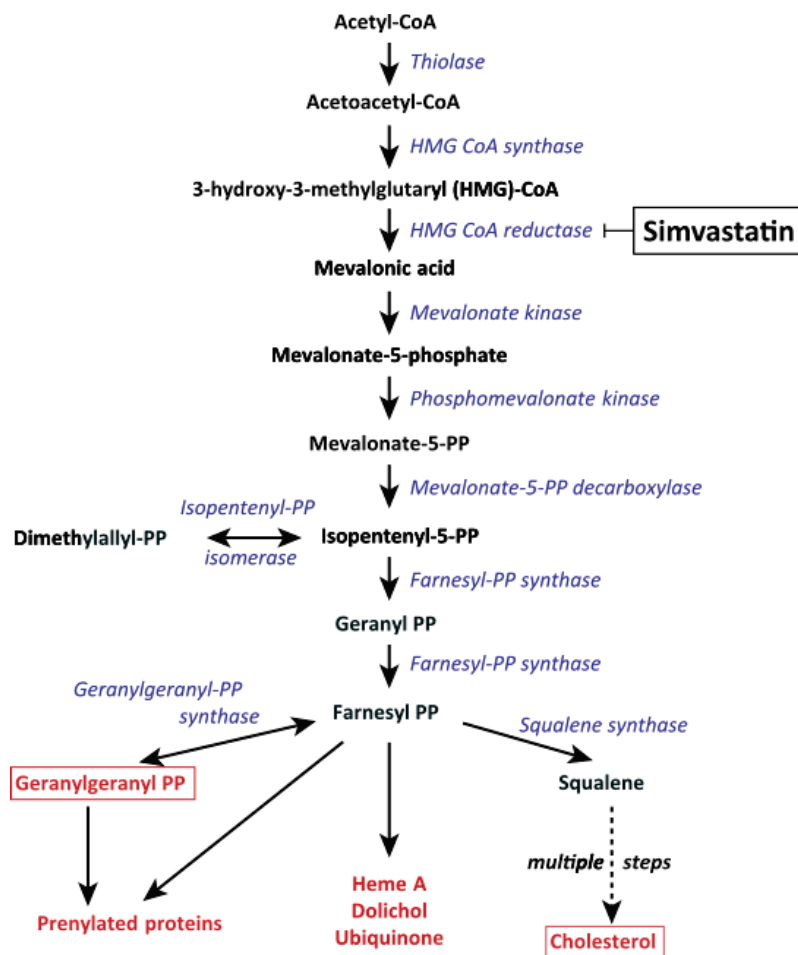


Figure 2. Mevalonate kinase pathway. Simvastatin, inhibitor of HMG-CoA reductase, is pictured on the right in a black box. Geranylgeranyl pyrophosphate (GGpp) and cholesterol are highlighted by red boxes (adapted from Fessler et al, 2016).

would act as a sensor of steroid metabolism in the cell. According to this model, pyrin activation in response to simvastatin treatment would go through the following mechanism: as cholesterol synthesis is inhibited by the statin, so is steroidogenesis since it is dependent on cholesterol. Steroids present in the cytoplasm of the cell would be progressively depleted, molecules that are most upstream of the steroidogenesis pathway (e.g. progesterone or testosterone) would decrease before their catabolites (e.g. pregnanolone or etiocholanolone). As the equilibrium between steroids and their catabolites shifts towards the catabolites, pyrin would sense the increasing concentration of steroid derivatives in comparison to the decreasing concentration of the steroids and trigger inflammasome activation (**Fig. 3**). This mode of steroid metabolism sensing would also explain slower cell death kinetics observed when monocytes expressing WT pyrin are treated with simvastatin: we begin to observe PI incorporation only 6-9 hours post-treatment. For reference, TcdA triggers cell death within 2-3 hours post-treatment in U937 monocytes and steroid catabolites trigger cell death within the first hour post-treatment.

To confirm this model several crucial steps need to be verified. First, we would like to clarify the effect of progesterone sensing on pyrin inflammasome activity. Our first observations suggested that pyrin was not able to sense progesterone because progesterone did not induce pyroptosis in pyrin-expressing cells unlike pregnanolone or etiocholanolone. Our more recent results presented in this manuscript demonstrate that progesterone counters pregnanolone-mediated pyrin activation, as long as progesterone concentration is higher than that of pregnanolone, which suggests that pyrin does sense progesterone, either directly or indirectly (Additional results, Fig. 2). The next step would be to test whether progesterone can counter pyrin activation by other stimuli such as TcdA, that activates pyrin by inhibiting RhoA or UCN-01 that activates p.M694V-expressing pyrin by promoting pyrin dephosphorylation.

Additionally, it would be important to establish whether this steroid/catabolite antagonistic sensing is also valid for the testosterone/etiocholanolone couple, etiocholanolone being the other steroid derivative we identified that is able to activate WT pyrin and is a catabolite of testosterone.

Local steroidogenesis by macrophages and monocytes does occur (Yamauchi et al., 2022), but to the best of our knowledge monocytes lack the 5 β -reductase - AKR1D1 - necessary to produce molecules such as pregnanolone or etiocholanolone (Chen and Penning, 2014; Schiffer et al., 2019). AKR1D1 is almost exclusively expressed in the liver. Therefore, the question remains open of how pyrin had evolved to sense such steroid derivatives not naturally produced by myeloid cells. It is possible that although in our

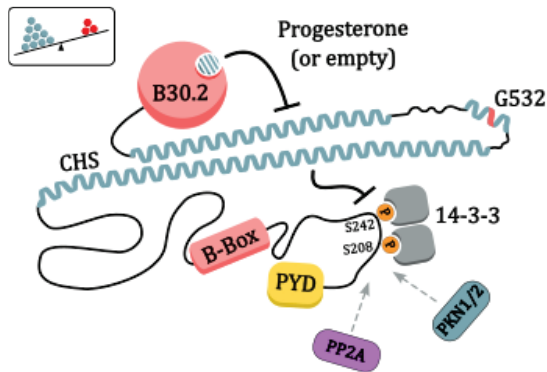
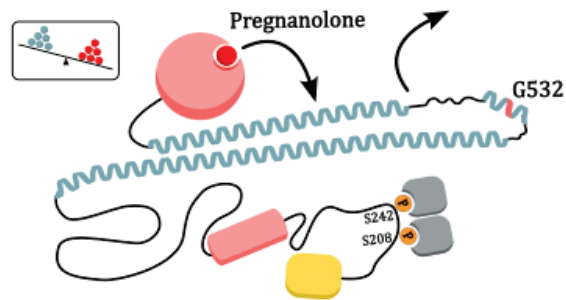
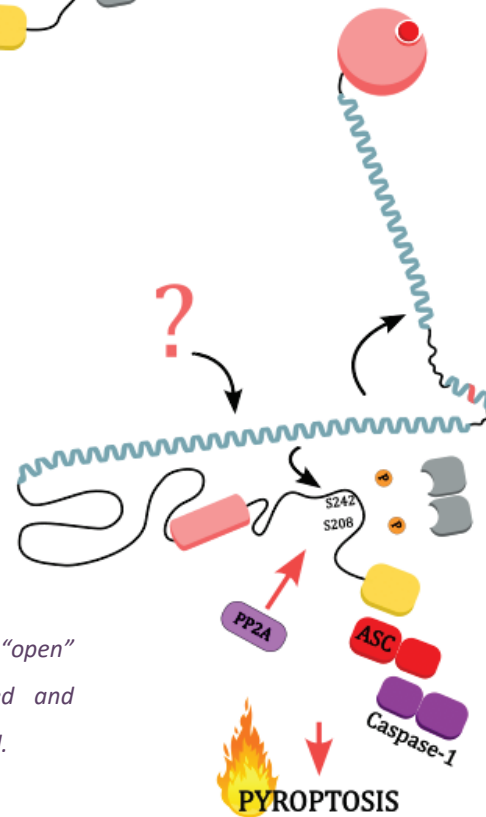


Figure 3. Model of pyrin activation by steroids.

(Top) Ligand-binding pocket of B30.2 is occupied by progesterone (or not occupied at all). Pyrin has a "closed" conformation, it is



(Middle) If/when pregnanolone becomes more present in the cell than progesterone, it replaces progesterone in the ligand-binding pocket of B30.2. This induces a change of conformation in the CHS.



(Bottom) Pyrin transitions into an "open" conformation, it is dephosphorylated and activated. The inflammasome is formed.

experiments we use specific steroid molecules, in physiological setting pyrin would sense different molecules that share stereochemical features with the steroids we use.

And finally, it is crucial to establish whether pyrin sensing of steroid metabolites is direct.

B30.2 steroid sensing

The question of direct binding of steroid molecules to the pyrin B30.2 is central for our understanding of pyrin activation by these molecules. Several pieces of evidence strongly suggest that steroids bind directly to the B30.2 of pyrin.

Pyrin activation by pregnanolone and etiocholanolone occurs within a very short time: pyroptosis is triggered within 30 minutes after treatment. Therefore, the mechanism of pyrin inflammasome activation by steroid catabolites is most likely non-genomic.

Pyrin inflammasome activation by pregnanolone and etiocholanolone is B30.2-dependent. When monocytes expressing pyrin without the B30.2 domain (Δ B30.2) were exposed to pregnanolone, we observed no PI incorporation, so no inflammasome activation (Magnotti et al., 2021). Pyrin B30.2 contains a hydrophobic cavity that could be a ligand-binding site. According to docking experiments performed *in silico* by our group, pregnanolone (and etiocholanolone) localized in the ligand-binding pocket of pyrin B30.2 (**Fig. 4A**). We also assessed steroid catabolite binding to the B-Box-CHS-B30.2 fragment of pyrin by microscale thermophoresis (MST). Although we were not able to obtain the K_d/K_a value for the interaction, we did observe a shift suggesting that there is an interaction between pyrin and pregnanolone (**Fig. 4B**). This experiment will require further optimisation to overcome technical difficulties linked to low solubility of steroid catabolites.

In addition, murine macrophages are deficient for steroid catabolites response in agreement with the murine pyrin protein not containing the B30.2 domain. Yet, ectopic expression of human pyrin in murine macrophages render them susceptible to steroid catabolites.

Finally, a genome-wide CRISPR/Cas9 screen on U937 pyrin-expressing monocytes treated (or not) with pregnanolone identified the *PYCARD* and *MEFV* genes, encoding the ASC and Pyrin proteins respectively. The same screen did not reveal any obvious steroid receptors to be involved in pyrin activation by pregnanolone (Dalmon S., unpublished data by our group).

Nevertheless, this evidence is secondary and not sufficient to definitively conclude that steroid catabolites directly bind pyrin B30.2. We would like to focus further effort on confirming this direct interaction.

Alternatively, steroids produce non-genomic effects on their target cells by interfering with the MAPK pathway or by modulating the intracellular Ca^{2+} (Foradori et al., 2008; Guo et al., 2002). Mobilisation of calcium is one of the triggers of the NLRP3 inflammasome (Murakami et al., 2012; Zhou et al., 2020). If pyrin activation by steroid derivatives is not direct and requires a mediator, then it could be triggered by Ca^{2+} signalling. This hypothesis remains to be tested experimentally.

Physiological pertinence of steroid sensing by pyrin

In physiological setting steroid catabolites reach plasma concentrations that are much smaller than those needed to fully activate pyrin inflammasome. In the last weeks of pregnancy when serum pregnanolone reaches its peak, it can be as high as 70 nM (Deligiannidis et al., 2016; Hill et al., 2007). Therefore, it is likely that steroid molecules alone are not naturally able to fully activate the WT pyrin inflammasome at least in circulating cells. However, they could mediate a “priming” of pyrin which would facilitate

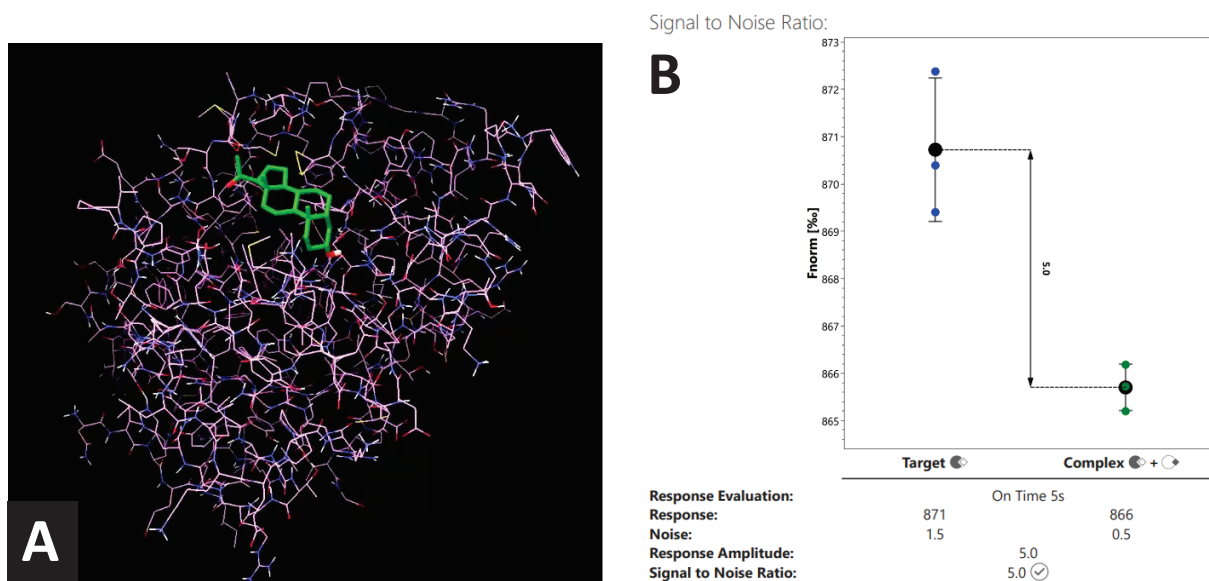


Figure 4. Thermophoresis Preliminary evidence suggesting direct binding of pregnanolone to pyrin. (A) *In silico* docking of pregnanolone (green) in the pyrin B30.2 domain (magenta), performed using AutoDoc4. Docking performed by Sarah Dalmon. (B) Microscale thermophoresis (MST) Binding check of recombinant Pyrin B-Box-CHS-B30.2 domain in the absence (blue dot) or presence (green dot) of pregnanolone (5 μM). Experiment performed by Flora Magnotti.

subsequent pyrin activation by other stimuli. Indeed, we observed that a low concentration of pregnanolone (6 μ M) not sufficient to activate WT pyrin, “sensitized” pyrin to the UCN-01 treatment or a suboptimal dose of TcdA which do not trigger WT pyrin activation under normal conditions (Magnotti et al., 2021).

Furthermore, while systemic concentrations of pregnanolone are likely not sufficient to trigger pyrin inflammasome, local concentrations of pregnanolone in tissue might prime or even activate pyrin. Similarly, extracellular ATP which is used at 5-10 mM to activate the NLRP3 inflammasome is thought to be a physiological activator of the NLRP3 inflammasome in tissues (Amores-Iniesta et al., 2017; Baron et al., 2015).

“Priming” of pyrin by steroid catabolites could be behind recurrent attacks of fever experienced by FMF patients. Emotional and physical stress are among the most common triggers of inflammatory bouts reported by FMF patients (Karadag et al., 2013; Kishida et al., 2020). Stress is also strongly associated with an increased concentration of pregnanolone in serum (Park et al., 2017; Ströhle et al., 2002). Between a third and a half of women with FMF report having menstruation-associated autoinflammatory attacks (Akar et al., 2006; Kishida et al., 2020). The beginning of the menstrual cycle is accompanied by a drastic drop in serum progesterone. When progesterone is eliminated from the body, it undergoes several biochemical modifications, one of the catabolites formed in this process is pregnanolone (Schiffer et al., 2019).

That being said, there is no significant difference in the incidence of FMF between men and women, despite adult women having a fluctuating but always higher progesterone level in serum than men (Bhatt and Cascella, 2022). Yet, this absence of sex bias in FMF might be due to the fact that etiocholanolone, a testosterone catabolite, can also activate pyrin although slightly less than pregnanolone.

Elevated progesterone and pregnanolone are characteristic of the last weeks of pregnancy, but some women with FMF experience a complete remission during pregnancy while others report no change in their symptoms or increased severity of febrile attacks (Ben-Chetrit and Levy, 2003). Puberty is associated with drastic hormonal changes in the body but, although the vast majority of FMF patients experience the first attack of the disease before the age of 20, there is no documented link between the onset of FMF and puberty.

Importance of specific residues in pyrin activity

As mentioned before, it is intriguing to see such a difference between the phenotypes of p.F479L and p.H478Y variants that impact amino acids located right next to each other on one α -helix of the CHS. This highlights the importance of specific amino acids, their biochemical properties, and their position in pyrin activity. Unfortunately, our attempts at elucidating specific intra- or inter-molecular interactions involved in the sensing of steroids and their catabolites by pyrin did not yield a clear understanding of the mechanism (Additional results, Fig.4 and Fig.5). It would be crucial for the understanding of pyrin activation to dig deeper into the interactions within pyrin oligomers before and during inflammasome activation by various stimuli. With more detailed knowledge about the structure of the entire protein we could better analyse the impact of pyrin mutations.

Pyrin-Associated Autoinflammatory Diseases (PAAD)

Classification of FMF-associated pyrin variants is notoriously difficult. There is no clear prediction algorithm to evaluate the pathogenicity of FMF mutations or the severity of disease they would produce. The scientific community proposed several attempts at classifying pyrin variants, but none have stuck so far.

Patients carrying the same mutation or the same combination of mutations can present with very different phenotypes: what can be a dominant PAAND in one patient, can be an asymptomatic carrier state for another (Kiyota et al., 2020; Masters et al., 2016). Some mutations occur frequently and are believed to be non-pathogenic by themselves but contribute to severity of disease when combined with other mutations (Miyashita et al., 2022). The difficulty of categorizing pyrin mutations is evident from the number of FMF-associated mutations listed in the Infevers database that are classified as Variants of Unknown Significance (VUS). Currently 115 mutations (29 %) are classified as VUS out of 391 mutations listed, while only 5 (1.3 %) mutations are classified as pathogenic and 57 (14.5 %) as likely pathogenic (**Fig. 5**) (Infevers database, consulted on 20/09/22).

The panoply of autoinflammatory diseases associated with aberrant pyrin inflammasome activation was illustrated earlier in this manuscript. Several of these disorders arise from mutations in genes other than *MEFV*. However, at least two well defined diseases – PAAND and FMF – are linked directly to mutations impacting pyrin and even they contain a considerable variability of clinical presentations. In light of such complexity the term pyrin-associated autoinflammatory disease (PAAD) has been recently suggested (Boursier et al., 2019).

We believe that this clinical complexity arises from the fact that pyrin protein inflammasome is regulated by multiple mechanisms, not all of which are well-known to science. Pyrin is inhibited by phosphorylation which is maintained by RhoA effectors PKN1/2. The breakdown of this checkpoint causes PAAND. Pyrin is also inhibited by a mechanism linked to microtubule dynamics. This mechanism appears to be broken down by B30.2 mutations that cause classical FMF which in most cases is a recessive disease. Finally, mutations located in the CHS domain of pyrin modulate passage of the activating signal from B30.2 to the phosphorylation sites of pyrin. At this time, it is still unclear whether these mutations cause a typical FMF or whether a particular symptomatology could be associated with these mutations possibly in relation with the physiology of sex hormones catabolism, secondary bile salt generation by the microbiota or cholesterol metabolism. Finally, it remains to be understood why certain *MEFV* mutations cause dominant FMF (e.g. p.H478Y, p.P373L, p.M694del) while other do not (e.g. p.F479L, p.M694V). Of note, our U937 model currently does not allow us to test the dominance/recessivity of pathogenic pyrin variants, which is one of the limitations of our experimental model.

Limitations of the model

The majority of experiments assembled in this manuscript were performed in U937 monocytes, where pyrin is under the control of a doxycycline promoter. This is an overexpression system prone to biases such as excessive inflammasome activation in response to more potent triggers. It is likely that this system is not well suited to study more subtle mechanisms that rely on an equilibrium of phosphorylation/dephosphorylation or delicate balances of cholesterol metabolism. Additionally, regulation of inflammasome activation differs between monocytes, macrophages, and neutrophils – different cell subsets that express pyrin.

The genetic construct introduced in our U937 monocytic cell lines contains only the coding DNA sequence (CDS). Some aspects of pyrin regulation such as non-coding RNA targeting 5'UTR or 3'UTR sequences are absent from our model.

Hence, we strive to systematically validate the observations from the U937 system in primary peripheral mononuclear cells obtained from healthy donors or patients with FMF or FMF-like diseases.

The cell culture medium used in our experiments is complemented with foetal calf serum which may contain pregnancy-associated hormones. We cannot exclude that this may influence pyrin inflammasome activation.

Additional difficulty in the study of the pyrin inflammasome through the prism of mutations linked to FMF is that there is an inevitable bias in the choice of residues that receive closer examination. It would be beneficial to develop methods that would allow to scan through pyrin residues in an unbiased manner to determine their importance in pyrin function.

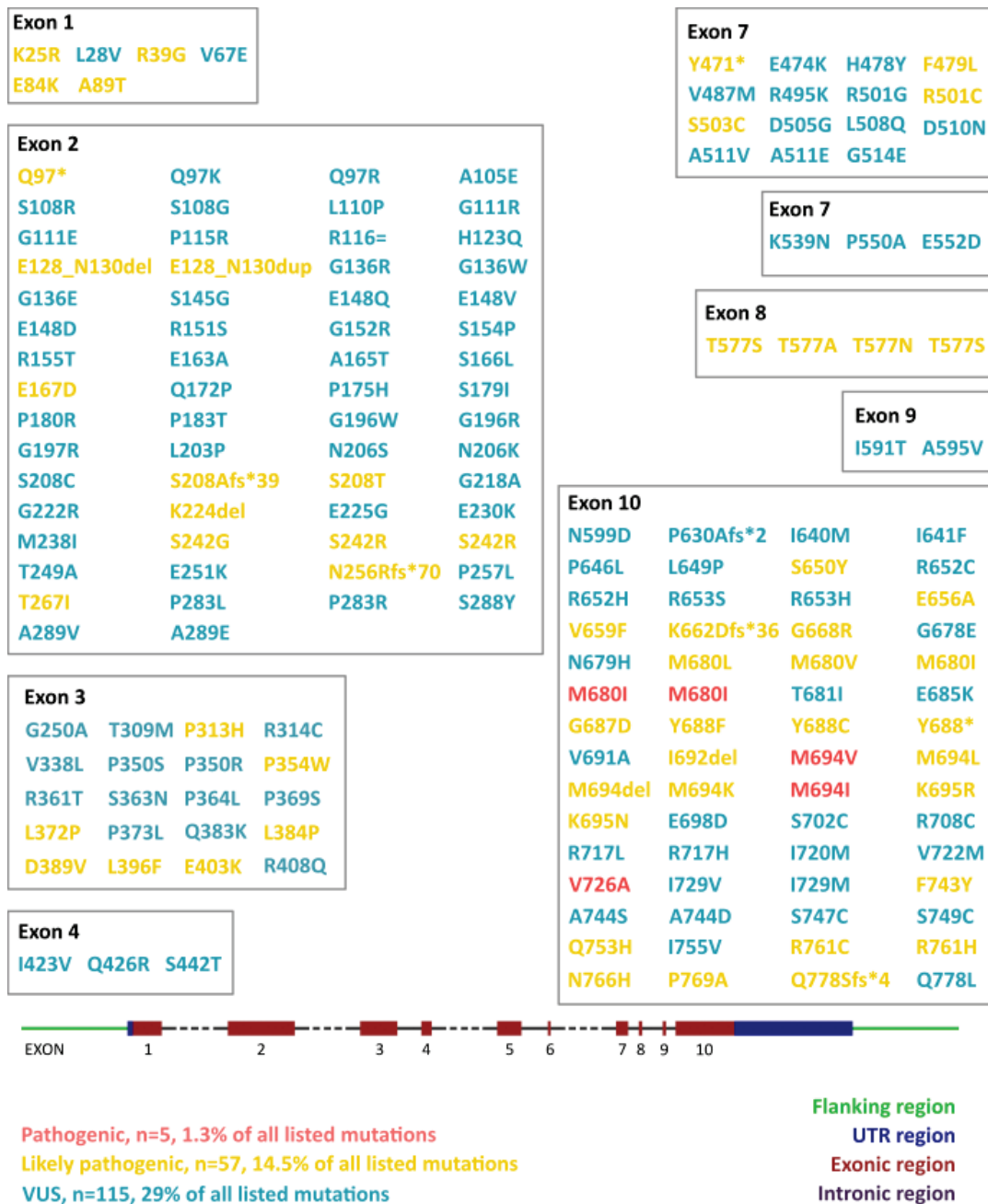


Figure 5. FMF-associated mutations located in the coding DNA sequence of the MEFV gene listed in the Infevers database (accessed on 20/09/2022). Pathogenic mutations appear in red, likely pathogenic are in yellow. Variants of unknown significance (VUS) appear in blue.

MATERIALS AND METHODS

The following section contains “Methods and Protocols” chapter published in *Methods in Molecular Biology* in June 2022. It includes a detailed description of key protocols used by our group for functional assessment of disease-associated pyrin variants.

Chapter 12

Functional assessment of disease-associated pyrin variants

Daria Chirita¹, Yvan Jamilloux^{1,2}, Thomas Henry^{1,@}, Flora Magnotti^{1,@}

¹CIRI, Centre International de Recherche en Infectiologie, Univ Lyon, Inserm U1111, Université Claude Bernard Lyon 1, CNRS, UMR5308, ENS de Lyon, Univ Lyon, F-69007, LYON, France

²Internal Medicine, University Hospital Croix-Rousse, Hospices Civils de Lyon, Lyon, France

@Correspondence to: thomas.henry@inserm.fr or flora.magnotti@inserm.fr

Running Head: Pyrin variants functionality and pathogenicity

Abstract

The pyrin inflammasome detects effectors and toxins that inhibit RhoA GTPases and triggers inflammatory cytokines release and a fast cell death termed pyroptosis. Ancient plague pandemics in the Mediterranean basin have selected in the human population pyrin variants that can trigger an autoinflammatory disease termed Familial Mediterranean Fever (FMF). In addition, distinct mutations in *MEFV*, the gene encoding pyrin, cause a different rare autoinflammatory disease termed, Pyrin-Associated Autoinflammation with Neutrophilic Dermatitis (PAAND). As of today, more than 385 *MEFV* variants have been described although for most of them, whether they are pathogenic variant or benign polymorphism is unknown.

Here, we describe different methods using primary human monocytes or engineered monocytic cell lines to functionally characterize *MEFV* variants, determine their potential pathogenicity and classify them as either FMF-like or PAAND-like variants.

Keywords: Pyrin, inflammasome, familial Mediterranean fever, Pyrin-Associated Autoinflammation with Neutrophilic Dermatitis, *MEFV*, pyroptosis, real time cell death assay, IL-1 β

1. Introduction:

MEFV encodes the pyrin protein, an important player of the antibacterial innate immune responses (Aubert et al., 2016; Chung et al., 2016; Jamilloux et al., 2018; Ratner et al., 2016; Xu et al., 2014).

Mutations in this gene are associated with two auto-inflammatory disorders: familial Mediterranean fever (FMF), the most frequent hereditary auto-inflammatory disease (“Ancient missense mutations in a new member of the RoRet gene family are likely to cause familial Mediterranean fever. The International FMF Consortium,” 1997; French FMF Consortium, 1997; Manukyan and Aminov, 2016), and a rare disease termed Pyrin-Associated Autoinflammation with Neutrophilic Dermatitis (PAAND) (Moghaddas et al., 2017). In these patients, *MEFV* mutations lead to a deregulation in the pyrin-associated inflammatory responses causing recurrent inflammation (Masters et al., 2016; Ozen et al., 2003).

Pyrin is an inflammasome sensor on the front line of the innate immune response against pathogens. Inflammasomes work as multi-protein complexes formed in response to cytosolic pathogen-associated molecular patterns (PAMPs), endogenous damage-associated molecular patterns (DAMPs) or homeostasis-altering molecular processes (HAMPs) (Fabio Martinon et al., 2002). Three major events characterize pyrin inflammasome formation and can be used as readouts to monitor inflammasome activation: 1) ASC (Apoptosis-associated Speck-like protein containing a CARD) speck formation. ASC is the inflammasome adaptor. It oligomerizes to form a “speck” in the cytosol as the inflammasome complex is assembled (Fernandes-Alnemri et al., 2007). ASC speck constitutes a platform onto which the inflammasome effector, caspase-1 is recruited, and activated; 2) Pyroptosis. Pyroptosis is an inflammatory form of cell death due to the caspase-1-mediated cleavage of Gasdermin D. Gasdermin D is a pore-forming protein that, upon cleavage, oligomerizes in the plasma membrane and mediates a fast necrotic cell death (Kayagaki et al., 2015; Liu et al., 2016); 3) the release of pro-inflammatory cytokines (Interleukin-1 β (IL-1 β) and Interleukin-18 (IL-18)) into the extracellular space (B. T. Cookson and Brennan, 2001; Fabio Martinon et al., 2002).

Pyrin acts as a guard mechanism for RhoA GTPases inhibition (Chung et al., 2016; Ratner et al., 2016; Xu et al., 2014). Numerous bacterial effectors such as YopE and YopT from *Yersinia* spp. (Chung et al., 2016; Ratner et al., 2016), TecA from *Burkholderia* (Aubert et al., 2016) and numerous toxins such as *Clostridioides difficile* toxins A and B (TcdA/TcdB) inhibit RhoA by covalent modifications. Pyrin does not recognize neither the bacterial effectors/toxins nor the covalent modifications, but senses RhoA inhibition (Xu et al., 2014). Indeed, at steady state, RhoA maintains pyrin inactive via the dynamic activation of the two RhoA effectors, PKN1 and PKN2. PKN1 and PKN2 are kinases from the PKC superfamily that phosphorylate Pyrin on two serine residues (S208 and S242). The phosphorylated Pyrin binds 14-3-3 chaperone proteins, which sequester Pyrin away from an active inflammasome (Gao et al., 2016; Park et al., 2016). When RhoA GTPases are inhibited, PKN1/2 are no longer activated, and Pyrin is no longer phosphorylated. In the dephosphorylated state, Pyrin is able to assemble the inflammasome complex and triggers the inflammatory response (Gao et al., 2016; Masters et al., 2016;

Park et al., 2016; Van Gorp et al., 2016). *MEFV* mutations affecting one the phosphorylation sites or 14-3-3 binding sites alleviate this regulatory mechanism and are causing PAAND (Hong et al., 2019; Masters et al., 2016; Moghaddas et al., 2017).

The Pysin inflammasome activation mechanism has not been fully deciphered but we demonstrated that Pysin dephosphorylation is insufficient to activate the inflammasome. Indeed, blocking Pysin phosphorylation through PKN1/2 inhibition (using the PKC superfamily inhibitor UCN-01) or genetic approaches (by mutating the S208/S242 residues), does not activate Pysin in primary monocytes from healthy donors. On the contrary, dephosphorylation of Pysin is sufficient to activate the pyrin inflammasome in monocytes from FMF patients (Magnotti et al., 2019). Pysin activation is thus controlled by two mechanisms, the first one depending on (de)phosphorylation which is constitutively activated in PAAND patients and a second poorly understood mechanism, which is constitutively activated in FMF patients. This differential response to pyrin dephosphorylation (i.e. to UCN-01 treatment) is at the basis of the assays described here to discriminate FMF-like *MEFV* variants patients from WT-like variants. Of note, another technique based on the *in vitro* resistance to colchicine inhibition has been previously described (Van Gorp et al., 2016). Furthermore, combining a PAAND mutation (constitutive activation of signal 1) with a FMF mutation (constitutive activation of signal 2) results in a constitutively active Pysin inflammasome. We thus present a technique based on genetic engineering of a monocytic cell line to classify *MEFV* variants for their potential pathogenicity (FMF-like or PAAND-like variant). Finally, we detail methods to investigate the impact of *MEFV* mutation on Pysin phosphorylation level. Altogether, the techniques presented here allow to monitor activation of the Pysin inflammasome using several stimuli and several readouts, in primary human monocytes and in *MEFV* variant-expressing monocytic cell lines to be able to assess the functional impact of *MEFV* mutations and determine their potential pathogenic impact.

2 Materials:

2.1 Pysin-expressing U937 cell lines

Generation of pyrin-expressing U937 cell lines is not described as a specific method since these cells are generated by standard transduction methods (Magnotti et al., 2019). 3xFLAG-*MEFV*-expressing lentiviral plasmids are available at Addgene (e.g. #134702, 134703, 134706 for 3xFLAG-WT, p.M694V and p.S208C/S242R/M694V *MEFV*-expressing plasmids, respectively). Site-directed mutagenesis of *MEFV* gene to generate novel sequence variant of interest can be performed either on the lentiviral plasmid or on the parental entry plasmid (Addgene #167018, 167118, 167020 for pENTR1A-WT, p.M694V, p.S242R *MEFV*) (Note 1). pINDUCER21 vector (Meerbrey et al., 2011) derivatives are used

and contains GFP for FACS sorting-based selection and a doxycycline-inducible promoter driving *MEFV* expression.

1. Cell culture medium: RPMI 1640 with GlutaMAX, 10% foetal calf serum (FCS).
2. Doxycycline (Sigma, D9891): stock at 1mg/mL in water, filter-sterilize, aliquot and store at -20°C. Final concentration: 1 µg/mL (Note 2).

2.2 Primary monocytes

Isolation of primary monocytes is not described as a specific method since standard procedures are used. Experimental work on primary human cells requires ethical approval. Procedures have been optimized to limit the cell number (Jamilloux et al., 2018) (Table 1) and we routinely perform several inflammasome stimuli and readouts with 4 mL of blood drawn in heparin-coated tubes. Tubes are kept overnight at room temperature (RT) before isolation the next day using density-gradient centrifugation and CD14-based positive selections (Magnotti et al., 2020, 2019).

2.3 Pysin phosphorylation level

1. Lysis buffer: 25 mM Tris HCl pH 7.0, 150 mM NaCl, 1 mM EDTA, 0.1% Igepal CA-630 (NP40) supplemented with: 10mM Sodium fluoride (phosphatase inhibitor), and cOmplete™ EDTA-free Protease Inhibitor Cocktail (Roche, 05056489001).
2. Anti-Flag beads: ANTI-FLAG M2 Affinity Gel (Sigma, A2220) or Anti-FLAG® M2 Magnetic Beads (Sigma, M8823).
3. WB blocking buffer: Tris buffered saline buffer (25 mM Tris-base, 137 mM NaCl, 2.7 mM KCl, pH 7.5), 1% (v/v) Tween, 5% (w/v) skimmed milk.
4. Antibodies: Anti-Pysin (phospho S241) antibody [EPR19570] (Abcam, ab200420) diluted 1:1000, anti-Pysin (phospho S205) antibody [EPR19567] (Abcam, ab201784) diluted 1:1000 (Note 3), anti-Pysin (human), pAb (AL196) (Adipogen, AG-25B-0020-C100) diluted 1:2000, Anti-Actin Antibody clone C4 (Millipore, MAB1501) diluted 1:5000.

2.4 ASC speck immunofluorescence

1. Fixative: 2% (w/v) paraformaldehyde in PBS.
2. Cyto centrifuge: Cytospin 3 (Shandon), cytofunnels, cyto clips, disposable filter cards (Thermo Scientific, 5991022).
3. Permeabilization buffer (PBS-T): PBS, 0.1% (v/v) Triton X100.
4. Blocking buffer: PBS, 0.1% (v/v) Triton X100, 3% (w/v) BSA, 3mM Na₃N.
5. PAP thick pen for immunostaining (Dutscher, 490001)
6. Antibodies: anti-ASC (Santa Cruz, sc22514R, 4µg/mL); Alexa 488-goat anti-rabbit antibodies (Invitrogen, A-110088, 10µg/mL)
7. DAPI: Stock at 1mg/mL in water, use at 100 ng/mL in PBS-T

8. Fluoromount-G Mounting medium (Invitrogen, 00-4958-02)

2.5 Inflammasome stimuli

Inflammasome stimuli are presented in Table 2.

2.6 Real time cell death assay

1. 96-well plates black flat bottom.
2. Supplemented CO₂-independent medium: CO₂-independent medium supplemented with 10% FCS, 2 mM glutamine.
3. Propidium iodide: stock 1 mg/mL in water, filter sterilize, use at 5 µg/mL final.
4. Triton X100 (Sigma, X100): stock at 10% (v/v) in water, use at 1 % final.
5. Required apparatus: Plate fluorimeter with thermoregulation (CO₂ Chamber dispensable).

2.7 ELISA

1. Nunc MaxiSorp™ flat-bottom, for ELISA assay.
2. Phorbol 12-myristate 13-acetate (PMA) (Invivogen, tlrl-pma): stock at 5 mg/mL in water, use at 100 ng/mL final
3. ELISA IL-1β: Human IL-1 beta/IL-1F2 DuoSet ELISA (R&D, DY201)
4. ELISA IL-18 : Capture antibody: Anti-human IL18 (R&D, D044-3) at 4µg/mL; Detection antibody: biotin labeled anti-human IL18 (R&D, D045-6) at 500µg/mL; Standard protein: recombinant human IL18 (R&D, B001-5)

3. Methods

To functionally assess the role of *MEFV* mutations, we evaluate the activity of the corresponding Pyrin inflammasome in response to various stimuli (e.g. UCN-01 for FMF-like variants) or by combining them with the well-known FMF mutation (p.M694V) or PAAND mutation (p.S242R). The decision tree to classify novel pyrin variants as FMF-like, PAAND-like or likely benign based on the techniques described here and the current knowledge in the field is presented in Fig. 1. Pysin phosphorylation level can be investigated as an additional mechanistic insight especially for PAAND-like mutations. Three readouts for pyrin inflammasome activation are routinely examined: i) ASC speck formation, ii) pyroptosis, and iii) the release of pro-inflammatory cytokines. All these analyses can be performed using *MEFV*-expressing U937 cell lines (see Material 1) or primary human monocytes, with the exception of Pysin phosphorylation monitoring by Western blot analysis, which has been optimized for cell lines.

3.1 Determination of pyrin phosphorylation level by immunoprecipitation followed by Western blot

This protocol aims at determining the phosphorylation level of serine 208 and 242 residues of Pysin using 3xFlag-*MEFV*-expressing U937 cell lines. Typical results are presented Fig. 2.

1. Incubate the cells in cell culture medium supplemented with 1µg/mL doxycycline overnight at 37°C, 5% CO₂, to induce *MEFV* expression. Keep 2*10⁶ U937 cells without doxycycline (or a control U937 cell line not expressing a flag-tagged protein) to saturate the anti-Flag beads.
2. Count the cells and seed the appropriate amount (Table 1) in fresh medium. Proceed to the treatment (e.g. UCN-01, 12.5 µM, 15 min).
3. Collect cells in 1.5 mL tubes. Wash the cells once with 1mL ice-cold PBS (centrifuge 5 min 120 rcf 4°C). Resuspend the cell pellet in 400 µL of ice-cold lysis buffer. Lyse cells during 1 h at 4°C on a rotating wheel or store at -80°C. Clarify the lysate by centrifuging 10 min at 14 000 rcf 4°C. Set aside 30 µL for input control (add 10 µL of loading dye, boil for 5 min at 95°C and store at -20°C).
4. Take 10 µL of beads slurry per sample. Wash 3 times with 1 mL lysis buffer. Add the clarified U937 lysates (400 µL, without doxycycline) to the beads to saturate the non-specific binding sites. Incubate on a rotating wheel at 4°C for 30 min. Wash once in lysis buffer and resuspend in 100 µL of lysis buffer / sample.
5. Add the clarified lysate sample to the 100 µL beads mix. Incubate on a rotating wheel at 4°C for 2 h. Wash the beads 3 times in ice-cold lysis buffer. Resuspend beads in 20 µL loading dye, boil for 5 min at 95°C and proceed to Western blot analysis or store at -20°C.
6. Perform a classic SDS-PAGE followed by transfer on PVDF membrane. Block membranes in WB blocking buffer for 1 h. Incubate membranes with primary antibodies diluted in WB blocking buffer for 1 h at RT or overnight at 4°C using anti-phospho pyrin, anti-pyrin and anti-actin antibodies. Proceed using regular Western blotting protocol.

Compare phosphorylation level to WT, p.S208C and p.S242R *MEFV*-expressing cells to evaluate whether the considered *MEFV* variant affects serine residue 208 or 242 phosphorylation level. If so, the considered variant can be classified as a PAAND-like variant. Do not conclude on negative results since PAAND can be caused by defects in 14-3-3 binding (Moghaddas et al., 2017).

3.2 ASC speck visualization by Immunofluorescence (IF)

1. Plate U937 cells and incubate overnight with 1 µg/mL doxycycline. Alternatively, for IF on primary monocytes, seed the cells and proceed immediately with the treatments. Count the cells and seed the appropriate cell number in a V-bottom 96-well plate.
2. Proceed with the treatments as applies in your experiment (typically, 1-untreated, 2-UCN-01 12.5 µM 30 min, 3-LPS 3 h followed by nigericin during 90 min).
3. Following the indicated incubation period, centrifuge the plate for 5 min 120 rcf at RT and wash with PBS.

4. Resuspend the cells in 100 μ L of paraformaldehyde 2% in PBS, incubate for 15 min at 37°C. Centrifuge for 5 min 120 rcf RT, wash the cells once with PBS. Resuspend in 100 μ L PBS. Proceed with the slide preparation or store at 4°C.
5. Use cytospin to transfer cells onto glass slides. Place the slide in the cytoclip, place the filter card (absorbent side up) and cytofunnel on top, close the cytoclip and make sure that the circles in the filter card and the cytofunnel align by looking at the bottom. Place the assembled device in the cytospin and deposit the sample through the funnel. Spin for 5 min at 450 rpm RT. Undo the cytoclip and carefully remove the filter card, without disturbing the cells now stuck onto the slide.
6. Delineate a circle around the samples using a hydrophobic marker and place the slide in PBS-T– the slides should be covered with liquid – to permeabilize the cells. Incubate for 10 min at RT. Replace the PBS-T with blocking buffer and incubate slides for 1 h at RT or store at 4°C overnight.
7. Prepare a humidity chamber to accommodate all your slides. Prepare 50 μ L per sample of anti-ASC antibody in blocking buffer. Refresh the hydrophobic marker circle around the samples. Carefully place 50 μ L of the antibody mix over the samples. Incubate in the humidity chamber for 1 h at RT.
8. Wash the slides 3 times by dipping them in 3 consecutive 50 mL tubes of PBS-T. Refresh the hydrophobic marker around the samples. Prepare 50 μ L per sample of the secondary antibody (e.g. Goat anti-Rabbit-Alexa 594) in blocking buffer and deposite it over the samples. Incubate 1 h at RT.
9. Wash 3 times as described above. Stain with DAPI for 5 min at RT.
10. Wash the slides twice and add one final wash with Milli-Ro water to remove salts. Place 2 μ L of the mounting solution in the centre of the cover glass, spread it with the tip of the pipette and carefully place the cover glass on top of the sample, avoiding bubbles. Let the slide dry away from daylight and preferably at 4°C.
11. Acquire images with a fluorescence microscope or confocal microscope (Fig. 3). If you observe specks formation in response to UCN-01, your cells likely harbour a FMF-like *MEFV* variant (Note 4). Compare with primary monocytes from healthy donors (HD) and p.M694V homozygous FMF patient or the corresponding U937 cell lines.

3.3 Real-time cell death analysis by propidium iodide (PI) incorporation:

1. Seed the cells in triplicates for each condition, plan an untreated condition and a “Triton X-100” condition, which will provide the fluorescence value corresponding to 100% of cell death.

2. Count the cells and seed cells in a black flat-bottom 96-well plate in supplemented CO₂-independent medium (see Note 5) in the presence or absence of doxycycline at 1 µg/mL.
3. Add Triton X-100 1% final in the "total cell death" wells. Add propidium iodide (PI) to each well (5 µg/mL final).
4. Immediately start the acquisition of the PI fluorescence, corresponding to the PI incorporation into dead cells, using a thermostatic fluorimeter (e.g. Tecan M200) at 37°C with the following wavelengths: excitation 535 nm (bandwidth 15 nm) and emission 635 nm (bandwidth 15 nm) (Christopher L. Case and Roy, 2011; Pierini et al., 2012). To evaluate the cell death associated with *MEFV* variant expression (constitutive activation), measure PI incorporation every 15 min for 16 h.
5. 16 h later, stop the fluorimeter and add inflammasome stimuli (e.g. UCN-01 at 12.5 µM, Note 6). Start a novel acquisition with readings every 5 min for 3 h (Note 7).
Alternatively, for primary monocytes, proceed immediately to inflammasome stimuli treatment and a short kinetics readings every 5 min for 3 h.
6. To determine the percentage of dead cells for each condition, analyse the data as follows: Calculate the average of the untreated triplicates for each time point. Calculate the average of the Triton X-100 triplicates for each time point. Select the maximum Triton X-100 mean value (this value corresponds to the PI fluorescence corresponding to 100% of dead cells). Determine the percentage of dead cells for each condition (each well) and time point using the following calculation $\text{Cell death}_{\text{well X}} = ((\text{fluorescence value well X} - \text{average Untreated}) / (\text{Max Triton X-100 mean value} - \text{average Untreated})) * 100$.
7. Plot the cell death results along time using the appropriate graphing software (e.g. GraphPad Prism) to obtain the cell death curves in relation with time (Figs. 4-5).
Quantifying the corresponding area under the curves (AUC) allows to compare statistically the real time cell death curves. The AUC can be calculated with specific software such as the GraphPad prism feature: Analyze/XY Analyses/Area under curve (Figs. 4C, 4F).

If when combined with p.M694V mutation, the studied *MEFV* mutation triggers constitutive cell death (i.e. in the presence of doxycycline), the corresponding mutation is a PAAND-like mutation. If when combined with the p.S242R mutation, the studied *MEFV* mutation triggers constitutive cell death (i.e. in the presence of doxycycline), the corresponding mutation is a FMF-like mutation. If the studied *MEFV* mutation triggers UCN-01-mediated cell death, the mutation classifies as a FMF-like mutation (Fig. 1) (Note 8).

3.4 Quantification of IL-1 β and IL-18 release by ELISA

1. Seed the cells in triplicates for each condition. To assess IL-1 β release, U937 cells require differentiation in macrophages with PMA treatment (See Note 9). IL-18 quantification does not require PMA differentiation but requires a greater cell number (Table 2). Primary monocytes do not require PMA neither for IL-1 β nor for IL-18. Include a “LPS alone” control.
2. Count and plate the cells in a flat-bottom 96-well plate at the required concentration in cell culture medium. For U937 cells and IL-1 β ELISA, seed cells at day 0 and perform a 3 h pulse with PMA (100 ng/mL). Wash cells and incubate for 24 h. On day 1, treat with doxycycline (1 μ g/mL). 12 to 16 h later (day 2), add the relevant stimuli. For U937 cells and IL-18 ELISA, start at the doxycycline step. For primary monocytes proceed directly with the treatments.
3. Spin the plate for 5 min and 120 rcf at RT and replace medium with fresh cell culture medium.
4. Prime with LPS during 3 h at 37°C, 5% CO₂.
5. Add the signal 2 (e.g. nigericin or UCN-01). Incubate at 37°C, 5% CO₂ for 3 h (1.5 h for primary monocytes).
6. Spin plates for 5 min and 120 rcf at RT and collect supernatant in a separate 96-well plate. Store at -80°C until the ELISA is performed according to manufacturer's protocol (Fig. 6).
Analyse the results in comparison to HD monocytes/ WT *MEFV* and p.M694V *MEFV*-expressing U937 cells and conclude on the nature of the studied *MEFV* variant using Fig. 1 decision tree.

4 Notes:

1. Site-directed mutagenesis to introduce novel mutation in the *MEFV* sequence can be performed in the lentiviral plasmid (e.g. pINDUCER21-WT *MEFV*) using a proofreading polymerase with high processivity (e.g. Pfu Ultra II, Agilent 600672). This can be challenging due to the large size of the vector (\approx 13kb). We routinely perform site-directed mutagenesis on the parental entry plasmid (e.g. pENTR1A-WT, p.M694V, p.S242R *MEFV*, \approx 5kb) and clone the mutated *MEFV* variant in pInducer 21 using Gateway cloning (Gateway® LR Clonase® Enzyme mix, Invitrogen 11791-019).
2. Doxycycline-mediated induction of *MEFV* is observed at the protein level as soon as 3-6 h post-doxycycline addition. We typically used overnight induction but shorter duration can be used. The doxycycline concentration routinely used (1 μ g/mL) is saturating. To titrate pyrin protein level, decrease the concentration to (50 ng/mL).
3. Antibodies against phospho-pyrin have been raised against murine pyrin (Gao et al., 2016d). Yet, they cross react against human phospho-pyrin. Serine 205 and 241 in murine Pyrin correspond to serine 208 and 242 in human Pyrin.

4. Counting the percentage of ASC-speck containing cells is strongly suggested. Yet, it can be challenging since ASC speck formation is associated with pyroptosis and cell loss.
5. For the real time cell death analysis, cells can be resuspended in supplemented RPMI if the assay is meant to last for < 5 h. If the plate stays longer inside the fluorimeter in the absence of CO₂ supply, it is recommended to seed the cells in supplemented CO₂-independent medium.
6. As positive control to monitor inflammasome activation, the NLRP3 inflammasome is primed with LPS during 3 h followed by addition of the NLRP3 signal 2, nigericin.
7. The real time cell death analysis can be performed on U937 cells or primary monocytes. Regarding the U937 cells, there are two possibilities, as shown in Fig. 4 and Fig. 5. Cells can be treated with doxycycline overnight, seeded and analysed for cell death only upon inflammasome stimulation the day after (3 h kinetics). This short kinetics aims at measuring the effects of the treatments when Pyrin is already produced. To investigate the potential constitutive activation of a particular Pyrin variant, cell death monitoring can be started at the time of doxycycline addition. 16h later, inflammasome activators (e.g. UCN-01) can be added before returning the plate to the fluorimeter.
8. Long term UCN-01 treatment can trigger apoptosis (Magnotti et al., 2019d). To conclude on pyroptosis, only the first 3 h post-UCN-01 addition should be considered and, in the case of U937 cells, the dependency on *MEFV* expression (i.e. the presence of doxycycline) should be checked.
9. PMA is a PKC activator. Since Pyrin inflammasome is under the control of the PKC superfamily PKN1/2, we recommend a 3 h PMA pulse followed by one wash and 36 h of incubation.

Acknowledgment

This work has received funding from the European Union's Horizon 2020 research and innovation programme under grant agreement #779295 (ImmunAID). We are grateful to Michel Popoff, Institut Pasteur, Paris for providing TcdA toxin.

Tables:

Table 1: Cell number required per sample for the different experiments

Experiment	Number of U937 cells / condition	U937 cells/mL	Number of primary cells / condition	Primary cells/mL
IP	$2 \cdot 10^6$	$1 \cdot 10^6$	-	-
IF	$2 \cdot 10^5$	$2 \cdot 10^6$	$12 \cdot 10^4$	$1 \cdot 10^6$
PI incorporation	$5 \cdot 10^4$	$0.5 \cdot 10^6$	$2 \cdot 10^4$	$0.2 \cdot 10^6$
ELISA IL-1 β	$5 \cdot 10^4$	$0.5 \cdot 10^6$	$5 \cdot 10^3$	$0.05 \cdot 10^6$
ELISA IL-18	$2 \cdot 10^5$	$2 \cdot 10^6$	$5 \cdot 10^3$	$0.05 \cdot 10^6$

Table 2: Inflammasome activators used, working and stock concentrations.

Compound	Working concentration in U937 assays	Working concentration in primary monocytes assays	Stock concentration; Solvent; Reference
LPS	0.5 $\mu\text{g/mL}$ for IL-1 β 1 $\mu\text{g/mL}$ for IL-18 and RT cell death assay (in the case of the LPS + nigericin stimulus)	10 ng/mL	5mg/ml; water; Invivogen (tlrl-3pelps)
Nigericin	50 $\mu\text{g/mL}$	5 $\mu\text{g/mL}$	5 mg/mL; ethanol; Invivogen (tlrl-nig)
TcdA	1 $\mu\text{g/mL}$	1 $\mu\text{g/mL}$	380 $\mu\text{g/mL}$; water; purified from <i>Clostridioides difficile</i> VPI10463 strain, as previously described (Popoff, 1987)
TcdB	-	125 ng/mL	200 $\mu\text{g/mL}$; water; Abcam (ab124001)
UCN-01	12,5 μM	12,5 μM	10.4 mM; DMSO; Sigma (U6508)

Figures:

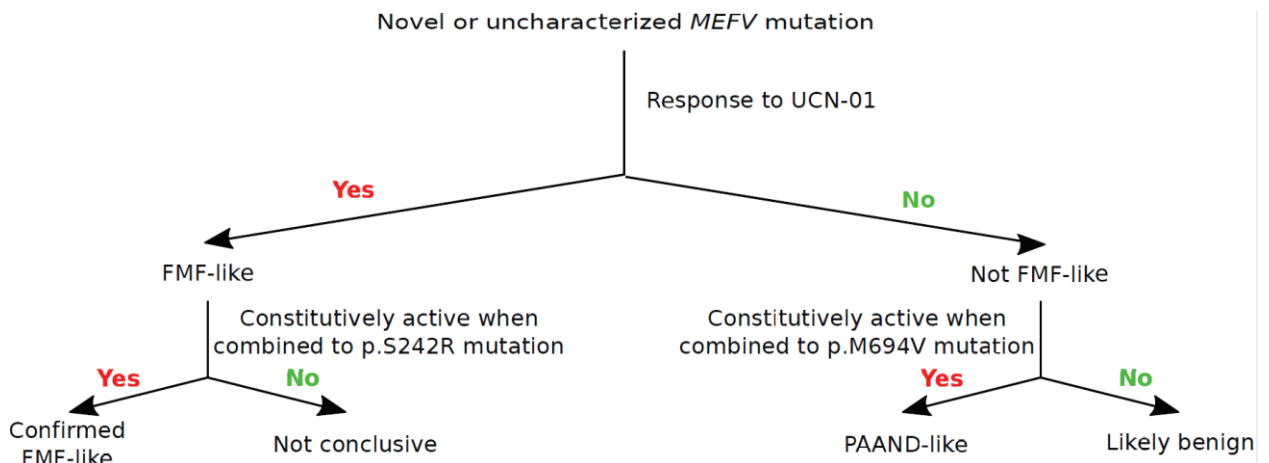


Figure 1 Decision tree to classify a novel or uncharacterized *MEFV* variant based on the techniques presented here and the current knowledge in the field. Only the first step is applicable to primary human monocytes.

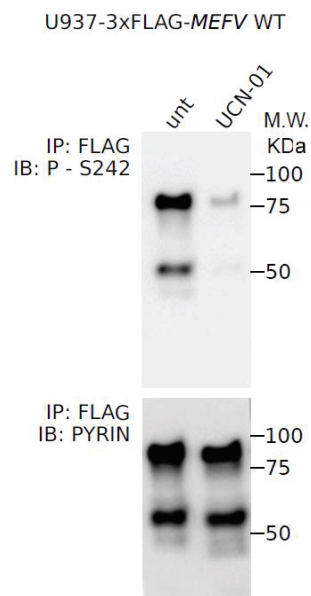


Figure 2. Phosphorylation level of Pyrin S242 as determined by immunoblotting (IB) following immunoprecipitation (IP). Treatment with UCN-01 (12.5 μ M, 15 min) triggers Pyrin S242 dephosphorylation. Unt: untreated. MW : molecular weight.

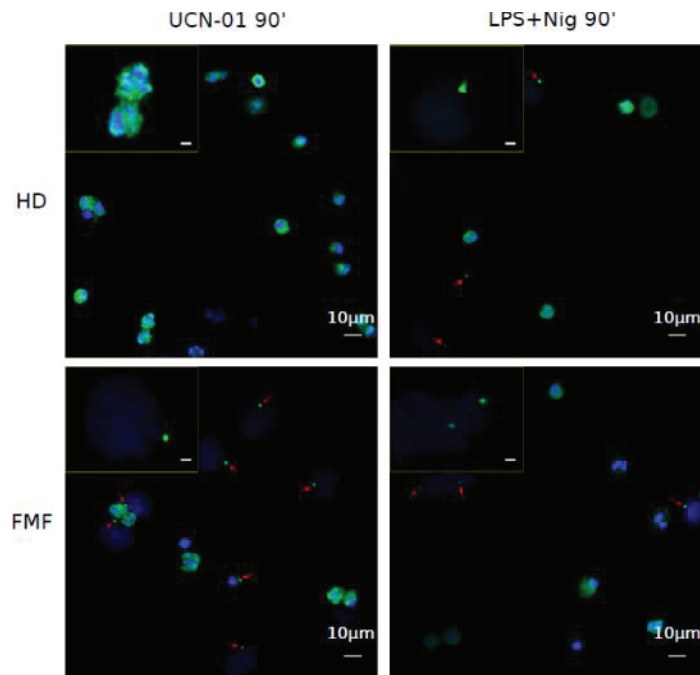


Figure 3. ASC specks formation in response to UCN-01 discriminates FMF patient's monocytes from healthy donor (HD) monocytes. ASC immunofluorescence on monocytes from one HD and one FMF patient (FMF) treated with the indicated stimuli for the indicated time points. The red arrows indicate the ASC specks. Left, cells were treated with UCN-01 for 90 min. Only FMF monocytes displayed ASC specks. Right, cells were treated with LPS for 3 h and nigericin for 90 min to activate the NLRP3 inflammasome as a positive control (see Note 5) for ASC specks formation occurring in monocytes from both HD and FMF patient.

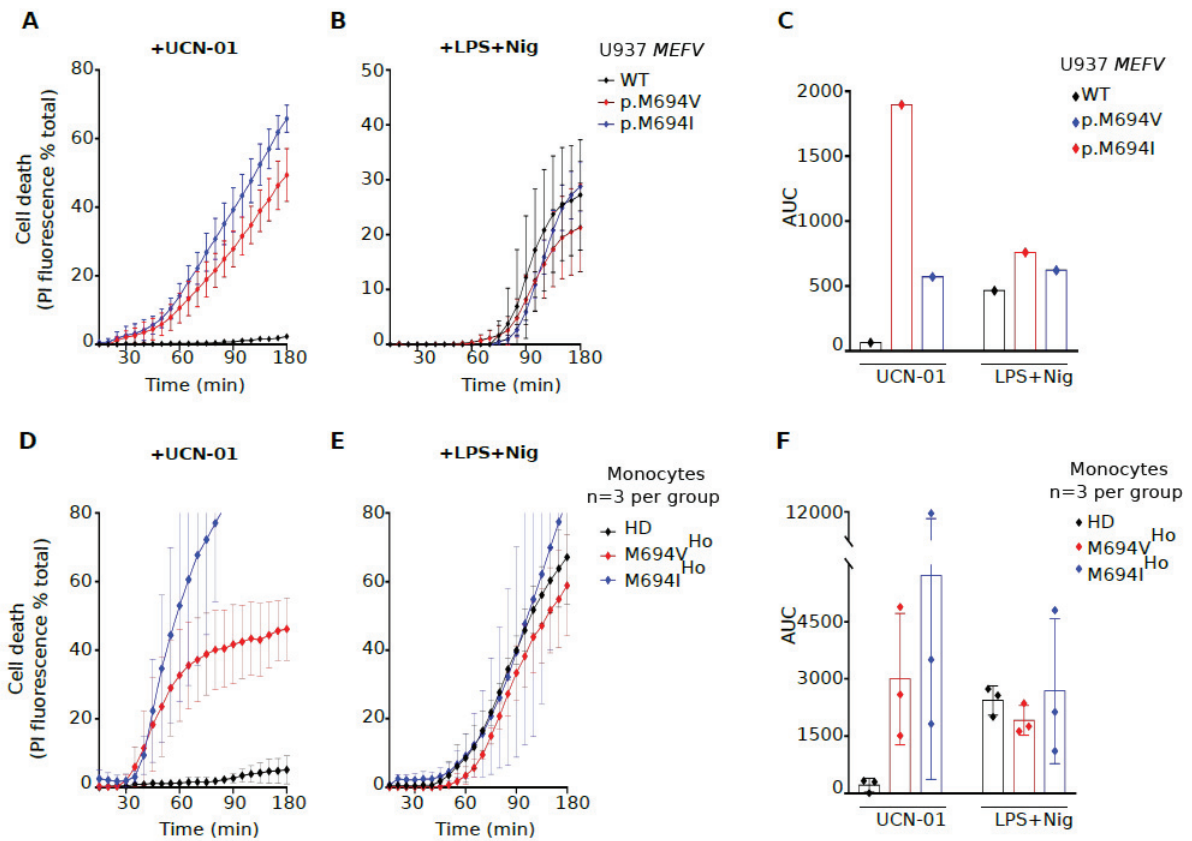


Figure 4. Characterization of *MEFV* variant by real time cell death assays (short kinetics). (A, B) Real time cell death analysis in U937 cells expressing WT *MEFV* and two prototypical FMF-associated *MEFV* variants p.M694V and p.M694I. (D, E) Real time cell death analysis in monocytes from 3 HD and 3 FMF patients homozygous for the same variants. UCN-01 treatment induces a fast cell death (after 30-40 min) when cells express a FMF-associated *MEFV* variant. No difference is detected after LPS + nigericin treatment. (C, F) To quantify these experiments, the Area Under the Curves (AUC) were computed. After UCN-01 treatment, the AUC value is higher when cells express a FMF-associated *MEFV* variant than when cells express the WT *MEFV*. On the contrary, the AUC values after to the LPS + nigericin treatment are similar.

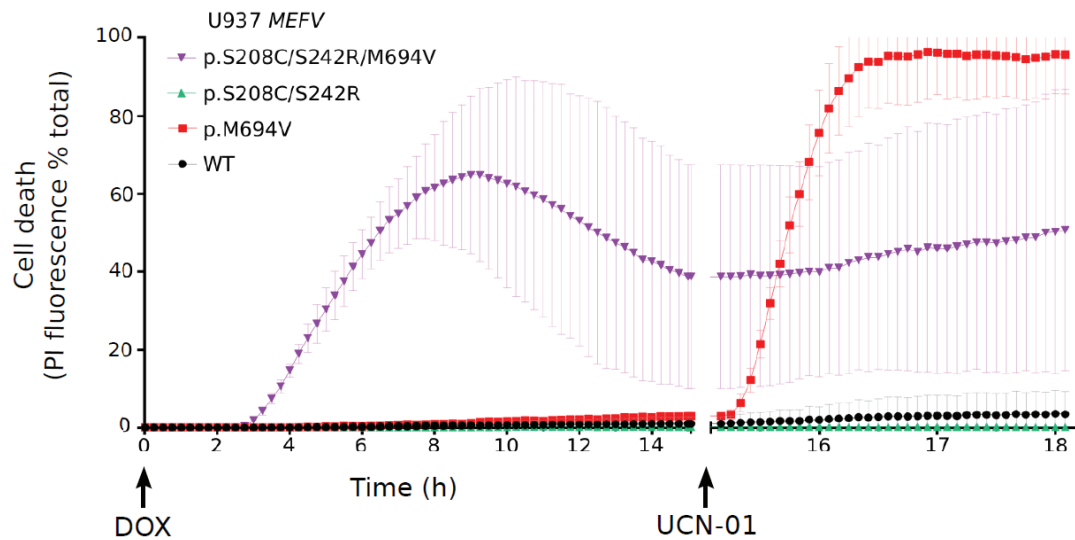


Figure 5. Characterization of *MEFV* variant by real time cell death assay (long kinetics). Real time cell death analysis in U937 cells expressing WT ; p.M694V ; p.S208C/S242R ; p.S208C/S242R/M694V *MEFV* variants. Cell death was monitored for 15 h following doxycycline treatment (DOX). Cells expressing the *MEFV* p.M694V variant, do not substantially die in response to doxycycline, indicating that the corresponding Pyrin variant is not constitutively active. Yet, these cells die after UCN-01 addition (red line). The p.S208C/S242R *MEFV* variant includes the two prototypical “PAAND” mutations. When the p.S208C/S242R mutations are associated to the “FMF” p.M694V mutation (purple line), the corresponding Pyrin variant is constitutively active and cell death is observed starting at 3 h post-doxycycline addition.

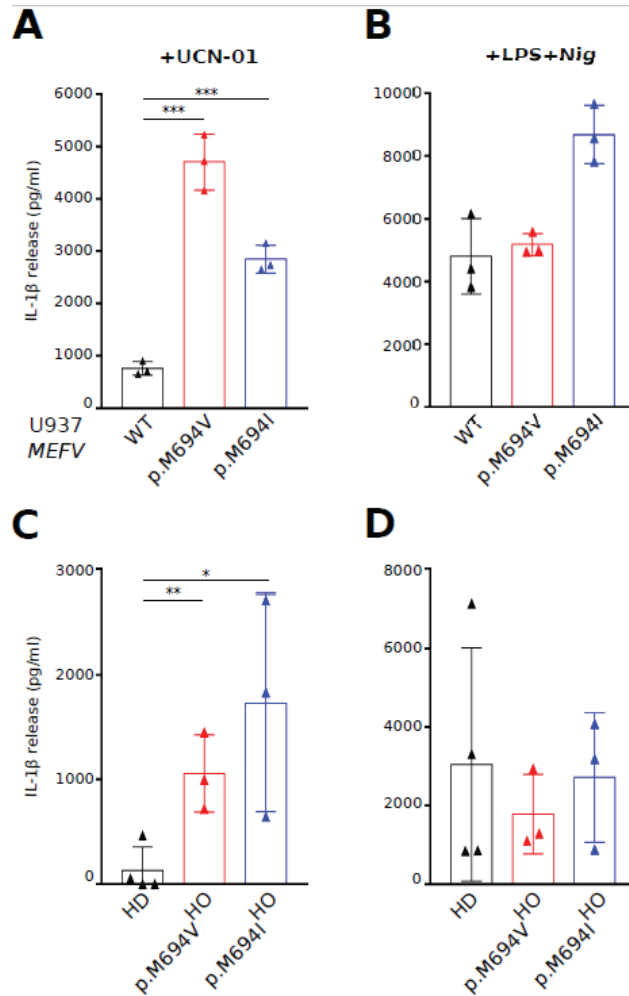


Figure 6. Characterization of *MEFV* variant by IL-1 β ELISA. IL-1 β quantification by ELISA in (A, B) U937 expressing WT (black); p.M694V (red) ; p.M694I (blue) *MEFV* after PMA differentiation and (C, D) primary monocytes from 3 HD (black), 3 patients homozygous for the p.M694V mutation (red) or the p.M694I mutation (blue). Higher levels of IL-1 β have been detected in the supernatant of cells expressing FMF *MEFV* variants than in the supernatant of cells expressing WT *MEFV*. (A-B) Each point represents the value of one well, the bar represents the mean and S.D. of the triplicate. (C-D) Each point represents the mean value of a triplicate for one individual, the bar represents the mean and S.D. of the values of three individuals.

Bibliography

- A candidate gene for familial Mediterranean fever. The French FMF Consortium, 1997. . *Nat Genet* 17, 25–31.
- Accetturo, M., D'Uggento, A.M., Portincasa, P., Stella, A., 2020. Improvement of MEFV gene variants classification to aid treatment decision making in familial Mediterranean fever. *Rheumatology* 59, 754–761. <https://doi.org/10.1093/rheumatology/kez332>
- Akar, S., Soyuturk, M., Onen, F., Tunca, M., 2006. The relations between attacks and menstrual periods and pregnancies of familial Mediterranean fever patients. *Rheumatol. Int.* 26, 676–679. <https://doi.org/10.1007/s00296-005-0041-z>
- Akula, M.K., Shi, M., Jiang, Z., Foster, C.E., Miao, D., Li, A.S., Zhang, X., Gavin, R.M., Forde, S.D., Germain, G., Carpenter, S., Rosadini, C.V., Gritsman, K., Chae, J.J., Hampton, R., Silverman, N., Gravalles, E.M., Kagan, J.C., Fitzgerald, K.A., Kastner, D.L., Golenbock, D.T., Bergo, M.O., Wang, D., 2016. Control of the innate immune response by the mevalonate pathway. *Nat. Immunol.* 17, 922–929. <https://doi.org/10.1038/ni.3487>
- Aldea, A., Campistol, J.M., Arostegui, J.I., Rius, J., Maso, M., Vives, J., Yagüe, J., 2004. A severe autosomal-dominant periodic inflammatory disorder with renal AA amyloidosis and colchicine resistance associated to the MEFV H478Y variant in a Spanish kindred: an unusual familial Mediterranean fever phenotype or another MEFV-associated periodic inflammatory disorder? *Am. J. Med. Genet. A.* 124A, 67–73. <https://doi.org/10.1002/ajmg.a.20296>
- Alenghat, F.J., Davis, A.M., 2019. Management of Blood Cholesterol. *JAMA* 321, 800–801. <https://doi.org/10.1001/jama.2019.0015>
- Alimov, I., Menon, S., Cochran, N., Maher, R., Wang, Q., Alford, J., Concannon, J.B., Yang, Z., Harrington, E., Llamas, L., Lindeman, A., Hoffman, G., Schuhmann, T., Russ, C., Reece-Hoyes, J., Canham, S.M., Cai, X., 2019. Bile acid analogues are activators of pyrin inflammasome. *J. Biol. Chem.* 294, 3359–3366. <https://doi.org/10.1074/jbc.RA118.005103>
- Amores-Iniesta, J., Barberà-Cremades, M., Martínez, C.M., Pons, J.A., Revilla-Nuin, B., Martínez-Alarcón, L., Di Virgilio, F., Parrilla, P., Baroja-Mazo, A., Pelegrín, P., 2017. Extracellular ATP Activates the NLRP3 Inflammasome and Is an Early Danger Signal of Skin Allograft Rejection. *Cell Rep.* 21, 3414–3426. <https://doi.org/10.1016/j.celrep.2017.11.079>
- Ancient missense mutations in a new member of the RoRet gene family are likely to cause familial Mediterranean fever. The International FMF Consortium, 1997. . *Cell* 90, 797–807. [https://doi.org/10.1016/s0092-8674\(00\)80539-5](https://doi.org/10.1016/s0092-8674(00)80539-5)
- Arakelov, G., Arakelov, V., Nazaryan, K., 2018. Complex formation dynamics of native and mutated pyrin's B30.2 domain with caspase-1. *Proteins Struct. Funct. Bioinforma.* 86, 676–683. <https://doi.org/10.1002/prot.25494>
- Arakelov, G.G., Osipov, O.V., Nazaryan, K.B., 2015. Effects of M680I and M694V pyrin mutations on the tertiary structure of domain B30.2 and its interaction with caspase-1: In silico analysis. *Mol. Biol.* 49, 736–741. <https://doi.org/10.1134/S0026893315050027>
- Aubert, D.F., Xu, H., Yang, J., Shi, X., Gao, W., Li, L., Bisaro, F., Chen, S., Valvano, M.A., Shao, F., 2016. A Burkholderia Type VI Effector Deamidates Rho GTPases to Activate the Pyrin Inflammasome and Trigger Inflammation. *Cell Host Microbe* 19, 664–674. <https://doi.org/10.1016/j.chom.2016.04.004>
- Ayroldi, E., Cannarile, L., Migliorati, G., Nocentini, G., Delfino, D.V., Riccardi, C., 2012. Mechanisms of the anti-inflammatory effects of glucocorticoids: genomic and

- nongenomic interference with MAPK signaling pathways. *FASEB J. Off. Publ. Fed. Am. Soc. Exp. Biol.* 26, 4805–4820. <https://doi.org/10.1096/fj.12-216382>
- Azlan, A., Salamonsen, L.A., Hutchison, J., Evans, J., 2020. Endometrial inflammasome activation accompanies menstruation and may have implications for systemic inflammatory events of the menstrual cycle. *Hum. Reprod. Oxf. Engl.* 35, 1363–1376. <https://doi.org/10.1093/humrep/deaa065>
- Baker, F.C., Sibozza, F., Fuller, A., 2020. Temperature regulation in women: Effects of the menstrual cycle. *Temp. Austin Tex* 7, 226–262. <https://doi.org/10.1080/23328940.2020.1735927>
- Balci-Peynircioglu, B., Waite, A.L., Hu, C., Richards, N., Staubach-Grosse, A., Yilmaz, E., Gumucio, D.L., 2008. Pypin, product of the MEFV locus, interacts with the proapoptotic protein, Siva. *J. Cell. Physiol.* 216, 595–602. <https://doi.org/10.1002/jcp.21435>
- Baron, L., Gombault, A., Fanny, M., Villeret, B., Savigny, F., Guillou, N., Panek, C., Le Bert, M., Lagente, V., Rassendren, F., Riteau, N., Couillin, I., 2015. The NLRP3 inflammasome is activated by nanoparticles through ATP, ADP and adenosine. *Cell Death Dis.* 6, e1629. <https://doi.org/10.1038/cddis.2014.576>
- Bauernfeind, F.G., Horvath, G., Stutz, A., Alnemri, E.S., MacDonald, K., Speert, D., Fernandes-Alnemri, T., Wu, J., Monks, B.G., Fitzgerald, K.A., Hornung, V., Latz, E., 2009. Cutting edge: NF- κ B activating pattern recognition and cytokine receptors license NLRP3 inflammasome activation by regulating NLRP3 expression. *J. Immunol.* 183, 787–91. <https://doi.org/10.4049/jimmunol.0901363>
- Beagley, K.W., Gockel, C.M., 2003. Regulation of innate and adaptive immunity by the female sex hormones oestradiol and progesterone. *FEMS Immunol. Med. Microbiol.* 38, 13–22. [https://doi.org/10.1016/S0928-8244\(03\)00202-5](https://doi.org/10.1016/S0928-8244(03)00202-5)
- Bekhouche, B., Tourville, A., Ravichandran, Y., Tacine, R., Abrami, L., Dussiot, M., Khau-Dancasius, A., Boccara, O., Khirat, M., Mangeney, M., Dingli, F., Loew, D., Boëda, B., Jordan, P., Molina, T.J., Bellon, N., Fraitag, S., Hadj-Rabia, S., Blanche, S., Puel, A., Etienne-Manneville, S., van der Goot, F.G., Cherfils, J., Hermine, O., Casanova, J.-L., Bodemer, C., Smahi, A., Delon, J., 2020. A toxic palmitoylation of Cdc42 enhances NF- κ B signaling and drives a severe autoinflammatory syndrome. *J. Allergy Clin. Immunol.* 146, 1201-1204.e8. <https://doi.org/10.1016/j.jaci.2020.03.020>
- Ben-Chetrit, E., Ben-Chetrit, A., 2001. Familial Mediterranean fever and menstruation. *BJOG Int. J. Obstet. Gynaecol.* 108, 403–407. <https://doi.org/10.1111/j.1471-0528.2001.00083.x>
- Ben-Chetrit, E., Levy, M., 2003. Reproductive system in familial Mediterranean fever: an overview. *Ann. Rheum. Dis.* 62, 916–919. <https://doi.org/10.1136/ard.62.10.916>
- Ben-Chetrit, E., Touitou, I., 2009. Familial mediterranean Fever in the world. *Arthritis Rheum.* 61, 1447–1453. <https://doi.org/10.1002/art.24458>
- Bergsbaken, T., Fink, S.L., Cookson, B.T., 2009. Pyroptosis: host cell death and inflammation. *Nat. Rev. Microbiol.* 7, 99–109. <https://doi.org/10.1038/nrmicro2070>
- Bhatt, H., Cascella, M., 2022. Familial Mediterranean Fever, in: *StatPearls*. StatPearls Publishing, Treasure Island (FL).
- Bodel, P., Dillard, M., 1968. Studies on steroid fever: *I. Production of leukocyte pyrogen in vitro by etiocholanolone*. *J. Clin. Invest.* 47, 107–117. <https://doi.org/10.1172/JCI105701>
- Bonnefont, J., Laforge, T., Plastre, O., Beck, B., Sorce, S., Dehay, C., Krause, K.-H., 2011. Primate-specific RFPL1 gene controls cell-cycle progression through cyclin B1/Cdc2 degradation. *Cell Death Differ.* 18, 293–303. <https://doi.org/10.1038/cdd.2010.102>

- Boonyaratanakornkit, V., Edwards, D.P., 2007. Receptor mechanisms mediating non-genomic actions of sex steroids. *Semin. Reprod. Med.* 25, 139–153. <https://doi.org/10.1055/s-2007-973427>
- Boucher, D., Monteleone, M., Coll, R.C., Chen, K.W., Ross, C.M., Teo, J.L., Gomez, G.A., Holley, C.L., Bierschenk, D., Stacey, K.J., Yap, A.S., Bezbradica, J.S., Schroder, K., 2018. Caspase-1 self-cleavage is an intrinsic mechanism to terminate inflammasome activity. *J. Exp. Med.* 215, 827–840. <https://doi.org/10.1084/jem.20172222>
- Boursier, G., Hentgen, V., Sarabay, G., Kone-Paut, I., Touitou, I., 2019. The Changing Concepts Regarding the Mediterranean Fever Gene: Toward a Spectrum of Pyrin-Associated Autoinflammatory Diseases with Variable Heredity. *J. Pediatr.* 209, 12–16.e1. <https://doi.org/10.1016/j.jpeds.2019.02.039>
- Broz, P., Monack, D.M., 2011. Molecular mechanisms of inflammasome activation during microbial infections. *Immunol. Rev.* 243, 174–190. <https://doi.org/10.1111/j.1600-065X.2011.01041.x>
- Cannon, J.G., Dinarello, C.A., 1985. Increased plasma interleukin-1 activity in women after ovulation. *Science* 227, 1247–1249. <https://doi.org/10.1126/science.3871966>
- Cano, C.E., Pasero, C., De Gassart, A., Kerneur, C., Gabriac, M., Fullana, M., Granarolo, E., Hoet, R., Scotet, E., Rafia, C., Herrmann, T., Imbert, C., Gorvel, L., Vey, N., Briantais, A., le Floch, A.C., Olive, D., 2021. BTN2A1, an immune checkpoint targeting V γ 9V δ 2 T cell cytotoxicity against malignant cells. *Cell Rep.* 36, 109359. <https://doi.org/10.1016/j.celrep.2021.109359>
- Cao, A., Kagan, J.C., 2022. Gasdermin Pore Forming Activities that Promote Inflammation from Living and Dead Cells. *J. Mol. Biol.* 434, 167427. <https://doi.org/10.1016/j.jmb.2021.167427>
- Case, Christopher L., Roy, C.R., 2011. Asc modulates the function of NLRP4 in response to infection of macrophages by *Legionella pneumophila*. *mBio* 2. <https://doi.org/10.1128/mBio.00117-11>
- Cato, A.C.B., Nestl, A., Mink, S., 2002. Rapid actions of steroid receptors in cellular signaling pathways. *Sci. STKE Signal Transduct. Knowl. Environ.* 2002, re9. <https://doi.org/10.1126/stke.2002.138.re9>
- Cekin, N., Akyurek, M.E., Pinarbasi, E., Ozen, F., 2017. MEFV mutations and their relation to major clinical symptoms of Familial Mediterranean Fever. *Gene* 626, 9–13. <https://doi.org/10.1016/j.gene.2017.05.013>
- Centola, M., Wood, G., Frucht, D.M., Galon, J., Aringer, M., Farrell, C., Kingma, D.W., Horwitz, M.E., Mansfield, E., Holland, S.M., O’Shea, J.J., Rosenberg, H.F., Malech, H.L., Kastner, D.L., 2000. The gene for familial Mediterranean fever, MEFV, is expressed in early leukocyte development and is regulated in response to inflammatory mediators. *Blood* 95, 3223–3231.
- Chae, Jae Jin, Centola, M., Aksentijevich, I., Dutra, A., Tran, M., Wood, G., Nagaraju, K., Kingma, D.W., Liu, P.P., Kastner, D.L., 2000. Isolation, genomic organization, and expression analysis of the mouse and rat homologs of MEFV, the gene for familial Mediterranean fever. *Mamm. Genome* 11, 428–435. <https://doi.org/10.1007/s003350010082>
- Chae, J.J., Cho, Y.-H., Lee, G.-S., Cheng, J., Liu, P.P., Feigenbaum, L., Katz, S.I., Kastner, D.L., 2011. Gain-of-function Pyrin mutations induce NLRP3 protein-independent interleukin-1 β activation and severe autoinflammation in mice. *Immunity* 34, 755–768. <https://doi.org/10.1016/j.immuni.2011.02.020>
- Chae, J.J., Wood, G., Masters, S.L., Richard, K., Park, G., Smith, B.J., Kastner, D.L., 2006. The B30.2 domain of pyrin, the familial Mediterranean fever protein, interacts directly

- with caspase-1 to modulate IL-1 β production. *Proc. Natl. Acad. Sci.* 103, 9982. <https://doi.org/10.1073/pnas.0602081103>
- Chae, J.J., Wood, G., Richard, K., Jaffe, H., Colburn, N.T., Masters, S.L., Gumucio, D.L., Shoham, N.G., Kastner, D.L., 2008. The familial Mediterranean fever protein, pyrin, is cleaved by caspase-1 and activates NF- κ B through its N-terminal fragment. *Blood* 112, 1794–1803. <https://doi.org/10.1182/blood-2008-01-134932>
- Chakraborty, S., Pramanik, J., Mahata, B., 2021. Revisiting steroidogenesis and its role in immune regulation with the advanced tools and technologies. *Genes Immun.* 22, 125–140. <https://doi.org/10.1038/s41435-021-00139-3>
- Chaudoreille, M.M., Peyrot, V., Braguer, D., Codaccioni, F., Crevat, A., 1991. Qualitative study of the interaction mechanism of estrogenic drugs with tubulin. *Biochem. Pharmacol.* 41, 685–693. [https://doi.org/10.1016/0006-2952\(91\)90067-f](https://doi.org/10.1016/0006-2952(91)90067-f)
- Chen, M., Penning, T.M., 2014. 5 β -Reduced steroids and human $\Delta(4)$ -3-ketosteroid 5 β -reductase (AKR1D1). *Steroids* 83, 17–26. <https://doi.org/10.1016/j.steroids.2014.01.013>
- Chen, W.Y., Bailey, E.C., McCune, S.L., Dong, J.Y., Townes, T.M., 1997. Reactivation of silenced, virally transduced genes by inhibitors of histone deacetylase. *Proc. Natl. Acad. Sci. U. S. A.* 94, 5798–5803. <https://doi.org/10.1073/pnas.94.11.5798>
- Choudhury, N.R., Heikel, G., Trubitsyna, M., Kubik, P., Nowak, J.S., Webb, S., Granneman, S., Spanos, C., Rappsilber, J., Castello, A., Michlewski, G., 2017. RNA-binding activity of TRIM25 is mediated by its PRY/SPRY domain and is required for ubiquitination. *BMC Biol.* 15. <https://doi.org/10.1186/s12915-017-0444-9>
- Chu, L.H., Gangopadhyay, A., Dorfleutner, A., Stehlik, C., 2015. An updated view on the structure and function of PYRIN domains. *Apoptosis Int. J. Program. Cell Death* 20, 157–173. <https://doi.org/10.1007/s10495-014-1065-1>
- Chung, L.K., Park, Y.H., Zheng, Y., Brodsky, I.E., Hearing, P., Kastner, D.L., Chae, J.J., Bliska, J.B., 2016. The Yersinia Virulence Factor YopM Hijacks Host Kinases to Inhibit Type III Effector-Triggered Activation of the Pyrin Inflammasome. *Cell Host Microbe* 20, 296–306. <https://doi.org/10.1016/j.chom.2016.07.018>
- Cookson, Brad T, Brennan, M.A., 2001. Pro-inflammatory programmed cell death. *Trends Microbiol.* 9, 113–114. [https://doi.org/10.1016/S0966-842X\(00\)01936-3](https://doi.org/10.1016/S0966-842X(00)01936-3)
- Cornut, M., Bourdonnay, E., Henry, T., 2020. Transcriptional Regulation of Inflammasomes. *Int. J. Mol. Sci.* 21, 8087. <https://doi.org/10.3390/ijms21218087>
- Coutinho, A.E., Chapman, K.E., 2011. The anti-inflammatory and immunosuppressive effects of glucocorticoids, recent developments and mechanistic insights. *Mol. Cell. Endocrinol.* 335, 2. <https://doi.org/10.1016/j.mce.2010.04.005>
- Cutolo, M., Accardo, S., Villaggio, B., Barone, A., Sulli, A., Balleari, E., Bason, C., Felli, L., Granata, O.M., Amodio, R., Castagnetta, L., 1995. Androgen metabolism and inhibition of interleukin-1 synthesis in primary cultured human synovial macrophages. *Mediators Inflamm.* 4, 138–143. <https://doi.org/10.1155/S096293519500024X>
- Cutolo, M., Straub, R.H., 2020. Sex steroids and autoimmune rheumatic diseases: state of the art. *Nat. Rev. Rheumatol.* 16, 628–644. <https://doi.org/10.1038/s41584-020-0503-4>
- D’Cruz, A.A., Babon, J.J., Norton, R.S., Nicola, N.A., Nicholson, S.E., 2013. Structure and function of the SPRY/B30.2 domain proteins involved in innate immunity. *Protein Sci.* 22, 1–10. <https://doi.org/10.1002/pro.2185>
- D’Cruz, A.A., Kershaw, N.J., Hayman, T.J., Linossi, E.M., Chiang, J.J., Wang, M.K., Dagley, L.F., Kolesnik, T.B., Zhang, J.-G., Masters, S.L., Griffin, M.D.W., Gack, M.U., Murphy, J.M., Nicola, N.A., Babon, J.J., Nicholson, S.E., 2018. Identification of a

- second binding site on the TRIM25 B30.2 domain. *Biochem. J.* 475, 429–440. <https://doi.org/10.1042/BCJ20170427>
- de Alba, E., 2019. Structure, interactions and self-assembly of ASC-dependent inflammasomes. *Arch. Biochem. Biophys.* 670, 15–31. <https://doi.org/10.1016/j.abb.2019.05.023>
- de Vasconcelos, N.M., Van Opdenbosch, N., Van Gorp, H., Parthoens, E., Lamkanfi, M., 2019. Single-cell analysis of pyroptosis dynamics reveals conserved GSDMD-mediated subcellular events that precede plasma membrane rupture. *Cell Death Differ.* 26, 146–161. <https://doi.org/10.1038/s41418-018-0106-7>
- Deligiannidis, K.M., Kroll-Desrosiers, A.R., Mo, S., Nguyen, H.P., Svenson, A., Jaitly, N., Hall, J.E., Barton, B.A., Rothschild, A.J., Shaffer, S.A., 2016. Peripartum neuroactive steroid and γ -aminobutyric acid profiles in women at-risk for postpartum depression. *Psychoneuroendocrinology* 70, 98–107. <https://doi.org/10.1016/j.psyneuen.2016.05.010>
- Demidowich, A.P., Freeman, A.F., Kuhns, D.B., Aksentijevich, I., Gallin, J.I., Turner, M.L., Kastner, D.L., Holland, S.M., 2012. Brief report: genotype, phenotype, and clinical course in five patients with PAPA syndrome (pyogenic sterile arthritis, pyoderma gangrenosum, and acne). *Arthritis Rheum.* 64, 2022–2027. <https://doi.org/10.1002/art.34332>
- Dierselhuis, M.P., Frenkel, J., Wulffraat, N.M., Boelens, J.J., 2005. Anakinra for flares of pyogenic arthritis in PAPA syndrome. *Rheumatol. Oxf. Engl.* 44, 406–408. <https://doi.org/10.1093/rheumatology/keh479>
- Dinareello, C.A., Chusid, M.J., Fauci, A.S., Gallin, J.I., Dale, D.C., Wolff, S.M., 1976. Effect of prophylactic colchicine therapy on leukocyte function in patients with familial Mediterranean fever. *Arthritis Rheum.* 19, 618–622. <https://doi.org/10.1002/art.1780190315>
- Drenth, J.P., Cuisset, L., Grateau, G., Vasseur, C., van de Velde-Visser, S.D., de Jong, J.G., Beckmann, J.S., van der Meer, J.W., Delpech, M., 1999. Mutations in the gene encoding mevalonate kinase cause hyper-IgD and periodic fever syndrome. International Hyper-IgD Study Group. *Nat. Genet.* 22, 178–181. <https://doi.org/10.1038/9696>
- Duzgun, N., Ates, A., Tuna, S., 2006. Regular abdominal pain and fever in each menstruation onset: an unusual menses-associated familial Mediterranean fever attacks and a favor result on colchicine treatment. *Rheumatol. Int.* 26, 760–761. <https://doi.org/10.1007/s00296-005-0055-6>
- Evavold, C.L., Ruan, J., Tan, Y., Xia, S., Wu, H., Kagan, J.C., 2018. The Pore-Forming Protein Gasdermin D Regulates Interleukin-1 Secretion from Living Macrophages. *Immunity* 48, 35-44.e6. <https://doi.org/10.1016/j.immuni.2017.11.013>
- Fayez, A.G., Eldeen, G.N., Zarouk, W.A., Hamed, K., Ramadan, A., Foda, B.M., Kobesiy, M.M., Zekrie, M.E., Lotfy, R.S., Sokkar, M.F., El-Bassyouni, H.T., 2022. Dynamic disequilibrium-based pathogenicity model in mutated pyrin's B30.2 domain-Casp1/p20 complex. *J. Genet. Eng. Biotechnol.* 20, 31. <https://doi.org/10.1186/s43141-022-00300-z>
- Federici, S., Calcagno, G., Finetti, M., Gallizzi, R., Meini, A., Vitale, A., Caroli, F., Cattalini, M., Caorsi, R., Zulian, F., Tommasini, A., Insalaco, A., Sormani, M.P., Baldi, M., Ceccherini, I., Martini, A., Gattorno, M., 2012. Clinical impact of MEFV mutations in children with periodic fever in a prevalent western European Caucasian population. *Ann. Rheum. Dis.* 71, 1961–1965. <https://doi.org/10.1136/annrheumdis-2011-200977>

- Fernandes-Alnemri, T., Wu, J., Yu, J.W., Datta, P., Miller, B., Jankowski, W., Rosenberg, S., Zhang, J., Alnemri, E.S., 2007. The pyroptosome: a supramolecular assembly of ASC dimers mediating inflammatory cell death via caspase-1 activation. *Cell Death Differ* 14, 1590–604.
- Foradori, C.D., Weiser, M.J., Handa, R.J., 2008. Non-genomic actions of androgens. *Front. Neuroendocrinol.* 29, 169–181. <https://doi.org/10.1016/j.yfrne.2007.10.005>
- French FMF Consortium, 1997. A candidate gene for familial Mediterranean fever. *Nat. Genet.* 17, 25–31. <https://doi.org/10.1038/ng0997-25>
- Frye, C.A., 2009. Steroids, reproductive endocrine function, and affect. A review. *Minerva Ginecol.* 61, 541–562.
- Funder, J.W., Krozowski, Z., Myles, K., Sato, A., Sheppard, K.E., Young, M., 1997. Mineralocorticoid receptors, salt, and hypertension. *Recent Prog. Horm. Res.* 52, 247–260; discussion 261–262.
- Gao, W., Yang, J., Liu, W., Wang, Y., Shao, F., 2016. Site-specific phosphorylation and microtubule dynamics control Pyrin inflammasome activation. *Proc. Natl. Acad. Sci. U. S. A.* 113, E4857–E4866. <https://doi.org/10.1073/pnas.1601700113>
- Gernez, Y., de Jesus, A.A., Alsaleem, H., Macaubas, C., Roy, A., Lovell, D., Jagadeesh, K.A., Alehashemi, S., Erdman, L., Grimley, M., Talarico, S., Bacchetta, R., Lewis, D.B., Canna, S.W., Laxer, R.M., Mellins, E.D., Goldbach-Mansky, R., Weinacht, K.G., 2019. Severe autoinflammation in 4 patients with C-terminal variants in cell division control protein 42 homolog (CDC42) successfully treated with IL-1 β inhibition. *J. Allergy Clin. Immunol.* 144, 1122–1125.e6. <https://doi.org/10.1016/j.jaci.2019.06.017>
- Goldfinger, S.E., 1972. Colchicine for familial Mediterranean fever. *N. Engl. J. Med.* 287, 1302. <https://doi.org/10.1056/NEJM197212212872514>
- Grandemange, S., Aksentijevich, I., Jeru, I., Gul, A., Touitou, I., 2011. The regulation of MEFV expression and its role in health and familial Mediterranean fever. *Genes Immun.* 12, 497–503. <https://doi.org/10.1038/gene.2011.53>
- Grütter, C., Briand, C., Capitani, G., Mittl, P.R.E., Papin, S., Tschopp, J., Grütter, M.G., 2006. Structure of the PRYSPRY-domain: implications for autoinflammatory diseases. *FEBS Lett.* 580, 99–106. <https://doi.org/10.1016/j.febslet.2005.11.076>
- Guo, Z., Benten, W.P.M., Krücken, J., Wunderlich, F., 2002. Nongenomic Testosterone Calcium Signaling: GENOTROPIC ACTIONS IN ANDROGEN RECEPTOR-FREE MACROPHAGES*. *J. Biol. Chem.* 277, 29600–29607. <https://doi.org/10.1074/jbc.M202997200>
- Hill, M., Cibula, D., Havlíková, H., Kancheva, L., Fait, T., Kancheva, R., Parížek, A., Stárka, L., 2007. Circulating levels of pregnanolone isomers during the third trimester of human pregnancy. *J. Steroid Biochem. Mol. Biol.* 105, 166–175. <https://doi.org/10.1016/j.jsbmb.2006.10.010>
- Honda, Y., Maeda, Y., Izawa, K., Shiba, T., Tanaka, T., Nakaseko, H., Nishimura, K., Mukoyama, H., Isa-Nishitani, M., Miyamoto, T., Nihira, H., Shibata, H., Hiejima, E., Ohara, O., Takita, J., Yasumi, T., Nishikomori, R., 2021. Rapid Flow Cytometry-Based Assay for the Functional Classification of MEFV Variants. *J. Clin. Immunol.* <https://doi.org/10.1007/s10875-021-01021-7>
- Hong, Y., Standing, A.S.I., Nanthapisal, S., Sebire, N., Jolles, S., Omoyinmi, E., Verstegen, R.H., Brogan, P.A., Eleftheriou, D., 2019. Autoinflammation due to homozygous S208 MEFV mutation. *Ann. Rheum. Dis.* 78, 571–573. <https://doi.org/10.1136/annrheumdis-2018-214102>

- Hosie, A.M., Wilkins, M.E., da Silva, H.M.A., Smart, T.G., 2006. Endogenous neurosteroids regulate GABAA receptors through two discrete transmembrane sites. *Nature* 444, 486–489. <https://doi.org/10.1038/nature05324>
- Hsiao, C.-H.C., Nguyen, K., Jin, Y., Vinogradova, O., Wiemer, A.J., 2022. Ligand-induced interactions between butyrophilin 2A1 and 3A1 internal domains in the HMBPP receptor complex. *Cell Chem. Biol.* 29, 985-995.e5. <https://doi.org/10.1016/j.chembiol.2022.01.004>
- Hughes, M.M., O’Neill, L.A.J., 2018. Metabolic regulation of NLRP3. *Immunol. Rev.* 281, 88–98. <https://doi.org/10.1111/imr.12608>
- Jamilloux, Y., Lefevre, L., Magnotti, F., Martin, A., Benezech, S., Allatif, O., Penel-Page, M., Hentgen, V., Sève, P., Gerfaud-Valentin, M., Duquesne, A., Desjonquères, M., Laurent, A., Rémy-Piccolo, V., Cimaz, R., Cantarini, L., Bourdonnay, E., Walzer, T., Py, B.F., Belot, A., Henry, T., 2018. Familial Mediterranean fever mutations are hypermorphic mutations that specifically decrease the activation threshold of the Pyrin inflammasome. *Rheumatology* 57, 100–111. <https://doi.org/10.1093/rheumatology/kex373>
- Jamilloux, Y., Magnotti, F., Belot, A., Henry, T., 2018. The pyrin inflammasome: from sensing RhoA GTPases-inhibiting toxins to triggering autoinflammatory syndromes. *Pathog. Dis.* 76. <https://doi.org/10.1093/femspd/fty020>
- Jeong, J., Rao, A.U., Xu, J., Ogg, S.L., Hathout, Y., Fenselau, C., Mather, I.H., 2009. The PRY/SPRY/B30.2 Domain of Butyrophilin 1A1 (BTN1A1) Binds to Xanthine Oxidoreductase: IMPLICATIONS FOR THE FUNCTION OF BTN1A1 IN THE MAMMARY GLAND AND OTHER TISSUES*. *J. Biol. Chem.* 284, 22444. <https://doi.org/10.1074/jbc.M109.020446>
- Jeru, I., Papin, S., L’hoste, S., Duquesnoy, P., Cazeneuve, C., Camonis, J., Amselem, S., 2005. Interaction of pyrin with 14.3.3 in an isoform-specific and phosphorylation-dependent manner regulates its translocation to the nucleus. *Arthritis Rheum.* 52, 1848–1857. <https://doi.org/10.1002/art.21050>
- Johansson-Haque, K., Palanichamy, E., Okret, S., 2008. Stimulation of MAPK-phosphatase 1 gene expression by glucocorticoids occurs through a tethering mechanism involving C/EBP. *J. Mol. Endocrinol.* 41, 239–249. <https://doi.org/10.1677/JME-08-0015>
- Kappas, A., Hellman, L., Fukushima, D.K., Gallagher, T.F., 1957. The pyrogenic effect of etiocholanolone. *J. Clin. Endocrinol. Metab.* 17, 451–453. <https://doi.org/10.1210/jcem-17-3-451>
- Kappas, A., Palmer, R.H., Glickman, P.B., 1961. Steroid fever. *Am. J. Med.* 31, 167–170. [https://doi.org/10.1016/0002-9343\(61\)90106-1](https://doi.org/10.1016/0002-9343(61)90106-1)
- Kappas, A., Ratkovits, B., 1960. Species specificity of steroid-induced fever. *J. Clin. Endocrinol. Metab.* 20, 898–900. <https://doi.org/10.1210/jcem-20-6-898>
- Kappas, A., Soybel, W., Glickman, P., Fukushima, D.K., 1960. Fever-producing steroids of endogenous origin in man. *Arch. Intern. Med.* 105, 701–708. <https://doi.org/10.1001/archinte.1960.00270170039005>
- Karadag, O., Tufan, A., Yazisiz, V., Ureten, K., Yilmaz, S., Cinar, M., Akdogan, A., Erdem, H., Ozturk, M.A., Pay, S., Dinc, A., 2013. The factors considered as trigger for the attacks in patients with familial Mediterranean fever. *Rheumatol. Int.* 33, 893–897. <https://doi.org/10.1007/s00296-012-2453-x>
- Kayagaki, N., Kornfeld, O.S., Lee, B.L., Stowe, I.B., O’Rourke, K., Li, Q., Sandoval, W., Yan, D., Kang, J., Xu, M., Zhang, J., Lee, W.P., McKenzie, B.S., Ulas, G., Payandeh, J., Roose-Girma, M., Modrusan, Z., Reja, R., Sagolla, M., Webster, J.D., Cho, V., Andrews, T.D., Morris, L.X., Miosge, L.A., Goodnow, C.C., Bertram, E.M., Dixit,

- V.M., 2021. NINJ1 mediates plasma membrane rupture during lytic cell death. *Nature* 591, 131–136. <https://doi.org/10.1038/s41586-021-03218-7>
- Kayagaki, N., Stowe, I.B., Lee, B.L., O'Rourke, K., Anderson, K., Warming, S., Cuellar, T., Haley, B., Roose-Girma, M., Phung, Q.T., Liu, P.S., Lill, J.R., Li, H., Wu, J., Kummerfeld, S., Zhang, J., Lee, W.P., Snipas, S.J., Salvesen, G.S., Morris, L.X., Fitzgerald, L., Zhang, Y., Bertram, E.M., Goodnow, C.C., Dixit, V.M., 2015. Caspase-11 cleaves gasdermin D for non-canonical inflammasome signalling. *Nature* 526, 666–671. <https://doi.org/10.1038/nature15541>
- Keown, J.R., Goldstone, D.C., 2016. Crystal structure of the Trim5 α Bbox2 domain from rhesus macaques describes a plastic oligomerisation interface. *J. Struct. Biol.* 195, 282–285. <https://doi.org/10.1016/j.jsb.2016.07.004>
- Khare, S., Ratsimandresy, R.A., de Almeida, L., Cuda, C.M., Rellick, S.L., Misharin, A.V., Wallin, M.C., Gangopadhyay, A., Forte, E., Gottwein, E., Perlman, H., Reed, J.C., Greaves, D.R., Dorfleutner, A., Stehlik, C., 2014. The PYRIN domain-only protein POP3 inhibits AIM2-like receptor inflammasomes and regulates responses to DNA virus infections. *Nat. Immunol.* 15, 343–353. <https://doi.org/10.1038/ni.2829>
- Kile, B.T., Panopoulos, A.D., Storzaker, R.A., Hacking, D.F., Tahtamouni, L.H., Willson, T.A., Mielke, L.A., Henley, K.J., Zhang, J.-G., Wicks, I.P., Stevenson, W.S., Nurden, P., Watowich, S.S., Justice, M.J., 2007. Mutations in the cofilin partner Aip1/Wdr1 cause autoinflammatory disease and macrothrombocytopenia. *Blood* 110, 2371–2380. <https://doi.org/10.1182/blood-2006-10-055087>
- Kim, J.-R., Kim, H.A., 2020. Molecular Mechanisms of Sex-Related Differences in Arthritis and Associated Pain. *Int. J. Mol. Sci.* 21, 7938. <https://doi.org/10.3390/ijms21217938>
- Kim, M.L., Chae, J.J., Park, Y.H., De Nardo, D., Storzaker, R.A., Ko, H.-J., Tye, H., Cengia, L., DiRago, L., Metcalf, D., Roberts, A.W., Kastner, D.L., Lew, A.M., Lyras, D., Kile, B.T., Croker, B.A., Masters, S.L., 2015. Aberrant actin depolymerization triggers the pyrin inflammasome and autoinflammatory disease that is dependent on IL-18, not IL-1 β . *J. Exp. Med.* 212, 927–938. <https://doi.org/10.1084/jem.20142384>
- Kimura, T., Jain, A., Choi, S.W., Mandell, M.A., Schroder, K., Johansen, T., Deretic, V., 2015. TRIM-mediated precision autophagy targets cytoplasmic regulators of innate immunity. *J. Cell Biol.* 210, 973–989. <https://doi.org/10.1083/jcb.201503023>
- Kishida, D., Nakamura, A., Yazaki, M., Oka, K., Tsuchiya-Suzuki, A., Ichikawa, T., Shimojima, Y., Sekijima, Y., 2020. Triggering factors for febrile attacks in Japanese patients with familial Mediterranean fever. *Clin. Exp. Rheumatol.* 38 Suppl 127, 76–79.
- Kiyota, M., Oya, M., Ayano, M., Niuro, H., Iwasaki, T., Fujiwara, M., Oda, Y., Fujimoto, K., Ida, H., 2020. First case of pyrin-associated autoinflammation with neutrophilic dermatosis complicated by amyloidosis. *Rheumatol. Oxf. Engl.* 59, e41–e43. <https://doi.org/10.1093/rheumatology/keaa005>
- Kuang, Z., Lewis, R.S., Curtis, J.M., Zhan, Y., Saunders, B.M., Babon, J.J., Kolesnik, T.B., Low, A., Masters, S.L., Willson, T.A., Kedzierski, L., Yao, S., Handman, E., Norton, R.S., Nicholson, S.E., 2010. The SPRY domain-containing SOCS box protein SPSB2 targets iNOS for proteasomal degradation. *J. Cell Biol.* 190, 129–141. <https://doi.org/10.1083/jcb.200912087>
- Lagrange, B., Benaoudia, S., Wallet, P., Magnotti, F., Provost, A., Michal, F., Martin, A., Di Lorenzo, F., Py, B.F., Molinaro, A., Henry, T., 2018. Human caspase-4 detects tetraacylated LPS and cytosolic Francisella and functions differently from murine caspase-11. *Nat. Commun.* 9, 242. <https://doi.org/10.1038/s41467-017-02682-y>

- Lam, M.T., Coppola, S., Krumbach, O.H.F., Prencipe, G., Insalaco, A., Cifaldi, C., Brigida, I., Zara, E., Scala, S., Di Cesare, S., Martinelli, S., Di Rocco, M., Pascarella, A., Niceta, M., Pantaleoni, F., Ciolfi, A., Netter, P., Carisey, A.F., Diehl, M., Akbarzadeh, M., Conti, F., Merli, P., Pastore, A., Levi Mortera, S., Camerini, S., Farina, L., Buchholzer, M., Pannone, L., Cao, T.N., Coban-Akdemir, Z.H., Jhangiani, S.N., Muzny, D.M., Gibbs, R.A., Basso-Ricci, L., Chiriaco, M., Dvorsky, R., Putignani, L., Carsetti, R., Janning, P., Stray-Pedersen, A., Erichsen, H.C., Horne, A., Bryceson, Y.T., Torralba-Raga, L., Ramme, K., Rosti, V., Bracaglia, C., Messia, V., Palma, P., Finocchi, A., Locatelli, F., Chinn, I.K., Lupski, J.R., Mace, E.M., Cancrini, C., Aiuti, A., Ahmadian, M.R., Orange, J.S., De Benedetti, F., Tartaglia, M., 2019. A novel disorder involving dyshematopoiesis, inflammation, and HLH due to aberrant CDC42 function. *J. Exp. Med.* 216, 2778–2799. <https://doi.org/10.1084/jem.20190147>
- LaRock, C.N., Cookson, B.T., 2012. The *Yersinia* virulence effector YopM binds caspase-1 to arrest inflammasome assembly and processing. *Cell Host Microbe* 12, 799–805. <https://doi.org/10.1016/j.chom.2012.10.020>
- Lindor, N.M., Arsenaault, T.M., Solomon, H., Seidman, C.E., McEvoy, M.T., 1997. A new autosomal dominant disorder of pyogenic sterile arthritis, pyoderma gangrenosum, and acne: PAPA syndrome. *Mayo Clin. Proc.* 72, 611–615. [https://doi.org/10.1016/S0025-6196\(11\)63565-9](https://doi.org/10.1016/S0025-6196(11)63565-9)
- Lindwall, E., Singla, S., Davis, W.E., Quinet, R.J., 2015. Novel PSTPIP1 gene mutation in a patient with pyogenic arthritis, pyoderma gangrenosum and acne (PAPA) syndrome. *Semin. Arthritis Rheum.* 45, 91–93. <https://doi.org/10.1016/j.semarthrit.2015.02.012>
- Liston, A., Masters, S.L., 2017. Homeostasis-altering molecular processes as mechanisms of inflammasome activation. *Nat. Rev. Immunol.* 17, 208–214. <https://doi.org/10.1038/nri.2016.151>
- Liu, X., Zhang, Z., Ruan, J., Pan, Y., Magupalli, V.G., Wu, H., Lieberman, J., 2016. Inflammasome-activated gasdermin D causes pyroptosis by forming membrane pores. *Nature* 535, 153–158. <https://doi.org/10.1038/nature18629>
- Livneh, A., Langevitz, P., Zemer, D., Zaks, N., Kees, S., Lidar, T., Migdal, A., Padeh, S., Pras, M., 1997. Criteria for the diagnosis of familial Mediterranean fever. *Arthritis Rheum.* 40, 1879–1885. <https://doi.org/10.1002/art.1780401023>
- Magnotti, F., Chirita, D., Dalmon, S., Martin, A., Bronnec, P., Sousa, J., Helyncck, O., Lee, W., Kastner, D., Chae, J.J., McDermott, M.F., Belot, A., Popoff, M., Sève, P., Georgin-Lavialle, S., Munier-Lehmann, H., Tran, T.A., Langhe, E.D., Wouters, C., Jamilloux, Y., Henry, T., 2021. Steroid hormone catabolites activate the pyrin inflammasome through a non-canonical mechanism. *bioRxiv* 2021.10.29.466454. <https://doi.org/10.1101/2021.10.29.466454>
- Magnotti, F., Lefeuvre, L., Benezech, S., Malsot, T., Waeckel, L., Martin, A., Kerever, S., Chirita, D., Desjonqueres, M., Duquesne, A., Gerfaud-Valentin, M., Laurent, A., Sève, P., Popoff, M., Walzer, T., Belot, A., Jamilloux, Y., Henry, T., 2019. Pyrin dephosphorylation is sufficient to trigger inflammasome activation in familial Mediterranean fever patients. *EMBO Mol. Med.* 11. <https://doi.org/10.15252/emmm.201910547>
- Magnotti, F., Malsot, T., Georgin-Lavialle, S., Abbas, F., Martin, A., Belot, A., Fauter, M., Rabilloud, M., Gerfaud-Valentin, M., Sève, P., Duquesne, A., Hot, A., Durupt, S., Savey, L., Giurgea, I., Grateau, G., Henry, T., Jamilloux, Y., 2020. Fast diagnostic test for familial Mediterranean fever based on a kinase inhibitor. *Ann. Rheum. Dis.* <https://doi.org/10.1136/annrheumdis-2020-218366>

- Magupalli, V.G., Negro, R., Tian, Y., Hauenstein, A.V., Di Caprio, G., Skillern, W., Deng, Q., Orning, P., Alam, H.B., Maliga, Z., Sharif, H., Hu, J.J., Evavold, C.L., Kagan, J.C., Schmidt, F.I., Fitzgerald, K.A., Kirchhausen, T., Li, Y., Wu, H., 2020. HDAC6 mediates an aggresome-like mechanism for NLRP3 and pyrin inflammasome activation. *Science* 369, eaas8995. <https://doi.org/10.1126/science.aas8995>
- Malik, H.S., Bliska, J.B., 2020. The pyrin inflammasome and the *Yersinia* effector interaction. *Immunol. Rev.* 297, 96–107. <https://doi.org/10.1111/imr.12907>
- Malik, H.S., Loeven, N.A., Delgado, J.M., Kettenbach, A.N., Bliska, J.B., 2022. Phosphoprotein Phosphatase Activity Positively Regulates Oligomeric Pyrin to Trigger Inflammasome Assembly in Response to Bacterial Effectors and Toxins that Inactivate RhoA in Macrophages. *bioRxiv* 2022.03.23.485108. <https://doi.org/10.1101/2022.03.23.485108>
- Mandey, S.H.L., Kuijk, L.M., Frenkel, J., Waterham, H.R., 2006. A role for geranylgeranylation in interleukin-1beta secretion. *Arthritis Rheum.* 54, 3690–3695. <https://doi.org/10.1002/art.22194>
- Mansfield, E., Chae, J.J., Komarow, H.D., Brotz, T.M., Frucht, D.M., Aksentjevich, I., Kastner, D.L., 2001. The familial Mediterranean fever protein, pyrin, associates with microtubules and colocalizes with actin filaments. *Blood* 98, 851–859. <https://doi.org/10.1182/blood.v98.3.851>
- Manthiram, K., Zhou, Q., Aksentjevich, I., Kastner, D.L., 2017. The monogenic autoinflammatory diseases define new pathways in human innate immunity and inflammation. *Nat. Immunol.* 18, 832–842. <https://doi.org/10.1038/ni.3777>
- Manukyan, G., Aminov, R., 2016. Update on Pyrin Functions and Mechanisms of Familial Mediterranean Fever. *Front. Microbiol.* 7, 456. <https://doi.org/10.3389/fmicb.2016.00456>
- Martinon, Fabio, Burns, K., Tschopp, J., 2002. The inflammasome: a molecular platform triggering activation of inflammatory caspases and processing of proIL-beta. *Mol. Cell* 10, 417–426. [https://doi.org/10.1016/s1097-2765\(02\)00599-3](https://doi.org/10.1016/s1097-2765(02)00599-3)
- Martinon, F., Mayor, A., Tschopp, J., 2009. The inflammasomes: guardians of the body. *Annu. Rev. Immunol.* 27, 229–265. <https://doi.org/10.1146/annurev.immunol.021908.132715>
- Masters, S.L., Lagou, V., Jéru, I., Baker, P.J., Van Eyck, L., Parry, D.A., Lawless, D., De Nardo, D., Garcia-Perez, J.E., Dagley, L.F., Holley, C.L., Dooley, J., Moghaddas, F., Pasciuto, E., Jeandel, P.-Y., Sciot, R., Lyras, D., Webb, A.I., Nicholson, S.E., De Somer, L., van Nieuwenhove, E., Ruuth-Praz, J., Copin, B., Cochet, E., Medlej-Hashim, M., Megarbane, A., Schroder, K., Savic, S., Goris, A., Amselem, S., Wouters, C., Liston, A., 2016. Familial autoinflammation with neutrophilic dermatosis reveals a regulatory mechanism of pyrin activation. *Sci. Transl. Med.* 8, 332ra45. <https://doi.org/10.1126/scitranslmed.aaf1471>
- Meerbrey, K.L., Hu, G., Kessler, J.D., Roarty, K., Li, M.Z., Fang, J.E., Herschkowitz, J.I., Burrows, A.E., Ciccia, A., Sun, T., Schmitt, E.M., Bernardi, R.J., Fu, X., Bland, C.S., Cooper, T.A., Schiff, R., Rosen, J.M., Westbrook, T.F., Elledge, S.J., 2011. The pINDUCER lentiviral toolkit for inducible RNA interference in vitro and in vivo. *Proc. Natl. Acad. Sci. U. S. A.* 108, 3665–3670. <https://doi.org/10.1073/pnas.1019736108>
- Milhavet, F., Cuisset, L., Hoffman, H.M., Slim, R., El-Shanti, H., Aksentjevich, I., Lesage, S., Waterham, H., Wise, C., Sarrauste de Menthiere, C., Touitou, I., 2008. The infevers autoinflammatory mutation online registry: update with new genes and functions. *Hum. Mutat.* 29, 803–808. <https://doi.org/10.1002/humu.20720>

- Miyashita, K., Matsuda, Y., Okajima, M., Toma, T., Yachie, A., Wada, T., 2022. Role of E148Q in familial Mediterranean fever with an exon 10 mutation in MEFV. *Pediatr. Int. Off. J. Jpn. Pediatr. Soc.* 64, e14696. <https://doi.org/10.1111/ped.14696>
- Moghaddas, F., Llamas, R., De Nardo, D., Martinez-Banaclocha, H., Martinez-Garcia, J.J., Mesa-del-Castillo, P., Baker, P.J., Gargallo, V., Mensa-Vilaro, A., Canna, S., Wicks, I.P., Pelegrin, P., Arostegui, J.I., Masters, S.L., 2017. A novel Pyrin-Associated Autoinflammation with Neutrophilic Dermatitis mutation further defines 14-3-3 binding of Pyrin and distinction to Familial Mediterranean Fever. *Ann. Rheum. Dis.* 76, 2085–2094. <https://doi.org/10.1136/annrheumdis-2017-211473>
- Moradian, M.M., Babikyan, D., Banoian, D., Hayrapetyan, H., Manvelyan, H., Avanesian, N., Sarkisian, T., 2017. Comprehensive analysis of mutations in the MEFV gene reveal that the location and not the substitution type determines symptom severity in FMF. *Mol. Genet. Genomic Med.* 5, 742–750. <https://doi.org/10.1002/mgg3.336>
- Murakami, T., Ockinger, J., Yu, J., Byles, V., McColl, A., Hofer, A.M., Horng, T., 2012. Critical role for calcium mobilization in activation of the NLRP3 inflammasome. *Proc. Natl. Acad. Sci. U. S. A.* 109, 11282–11287. <https://doi.org/10.1073/pnas.1117765109>
- Newton, K., Dixit, V.M., Kayagaki, N., 2021. Dying cells fan the flames of inflammation. *Science* 374, 1076–1080. <https://doi.org/10.1126/science.abi5934>
- Nishitani-Isa, M., Mukai, K., Honda, Y., Nihira, H., Tanaka, T., Shibata, H., Kodama, K., Hiejima, E., Izawa, K., Kawasaki, Y., Osawa, M., Katata, Y., Onodera, S., Watanabe, T., Uchida, T., Kure, S., Takita, J., Ohara, O., Saito, M.K., Nishikomori, R., Taguchi, T., Sasahara, Y., Yasumi, T., 2022. Trapping of CDC42 C-terminal variants in the Golgi drives pyrin inflammasome hyperactivation. *J. Exp. Med.* 219, e20211889. <https://doi.org/10.1084/jem.20211889>
- Normand, S., Massonnet, B., Delwail, A., Favot, L., Cuisset, L., Grateau, G., Morel, F., Silvain, C., Lecron, J.-C., 2009. Specific increase in caspase-1 activity and secretion of IL-1 family cytokines: a putative link between mevalonate kinase deficiency and inflammation. *Eur. Cytokine Netw.* 20, 101–107. <https://doi.org/10.1684/ecn.2009.0163>
- Omenetti, A., Carta, S., Delfino, L., Martini, A., Gattorno, M., Rubartelli, A., 2014. Increased NLRP3-dependent interleukin 1beta secretion in patients with familial Mediterranean fever: correlation with MEFV genotype. *Ann. Rheum. Dis.* 73, 462–469. <https://doi.org/10.1136/annrheumdis-2012-202774>
- Ozen, S., Bakkaloglu, A., Yilmaz, E., Duzova, A., Balci, B., Topaloglu, R., Besbas, N., 2003. Mutations in the gene for familial Mediterranean fever: do they predispose to inflammation? *J. Rheumatol.* 30, 2014–2018.
- Palmer, R.H., Ratkovits, B., Kappas, A., 1961. Steroid pyrogen studies in laboratory and domestic animals. *J. Appl. Physiol.* 16, 345–347. <https://doi.org/10.1152/jappl.1961.16.2.345>
- Papin, S., Cuenin, S., Agostini, L., Martinon, F., Werner, S., Beer, H.D., Grutter, C., Grutter, M., Tschopp, J., 2007. The SPRY domain of Pyrin, mutated in familial Mediterranean fever patients, interacts with inflammasome components and inhibits proIL-1beta processing. *Cell Death Differ* 14, 1457–66.
- Papin, S., Duquesnoy, P., Cazeneuve, C., Pantel, J., Coppey-Moisan, M., Dargemont, C., Amselem, S., 2000. Alternative splicing at the MEFV locus involved in familial Mediterranean fever regulates translocation of the marenostin/pyrin protein to the nucleus. *Hum. Mol. Genet.* 9, 3001–3009. <https://doi.org/10.1093/hmg/9.20.3001>

- Park, M.H., Rehman, S.U., Kim, I.S., Choi, M.S., Yoo, H.H., 2017. Stress-induced changes of neurosteroid profiles in rat brain and plasma under immobilized condition. *J. Pharm. Biomed. Anal.* 138, 92–99. <https://doi.org/10.1016/j.jpba.2017.02.007>
- Park, Y.H., Remmers, E.F., Lee, W., Ombrello, A.K., Chung, L.K., Shilei, Z., Stone, D.L., Ivanov, M.I., Loeven, N.A., Barron, K.S., Hoffmann, P., Nehrebecky, M., Akkaya-Ulum, Y.Z., Sag, E., Balci-Peynircioglu, B., Aksentijevich, I., Gül, A., Rotimi, C.N., Chen, H., Bliska, J.B., Ozen, S., Kastner, D.L., Shriner, D., Chae, J.J., 2020. Ancient familial Mediterranean fever mutations in human pyrin and resistance to *Yersinia pestis*. *Nat. Immunol.* 21, 857–867. <https://doi.org/10.1038/s41590-020-0705-6>
- Park, Y.H., Wood, G., Kastner, D.L., Chae, J.J., 2016. Pyrin inflammasome activation and RhoA signaling in the autoinflammatory diseases FMF and HIDS. *Nat. Immunol.* 17, 914–921. <https://doi.org/10.1038/ni.3457>
- Peckham, D., Scambler, T., Savic, S., McDermott, M.F., 2017. The burgeoning field of innate immune-mediated disease and autoinflammation. *J. Pathol.* 241, 123–139. <https://doi.org/10.1002/path.4812>
- Perfetto, L., Gherardini, P.F., Davey, N.E., Diella, F., Helmer-Citterich, M., Cesareni, G., 2013. Exploring the diversity of SPRY/B30.2-mediated interactions. *Trends Biochem. Sci.* 38, 38–46. <https://doi.org/10.1016/j.tibs.2012.10.001>
- Pierini, R., Juruj, C., Perret, M., Jones, C.L., Mangeot, P., Weiss, D.S., Henry, T., 2012. AIM2/ASC triggers caspase-8-dependent apoptosis in *Francisella*-infected caspase-1-deficient macrophages. *Cell Death Differ.* 19, 1709–21. <https://doi.org/10.1038/cdd.2012.51>
- Planès, R., Pinilla, M., Santoni, K., Hessel, A., Passemar, C., Lay, K., Paillette, P., Valadão, A.-L.C., Robinson, K.S., Bastard, P., Lam, N., Fadrique, R., Rossi, I., Pericat, D., Bagayoko, S., Leon-Icaza, S.A., Rombouts, Y., Perouzel, E., Tiraby, M., COVID Human Genetic Effort, Zhang, Q., Cicuta, P., Jouanguy, E., Neyrolles, O., Bryant, C.E., Floto, A.R., Goujon, C., Lei, F.Z., Martin-Blondel, G., Silva, S., Casanova, J.-L., Cougoule, C., Reversade, B., Marcoux, J., Ravet, E., Meunier, E., 2022. Human NLRP1 is a sensor of pathogenic coronavirus 3CL proteases in lung epithelial cells. *Mol. Cell* 82, 2385-2400.e9. <https://doi.org/10.1016/j.molcel.2022.04.033>
- Polan, M.L., Loukides, J., Nelson, P., Carding, S., Diamond, M., Walsh, A., Bottomly, K., 1989. Progesterone and estradiol modulate interleukin-1 beta messenger ribonucleic acid levels in cultured human peripheral monocytes. *J. Clin. Endocrinol. Metab.* 69, 1200–1206. <https://doi.org/10.1210/jcem-69-6-1200>
- Popoff, M.R., 1987. Purification and characterization of *Clostridium sordellii* lethal toxin and cross-reactivity with *Clostridium difficile* cytotoxin. *Infect. Immun.* 55, 35–43.
- Pras, M., Frangione, B., Franklin, E.C., Gafni, J., 1982. Idiopathic AL-kiv amyloidosis presenting as giant hepatomegaly. *Isr. J. Med. Sci.* 18, 866–869.
- Py, B.F., Kim, M.-S., Vakifahmetoglu-Norberg, H., Yuan, J., 2013. Deubiquitination of NLRP3 by BRCC3 critically regulates inflammasome activity. *Mol. Cell* 49, 331–338. <https://doi.org/10.1016/j.molcel.2012.11.009>
- Rathinam, V.A.K., Fitzgerald, K.A., 2016. Inflammasome Complexes: Emerging Mechanisms and Effector Functions. *Cell* 165, 792–800. <https://doi.org/10.1016/j.cell.2016.03.046>
- Ratner, D., Orning, M.P.A., Proulx, M.K., Wang, D., Gavrilin, M.A., Wewers, M.D., Alnemri, E.S., Johnson, P.F., Lee, B., Meccas, J., Kayagaki, N., Goguen, J.D., Lien, E., 2016. The *Yersinia pestis* Effector YopM Inhibits Pyrin Inflammasome Activation. *PLoS Pathog.* 12, e1006035. <https://doi.org/10.1371/journal.ppat.1006035>

- Ratsimandresy, R.A., Chu, L.H., Khare, S., de Almeida, L., Gangopadhyay, A., Indramohan, M., Misharin, A.V., Greaves, D.R., Perlman, H., Dorfleutner, A., Stehlik, C., 2017. The PYRIN domain-only protein POP2 inhibits inflammasome priming and activation. *Nat. Commun.* 8. <https://doi.org/10.1038/ncomms15556>
- Reamy, B.V., Viera, A.J., 2022. Cardiovascular Disease Prevention: Pharmacologic Prevention. *FP Essent.* 520, 20–25.
- Regan, J.C., Brandão, A.S., Leitão, A.B., Mantas Dias, A.R., Sucena, E., Jacinto, A., Zaidman-Rémy, A., 2013. Steroid hormone signaling is essential to regulate innate immune cells and fight bacterial infection in *Drosophila*. *PLoS Pathog.* 9, e1003720. <https://doi.org/10.1371/journal.ppat.1003720>
- Rhodes, D.A., de Bono, B., Trowsdale, J., 2005. Relationship between SPRY and B30.2 protein domains. Evolution of a component of immune defence? *Immunology* 116, 411–417. <https://doi.org/10.1111/j.1365-2567.2005.02248.x>
- Richardson, M.W., Guo, L., Xin, F., Yang, X., Riley, J.L., 2014. Stabilized Human TRIM5 α Protects Human T Cells From HIV-1 Infection. *Mol. Ther.* 22, 1084–1095. <https://doi.org/10.1038/mt.2014.52>
- Rigau, M., Ostrouska, S., Fulford, T.S., Johnson, D.N., Woods, K., Ruan, Z., McWilliam, H.E.G., Hudson, C., Tutuka, C., Wheatley, A.K., Kent, S.J., Villadangos, J.A., Pal, B., Kurts, C., Simmonds, J., Pelzing, M., Nash, A.D., Hammet, A., Verhagen, A.M., Vairo, G., Maraskovsky, E., Panousis, C., Gherardin, N.A., Cebon, J., Godfrey, D.I., Behren, A., Uldrich, A.P., 2020. Butyrophilin 2A1 is essential for phosphoantigen reactivity by $\gamma\delta$ T cells. *Science* 367, eaay5516. <https://doi.org/10.1126/science.aay5516>
- Rodal, A.A., Tetreault, J.W., Lappalainen, P., Drubin, D.G., Amberg, D.C., 1999. Aip1p interacts with cofilin to disassemble actin filaments. *J. Cell Biol.* 145, 1251–1264. <https://doi.org/10.1083/jcb.145.6.1251>
- Romero, R., Mazor, M., Tartakovsky, B., 1991. Systemic administration of interleukin-1 induces preterm parturition in mice. *Am. J. Obstet. Gynecol.* 165, 969–971. [https://doi.org/10.1016/0002-9378\(91\)90450-6](https://doi.org/10.1016/0002-9378(91)90450-6)
- Romero, R., Xu, Y., Plazyo, O., Chaemsaitong, P., Chaiworapongsa, T., Unkel, R., Than, N.G., Chiang, P.J., Dong, Z., Xu, Z., Tarca, A.L., Abrahams, V.M., Hassan, S.S., Yeo, L., Gomez-Lopez, N., 2018. A Role for the Inflammasome in Spontaneous Labor at Term. *Am. J. Reprod. Immunol. N. Y. N* 1989 79, e12440. <https://doi.org/10.1111/aji.12440>
- Rowczenio, D.M., Youngstein, T., Trojer, H., Omoyinmi, E., Baginska, A., Brogan, P., Papadopoulou, C., Rezk, T., Hawkins, P.N., Lachmann, H.J., 2020. British kindred with dominant FMF associated with high incidence of AA amyloidosis caused by novel MEFV variant, and a review of the literature. *Rheumatol. Oxf. Engl.* 59, 554–558. <https://doi.org/10.1093/rheumatology/kez334>
- Ryan, J., Masters, S., Booty, M., Habal, N., Alexander, J., Barham, B., Remmers, E., Barron, K., Kastner, D., Aksentijevich, I., 2010. Clinical features and functional significance of the P369S/R408Q variant in pyrin, the familial Mediterranean fever protein. *Ann. Rheum. Dis.* 69, 1383–1388. <https://doi.org/10.1136/ard.2009.113415>
- Salim, M., Knowles, T.J., Baker, A.T., Davey, M.S., Jeeves, M., Sridhar, P., Wilkie, J., Willcox, C.R., Kadri, H., Taher, T.E., Vantourout, P., Hayday, A., Mehellou, Y., Mohammed, F., Willcox, B.E., 2017. BTN3A1 discriminates $\gamma\delta$ T cell phosphoantigens from non-antigenic small molecules via a conformational sensor in its B30.2 domain. *ACS Chem. Biol.* 12, 2631–2643. <https://doi.org/10.1021/acscchembio.7b00694>

- Samukawa, S., Yoshimi, R., Kirino, Y., Nakajima, H., 2021. The PRY/SPRY domain of pyrin/TRIM20 interacts with β 2-microglobulin to promote inflammasome formation. *Sci. Rep.* 11, 23613. <https://doi.org/10.1038/s41598-021-03073-6>
- Sanchez, J.G., Sparrer, K.M.J., Chiang, C., Reis, R.A., Chiang, J.J., Zurenski, M.A., Wan, Y., Gack, M.U., Pornillos, O., 2018. TRIM25 binds RNA to modulate cellular anti-viral defense. *J. Mol. Biol.* 430, 5280–5293. <https://doi.org/10.1016/j.jmb.2018.10.003>
- Sandstrom, A., Mitchell, P.S., Goers, L., Mu, E.W., Lesser, C.F., Vance, R.E., 2019. Functional degradation: A mechanism of NLRP1 inflammasome activation by diverse pathogen enzymes. *Science* 364, eaau1330. <https://doi.org/10.1126/science.aau1330>
- Sandstrom, A., Peigné, C.-M., Léger, A., Crooks, J.E., Konczak, F., Gesnel, M.-C., Breathnach, R., Bonneville, M., Scotet, E., Adams, E.J., 2014. The intracellular B30.2 domain of Butyrophilin 3A1 binds phosphoantigens to mediate activation of human V γ 9V δ 2 T cells. *Immunity* 40, 490–500. <https://doi.org/10.1016/j.immuni.2014.03.003>
- Sardiello, M., Cairo, S., Fontanella, B., Ballabio, A., Meroni, G., 2008. Genomic analysis of the TRIM family reveals two groups of genes with distinct evolutionary properties. *BMC Evol. Biol.* 8, 225. <https://doi.org/10.1186/1471-2148-8-225>
- Schaner, Philip, Richards, N., Wadhwa, A., Aksentijevich, I., Kastner, D., Tucker, P., Gumucio, D., 2001. Episodic evolution of pyrin in primates: human mutations recapitulate ancestral amino acid states. *Nat. Genet.* 27, 318–321. <https://doi.org/10.1038/85893>
- Schiffer, L., Barnard, L., Baranowski, E.S., Gilligan, L.C., Taylor, A.E., Arlt, W., Shackleton, C.H.L., Storbeck, K.-H., 2019. Human steroid biosynthesis, metabolism and excretion are differentially reflected by serum and urine steroid metabolomes: A comprehensive review. *J. Steroid Biochem. Mol. Biol.* 194, 105439. <https://doi.org/10.1016/j.jsbmb.2019.105439>
- Shiba, T., Tanaka, T., Ida, H., Watanabe, M., Nakaseko, H., Osawa, M., Shibata, H., Izawa, K., Yasumi, T., Kawasaki, Y., Saito, M.K., Takita, J., Heike, T., Nishikomori, R., 2019. Functional evaluation of the pathological significance of MEFV variants using induced pluripotent stem cell-derived macrophages. *J. Allergy Clin. Immunol.* 144, 1438-1441.e12. <https://doi.org/10.1016/j.jaci.2019.07.039>
- Shimba, A., Ejima, A., Ikuta, K., 2021. Pleiotropic Effects of Glucocorticoids on the Immune System in Circadian Rhythm and Stress. *Front. Immunol.* 12, 706951. <https://doi.org/10.3389/fimmu.2021.706951>
- Shoham, N.G., Centola, M., Mansfield, E., Hull, K.M., Wood, G., Wise, C.A., Kastner, D.L., 2003. Pyrin binds the PSTPIP1/CD2BP1 protein, defining familial Mediterranean fever and PAPA syndrome as disorders in the same pathway. *Proc. Natl. Acad. Sci. U. S. A.* 100, 13501–13506. <https://doi.org/10.1073/pnas.2135380100>
- Sivaramakrishnan, G., Sun, Y., Rajmohan, R., Lin, V.C.L., 2009. B30.2/SPRY domain in tripartite motif-containing 22 is essential for the formation of distinct nuclear bodies. *FEBS Lett.* 583, 2093–2099. <https://doi.org/10.1016/j.febslet.2009.05.036>
- Skinner, O.P., Jurczyk, J., Baker, P.J., Masters, S.L., Rios Wilks, A.G., Clearwater, M.S., Robertson, A.A.B., Schroder, K., Mehr, S., Munoz, M.A., Rogers, M.J., 2019. Lack of protein prenylation promotes NLRP3 inflammasome assembly in human monocytes. *J. Allergy Clin. Immunol.* 143, 2315-2317.e3. <https://doi.org/10.1016/j.jaci.2019.02.013>
- Solak, M., Yildiz, H., Koken, R., Erdogan, M., Eser, B., Sen, T., Evirgen, N., Erdem, S., Arikan, E., 2008. Analysis of familial Mediterranean fever gene mutations in 202

- patients with familial Mediterranean fever. *Genet. Test.* 12, 341–344.
<https://doi.org/10.1089/gte.2008.0009>
- Srinivasula, S.M., Poyet, J.-L., Razmara, M., Datta, P., Zhang, Z., Alnemri, E.S., 2002. The PYRIN-CARD Protein ASC Is an Activating Adaptor for Caspase-1. *J. Biol. Chem.* 277, 21119–21122. <https://doi.org/10.1074/jbc.C200179200>
- Stacey, K.B., Breen, E., Jefferies, C.A., 2012. Tyrosine Phosphorylation of the E3 Ubiquitin Ligase TRIM21 Positively Regulates Interaction with IRF3 and Hence TRIM21 Activity. *PLoS ONE* 7. <https://doi.org/10.1371/journal.pone.0034041>
- Stamerra, C.A., Di Giosia, P., Ferri, C., Giorgini, P., Reiner, Z., Johnston, T.P., Sahebkar, A., 2021. Statin therapy and sex hormones. *Eur. J. Pharmacol.* 890, 173745.
<https://doi.org/10.1016/j.ejphar.2020.173745>
- Standing, A.S.I., Malinova, D., Hong, Y., Record, J., Moulding, D., Blundell, M.P., Nowak, K., Jones, H., Omoyinmi, E., Gilmour, K.C., Medlar, A., Stanescu, H., Kleta, R., Anderson, G., Nanthapisal, S., Gomes, S.M., Klein, N., Eleftheriou, D., Thrasher, A.J., Brogan, P.A., 2017. Autoinflammatory periodic fever, immunodeficiency, and thrombocytopenia (PFIT) caused by mutation in actin-regulatory gene WDR1. *J. Exp. Med.* 214, 59–71. <https://doi.org/10.1084/jem.20161228>
- Stark, K., Straub, R.H., Rovenský, J., Blažičková, S., Eiselt, G., Schmidt, M., 2015. CYB5A polymorphism increases androgens and reduces risk of rheumatoid arthritis in women. *Arthritis Res. Ther.* 17, 56. <https://doi.org/10.1186/s13075-015-0574-9>
- Stehlik, C., Krajewska, M., Welsh, K., Krajewski, S., Godzik, A., Reed, J.C., 2003. The PAAD/PYRIN-only protein POP1/ASC2 is a modulator of ASC-mediated nuclear-factor-kappa B and pro-caspase-1 regulation. *Biochem. J.* 373, 101–113.
<https://doi.org/10.1042/BJ20030304>
- Steinetz, B.G., Randolph, C., Werner, R., Mahoney, C.J., 1998. Pyrogenicity of etiocholanolone and interleukin-1 in New and Old World Monkeys. *Proc. Soc. Exp. Biol. Med. Soc. Exp. Biol. Med. N. Y.* N 217, 435–438.
<https://doi.org/10.3181/00379727-217-44253>
- Stelzer, I.A., Ghaemi, M.S., Han, X., Ando, K., Hédou, J.J., Feyaerts, D., Peterson, L.S., Rumer, K.K., Tsai, E.S., Ganio, E.A., Gaudillière, D.K., Tsai, A.S., Choisy, B., Gaigne, L.P., Verdonk, F., Jacobsen, D., Gavasso, S., Traber, G.M., Ellenberger, M., Stanley, N., Becker, M., Culos, A., Fallahzadeh, R., Wong, R.J., Darmstadt, G.L., Druzin, M.L., Winn, V.D., Gibbs, R.S., Ling, X.B., Sylvester, K., Carvalho, B., Snyder, M.P., Shaw, G.M., Stevenson, D.K., Contrepolis, K., Angst, M.S., Aghaeepour, N., Gaudillière, B., 2021. Integrated trajectories of the maternal metabolome, proteome, and immunome predict labor onset. *Sci. Transl. Med.* 13, eabd9898. <https://doi.org/10.1126/scitranslmed.abd9898>
- Stichweh, D.S., Punaro, M., Pascual, V., 2005. Dramatic improvement of pyoderma gangrenosum with infliximab in a patient with PAPA syndrome. *Pediatr. Dermatol.* 22, 262–265. <https://doi.org/10.1111/j.1525-1470.2005.22320.x>
- Stremmlau, M., Perron, M., Welikala, S., Sodroski, J., 2005. Species-Specific Variation in the B30.2(SPRY) Domain of TRIM5 α Determines the Potency of Human Immunodeficiency Virus Restriction. *J. Virol.* 79, 3139–3145.
<https://doi.org/10.1128/JVI.79.5.3139-3145.2005>
- Ströhle, A., Romeo, E., di Michele, F., Pasini, A., Yassouridis, A., Holsboer, F., Rupprecht, R., 2002. GABA(A) receptor-modulating neuroactive steroid composition in patients with panic disorder before and during paroxetine treatment. *Am. J. Psychiatry* 159, 145–147. <https://doi.org/10.1176/appi.ajp.159.1.145>

- Stutz, A., Kolbe, C.-C., Stahl, R., Horvath, G.L., Franklin, B.S., van Ray, O., Brinkschulte, R., Geyer, M., Meissner, F., Latz, E., 2017. NLRP3 inflammasome assembly is regulated by phosphorylation of the pyrin domain. *J. Exp. Med.* 214, 1725–1736. <https://doi.org/10.1084/jem.20160933>
- Sun, Y., Keown, J.R., Black, M.M., Raclot, C., Demarais, N., Trono, D., Turelli, P., Goldstone, D.C., 2019. A Dissection of Oligomerization by the TRIM28 Tripartite Motif and the Interaction with Members of the Krab-ZFP Family. *J. Mol. Biol.* 431, 2511–2527. <https://doi.org/10.1016/j.jmb.2019.05.002>
- Tang, B.L., 2022. Cholesterol synthesis inhibition or depletion in axon regeneration. *Neural Regen. Res.* 17, 271–276. <https://doi.org/10.4103/1673-5374.317956>
- The French FMF Consortium, Bernot, A., Clepet, C., Dasilva, C., Devaud, C., Petit, J.-L., Caloustian, C., Cruaud, C., Samson, D., Pulcini, F., Weissenbach, J., Heilig, R., Notanicola, C., Domingo, C., Rozenbaum, M., Benchetrit, E., Topaloglu, R., Dewalle, M., Dross, C., Hadjari, P., Dupont, M., Demaille, J., Touitou, I., Smaoui, N., Nedelec, B., Méry, J.-P., Chaabouni, H., Delpech, M., Grateau, G., 1997. A candidate gene for familial Mediterranean fever. *Nat. Genet.* 17, 25–31. <https://doi.org/10.1038/ng0997-25>
- The International FMF Consortium, 1997. Ancient Missense Mutations in a New Member of the RoRet Gene Family Are Likely to Cause Familial Mediterranean Fever. *Cell* 90, 797–807. [https://doi.org/10.1016/S0092-8674\(00\)80539-5](https://doi.org/10.1016/S0092-8674(00)80539-5)
- Touitou, I., 2001. The spectrum of Familial Mediterranean Fever (FMF) mutations. *Eur. J. Hum. Genet. EJHG* 9, 473–483. <https://doi.org/10.1038/sj.ejhg.5200658>
- Tufan, A., Lachmann, H.J., 2020. Familial Mediterranean fever, from pathogenesis to treatment: a contemporary review. *Turk. J. Med. Sci.* 50, 1591–1610. <https://doi.org/10.3906/sag-2008-11>
- Ueda, N., Ida, H., Washio, M., Miyahara, H., Tokunaga, S., Tanaka, F., Takahashi, H., Kusuhara, K., Ohmura, K., Nakayama, M., Ohara, O., Nishikomori, R., Minota, S., Takei, S., Fujii, T., Ishigatsubo, Y., Tsukamoto, H., Tahira, T., Horiuchi, T., 2016. Clinical and Genetic Features of Patients With TNFRSF1A Variants in Japan: Findings of a Nationwide Survey. *Arthritis Rheumatol. Hoboken NJ* 68, 2760–2771. <https://doi.org/10.1002/art.39793>
- Vahidnezhad, H., Youssefian, L., Saeidian, A.H., Ziaee, V., Mahmoudi, H., Parvaneh, N., Ashjaei, B., Shahrokh, S., Kamyab Hesari, K., Soltani Zangbar, M., Yousefi, M., Zeinali, S., Uitto, J., 2021. Homozygous MEFV Gene Variant and Pyrin-Associated Autoinflammation With Neutrophilic Dermatitis: A Family With a Novel Autosomal Recessive Mode of Inheritance. *JAMA Dermatol.* 157, 1466–1471. <https://doi.org/10.1001/jamadermatol.2021.3899>
- Vajjhala, P.R., Kaiser, S., Smith, S.J., Ong, Q.-R., Soh, S.L., Stacey, K.J., Hill, J.M., 2014. Identification of Multifaceted Binding Modes for Pyrin and ASC Pyrin Domains Gives Insights into Pyrin Inflammasome Assembly. *J. Biol. Chem.* 289, 23504–23519. <https://doi.org/10.1074/jbc.M114.553305>
- Vajjhala, P.R., Mirams, R.E., Hill, J.M., 2012. Multiple Binding Sites on the Pyrin Domain of ASC Protein Allow Self-association and Interaction with NLRP3 Protein. *J. Biol. Chem.* 287, 41732–41743. <https://doi.org/10.1074/jbc.M112.381228>
- Van Gorp, H., Saavedra, P.H.V., de Vasconcelos, N.M., Van Opdenbosch, N., Vande Walle, L., Matusiak, M., Prencipe, G., Insalaco, A., Van Hauwermeiren, F., Demon, D., Bogaert, D.J., Dullaers, M., De Baere, E., Hochepped, T., Dehoorne, J., Vermaelen, K.Y., Haerynck, F., De Benedetti, F., Lamkanfi, M., 2016. Familial Mediterranean fever mutations lift the obligatory requirement for microtubules in Pyrin

- inflammasome activation. *Proc. Natl. Acad. Sci. U. S. A.* 113, 14384–14389. <https://doi.org/10.1073/pnas.1613156113>
- Van Nieuwenhove, E., De Langhe, E., Dooley, J., Van Den Oord, J., Shahrooei, M., Parvaneh, N., Ziaee, V., Savic, S., Kacar, M., Bossuyt, X., Humblet-Baron, S., Liston, A., Wouters, C., 2021. Phenotypic analysis of Pyrin-Associated Autoinflammation with Neutrophilic Dermatitis patients during treatment. *Rheumatol. Oxf. Engl.* <https://doi.org/10.1093/rheumatology/keab221>
- Vance, R.E., 2015. The NAIP/NLRC4 inflammasomes. *Curr. Opin. Immunol.* 32, 84–89. <https://doi.org/10.1016/j.coi.2015.01.010>
- von Eichel-Streiber, C., Harperath, U., Bosse, D., Hadding, U., 1987. Purification of two high molecular weight toxins of *Clostridium difficile* which are antigenically related. *Microb. Pathog.* 2, 307–318.
- Waite, A.L., Schaner, P., Richards, N., Balci-Peynircioglu, B., Masters, S.L., Brydges, S.D., Fox, M., Hong, A., Yilmaz, E., Kastner, D.L., Reinherz, E.L., Gumucio, D.L., 2009. Pyrin Modulates the Intracellular Distribution of PSTPIP1. *PLoS ONE* 4. <https://doi.org/10.1371/journal.pone.0006147>
- Wang, D., Li, Z., Messing, E.M., Wu, G., 2005. The SPRY Domain-containing SOCS Box Protein 1 (SSB-1) Interacts with MET and Enhances the Hepatocyte Growth Factor-induced Erk-Elk-1-Serum Response Element Pathway. *J. Biol. Chem.* 280, 16393–16401. <https://doi.org/10.1074/jbc.M413897200>
- Wei, X., Xie, F., Zhou, X., Wu, Y., Yan, H., Liu, T., Huang, J., Wang, F., Zhou, F., Zhang, L., 2022. Role of pyroptosis in inflammation and cancer. *Cell. Mol. Immunol.* <https://doi.org/10.1038/s41423-022-00905-x>
- Weinert, C., Grütter, C., Roschitzki-Voser, H., Mittl, P.R.E., Grütter, M.G., 2009. The Crystal Structure of Human Pyrin B30.2 Domain: Implications for Mutations Associated with Familial Mediterranean Fever. *J. Mol. Biol.* 394, 226–236. <https://doi.org/10.1016/j.jmb.2009.08.059>
- Weinert, C., Morger, D., Djekic, A., Grütter, M.G., Mittl, P.R.E., 2015. Crystal structure of TRIM20 C-terminal coiled-coil/B30.2 fragment: implications for the recognition of higher order oligomers. *Sci. Rep.* 5, 10819. <https://doi.org/10.1038/srep10819>
- Wise, C.A., Gillum, J.D., Seidman, C.E., Lindor, N.M., Veile, R., Bashiardes, S., Lovett, M., 2002. Mutations in CD2BP1 disrupt binding to PTP PEST and are responsible for PAPA syndrome, an autoinflammatory disorder. *Hum. Mol. Genet.* 11, 961–969. <https://doi.org/10.1093/hmg/11.8.961>
- Xie, Y., Xie, J., Meijer, A.H., Schaaf, M.J.M., 2021. Glucocorticoid-Induced Exacerbation of Mycobacterial Infection Is Associated With a Reduced Phagocytic Capacity of Macrophages. *Front. Immunol.* 12, 618569. <https://doi.org/10.3389/fimmu.2021.618569>
- Xu, H., Shi, J., Gao, H., Liu, Y., Yang, Z., Shao, F., Dong, N., 2019. The N-end rule ubiquitin ligase UBR2 mediates NLRP1B inflammasome activation by anthrax lethal toxin. *EMBO J.* 38, e101996. <https://doi.org/10.15252/embj.2019101996>
- Xu, H., Yang, J., Gao, W., Li, L., Li, P., Zhang, L., Gong, Y.-N., Peng, X., Xi, J.J., Chen, S., Wang, F., Shao, F., 2014. Innate immune sensing of bacterial modifications of Rho GTPases by the Pyrin inflammasome. *Nature* 513, 237–241. <https://doi.org/10.1038/nature13449>
- Yamauchi, S., Yamamoto, K., Ogawa, K., 2022. Testicular Macrophages Produce Progesterone De Novo Promoted by cAMP and Inhibited by M1 Polarization Inducers. *Biomedicines* 10, 487. <https://doi.org/10.3390/biomedicines10020487>




- Yang, Y., Li, L., Yuan, L., Zhou, X., Duan, J., Xiao, H., Cai, N., Han, S., Ma, X., Liu, Weidong, Chen, C.-C., Wang, L., Li, X., Chen, Jiahuan, Kang, N., Chen, Jing, Shen, Z., Malwal, S.R., Liu, Wanli, Shi, Y., Oldfield, E., Guo, R.-T., Zhang, Y., 2019. A Structural Change in Butyrophilin upon Phosphoantigen Binding Underlies Phosphoantigen-Mediated V γ 9V δ 2 T Cell Activation. *Immunity* 50, 1043-1053.e5. <https://doi.org/10.1016/j.immuni.2019.02.016>
- Yilmaz, C., Karali, K., Fodelianaki, G., Gravanis, A., Chavakis, T., Charalampopoulos, I., Alexaki, V.I., 2019. Neurosteroids as regulators of neuroinflammation. *Front. Neuroendocrinol.* 55, 100788. <https://doi.org/10.1016/j.yfrne.2019.100788>
- Yu, J.-W., Farias, A., Hwang, I., Fernandes-Alnemri, T., Alnemri, E.S., 2013. Ribotoxic Stress through p38 Mitogen-activated Protein Kinase Activates in Vitro the Human Pyrin Inflammasome*. *J. Biol. Chem.* 288, 11378–11383. <https://doi.org/10.1074/jbc.M112.448795>
- Yu, J.-W., Fernandes-Alnemri, T., Datta, P., Wu, J., Juliana, C., Solorzano, L., McCormick, M., Zhang, Z., Alnemri, E.S., 2007. Pyrin activates the ASC pyroptosome in response to engagement by autoinflammatory PSTPIP1 mutants. *Mol. Cell* 28, 214–227. <https://doi.org/10.1016/j.molcel.2007.08.029>
- Yu, P., Zhang, X., Liu, N., Tang, L., Peng, C., Chen, X., 2021. Pyroptosis: mechanisms and diseases. *Signal Transduct. Target. Ther.* 6, 128. <https://doi.org/10.1038/s41392-021-00507-5>
- Zanchetta, M.E., Meroni, G., 2019. Emerging Roles of the TRIM E3 Ubiquitin Ligases MID1 and MID2 in Cytokinesis. *Front. Physiol.* 10, 274. <https://doi.org/10.3389/fphys.2019.00274>
- Zhou, Y., Tong, Z., Jiang, S., Zheng, W., Zhao, J., Zhou, X., 2020. The Roles of Endoplasmic Reticulum in NLRP3 Inflammasome Activation. *Cells* 9, E1219. <https://doi.org/10.3390/cells9051219>
- Zurek, B., Schoultz, I., Neerincx, A., Napolitano, L.M., Birkner, K., Bennek, E., Sellge, G., Lerm, M., Meroni, G., Söderholm, J.D., Kufer, T.A., 2012. TRIM27 Negatively Regulates NOD2 by Ubiquitination and Proteasomal Degradation. *PLoS ONE* 7. <https://doi.org/10.1371/journal.pone.0041255>

ANNEX I

The following section contains a scientific article published in EMBO Molecular Medicine in November 2019. Here, we reveal that pyrin dephosphorylation is sufficient to activate pyrin inflammasome in FMF, but not in cells expressing WT pyrin. Thus, we demonstrate that a second control mechanism downstream of pyrin (de)phosphorylation exists in healthy donors.

SOURCE
DATATRANSPARENT
PROCESSOPEN
ACCESS

Pyrin dephosphorylation is sufficient to trigger inflammasome activation in familial Mediterranean fever patients

Flora Magnotti¹, Lucie Lefevre^{1,2}, Sarah Benezech^{1,2,‡} , Tiphaine Malsot¹, Louis Waeckel^{1,2}, Amandine Martin¹, Sébastien Kerever³, Daria Chirita¹, Marine Desjonqueres^{2,4}, Agnès Duquesne^{2,4}, Mathieu Gerfaud-Valentin^{2,5}, Audrey Laurent^{2,4}, Pascal Sève^{2,5}, Michel-Robert Popoff⁶, Thierry Walzer¹, Alexandre Belot^{1,2,4}, Yvan Jamilloux^{1,2,5,*}  & Thomas Henry^{1,**} 

Abstract

Familial Mediterranean fever (FMF) is the most frequent hereditary systemic autoinflammatory syndrome. FMF is usually caused by biallelic mutations in the *MEFV* gene, encoding Pyrin. Conclusive genetic evidence lacks for about 30% of patients diagnosed with clinical FMF. Pyrin is an inflammasome sensor maintained inactive by two kinases (PKN1/2). The consequences of *MEFV* mutations on inflammasome activation are still poorly understood. Here, we demonstrate that PKC superfamily inhibitors trigger inflammasome activation in monocytes from FMF patients while they trigger a delayed apoptosis in monocytes from healthy donors. The expression of the pathogenic p.M694V *MEFV* allele is necessary and sufficient for PKC inhibitors (or mutations precluding Pyrin phosphorylation) to trigger caspase-1- and gasdermin D-mediated pyroptosis. In line with colchicine efficacy in patients, colchicine fully blocks this response in FMF patients' monocytes. These results indicate that Pyrin inflammasome activation is solely controlled by Pyrin (de)phosphorylation in FMF patients while a second control mechanism restricts its activation in healthy donors/non-FMF patients. This study paves the way toward a functional characterization of *MEFV* variants and a functional test to diagnose FMF.

Keywords autoinflammation; caspase-1; colchicine; diagnosis; pyroptosis

Subject Categories Genetics, Gene Therapy & Genetic Disease; Immunology

DOI 10.15252/emmm.201910547 | Received 6 March 2019 | Revised 4 September 2019 | Accepted 13 September 2019 | Published online 7 October 2019

EMBO Mol Med (2019) 11: e10547

Introduction

Familial Mediterranean fever (FMF) is the most frequent hereditary systemic autoinflammatory disorder characterized by recurrent episodes of fever, serositis, and abdominal pain (Sonmez *et al*, 2016). Its feared complication is secondary AA amyloidosis, which can lead to end-stage kidney disease. Colchicine, an inhibitor of microtubule polymerization, decreases chronic inflammation and represents the cornerstone of FMF treatment (Goldfinger, 1972). Daily and lifelong administration of colchicine is currently recommended for FMF patients.

Familial Mediterranean fever diagnosis relies first on clinical criteria. Due to the absence of pathognomonic clinical signs and to heterogeneity in clinical presentations (Mor *et al*, 2003; Padeh *et al*, 2010), FMF diagnosis can be challenging (Giancane *et al*, 2015). Familial Mediterranean fever is associated with mutations in the *MEFV* gene. Mendelian transmission of the disease occurs mostly in an autosomal recessive mode. As of today, genetic screening confirms the FMF diagnosis upon identification of biallelic mutations in clearly pathogenic *MEFV* variants (Shinar *et al*, 2012). Nine sequence variants of *MEFV* are considered clearly pathogenic (Shinar *et al*, 2012). Yet, there are 365 *MEFV* variants listed in the Infevers database (Sarrauste de Menthiere *et al*, 2003), most of them of uncertain significance, which can result in misdiagnosis or diagnosis delay (Lidar *et al*, 2005). Furthermore, a substantial proportion of clinically diagnosed FMF patients (up to 30%) presents only a single *MEFV* pathogenic variant (Dode *et al*, 2000; Lachmann *et al*, 2006; Jeru *et al*, 2013). Finally, no *MEFV* variant is found in 5–14% of clinically diagnosed

1 CIRI, Centre International de Recherche en Infectiologie, Inserm, U1111, Université Claude Bernard Lyon 1, CNRS, UMR5308, École Normale Supérieure de Lyon, Univ. Lyon, Lyon, France

2 Hospices Civils de Lyon, Lyon, France

3 Department of Anesthesiology and Critical Care, St Louis-Lariboisière University Hospital, AP-HP, ECSTRA Team, Epidemiology and Biostatistics, Sorbonne Paris Cité Research Centre, UMR 1153, Inserm, University Denis Diderot-Paris VII, Paris, France

4 Service de Néphrologie, Rhumatologie, Dermatologie pédiatriques, HFME, Bron, France

5 Service de Médecine Interne, Hôpital de la Croix-Rousse, Lyon, France

6 Bacterial Toxins, Institut Pasteur, Paris, France

*Corresponding author. Tel: +33 4 37 28 23 72; E-mail: yvan.jamilloux@inserm.fr

**Corresponding author. Tel: +33 4 37 28 23 72; E-mail: thomas.henry@inserm.fr

†These authors contributed equally to this work as senior authors

‡Present address: Institut d'Hématologie et Oncologie Pédiatrique, Lyon, France

FMF patients (Lachmann *et al*, 2006; Toplak *et al*, 2012). Due to all these situations, genetic testing has a 70–80% positive predictive value (Soriano & Manna, 2012) and the median delay between disease onset and diagnosis remains long (1.4 years for patients born in the 21st century; Toplak *et al*, 2012). Furthermore, the generalization of next-generation sequencing leads to the identification of novel rare variants of unknown impact. Functional assays robustly discriminating pathogenic *MEFV* variants from non-pathogenic *MEFV* polymorphisms are needed to sustain diagnosis and the development of personalized medicine (Van Gorp *et al*, 2016).

MEFV encodes Pylrin, an inflammasome sensor detecting Rho A GTPase inhibition (Xu *et al*, 2014). Inactivation of Rho A by various bacterial toxins triggers activation of the Pylrin inflammasome, i.e., oligomerization of the inflammasome adaptor ASC, caspase-1 activation, secretion of the pro-inflammatory cytokines IL-1 β and IL-18, and an inflammatory cell death termed pyroptosis (Cookson & Brennan, 2001; Martinon *et al*, 2002; Xu *et al*, 2014). At steady state, Pylrin is maintained inactive by phosphorylation of its serine residues S208 and S242. Two kinases (PKN1/2) from the PKC superfamily phosphorylate Pylrin, leading to its sequestration by 14-3-3 chaperone proteins (Gao *et al*, 2016; Masters *et al*, 2016; Park *et al*, 2016; Van Gorp *et al*, 2016). Rho A inhibition leads to dephosphorylation of Pylrin, its release from the 14-3-3 proteins and the assembly/activation of the Pylrin inflammasome. Of note, in healthy individuals, the transition from 14-3-3-free Pylrin to ASC oligomerization and Pylrin inflammasome activation requires microtubule dynamics (Gao *et al*, 2016). Colchicine specifically blocks the Pylrin inflammasome downstream of Pylrin release from the 14-3-3 proteins and upstream of ASC oligomerization (Gao *et al*, 2016). In FMF patients, the microtubule-dependent mechanism might be deficient since a recent report indicated that colchicine is inefficient to block Pylrin inflammasome activation in PBMCs from FMF patients (Van Gorp *et al*, 2016). This *in vitro* result, at odds with the clinical efficacy of colchicine in FMF patients, is still poorly understood. A two-step activation model is emerging with (i) dephosphorylation of Pylrin following inhibition of PKN1/2 and (ii) Pylrin inflammasome maturation involving a colchicine-targetable microtubule dynamics event (Gao *et al*, 2016). The link between the two steps remains unclear. Particularly, it is unknown whether dephosphorylation of Pylrin automatically leads to Pylrin inflammasome activation in cells with intact microtubule dynamics. Finally, the impact of *MEFV* mutations on each step is controversial (Gao *et al*, 2016; Masters *et al*, 2016; Park *et al*, 2016; Van Gorp *et al*, 2016).

In this work, we demonstrate that PKC superfamily inhibitors trigger inflammasome activation, IL-1 β secretion, and pyroptosis in monocytes from FMF patients while they fail to do so in monocytes from healthy donors (HD) in which they trigger a delayed apoptosis. PKC superfamily inhibitor-mediated inflammasome activation was blocked by colchicine in FMF patients' monocytes in line with the efficacy of this drug in patients. The mechanism of the differential control of the Pylrin inflammasome was pinpointed to specific *MEFV* mutations in human monocyte cell lines expressing either one of three common clearly pathogenic *MEFV* variants, p.M694V, p.M694I, or p.M680I. Importantly, the cytotoxic effect of PKC superfamily inhibitors on the p.M694V allele-expressing cells could be recapitulated genetically by mutating the Pylrin Serine 242 or S208 residues. These results suggest that, while Pylrin inflammasome is controlled by two independent mechanisms in healthy donors, in FMF patients, the Pylrin

inflammasome lacks one safeguard mechanism and is only regulated by Pylrin phosphorylation. Finally, our results indicate that these differences could be exploited to develop a functional diagnostic test.

Results

PKC inhibitors trigger IL-1 β release in monocytes from FMF patients

The current model for Pylrin inflammasome activation indicates that activation results from the dephosphorylation of Pylrin following the lack of sustained activation of PKN1/2, two kinases from the PKC superfamily (Park *et al*, 2016). To explore the mechanisms underlying deregulation of the Pylrin inflammasome in FMF patients, we decided to assess the efficacy of staurosporine (a potent PKC superfamily inhibitor targeting PKN1/2; Davis *et al*, 2011) to trigger IL-1 β release in primary monocytes from HD or FMF patients. We observed no to very low IL-1 β release from monocytes isolated from HD in response to LPS + staurosporine (Fig 1A). In our experimental conditions, monocytes from 31 out of the 33 HD (94%) released < 50 pg/ml of IL-1 β (Fig 1A). In sharp contrast, monocytes from FMF patients released moderate to high levels of IL-1 β , leading to an average level 17-fold higher (422 pg/ml, $P < 0.0001$) than the average level in the supernatant of HD monocytes (25 pg/ml) (Fig 1A and Appendix Fig S1A for a detailed version including patients' genotype). These differences were conserved over several staurosporine concentrations and at several times post-treatment (Appendix Fig S2A and B). This result indicates strongly differing inflammasome responses to PKC superfamily inhibition between FMF patients and HD. To confirm this result, we used UCN-01, a hydroxylated derivative of staurosporine, which displays a better selectivity for PKC superfamily kinases (Tamaoki, 1991). Similar findings were observed (Fig 1B and Appendix Fig S1B) with monocytes from FMF patients releasing > 10-fold higher IL-1 β levels than HD monocytes did. The same trend (Appendix Fig S2C and D) was observed using the bisindolylmaleimide RO 31-8220, another PKC superfamily inhibitor of different chemical structure (Davis *et al*, 1992). IL-1 β levels following treatment with UCN-01 and staurosporine were significantly correlated in the different patients (Appendix Fig S2E). As seen with staurosporine, the difference in IL-1 β response between monocytes from HD and FMF patients was conserved over a large range of concentrations of UCN-01 (Appendix Fig S2F). The hyper-responsiveness of FMF monocytes to PKC superfamily inhibitors thus differs from their hyper-responsiveness to *Clostridioides difficile* toxin TcdB, which was observed only at low doses of TcdB (Jamilloux *et al*, 2018).

IL-1 β levels were substantially decreased upon addition, 30 min before UCN-01, of the caspase-1 inhibitors VX-765 or YVAD-FMK (Appendix Fig S2G). Neither the caspase-3 inhibitor (DEVD-FMK) nor the caspase-8 inhibitor (IETD-FMK) demonstrated a robust inhibition of IL-1 β release. This result suggests that UCN-01 triggers inflammasome activation in FMF patient monocytes. As previously described (Van Gorp *et al*, 2016), we did not observe any difference in IL-1 β release in response to engagement of the NLRP3 inflammasome by LPS + ATP (Appendix Fig S2H) or of the NLRC4 inflammasome (Jamilloux *et al*, 2018). Furthermore, LPS + staurosporine treatment did not lead to differential TNF secretion between monocytes from HD and FMF patients (Fig 1C), indicating that the

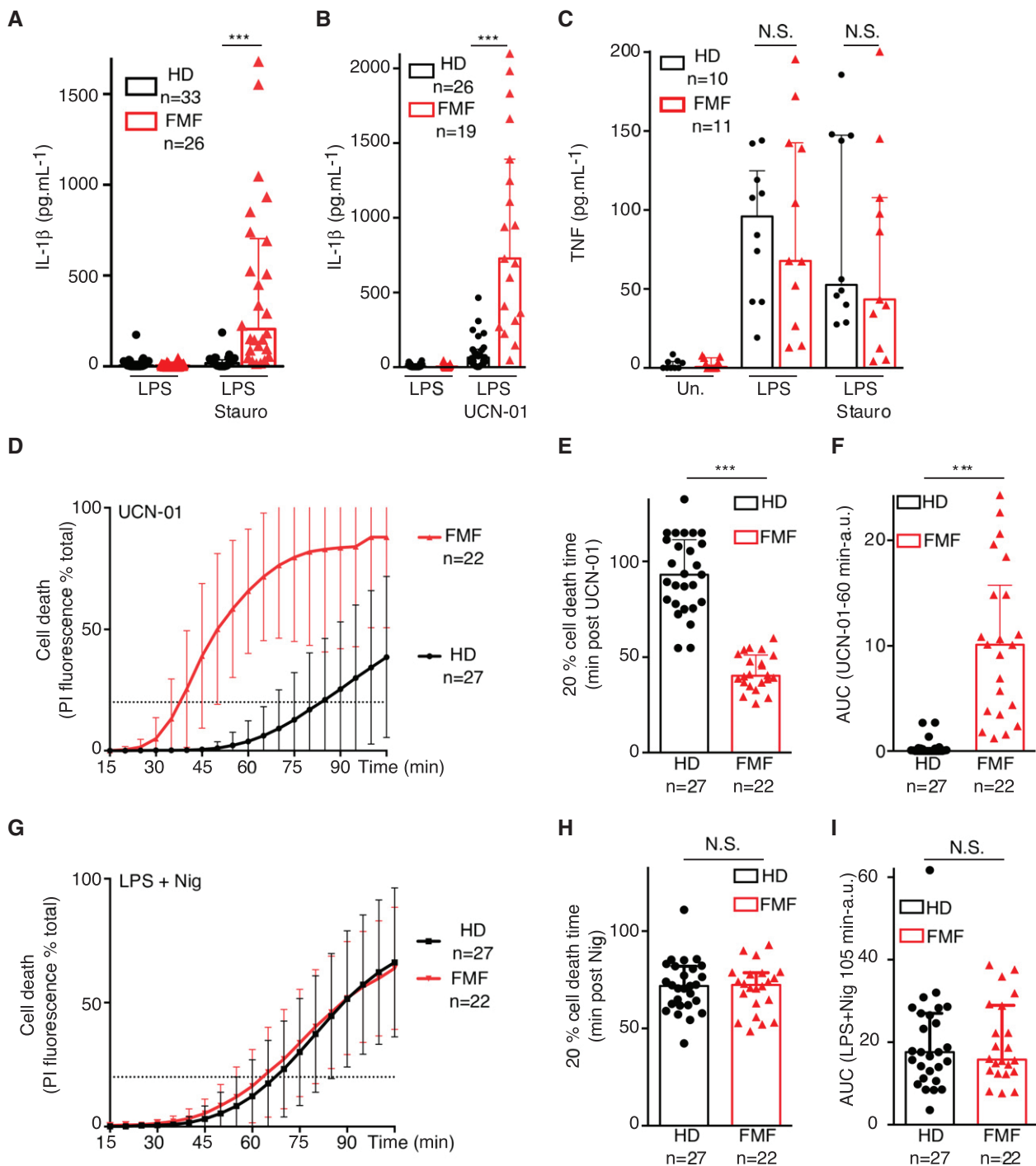


Figure 1. PKC inhibitors specifically trigger IL-1 β release and a fast cell death in monocytes from FMF patients.

A–I Monocytes from healthy donors (HD) or FMF patients were either primed with LPS (A–C, G–I) or not (D–F) and treated with (A, C) 1.25 μ M staurosporine (Stauro), (B, D–F) 12.5 μ M UCN-01, or (G–I) 5 μ M nigericin (Nig). (A, B) IL-1 β and (C) TNF level were quantified by ELISA at 90 min post stimulation. (D, G) Cell death was monitored in real time by measuring propidium iodide influx/fluorescence every 5 min. (E, H) The time required to reach 20% cell death and (F, I) the area under the curve (AUC) were computed for each HD or FMF patients.

Data information: (A–C, E–F, H, I) Each dot represents the mean value from three biological replicates for one HD or patient. The bar represents the median \pm interquartile range. a.u.: arbitrary units. (D, G) Each point of the curve corresponds to the average cell death values from the indicated number of HD or FMF patients (for each individual, the value is the mean of a biological triplicate). The dotted line indicates the 20% cell death value. (A, B, F) *** P < 0.0001 by Wilcoxon rank-sum test. (C) One-way ANOVA with Sidak's multiple comparison tests was performed. LPS: N.S. Not significant P = 0.99; LPS + Staurosporine N.S.: P = 0.77. (H) Unpaired t -tests were performed, and two-tailed P -values are shown. (E) *** P < 0.0001, (H) N.S.: P = 0.79. (I) N.S. P = 0.9 by Wilcoxon rank-sum test. Source data are available online for this figure.

differing response to PKC inhibitors between HD and FMF patients is specific to inflammasome activation. These results suggest that dephosphorylation of Pypin is sufficient to trigger inflammasome activation in monocytes from FMF patients while a PKC-independent mechanism limits IL-1 β release in HD monocytes.

PKC inhibitors trigger fast cell death in monocytes from FMF patients

Inflammasome activation is often associated with a fast cell death process termed pyroptosis. We thus investigated whether PKC inhibitors, in the absence of LPS priming, trigger cell death in monocytes from HD and FMF patients. Indeed, UCN-01 triggered a very rapid influx of propidium iodide in monocytes from FMF patients while it was much delayed in monocytes from HD (Fig 1D). These kinetics were determined to be significantly different by quantifying the time post-UCN-01 addition leading to 20% cell death (dotted line in Fig 1D and E, $P < 0.0001$) and the area under the curve (AUC, Fig 1F, $P < 0.0001$). The difference in cell death was specific to PKC inhibitors since NLRP3 inflammasome activation by LPS + nigericin (Mariathasan *et al*, 2006) triggered propidium iodide influx with similar kinetics in monocytes from HD and FMF patients (Fig 1G–I and Appendix Fig S2I). Importantly, the UCN-01-mediated fast cell death was observed in the absence of LPS treatment, indicating that the Pypin inflammasome does not require TLR-mediated priming, as previously demonstrated following *C. difficile* toxin treatment (Van Gorp *et al*, 2016; Jamilloux *et al*, 2018).

PKC inhibitors differentially trigger pyroptosis or apoptosis in monocytes from FMF patients and HD

The kinetics of monocytes death and its association with IL-1 β release suggest that PKC inhibitors trigger pyroptosis in monocytes from FMF patients. To strengthen this finding, we directly evaluated the ability of the inflammasome adaptor ASC to form specks as a readout of inflammasome complex formation. At 40 min post-UCN-01 treatment, monocytes were fixed and immuno-stained for ASC. More than 35% of monocytes from FMF patients displayed ASC

specks while UCN-01 treatment did not substantially increase the frequency of speck-containing cells in HD monocytes (Fig 2A and B and control experiment in Appendix Fig S3). This result indicates that the Pypin inflammasome activation is controlled by a phosphorylation-independent mechanism upstream of ASC oligomerization in monocytes from HD and that this control mechanism is defective in FMF patients.

The UCN-01-mediated induction of inflammasome activation in monocytes from FMF patients was further confirmed by quantifying cells containing active caspase-1, using the fluorescent inhibitor probe FAM-YVAD-FMK, referred to as FLICA-Casp1. As quantified by flow cytometry, 33% of monocytes from FMF patients stained positive for FLICA-Casp1 at 40 min post-UCN-01 addition, while only 6% of monocytes from HD did, a proportion similar to the one observed in the untreated samples (Fig 2C).

These results establish that PKC inhibitors specifically trigger pyroptosis in monocytes from FMF patients. Yet, PKC inhibitors also lead to a late cell death in HD monocytes (Fig 1D). Based on the well-known activity of PKC inhibitors to trigger apoptosis (Nie *et al*, 2014), and on the absence of signs of inflammasome activation (Figs 1B and 2A–C), we hypothesized that UCN-01 might trigger apoptosis in HD monocytes. We thus monitored phosphatidyl serine externalization in propidium iodide-negative cells as an early marker of apoptosis following UCN-01 (Fig 2D and E) or staurosporine (Appendix Fig S4) treatment. At 90 min post-treatment with PKC superfamily inhibitors, a large number of HD monocytes stained positive for Annexin-V and were negative for propidium iodide, strongly suggesting that HD monocytes died by apoptosis. In contrast, we did not detect any Annexin-V-positive/propidium iodide (PI)-negative cells induced by UCN-01 in monocytes from FMF patients, which is consistent with FMF patients' monocytes dying by pyroptosis upon PKC inhibitor exposure. As expected, in response to LPS + nigericin, we did not detect a substantial proportion of Annexin-V⁺/PI⁻ cells, neither in monocytes from HD nor from FMF patients (Fig 2E).

Altogether, these results indicate that PKC inhibitors trigger inflammasome activation, IL-1 β release, and pyroptosis in monocytes from FMF patients, while inflammasome is not activated in monocytes from HD.

Figure 2. The PKC inhibitor, UCN-01, triggers pyroptosis or apoptosis in monocytes from FMF patients and HD, respectively.

- A, B Monocytes from HD or FMF patients were treated with 12.5 μ M UCN-01 for 40 min or primed with LPS (3 h) and treated with 5 μ M nigericin (Nig) for 90 min. (A) Cells were immuno-stained for ASC. ASC specks are indicated by red arrowheads. Representative confocal microscopy images from one HD (top panels) and one FMF patient (bottom panels) are shown. Scale bars: 10 μ m and 2.5 μ m in the main figures and onsets, respectively. (B) Quantification of ASC specks in HD and FMF patients' monocytes by immunofluorescence.
- C The frequency of cells positive for active caspase-1 was quantified by flow cytometry, using FLICA-Caspase-1 in HD and FMF patients.
- D, E Cell death was assessed at 90 min post-UCN-01 or post-LPS + nigericin treatment by determining the percentage of Annexin-V⁺/PI⁻ cells and of PI⁺ cells among dead cells (Annexin-V⁺ and/or PI⁺ cells) using flow cytometry. (D) Representative FACS plots from one healthy donor (HD) and one FMF patient are shown. Percentage are indicated for the two right gates. (E) Cell death modality was assessed by determining the percentage of treatment-induced Annexin-V⁺/PI⁻ cells and of PI⁺ cells among dead cells, using flow cytometry.

Data information: (B, C, E) Kruskal–Wallis with Dunn's multiple comparison tests were performed to compare HD and FMF responses. Adjusted P -values are detailed below. (B) Each dot (HD)/symbol (FMF) represents the percentage of cells containing an ASC speck for one individual. Symbol to FMF patient #: square #2 (M694I/M694I), round #26 (V726A/V726A), triangle #13 (M694V/R761H), diamond #18 (M694I/M694I). UCN-01 $^{**}P = 0.0095$; LPS + nigericin N.S. $P = 0.75$. (C) Each dot (HD)/symbol (FMF) represents the percentage of cells stained with FLICA-Casp1 for one individual, the bar represents the median (\pm interquartile range). Symbol to FMF patient #: round #26 (V726A/V726A), triangle #13 (M694V/R761H), triangle pointing down #23 (M694V/M694V), hexagon #24 (M694V/M694V), star #10 (M694V/M694V). Untreated: N.S. $P = 1$; UCN-01: $^{***}P = 0.0069$; LPS + nigericin: N.S. $P = 1$. (E) Each dot (HD)/triangle (FMF) represents the value for one individual, and the bar represents the median (\pm interquartile range). UCN-01: $^{***}P < 0.0001$; LPS + nigericin N.S. $P = 0.51$. Source data are available online for this figure.

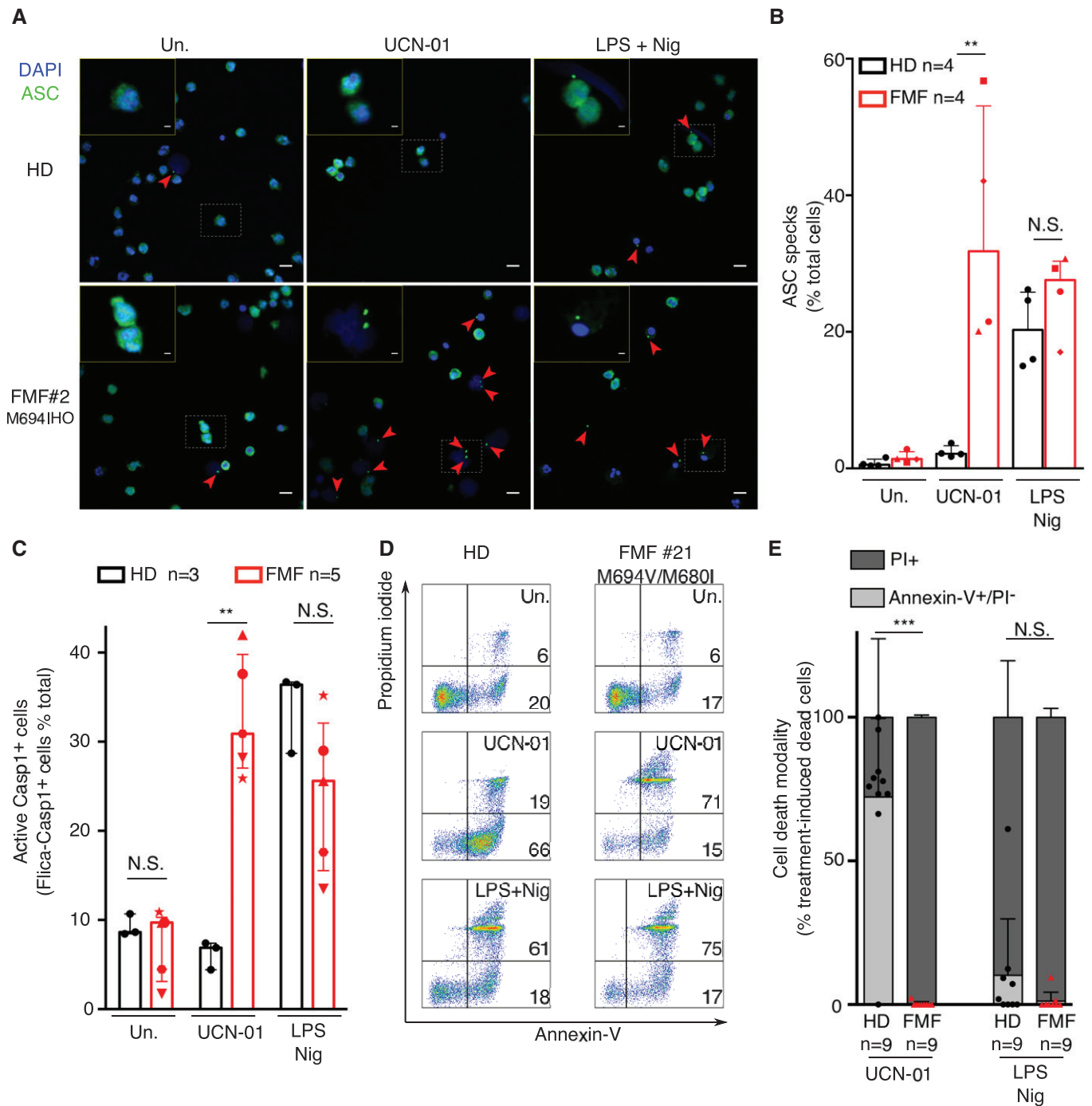


Figure 2.

Inflammasome activation in FMF patients upon PKC inhibition is blocked by colchicine

The link between Pyrin and NLRP3 inflammasomes in FMF patients is still unclear (Chae *et al*, 2011; Omenetti *et al*, 2014). We thus tested whether NLRP3 could contribute to UCN-01-mediated inflammasome activation. As expected, MCC950-mediated inhibition of the NLRP3 inflammasome (Coll *et al*, 2015) abolished IL-1 β release upon LPS + nigericin treatment (Fig 3A). MCC950 treatment

did not affect IL-1 β release by FMF patients' monocytes exposed to TcdB in line with previous results obtained in PBMCs from HD exposed to TcdA (Van Gorp *et al*, 2016). In addition, MCC950 treatment did not affect IL-1 β release upon UCN-01 treatment, indicating that this response is independent of NLRP3 (Fig 3A and Appendix Fig S5).

Colchicine specifically blocks the Pyrin inflammasome in murine macrophages and in PBMCs from healthy donors (Gao *et al*, 2016; Park *et al*, 2016; Van Gorp *et al*, 2016). Despite its long

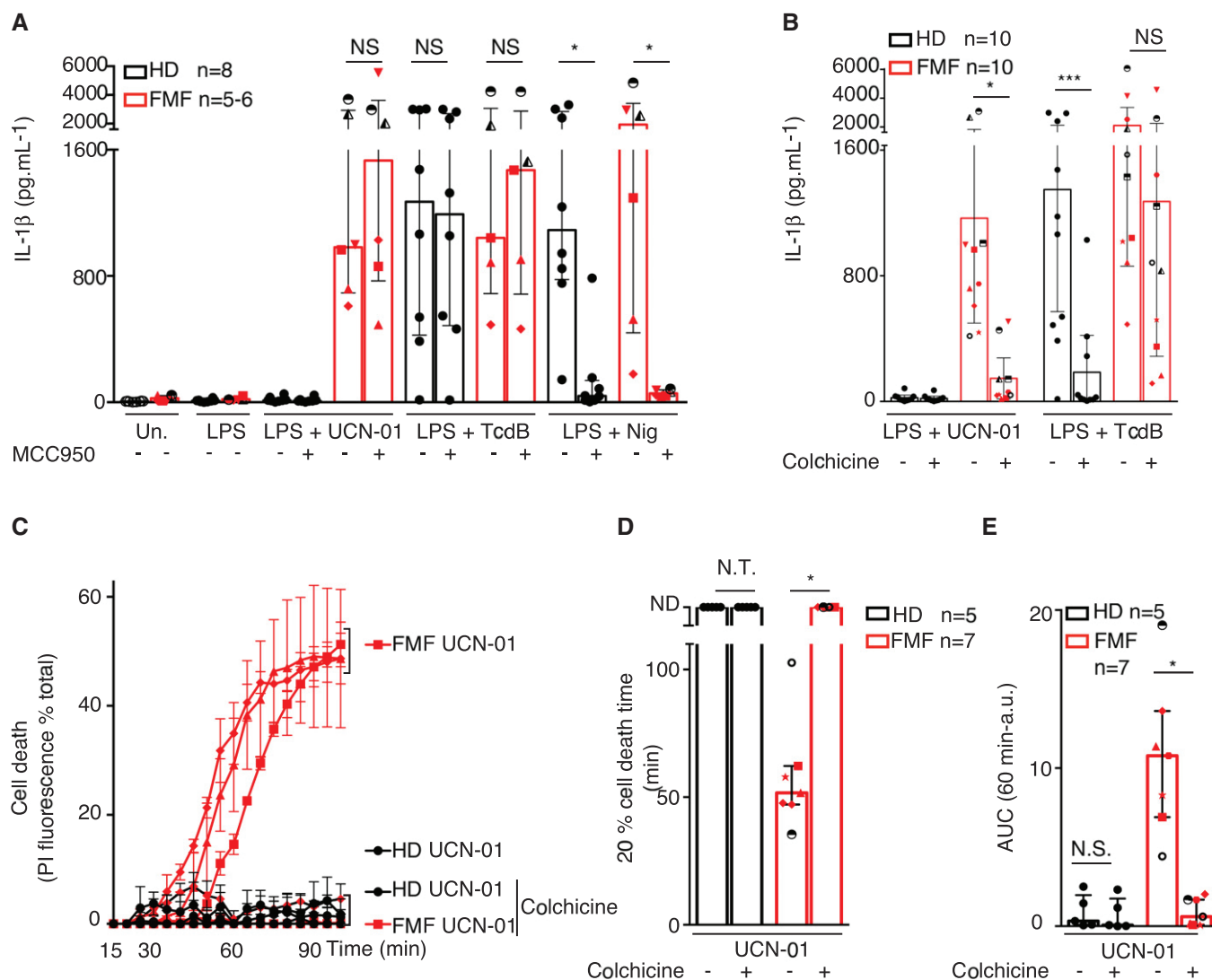


Figure 3. Colchicine blocks inflammasome activation in monocytes from FMF patients following PKC inhibitor treatment.

Monocytes from healthy donors (HD) or FMF patients were primed for 3 h as indicated with LPS (A, B) or not (C–E). When indicated, (A) the NLRP3 inhibitor MCC950 (10 μ M) or (B–E) colchicine (1 μ M) were added 30 min before addition of 12.5 μ M UCN-01, 125 ng/ml TcdB, or 5 μ M nigericin.

A, B IL-1 β level was quantified by ELISA at 90 min post-stimulation.

C–E Cell death was monitored in real time by measuring propidium iodide influx/fluorescence every 5 min.

Data information: (A, B, D, E) Each symbol represents the mean value from three biological replicates for one HD or patient. The bar represents the median value (\pm interquartile range). (C) Each point of the curve corresponds to the average cell death values from three biological replicates of monocytes from HD or FMF patients (diamond #32 (p.M694V/p.M694V); triangle #33 (p.M694V/p.M694V); square #1 (p.M694I/p.V726A)). The curves are displayed for each patient/HD. The time required to reach 20% cell death (D) and the area under the curve (AUC) (E) were computed for each HD or FMF patients. Each symbol represents the mean value from one HD or patient. The bar represents the median (\pm interquartile range). (D) ND indicates that the average cell death was below 20% at the end of the kinetics. (A) Wilcoxon matched-pairs signed rank test was used to compare untreated and MCC950-treated groups since all the groups did not contain an identical number of individuals. FMF, UCN-01 NS: $P = 0.84$, HD TcdB NS: $P = 0.81$, FMF TcdB NS: $P = 0.84$, HD Nig * $P = 0.039$, FMF Nig * $P = 0.031$. Individual genotypes are presented in Appendix Figure S5A. (B) Friedman paired test with Dunn's correction for multiple comparisons was applied to compare untreated and colchicine-treated groups. Adjusted P -values are as follow: FMF UCN-01 * $P = 0.036$; HD TcdB *** $P = 0.0006$; and FMF TcdB NS $P = 0.28$. (D, E) Wilcoxon matched-pairs signed rank test was used to compare untreated and colchicine-treated groups. Adjusted P -values are as follow: (D) N.T.: not tested. FMF * $P = 0.016$; (E) HD N.S. $P = 0.62$, FMF * $P = 0.016$.

Source data are available online for this figure.

demonstrated clinical efficacy in FMF patients, colchicine was recently shown to be inefficient in blocking IL-1 β release in PBMCs from FMF patients exposed to TcdA (Van Gorp *et al*, 2016). Although we did see a partial (40%) inhibition of TcdB-mediated IL-1 β response in monocytes from FMF patients, with a large

inter-patient variability, this inhibition was consistent and almost total (86%) in HD monocytes, thus confirming that toxin-mediated Pyrin inflammasome activation is less sensitive to colchicine inhibition in FMF patients than in HD monocytes (Fig 3B and Appendix Fig S5). In contrast to the lack of (Van Gorp *et al*, 2016)/

partial (our result) inhibition observed upon TcdA/B-mediated Pyrin inflammasome activation, colchicine strongly reduced (86%) IL-1 β release and fully abolished pyroptosis upon PKC inhibition (Fig 3B–E). Similarly, and in line with previous work using TcdA to stimulate the Pyrin inflammasome (Van Gorp *et al*, 2016), nocodazole abolished UCN-01-mediated IL-1 β release, and cell death (Fig EV1A and B). No substantial reduction was observed when using Taxol (Fig EV1A and B). Colchicine decreased UCN-01-mediated IL-1 β release from FMF monocytes (Fig EV1C) and TcdB-mediated IL-1 β release from HD monocytes (Fig EV1D) with a similar dose response. This result suggests that *C. difficile* toxins TcdA/B and PKC superfamily inhibitors differentially affect Pyrin inflammasome activation in FMF patients' monocytes. Based on the efficacy of colchicine in FMF patients, it is tempting to speculate that PKC inhibitors better mimic the endogenous stimuli triggering Pyrin inflammasome during inflammatory flares.

Expression of p.M694V MEFV is necessary and sufficient to trigger caspase-1- and gasdermin D-dependent responses to PKC inhibitors

To demonstrate that the difference in PKC inhibitor responses in monocytes from FMF patients and HD was specifically due to *MEFV* mutation, we generated U937 cells expressing either WT *MEFV* or p.M694V *MEFV*. U937 were invalidated for the *MEFV* gene (Lagrange *et al*, 2018) to avoid any possible confounding factor and complemented with either 3xFLAG-WT (Lagrange *et al*, 2018) or 3xFLAG-p.M694V *MEFV* under the control of a doxycycline-inducible promoter (Fig EV2A). The Pyrin immunoblot pattern obtained upon doxycycline addition was similar to the pattern previously described in PBMCs (Chae *et al*, 2008) with a major cleavage band around 50 kDa (Fig EV2B). Importantly, doxycycline-mediated expression of p.M694V *MEFV* rendered U937 sensitive to UCN-01, as determined by their fast cell death, while the expression of WT *MEFV* did not (Fig 4A). As expected, in the absence of doxycycline, no cell death was observed during 3 h post-UCN-01 treatment. These results demonstrate that the expression of p.M694V Pyrin is necessary and sufficient for the fast cell death response to UCN-01. In contrast, the expression of WT or p.M694V Pyrin did not substantially affect the cell death response following NLRP3 stimulation (Fig 4B). Similar results were obtained with the two clearly pathogenic *MEFV* variants, p.M694I and p.M680I (Fig EV3A–H). In contrast, the expression of the variant of unknown significance, p.P369S, did not trigger such a response suggesting that it is either a non-pathogenic variant (in line with its higher frequency in the human population Fig EV3I), that its pathogenicity is undetectable in our experimental system, or that its pathogenicity is associated with another molecular mechanism.

Importantly, the UCN-01-mediated cell death was strongly delayed when p.M694V Pyrin was expressed in *CASP1* or *GSDMD* knock-out cells, indicating that UCN-01 triggers pyroptosis in p.M694V Pyrin-expressing cells (Fig 4C). Invalidation of *GSDMD* did not impact cell death kinetics as much as *CASP1* invalidation. Such differences in cell death kinetics have been reported in several studies comparing cell death kinetics upon invalidation of individual inflammasome components and likely reflect the existence of alternative/secondary cell death pathways (Pierini *et al*, 2012; Sagulenko *et al*, 2013; Schneider *et al*, 2017).

Doxycycline-mediated expression of p.M694V Pyrin was necessary and sufficient to trigger a robust production of IL-1 β (Fig 4D) and IL-18 (Fig EV2C) in response to PKC inhibitors. Once again, the differences between WT and p.M694V Pyrin-expressing cell lines in terms of IL-1 β secretion were largely specific for PKC inhibitors, although low levels of IL-1 β and IL-18 secretion were observed in p.M694V Pyrin-expressing cells in the absence of PKC inhibitors, possibly due to the use of PMA (Figs 4D and EV2C). UCN-01/p.M694V Pyrin-mediated IL-1 β was dependent on both *CASP1* and *GSDMD* (Fig 4E), indicating that this response is a bona-fide inflammasome response.

UCN-01 is a PKC superfamily inhibitor and thereby not a specific inhibitor of PKN1/2. We were unable to invalidate *PKN2* by CRISPR/Cas9 despite multiple assays and more than 50 other human genes successfully invalidated in the meantime in the same cellular system (Benaoudia *et al*, 2019). *PKN2*-edited clones were recovered but contained small deletions/insertions not affecting the open-reading frames (see one example in Appendix Fig S7), suggesting that *PKN2* is necessary for cell growth/survival of U937 cells. This observation is in line with the embryonic lethality of *Pkn2* knock-out in mice (Danno *et al*, 2017). We thus generated *PKN1*^{KO} clones expressing either WT or p.M694V Pyrin (Fig EV4A) and performed siRNA-mediated knock-down (KD) of *PKN2*. We were unable to detect *PKN2* protein by Western blot analysis likely due to its low expression in U937 cells (Fig EV4B). Yet, two (siRNA #12 and 13) out of three siRNA gave us a strong reduction in *PKN2* transcript levels (Fig EV4C). Doxycycline-mediated induction of p.M694V Pyrin in *PKN1*^{KO} *PKN2*^{KD} cells increased cell death levels (Fig EV4D–E) compared to (i) cells not expressing Pyrin, (ii) cells expressing WT Pyrin, and (iii) p.M694V-expressing cells treated with a non-targeting (NT) siRNA or an inefficient *PKN2*-targeting siRNA (siRNA #14, Fig EV4F). Although the cell death levels were low, these results suggest that *PKN1/2* genetic invalidation mimics UCN-01 treatment and, in the presence of p.M694V Pyrin, is sufficient to trigger cell death.

PKC superfamily inhibitors regulate serine 242 phosphorylation to trigger cell death in p.M694V-expressing cells

To validate that the absence of inflammasome activation in WT Pyrin-expressing U937 cells was not due to a lack of UCN-01 efficacy and a lack of Pyrin dephosphorylation, we assessed the (de)phosphorylation of Pyrin Ser242 by Western blot analysis. The specificity of the antibody (Gao *et al*, 2016) was validated in our experimental system using a cell line expressing p.S242R Pyrin (Appendix Fig S8). Importantly, we observed dephosphorylation of Pyrin Ser242 residue upon UCN-01 treatment in WT Pyrin-expressing cells (Fig 4F) that was similar to the dephosphorylation pattern observed in p.M694V Pyrin-expressing cells.

Since the dephosphorylation of Pyrin only leads to pyroptosis in the presence of the p.M964V mutation, we reasoned that the p.S242R mutation, which blocks phosphorylation of Pyrin on this key residue, should be cytotoxic in the presence of the p.M694V mutation. Indeed, induction of the expression of a Pyrin protein containing both the p.S242R and the p.M694V mutations in U937 cells was cytotoxic per se in the absence of PKC superfamily inhibitors (Fig 5A and C). Similarly, induction of the expression of a Pyrin protein expressing the p.S208C mutation and the p.M694V mutations was also cytotoxic (Fig 5A and C). Cell death upon induction

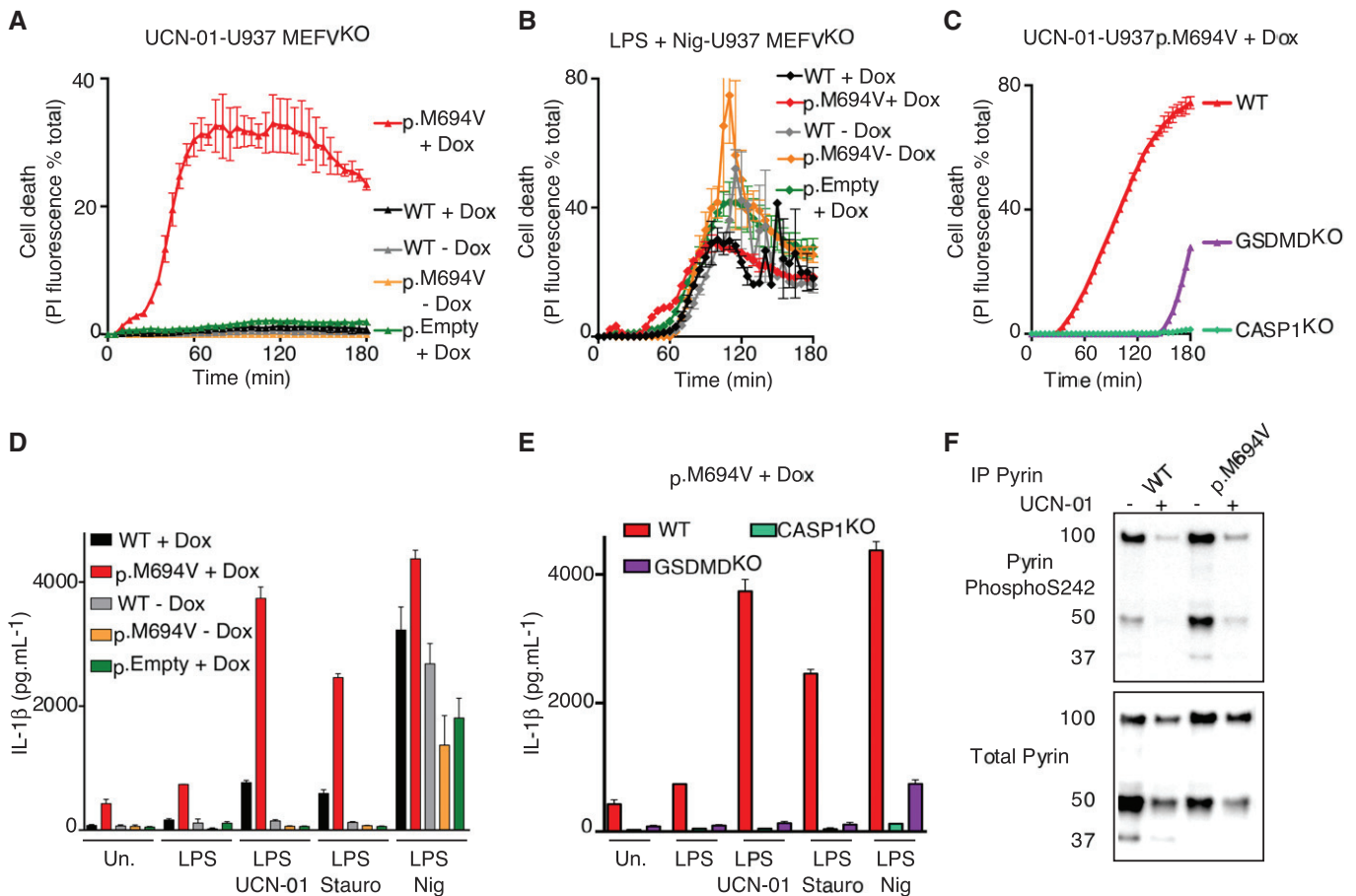


Figure 4. Expression of p.M694V Pyrin is necessary and sufficient to confer to PKC inhibitors the ability to activate the inflammasome.

A–C U937 cells of the indicated genotype and expressing the indicated plasmids were treated with (A, C) UCN-01 or LPS + nigericin (Nig). Propidium iodide (PI) influx/fluorescence was monitored every 5 min for 3 h.

D, E PMA-differentiated U937 cells of the indicated genotype and expressing the indicated plasmids were primed with LPS for 3 h and treated with UCN-01, staurosporine (Stauro) or nigericin as indicated. IL-1 β level in the supernatant was quantified by ELISA at 3 h post-treatment.

F Pyrin S242 phosphorylation was assessed by Western blot in the indicated cell lines with and without UCN-01 treatment for 15 min.

Data information: (A–C) One experiment representative of three independent experiments is shown. Mean and standard deviations from two biological replicates are shown. (D, E) Mean and standard deviations from three independent experiments are shown.

Source data are available online for this figure.

of these double mutants was reproducibly observed although the maximal cell death levels were variable between experiments (mean = 36.7% \pm 20.1(SE) [min: 11.2, max 67.1; n = 7] for p.S242R/M694V and mean = 24.4% \pm 6.7 (SE) [min 15.8, max 27.9; n = 4] for p.S208C/M694V). Interestingly, the level of cell death observed in cells expressing a Pyrin protein containing the two phospho-null mutations and the p.M694V mutations (triple mutant p.S208C/S242R/M694V) was consistently higher than the one of the cells expressing a single phospho-null mutation in combination with the p.M694V mutation (Fig 5B and C). The cell death kinetics correlated with the kinetics of protein expression following doxycycline-mediated induction (Fig EV2A and B, and Appendix Fig S9). In contrast, neither expression of the single or double phospho-null mutant (p.S208C; p.S242R; p.S208C/S242R) nor of the p.M694V single mutant proteins triggered substantial cell death. Addition of UCN-01 at 20 h post-doxycycline addition had a minor additional cytotoxic effect on the p.S208C/M694V and the

p.S242R/M694V-expressing cell lines (Fig 5A and D). No additional cytotoxic effect could be detected on the p.S208C/S242R/M694V-expressing cell line since all the cells were dead at 20 h post-doxycycline addition. Interestingly, colchicine addition could block the cell death induced by the doxycycline-mediated expression of pS208C/M694V, pS242R/M694V, and pS208C/S242R/M694V Pyrin variants (Fig EV5), suggesting that colchicine acts independently (and downstream; Van Gorp *et al*, 2016; Gao *et al*, 2016) of Pyrin dephosphorylation.

Similarly, doxycycline-mediated induction of p.S208C/M694V or p.S242R/M694V triggered IL-18 release in the absence of PKC inhibitors (Fig 5E). When added onto the p.M694V background, the two phospho-null mutations had an additive effect in regard to IL-18 concentration in the supernatant (Fig 5E). As described above for the cell death, IL-18 was not substantially released upon doxycycline induction of p.M694V, p.S208C, p.S242R, or p.S208C/S242R Pyrin proteins (Fig 5E). As expected, a further addition of UCN-01

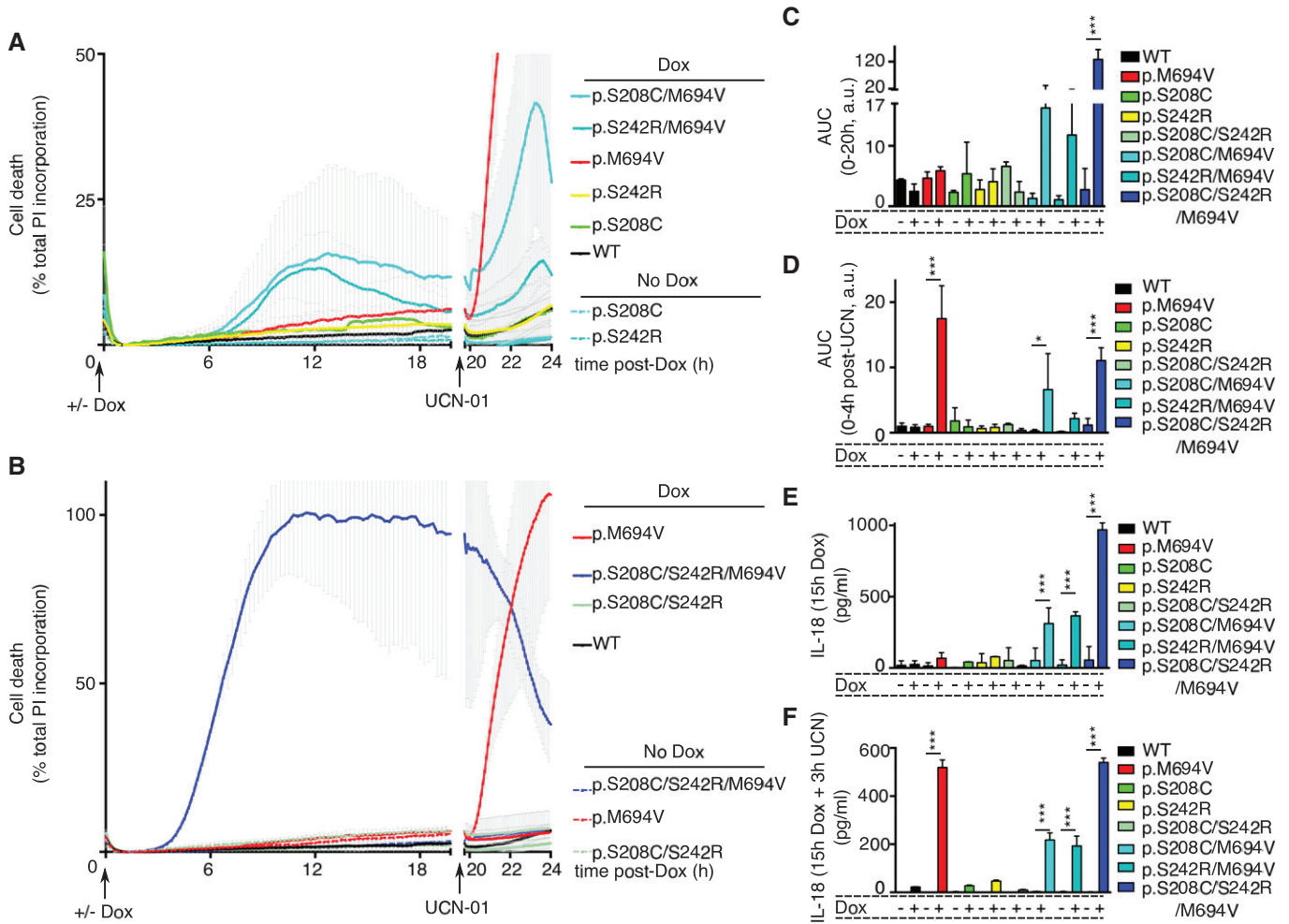


Figure 5. Expression of p.M694V Pyrin is necessary and sufficient to confer to the phospho-null p.S242R/p.S208C variants the ability to activate the inflammasome.

U937 cells bearing the indicated plasmids were treated as indicated at time 0 with doxycycline (Dox) and at 20 h post-Dox addition with UCN-01

A, B Propidium iodide (PI) influx/fluorescence was monitored every 15 min for 20 h and every 5 min for an additional 4 h.

C, D Area under the curve (AUC) corresponding to Fig 5A and B was computed from $t = 0$ to $t = 20$ h (C) and from 20 to 24 h (D).

E, F IL-18 was quantified in the supernatant of the indicated U937 cells at 15 h post-doxycycline/PBS addition (E) or in the supernatant of U937 cells exposed to 15 h of doxycycline/PBS and an additional 3 h of incubation with UCN-01 (F).

Data information: (A–F) One experiment representative of three independent experiments is shown. (A, B) Each dot represents the mean \pm SD of a biological triplicate. Values right after UCN-01 addition were corrected to match values right before UCN-01 addition to correct for a reading artifact, and the correction factor was applied until the end of the experiment. Data presented in (A and B) are from the same experiment and have been split for clarity. The WT and p.M694V controls are duplicated in (A and B). (C–F) The bar represents the mean \pm SD of a biological triplicate. One-way ANOVA with Holm–Sidak’s multiple comparisons test was performed to compare untreated and doxycycline-treated samples: (C) p.S208C/S242R/M694V $***P < 0.0001$ (D) p.M694V $***P < 0.0001$; p.S208C/M694V $*P = 0.016$; p.S208C/S242R/M694V $***P = 0.0004$. (E) p.S208C/M694V $***P = 0.0001$; p.S242R/M694V $***P < 0.0001$; p.S208C/S242R/M694V $***P < 0.0001$. (F) p.M694V $***P < 0.0001$; p.S208C/M694V $***P < 0.0001$; p.S242R/M694V $***P < 0.0001$; p.S208C/S242R/M694V $***P < 0.0001$.

Source data are available online for this figure.

triggered the fast release of IL-18 in p.M694V-expressing cells while no IL-18 was observed in cells expressing only the phospho-null Pyrin mutants (Fig 5F).

These data provide genetic evidence that dephosphorylation of Pyrin (or lack of phosphorylation) in the context of the p.M694V mutation is necessary and sufficient to promote full Pyrin inflammasome activation. Our data suggest that dephosphorylation of the S208 and of the S242 residues have an additive (IL-18) or possibly synergistic (cell death) effect to trigger Pyrin inflammasome

activation in the context of p.M694V mutation. Further, these results strongly suggest that UCN-01 acts on both S242 and S208 to trigger the fast cell death observed in primary monocytes from FMF patients and in U937 cells expressing the p.M694V Pyrin variant. Dephosphorylation of p.M694V Pyrin is thus sufficient to trigger inflammasome activation while another safeguard mechanism exists to control activation of dephosphorylated WT Pyrin. Finally, these results provide the proof of concept that U937 cells and PKC inhibitors could be used to functionally characterize *MEFV* variants for their pathogenicity.

PKC inhibitor responses functionally discriminate FMF patients from patients with unrelated inflammatory conditions

To exclude that the response of monocytes from FMF patients might be due to inflammation, we then studied the responses of monocytes from patients presenting various inflammatory syndromes and infection-associated inflammation including Behcet's disease, inflammatory bowel disease, and sepsis (Appendix Table S1). While each disease was represented by a low number of patients, none of the non-FMF patients (termed "Disease control-DC" in Fig 6) responded to the two PKC inhibitors by producing large amount of IL-1 β (Fig 6A and B) or by triggering a fast monocyte death (Fig 6C–E, Appendix Fig S10A–C). Even though larger cohorts of patients with "control diseases" are required to validate statistically this difference for each inflammatory syndrome, these data strongly suggest that inflammasome activation in response to PKC inhibitors is not due to underlying inflammation but is specific to FMF patients.

Due to this discrimination between FMF patients and other patients suffering from various conditions with an inflammatory component, we assessed whether the functional response to PKC inhibitors has the potential to be exploited for FMF diagnosis. We thus generated receiver operating characteristic (ROC) curves to determine the sensitivity and specificity of a functional test based on IL-1 β release following staurosporine (Fig 6F) or UCN-01 treatment (Fig 6G) or based on cell death kinetics parameters (time to reach 20% cell death; Fig 6H or AUC of the cell death kinetics; Fig 6I). The predictive values (Appendix Table S2) and the areas under the ROC curves, which are very close to 1 (1 corresponding to 100% specificity and 100% sensitivity), suggest that these functional assays accurately discriminate FMF patients from other patients presenting inflammatory conditions and from HD (Appendix Fig S10D–G). As an example, and keeping in mind that such a diagnostic use remains to be thoroughly tested in larger and multicentric cohorts, an IL-1 β concentration threshold at 224 pg/ml in response to UCN-01 discriminates FMF patients with a sensitivity of 89% and a specificity of 96%. Interestingly, the tests based on the cell death kinetics have slightly better positive and negative predictive values (Appendix Table S2) than the tests based on IL-1 β , suggesting that pyroptosis monitoring better discriminates FMF patients from HD (Appendix Fig S10F–G) and from patients with other inflammatory conditions (Fig 6H and I) than quantifying IL-1 β release does.

In conclusion, our study demonstrates that PKC inhibitor treatment is sufficient to trigger inflammasome activation in monocytes from FMF patients, which (i) expands our knowledge on the molecular basis sustaining Pyrin inflammasome deregulation in FMF, (ii) offers a potential functional assay to characterize *MEFV* variants, and (iii) provides a fast biological test that may discriminate FMF patients from patients suffering from other inflammatory conditions.

Discussion

The links between *MEFV* mutations, the dysfunctional Pyrin inflammasome, and FMF remain poorly understood. In contrast to the typical gain-of-function mutations of *NLRP3* or *NLRP4* observed in cryopyrin-associated periodic syndromes and *NLRP4*-associated syndromes, *MEFV* mutations do not lead to a spontaneous activation of the Pyrin inflammasome in the absence of a specific stimulus

(Van Gorp *et al*, 2016; Jamilloux *et al*, 2018). We have previously shown that *MEFV* mutations lower the activation threshold of the Pyrin inflammasome in response to a Pyrin inflammasome stimulus (Jamilloux *et al*, 2018). While our previous work demonstrated a shift in a dose–response experiment between monocytes of FMF patients and of healthy donors, here we identified an "all or nothing" response that discriminates FMF patients' monocytes from healthy donors' monocytes across a large concentration of PKC superfamily inhibitors.

MEFV mutations were described to lift the obligatory requirement for microtubule in Pyrin inflammasome activation (Van Gorp *et al*, 2016). In the work by van Gorp and colleagues, colchicine was inefficient at inhibiting TcdA-mediated Pyrin inflammasome in FMF patients PBMCs. Here, we took a reverse approach not based on inhibition of the Pyrin inflammasome (by colchicine) but on activation of the Pyrin inflammasome, which we demonstrated to be specific for FMF patients' monocytes following PKC superfamily inhibitor addition. We believe our results are important since they clearly demonstrate that dephosphorylation of Pyrin is sufficient to promote full inflammasome activation in FMF patients while it is not sufficient in healthy donors.

Our results partially concur with the conclusions from van Gorp and colleagues that FMF mutations affect the ability of colchicine to inhibit Pyrin inflammasome activation. Yet, our results demonstrate that the phenotype of FMF monocytes (and likely FMF patients) cannot be explained by a full loss of microtubule-dependent activation. The interaction of *MEFV* mutations with this microtubule-dependent step is likely much more complex. While colchicine fully inhibited TcdB-mediated IL-1 β in healthy donor monocytes, colchicine inhibited only partially IL-1 β release in FMF patients' monocytes. Furthermore, colchicine fully inhibited pyroptosis and IL-1 β release in response to PKC inhibition in FMF patients' monocytes. Similarly, colchicine inhibited cell death induced by the expression of a Pyrin protein containing both the p.S242R/S208C and the p.M694V mutations (Fig EV5). This *in vitro* efficacy of colchicine is in line with the efficacy of colchicine observed in FMF patients and with the previous *in vitro* assays performed on FMF monocytes following LPS stimulation (Park *et al*, 2016). One important message of our work is thus that colchicine is efficient at inhibiting the Pyrin inflammasome (at least in response to some stimuli) in FMF patients.

Our results demonstrate that, while the PKC superfamily inhibitors are efficient to dephosphorylate both WT Pyrin and p.M694V Pyrin (Park *et al*, 2016), ASC oligomerization, pyroptosis, and robust IL-1 β release are only triggered when these inhibitors are added on cells expressing p.M694V *MEFV* gene. This study thus reinforces the data indicating that p.M694V mutation does not impact Pyrin phosphorylation status in a major way (Gao *et al*, 2016; Masters *et al*, 2016; Van Gorp *et al*, 2016), but affects another control mechanism, likely related to a complex process implicating microtubule dynamics (Gao *et al*, 2016; Van Gorp *et al*, 2016).

PAAND patients presenting the p.S242R mutation, which abolishes one Pyrin phosphorylation site (Masters *et al*, 2016) or patients presenting the p.E244K mutation, which abolishes 14-3-3 binding site (Moghaddas *et al*, 2017), have a constitutive activation of the Pyrin inflammasome. Yet, the level of IL-1 β released by PAAND patients' monocytes upon LPS stimulation is moderate (Masters *et al*, 2016) and at least 10 times lower than the level of IL-1 β released upon stimulation with LPS + TcdB. This observation suggests that in PAAND

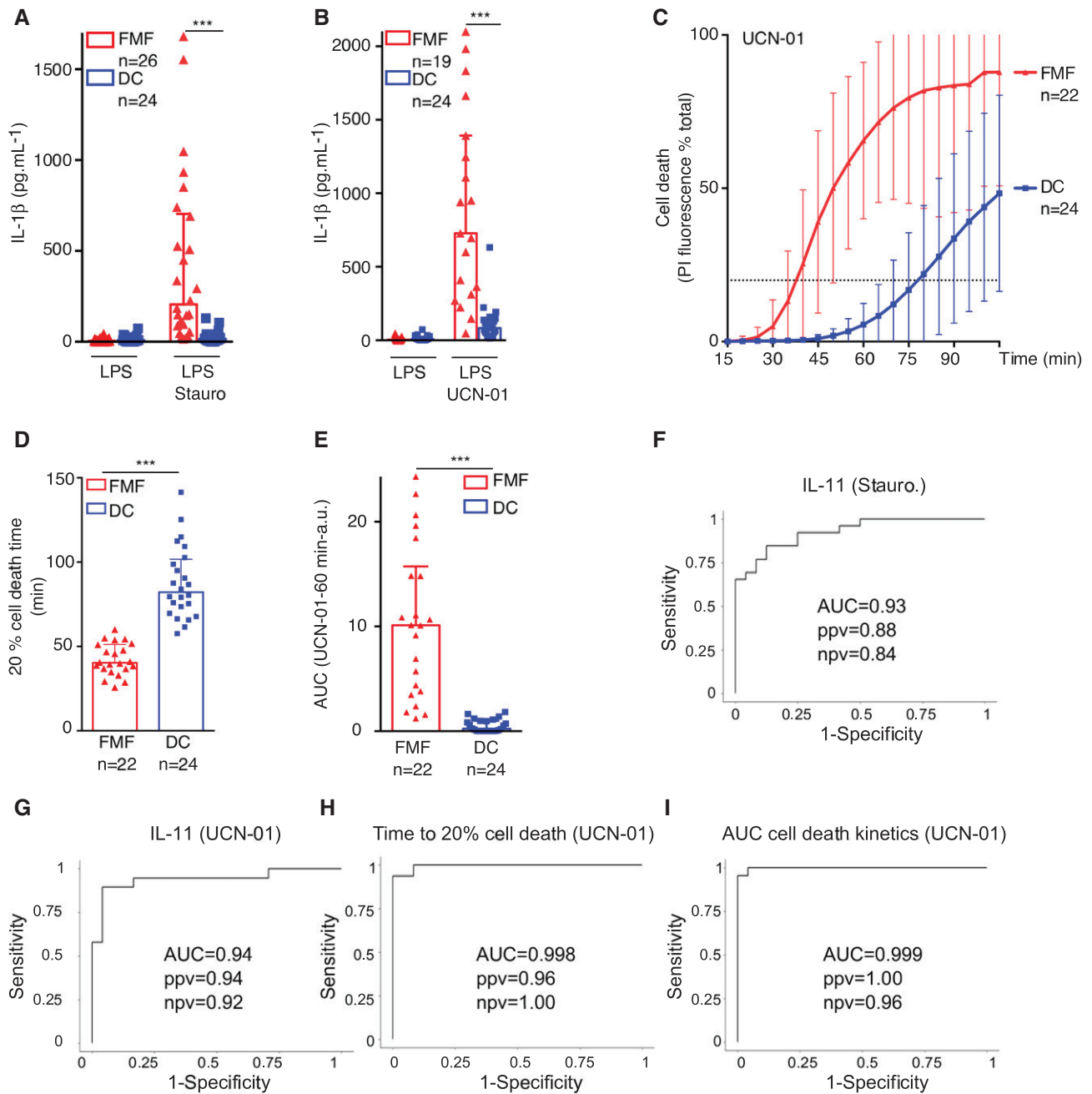


Figure 6. PKC inhibitor-mediated inflammasome activation discriminates FMF patients from patients suffering from unrelated inflammatory conditions.

Monocytes from FMF patients or from control diseases patients (DC) were either primed with LPS (A, B) or not (C–E) and treated with (A) 1.25 μ M staurosporine (Stauro), (B, C–E) 12.5 μ M UCN-01.

A, B IL-1 β level was quantified by ELISA at 90 min post-stimulation.

C–E Cell death was monitored in real time by measuring propidium iodide (PI) influx/fluorescence every 5 min. (D) The time required to obtain 20% of cell death and (E) the area under the kinetics curve (AUC) were computed for each patient.

F–I Receiver operating characteristic (ROC) curves were computed for IL-1 β concentrations following (F) staurosporine or (G) UCN-01 treatment, (H) the time to obtain 20% cell death, and (I) the area under the cell death kinetics curve. For each ROC curve, the AUC, the positive (ppv), and negative (npv) predictive values are indicated.

Data information: (A, B) Each symbol represents the mean value from three biological replicates for one patient. The bar represents the median \pm interquartile range. (C) Each point of the curve corresponds to the average of the mean cell death values from three biological replicates of monocytes from the indicated number of patients. The dotted line indicates the 20% cell death value. (D–E) Each dot represents the value from one patient. The bar represents the median \pm interquartile range. (A, B): *** P < 0.0001 by Wilcoxon rank-sum test. (D, E) *** P < 0.0001 by unpaired t -test. (A–E) Values from FMF patients are identical as the ones presented in Fig 1. The figures were not merged for clarity issues.

Source data are available online for this figure.

patients' monocytes, an additional control mechanism independent of phosphorylation/14-3-3-binding still partially limits Pyrin inflammasome activation. In agreement with this hypothesis, ectopic expression of a double mutant p.S242R/p.M694V Pyrin protein in HEK293T cells was found to promote more GFP-ASC speck formation than a single p.S242R Pyrin protein (Masters *et al*, 2016). Similarly, controlled expression of phosphorylation-mutant Pyrin in the mouse dendritic cell line DC2.4 was reported to trigger $\approx 20\%$ cell death (Gao *et al*, 2016). We did not observe substantial cell death in U937 cells expressing p.S242R (or p.S208C/S242R) Pyrin in contrast to the cytotoxicity associated with the expression of p.S242R/M694V double mutant (or p.S208C/S242R/M694V triple mutant). All together, our results combined with previous data from the literature emphasize that the WT Pyrin inflammasome is controlled by two largely independent mechanisms. In contrast, in FMF patients, the Pyrin inflammasome activation is solely under the control of PKC superfamily kinases and lacks a second negative control mechanism likely explaining its hyper-reactivity and the associated recurrent inflammation observed in FMF patients. Similarly, in PAAND patients where the phosphorylation regulation is affected, we believe the Pyrin inflammasome is not fully activated due to the control by the second colchicine-targetable mechanism. Yet, clinical evidence demonstrates that missing one of these two control mechanisms is associated with disease highlighting the key requirement for a tight inflammasome control. A key challenge in the field is now to identify the factors that could mimic PKC superfamily inhibitors and be responsible for inflammatory flares in patients.

In the present study, most FMF patients were under colchicine treatment (Appendix Table S1). Colchicine treatment is unlikely to explain the hyper-reactivity of FMF patients to PKC superfamily inhibitors since (i) we could recapitulate the findings in U937 cells; (ii) *in vitro*, colchicine reduces inflammasome activation (Gao *et al*, 2016; Park *et al*, 2016; Van Gorp *et al*, 2016); and (iii) three patients with Behcet's disease under colchicine were included in the disease control group and their monocytes did not display an FMF-like phenotype. Although our data suggest that a single clearly pathogenic *MEFV* variant is sufficient to confer to PKC inhibitors the ability to trigger inflammasome activation, our cohort of FMF patients is currently too small to draw robust conclusions regarding the number (biallelic mutations vs. mono-allelic) of clearly pathogenic variants. Furthermore, due to the large number of *MEFV* variants present in our cohort, conclusions on specific *MEFV* variants will require the recruitment of a large number of FMF patients coupled to the functional characterization of *MEFV* variants in genetically engineered cell lines.

Here, we show that the response of monocytes from FMF patients to PKC inhibitors could discriminate FMF patients from other patients presenting inflammatory conditions. Our results thus pave the way toward the development of a functional diagnostic test for FMF. Of note, several limitations of the current study remain to be overcome to fully evaluate the diagnostic potential of this assay. First, the sensitivity of the test has to be defined with respect to the different *MEFV* genotypes. Second, the assay would have to be validated in whole blood to be compatible with clinical laboratory. Third, the test remains to be validated in a large independent, multi-centric cohort of patients in a prospective manner. Such a test could be used upstream of genetic tests to narrow-down the diagnosis or downstream of the genetic test in the case of non-conclusive results, which represent about 25% of the current genetic diagnosis

(Grateau *et al*, 2000; Lachmann *et al*, 2006; Booty *et al*, 2009; Giancane *et al*, 2015). Furthermore, a functional assay might help physicians to take decisions regarding the weaning of the lifelong colchicine treatment in FMF patients possessing a single *MEFV* pathogenic variant (Sonmez *et al*, 2017). The lack of colchicine inhibition of the Pyrin inflammasome in response to TcdA can also be used to discriminate FMF patients from HD (Van Gorp *et al*, 2016). Interestingly, our functional test does not require the manipulation of the highly potent *C. difficile* toxins and might be thus easier to implement in the hospital/diagnostic laboratory environment. The *in vitro* efficacy of colchicine could thus be combined to the responsiveness to PKC inhibitors to further increase the potential of functional assays to discriminate HD and FMF patients.

Materials and Methods

Subjects

Thirty-nine patients with FMF (Appendix Table S1) were included along with patients suffering from other inflammatory conditions (mevalonate kinase deficiency ($n = 3$), Behcet's disease ($n = 4$), lupus ($n = 2$), Still's disease ($n = 5$), non-systemic juvenile idiopathic arthritis ($n = 1$), sepsis ($n = 3$), inflammatory bowel disease ($n = 4$), H syndrome ($n = 1$), A20 deficiency ($n = 1$)), and 45 HD. All FMF patients fulfilled the Tel HaShomer criteria for FMF and had at least one mutation in the *MEFV* gene. The potential carriage of *MEFV* mutations in HD was not assessed. Blood samples from HD were drawn on the same day as patients. Allele frequency was extracted from <https://gnomad.broadinstitute.org/> (Lek *et al*, 2016).

Monocyte isolation

Blood was drawn in heparin-coated tubes and kept at room temperature overnight. The next day, peripheral blood mononuclear cells (PBMCs) were isolated by density-gradient centrifugation using lymphocyte separation medium (Eurobio; Noble & Cutts, 1968). Monocytes were isolated from PBMCs by magnetic selection using CD14 MicroBeads (Miltenyi Biotec) (Lyons *et al*, 2007) and the AutoMACS Pro Separator (Miltenyi Biotec) following manufacturer's instructions. Monocytes were enumerated in the presence of a viability marker (propidium iodide, 10 $\mu\text{g/ml}$) by flow cytometry (BD Accuri C6 Flow Cytometer[®]) (Schuerwegh *et al*, 2001).

Inflammasome activation

Primary monocytes were seeded into 96-well plates at 5×10^3 cells/well, in RPMI 1640, GlutaMAX medium (Thermo Fisher Scientific) supplemented with 10% fetal calf serum (Lonza). When indicated, primary monocytes were incubated for 3 h in the presence of LPS (10 ng/ml, InvivoGen). Unless otherwise indicated, primary monocytes were then treated for 90 min with nigericin (5 μM , InvivoGen), ATP (2.5 mM, Sigma) (Mariathan *et al*, 2006), staurosporine (1.25 μM , Tocris), UCN-01 (12.5 μM , Sigma), or Ro31-8820 (100 μM , Tocris). When indicated, monocytes were treated with colchicine (1 μM or at the indicated concentration, Sigma), MCC950 (10 μM , Adipogen AG-CR1-3615), paclitaxel (Taxol, 5 μM , Sigma), nocodazole (5 μM , Sigma), z-YVAD-FMK, z-IETD-FMK, z-DEVD-FMK (at the

indicated concentrations, Bachem, #4027532, #4034771, #4027402, respectively), VX-765 (InvivoGen), 30 min before addition of UCN-01, TcdB (Abcam, #ab124001, 125 ng/ml), and TcdA (1 µg/ml) or nigericin. TcdA was purified from *Clostridioides difficile* VPI10463 strain, as previously described (von Eichel-Streiber et al, 1987; Popoff, 1987). Following the incubation, cells were centrifuged and supernatants were collected.

Immunofluorescence

Monocytes (1.2×10^5 per sample) stimulated as indicated above were fixed with paraformaldehyde 2% for 20 min at 37°C, washed three times in PBS, and spread onto poly-lysine adhesion slides (Thermo Fisher Scientific™) using the Cytospin 3 (Shandon) 5 min at 450 rpm. Following permeabilization with Triton X-100 (0.1% in PBS) and overnight incubation in blocking buffer (PBS, 3% BSA), cells were stained using anti-ASC (Santa Cruz, sc22514R, 4 µg/ml, 1 h of room temperature), Alexa 488-goat anti-rabbit antibodies (Invitrogen, A-110088, 10 µg/ml, 20 min of room temperature), and DAPI (100 ng/ml) all diluted in a 50 µl drop of blocking buffer. Coverslips were mounted onto the slides using mowiol. ASC specks and DAPI stained nuclei were visualized on the Zeiss LSM800 confocal microscope. Quantification was performed on 10 fields per sample.

FLICA-Casp1 and Annexin-V staining

Monocytes were stimulated as described above and stained with the FAM FLICA-Caspase-1 Kit (Bio-Rad ICT098), at the indicated time points, following manufacturer's instructions. Cells were extemporaneously analyzed on a Canto II cytometer. Annexin-V staining was performed using the Annexin-V Apoptosis Detection Kit (Invitrogen, 88-8005-74). Cells were then stained with propidium iodide (5 µg/ml) before acquisition on a CantoII cytometer. To obtain the response induced by the treatment, values from untreated samples were subtracted from values obtained following treatment. The sum of Annexin-V⁺ and PI⁺ cells defined the total dead cells. The ratio was calculated as the % of Annexin-V⁺/PI⁻ over total dead cells.

Cell lines and genetic manipulation

The human myeloid cell line U937 (CelluloNet, Lyon, France) was grown in RPMI 1640 medium with glutaMAX-I supplemented with 10% (vol/vol) FCS, 2 mM L-glutamine, 100 IU/ml penicillin, and 100 µg/ml streptomycin (Thermo Fisher Scientific). *MEFV*^{KO}, *Casp1*^{KO}, and *GSDMD*^{KO} cell lines generated by CRISPR/Cas9-mediated gene inactivations have been previously described (Lagrange et al, 2018). The sgRNA targeting *PKN1* and *PKN2* (Appendix Table S3) were selected from the Brunello library (Addgene) and cloned into the PGKpuro2ABFP vector (from Kosuke Yusa; Addgene plasmid # 50946). sgRNA plasmids were transduced in a previously described Cas9-expressing U937 clone (Lagrange et al, 2018) by spinoculation. The resulting cell lines were selected with 2 µg/ml Puromycin (Sigma-Aldrich) at 72 h post-transduction for 2 weeks. Except for *PKN1* and *PKN2* inactivation (due to low to zero efficiency of the KO process), the knock-out cells were kept polyclonal and were screened by Western blotting analysis or sequencing of a PCR fragment corresponding to the genomic region flanking the targeted sequence. The obtained sequence files were analyzed using

the sequence trace decomposition software TIDE (Brinkman et al, 2014; Appendix Fig S7).

WT, p.M694V, p.S242R, and p.S242R/M694V *MEFV* were cloned into the GFP-expressing plasmid pINDUCER21 (Meerbrey et al, 2011) under the control of a doxycycline-inducible promoter through the pENTR1A (Invitrogen) vector using a synthetic DNA fragment (GeneArt) encoding the p.M694V Pypin protein. The point mutants were generated using the QuikChange II Site-Directed Mutagenesis Kit (Agilent) and primers indicated in Appendix Table S3. Lentiviral particles were produced in 293T cells using pMD2.G and psPAX2 (from Didier Trono, Addgene plasmids #12259 and #12260), and pINDUCER-21 plasmids expressing WT, p.M694V, p.S242R, p.S242R/M694V Pypin, or no insert (pEmpty). The various U937 cell lines were transduced by spinoculation and sorted at day 7 post-transduction based on GFP expression on an Aria cell sorter. Pypin expression was induced by treatment with doxycycline (1 µg/ml) for 16 h before stimulation. For real-time cell death assay, U937 cells were seeded at 4×10^4 per wells before stimulation with relevant inflammasome stimuli. For IL-18 ELISA, 2×10^5 U937 cells per wells were seeded. To assess IL-1β release, 8×10^4 U937 cells per wells were exposed to 100 ng/ml of phorbol 12-myristate 13-acetate (PMA; InvivoGen) for 48 h and primed with LPS at 1 µg/ml for 3 h. When applicable, nigericin was used at 50 µg/ml. Supernatant was collected at 3 h post-treatment. 293T and U937 parental cell lines were tested negative for mycoplasma contamination (Cellulonet, Lyon, France) in January 2018.

siRNA targeting *PKN2* (ON TARGET plus, Dharmacon, # J0004612-12-0002; J0004612-13-0002; J0004612-14-0002) is indicated in Appendix Table S3. siRNA was electroporated into U937 cell lines using the Neon electroporator (Thermo Fisher Scientific) using the following parameters: 1,300 V, 1 pulse of 30 ms. 10^6 cells per condition were washed once at room temperature with PBS and suspended in 110 µl of buffer R containing 10 pmoles of siRNA. Following electroporation, cells were transferred into a well of a pre-warmed p12 plate containing complete medium without antibiotics. When applicable, doxycycline was added at 24 h post-siRNA electroporation.

Immunoprecipitation and immunoblot analysis

Cells were lysed in 25 mM Tris-HCl, 150 mM NaCl, 1 mM EDTA, and 0.1% NP-40 buffer containing Mini Protease Inhibitor Mixture (Roche) and sodium fluoride (Sigma) by a quick freezing and thawing step. Flag-Pypin was immuno-precipitated using anti-Flag M2 affinity gel (Sigma). Proteins were separated by SDS-PAGE on precast 4–15% acrylamide gels (Bio-Rad) and transferred to TransBlot® Turbo™ Midi-size PVDF membranes (Bio-Rad). Antibodies used were mouse monoclonal anti-FLAG® (Sigma-Aldrich, clone M2; 1:1,000 dilution), anti-Pypin (Adipogen, AL196, 1: 1,000 dilution), anti-phospho S242 Pypin (Abcam, ab200420; 1:1,000 dilution; Gao et al, 2016), and anti-PKN1 (Becton Dickinson, BD 610687; 1:1,000 dilution). Cell lysates were re-probed with a mouse monoclonal antibody anti-β-actin (clone C4, Millipore; 1:5,000 dilution). Full Western blot images are presented in Source Data.

Cytokine detection and cell death assay

Levels of IL-1β in monocyte supernatant were quantified by ELISA (R&D Systems). IL-18 levels were quantified using the following

antibodies for capture and detection: anti-human IL-18 antibody (4 µg/ml; # D044-3, MBL, Woburn, MA, USA) and anti-human IL-18 antibody coupled to biotin (20 ng/ml, # D045-6, MBL). Cell death was monitored by incubating 2×10^4 monocytes per well of a black 96-well plate (Costar, Corning) with propidium iodide (PI, Sigma) at 5 µg/ml. Three technical replicates per conditions were done. UCN-01 was added at 12.5 µM in the absence of any priming signal. Nigericin was added at 5 µM after a 3-h priming with LPS at 10 ng/ml. Real-time PI incorporation was measured every 5 min from 15 min to 105 min (for primary monocytes) or from 0 to 180 min (for U937 cells) post-nigericin/UCN-01 intoxication on a fluorimeter (Tecan) using the following wavelengths: excitation 535 nm (bandwidth 15 nm) and emission 635 nm (bandwidth 15 nm) (Case & Roy, 2011; Pierini *et al*, 2012). Cell death was normalized using PI incorporation in monocytes treated with Triton X-100 for 15 min (=100% cell death). Of note, PI value can artificially decline after several hours. As a further correction, the first time point of the kinetics was set to 0. When the reading was stopped (for < 5 min) to add UCN-01 at 20 h post-doxycycline addition, the values after UCN-01 addition were corrected so that the values right after UCN-01 addition matched the values obtained right before. The areas under the curve were computed using the trapezoid rule (Prism 6; GraphPad). Kinetics until 60 and 105 min post-UCN-01 and post-nigericin treatments, respectively, were retained. To extract the time corresponding to 20% cell death, a non-linear regression analysis (Prism 6; GraphPad) was used to fit a sixth-order polynomial curve to the normalized cell death kinetics using the least squares fit as the fitting method. The obtained curve was used to interpolate the time corresponding to 20% cell death.

Statistics

For HD/patient data, normal distribution was verified using D'Agostino–Pearson omnibus normality test. When Gaussian distribution could not be demonstrated for the compared variables, non-parametric tests were used. Results were expressed as median ± interquartile range. When two groups (e.g., HD and FMF), including at least one that did not pass the normality test, were compared, Wilcoxon rank-sum test was performed, and two-tailed *p*-values are shown. When two groups (e.g., HD and FMF) that passed the normality test were compared, unpaired *t*-test was performed, and two-tailed *P*-values are shown. When multiple comparisons between groups (e.g., HD and FMF) that all passed the normality test were made, one-way ANOVA with Sidak's multiple comparison tests was performed. When multiple comparisons between groups (e.g., HD and FMF), some of them that did not pass the normality test, were made, Kruskal–Wallis with Dunn's multiple comparison tests were performed. Multiplicity-adjusted *P*-values are shown. When multiple comparisons between paired groups of identical numbers (e.g., FMF and FMF + inhib.), some of them that did not pass the normality test, were made, Friedman with Dunn's multiple comparison tests were performed. Multiplicity-adjusted *P*-values are shown. When a comparison between two paired groups (e.g., FMF and FMF + inhib.), at least one of each did not pass the normality test, was made, Wilcoxon matched-pairs signed rank test was used. Two-tailed *P*-value is shown. Correlation significance was determined by Spearman test. The predictive power of the mechanisms of interest was assessed using receiver operating curve (ROC) analyses. The area under the ROC (AUC) and its 95% CI were estimated for each

The paper explained

Problem

Familial Mediterranean fever (FMF) is the most frequent hereditary systemic autoinflammatory disease. FMF is, in most cases, associated with biallelic mutations of the *MEFV* gene encoding Pyrin, an inflammasome sensor. The link between *MEFV* mutations and the dysregulated Pyrin inflammasome activation observed in FMF patients is unclear. Furthermore, most of the 365 described *MEFV* variants are of uncertain significance and the genetic validation of the clinical FMF diagnosis remains challenging.

Results

Thanks to the use of protein kinase inhibitors and phospho-null mutants; this study demonstrates that Pyrin dephosphorylation triggers full inflammasome activation in FMF patients' monocytes but not in healthy donors' monocytes. Furthermore, the pathogenic p.M694V *MEFV* mutation, most frequently observed in FMF patient, triggers constitutive inflammasome activation only when combined to phospho-null *MEFV* mutations. These results indicate that Pyrin inflammasome activation is controlled by two independent mechanisms in healthy donors but only by phosphorylation/dephosphorylation in FMF patients. This difference can be exploited using protein kinase inhibitors and primary monocytes from patients to functionally diagnose FMF.

Clinical impact

This study increases our knowledge of the molecular mechanisms underlying inflammation in FMF patients. Furthermore, it should improve FMF diagnosis by providing a quick and easy test in primary monocytes to discriminate FMF patients from patients with unrelated inflammatory conditions. Finally, this study provides means to determine the pathogenicity of *MEFV* variants, which should reduce in the future the number of variants of uncertain significance and improve genetic testing.

mechanism. Threshold values for the prediction of patients with FMF were determined by maximizing the Youden index. All tests were two-sided at the 0.05 significance level. Correlation coefficient was computed using non-parametric Spearman correlation. Statistical analyses were carried out with Prism 6 and R version 3.1.1 (<http://www.R-project.org>).

Study approval

The study was approved by the French Comité de Protection des Personnes (CPP, #L16-189) and by the French Comité Consultatif sur le Traitement de l'Information en matière de Recherche dans le domaine de la Santé (CCTIRS, #16.864). The experiments conformed to the principles set out in the WMA Declaration of Helsinki and the Department of Health and Human Services' Belmont Report. HD blood was provided by the Etablissement Français du Sang in the framework of the convention #14-1820. Informed consent was received from participants prior to inclusion in the study.

Data availability

All data are available within the manuscript, its appendix, and Source Data files.

Expanded View for this article is available online.

Acknowledgements

This work was performed in the framework of the Centre National de Référence RAISE. We acknowledge the contribution of the Etablissement Français du Sang Auvergne—Rhône-Alpes and of SFR Biosciences (UMS3444/CNRS, US8/Inserm, ENS de Lyon, UCBL) Cytometry, Microscopy, and Vectorology facilities. Funding: This work is supported by an ANR grant (FMFgeneToDiag #ANR-17-CE17-0021), an ERC-2012-StG_3115 and funding from the European Union's Horizon 2020 research and innovation program under grant agreement #779295 (ImmunAID).

Author contributions

FM, LL, SB, TM, LW, AM, and DC performed the experiments; SK performed the statistical analysis. MD, AD, MG-V, AL, and PS provided substantial clinical inputs on the work; M-RP provided key reagents; TW, AB, YJ, and TH designed and interpreted the work, YJ and TH wrote the manuscript, all authors reviewed and approved the manuscript.

Conflict of interest

FM, LL, AM, AB, YJ, and TH are listed on a patent related to FMF diagnosis.

For more information

- (i) FMF description on Orphanet (the portal for rare diseases and orphan drugs) https://www.orpha.net/consor/www/cgi-bin/OC_Exp.php?lng=EN&Expert=342
- (ii) FMF OMIM (An Online Catalog of Human Genes and Genetic Disorders): <https://omim.org/entry/249100>
- (iii) Patient association: FMF and AID Global association: <https://www.fmfanda.id.org/>
- (iv) MEFV sequence variants (Infevers, the registry of Hereditary Auto-Inflammatory Disorders Mutations) <https://infevers.umai-montpellier.fr/web/search.php?n=1>
- (v) CIRI website: <http://ciri.inserm.fr/en/>
- (vi) ImmunAID website: Immunome project consortium for AutoInflammatory Disorders <https://www.immunaid.eu/>
- (vii) International Patent filed from this work. <https://patentscope.wipo.int/search/en/detail.jsf?docId=WO2019048569>

References

- Benaoudia S, Martin A, Puig Gamez M, Gay G, Lagrange B, Cornut M, Krasnykov K, Claude J-B, Bourgeois CF, Hughes S et al (2019) A genome-wide screen identifies IRF2 as a key regulator of caspase-4 in human cells. *EMBO Rep* 20: e48235
- Booty MG, Chae JJ, Masters SL, Remmers EF, Barham B, Le JM, Barron KS, Holland SM, Kastner DL, Aksentijevich I (2009) Familial Mediterranean fever with a single MEFV mutation: where is the second hit? *Arthritis Rheum* 60: 1851–1861
- Brinkman EK, Chen T, Amendola M, van Steensel B (2014) Easy quantitative assessment of genome editing by sequence trace decomposition. *Nucleic Acids Res* 42: e168
- Case CL, Roy CR (2011) Asc modulates the function of NLRC4 in response to infection of macrophages by *Legionella pneumophila*. *mBio* 2: e00117-11
- Chae JJ, Wood G, Richard K, Jaffe H, Colburn NT, Masters SL, Gumucio DL, Shoham NG, Kastner DL (2008) The familial Mediterranean fever protein, pyrin, is cleaved by caspase-1 and activates NF-kappaB through its N-terminal fragment. *Blood* 112: 1794–1803
- Chae JJ, Cho Y-H, Lee G-S, Cheng J, Liu PP, Feigenbaum L, Katz SI, Kastner DL (2011) Gain-of-function Pyrin mutations induce NLRP3 protein-independent interleukin-1beta activation and severe autoinflammation in mice. *Immunity* 34: 755–768
- Coll RC, Robertson AAB, Chae JJ, Higgins SC, Munoz-Planillo R, Inserra MC, Vetter I, Dungan LS, Monks BG, Stutz A et al (2015) A small-molecule inhibitor of the NLRP3 inflammasome for the treatment of inflammatory diseases. *Nat Med* 21: 248–255
- Cookson BT, Brennan MA (2001) Pro-inflammatory programmed cell death. *Trends Microbiol* 9: 113–114
- Danno S, Kubouchi K, Mehruba M, Abe M, Natsume R, Sakimura K, Eguchi S, Oka M, Hirashima M, Yasuda H et al (2017) PKN2 is essential for mouse embryonic development and proliferation of mouse fibroblasts. *Genes Cells Devoted Mol Cell Mech* 22: 220–236
- Davis PD, Elliott LH, Harris W, Hill CH, Hurst SA, Keech E, Kumar MK, Lawton G, Nixon JS, Wilkinson SE (1992) Inhibitors of protein kinase C. 2. Substituted bisindolylmaleimides with improved potency and selectivity. *J Med Chem* 35: 994–1001
- Davis MI, Hunt JP, Herrgard S, Ciceri P, Wodicka LM, Pallares G, Hocker M, Treiber DK, Zarrinkar PP (2011) Comprehensive analysis of kinase inhibitor selectivity. *Nat Biotechnol* 29: 1046–1051
- Dode C, Pecheux C, Cazeneuve C, Cattan D, Dervichian M, Goossens M, Delpech M, Amselem S, Grateau G (2000) Mutations in the MEFV gene in a large series of patients with a clinical diagnosis of familial Mediterranean fever. *Am J Med Genet* 92: 241–246
- von Eichel-Streiber C, Harperath U, Bosse D, Hadding U (1987) Purification of two high molecular weight toxins of *Clostridium difficile* which are antigenically related. *Microb Pathog* 2: 307–318
- Gao W, Yang J, Liu W, Wang Y, Shao F (2016) Site-specific phosphorylation and microtubule dynamics control Pyrin inflammasome activation. *Proc Natl Acad Sci USA* 113: E4857–E4866
- Giancane G, Ter Haar NM, Wulffraat N, Vastert SJ, Barron K, Hentgen V, Kallinich T, Ozdogan H, Anton J, Brogan P et al (2015) Evidence-based recommendations for genetic diagnosis of familial Mediterranean fever. *Ann Rheum Dis* 74: 635–641
- Goldfinger SE (1972) Colchicine for familial Mediterranean fever. *N Engl J Med* 287: 1302
- Grateau G, Pêcheux C, Cazeneuve C, Cattan D, Dervichian M, Goossens M, Delpech M, Amselem S, Dodé C (2000) Clinical versus genetic diagnosis of familial Mediterranean fever. *QJM* 93: 223–229
- Jamilloux Y, Lefeuvre L, Magnotti F, Martin A, Benezech S, Allatif O, Penel-Page M, Hentgen V, Seve P, Gerfaud-Valentin M et al (2018) Familial Mediterranean fever mutations are hypermorphic mutations that specifically decrease the activation threshold of the Pyrin inflammasome. *Rheumatology (Oxford)* 57: 100–111
- Jeru I, Hentgen V, Cochet E, Duquesnoy P, Le Borgne G, Grimprel E, Stojanovic KS, Karabina S, Grateau G, Amselem S (2013) The risk of familial Mediterranean fever in MEFV heterozygotes: a statistical approach. *PLoS One* 8: e68431
- Lachmann HJ, Sengul B, Yavuzsen TU, Booth DR, Booth SE, Bybee A, Gallimore JR, Soyuturk M, Akar S, Tunca M et al (2006) Clinical and subclinical inflammation in patients with familial Mediterranean fever and in heterozygous carriers of MEFV mutations. *Rheumatology (Oxford)* 45: 746–750
- Lagrange B, Benaoudia S, Wallet P, Magnotti F, Provost A, Michal F, Martin A, Di Lorenzo F, Py BF, Molinaro A et al (2018) Human caspase-4 detects

- tetra-acylated LPS and cytosolic Francisella and functions differently from murine caspase-11. *Nat Commun* 9: 242
- Lek M, Karczewski KJ, Minikel EV, Samocha KE, Banks E, Fennell T, O'Donnell-Luria AH, Ware JS, Hill AJ, Cummings BB *et al* (2016) Analysis of protein-coding genetic variation in 60,706 humans. *Nature* 536: 285
- Lidar M, Tokov I, Chetrit A, Zaks N, Langevitz P, Livneh A (2005) Diagnosis delay in familial Mediterranean fever (FMF): social and gender gaps disclosed. *Clin Exp Rheumatol* 23: 357–363
- Lyons PA, Koukoulaki M, Hatton A, Doggett K, Woffendin HB, Chaudhry AN, Smith KG (2007) Microarray analysis of human leucocyte subsets: the advantages of positive selection and rapid purification. *BMC Genom* 8: 64
- Mariathasan S, Weiss DS, Newton K, McBride J, O'Rourke K, Roose-Girma M, Lee WP, Weinrauch Y, Monack DM, Dixit VM (2006) Cryopyrin activates the inflammasome in response to toxins and ATP. *Nature* 440: 228–232
- Martinon F, Burns K, Tschopp J (2002) The inflammasome: a molecular platform triggering activation of inflammatory caspases and processing of proIL-beta. *Mol Cell* 10: 417–426
- Masters SL, Lagou V, Jeru I, Baker PJ, Van Eyck L, Parry DA, Lawless D, De Nardo D, Garcia-Perez JE, Dagley LF *et al* (2016) Familial autoinflammation with neutrophilic dermatosis reveals a regulatory mechanism of pyrin activation. *Sci Transl Med* 8: 332ra45
- Meerbrey KL, Hu G, Kessler JD, Roarty K, Li MZ, Fang JE, Herschkowitz JL, Burrows AE, Ciccio A, Sun T *et al* (2011) The pINDUCER lentiviral toolkit for inducible RNA interference *in vitro* and *in vivo*. *Proc Natl Acad Sci USA* 108: 3665–3670
- Moghaddas F, Llamas R, De Nardo D, Martinez-Banaclocha H, Martinez-Garcia JJ, Mesa-del-Castillo P, Baker PJ, Gargallo V, Mensa-Vilaro A, Canna S *et al* (2017) A novel pyrin-associated autoinflammation with neutrophilic dermatosis mutation further defines 14-3-3 binding of pyrin and distinction to familial Mediterranean fever. *Ann Rheum Dis* 76: 2085–2094
- Mor A, Gal R, Livneh A (2003) Abdominal and digestive system associations of familial Mediterranean fever. *Am J Gastroenterol* 98: 2594–2604
- Nie C, Luo Y, Zhao X, Luo N, Tong A, Liu X, Yuan Z, Wang C, Wei Y (2014) Caspase-9 mediates Puma activation in UCN-01-induced apoptosis. *Cell Death Dis* 5: e1495
- Noble PB, Cutts JH (1968) Isolation of individual leukocyte types from peripheral blood. *J Lab Clin Med* 72: 533–538
- Omenetti A, Carta S, Delfino L, Martini A, Gattorno M, Rubartelli A (2014) Increased NLRP3-dependent interleukin 1beta secretion in patients with familial Mediterranean fever: correlation with MEFV genotype. *Ann Rheum Dis* 73: 462–469
- Padeh S, Livneh A, Pras E, Shinar Y, Lidar M, Feld O, Berkun Y (2010) Familial Mediterranean fever in children presenting with attacks of fever alone. *J Rheumatol* 37: 865–869
- Park YH, Wood G, Kastner DL, Chae JJ (2016) Pyrin inflammasome activation and RhoA signaling in the autoinflammatory diseases FMF and HIDS. *Nat Immunol* 17: 914–921.
- Pierini R, Juruj C, Perret M, Jones CL, Mangeot P, Weiss DS, Henry T (2012) AIM2/ASC triggers caspase-8-dependent apoptosis in Francisella-infected caspase-1-deficient macrophages. *Cell Death Differ* 19: 1709–1721
- Popoff MR (1987) Purification and characterization of Clostridium sordellii lethal toxin and cross-reactivity with Clostridium difficile cytotoxin. *Infect Immun* 55: 35–43
- Sagulenko V, Thygesen SJ, Sester DP, Idris A, Cridland JA, Vajjhala PR, Roberts TL, Schroder K, Vince JE, Hill JM *et al* (2013) AIM2 and NLRP3 inflammasomes activate both apoptotic and pyroptotic death pathways via ASC. *Cell Death Differ* 3: 1–12
- Sarrauste de Menthiere C, Terriere S, Pugnere D, Ruiz M, Demaille J, Toutou I (2003) INFEVERS: the Registry for FMF and hereditary inflammatory disorders mutations. *Nucleic Acids Res* 31: 282–285
- Schneider KS, Gross CJ, Dreier RF, Saller BS, Mishra R, Gorka O, Heilig R, Meunier E, Dick MS, Cikovic T *et al* (2017) The inflammasome drives GSDMD-independent secondary pyroptosis and IL-1 release in the absence of caspase-1 protease activity. *Cell Rep* 21: 3846–3859
- Schuerwegh AJ, Stevens WJ, Bridts CH, De Clerck LS (2001) Evaluation of monensin and brefeldin A for flow cytometric determination of interleukin-1 beta, interleukin-6, and tumor necrosis factor-alpha in monocytes. *Cytometry* 46: 172–176
- Shinar Y, Obici L, Aksentijevich I, Bennetts B, Austrup F, Ceccherini I, Costa JM, De Leener A, Gattorno M, Kania U *et al* (2012) Guidelines for the genetic diagnosis of hereditary recurrent fevers. *Ann Rheum Dis* 71: 1599–1605
- Sonmez HE, Batu ED, Ozen S (2016) Familial Mediterranean fever: current perspectives. *J Inflamm Res* 9: 13–20
- Sonmez HE, Batu ED, Bilginer Y, Ozen S (2017) Discontinuing colchicine in symptomatic carriers for MEFV (Mediterranean FeVer) variants. *Clin Rheumatol* 36: 421–425
- Soriano A, Manna R (2012) Familial Mediterranean fever: new phenotypes. *Autoimmun Rev* 12: 31–37
- Tamaoki T (1991) Use and specificity of staurosporine, UCN-01, and calphostin C as protein kinase inhibitors. *Methods Enzymol* 201: 340–347
- Toplak N, Frenkel J, Ozen S, Lachmann HJ, Woo P, Kone-Paut I, De Benedetti F, Neven B, Hofer M, Dolezalova P *et al* (2012) An international registry on autoinflammatory diseases: the Eurofever experience. *Ann Rheum Dis* 71: 1177–1182
- Van Gorp H, Saavedra PHV, de Vasconcelos NM, Van Opendbosch N, Vande Walle L, Matusiak M, Prencipe G, Insalaco A, Van Hauwermeiren F, Demon D *et al* (2016) Familial Mediterranean fever mutations lift the obligatory requirement for microtubules in Pyrin inflammasome activation. *Proc Natl Acad Sci USA* 113: 14384–14389
- Xu H, Yang J, Gao W, Li L, Li P, Zhang L, Gong Y-N, Peng X, Xi JJ, Chen S *et al* (2014) Innate immune sensing of bacterial modifications of Rho GTPases by the Pyrin inflammasome. *Nature* 513: 237–241



License: This is an open access article under the terms of the Creative Commons Attribution 4.0 License, which permits use, distribution and reproduction in any medium, provided the original work is properly cited.

Résumé

Introduction

L'immunité innée représente la première ligne de défense du corps humain contre des pathogènes. Elle se repose sur des récepteurs codés par la lignée germinale qui détectent les motifs moléculaires associés aux pathogènes (PRR). Les inflammasomes sont des complexes protéiques dont les récepteurs ou senseurs font partie des PRRs. Un inflammasome est typiquement constitué d'un senseur, un adaptateur et un effecteur. Les senseurs de l'inflammasome sont des PRRs qui détectent les signaux de danger. La détection d'un tel signal enclenche l'oligomérisation du senseur avec l'adaptateur ASC et l'effecteur caspase-1. L'activation de l'inflammasome induit le clivage et l'activation de caspase-1, ainsi que la sécrétion de cytokines pro-inflammatoires telles qu'IL-1 β et IL-18. Parmi les inflammasomes, l'inflammasome pyrine se distingue puisqu'il détecte les modifications de l'homéostasie cellulaire (HAMP) sans interaction directe avec un PAMP ou un DAMP.

La protéine pyrine est une protéine de la famille TRIM de 781 acides aminés, codée par le gène *MEFV*. Comme la plupart des senseurs de l'inflammasome, elle contient un domaine PYD à son extrémité N-terminale qui permet l'interaction et l'oligomérisation avec l'adaptateur ASC. Le PYD de pyrine est suivi d'un domaine contenant deux sites de phosphorylation (S208 et S242) qui sont cruciaux pour la régulation de pyrine. Les résidus de 370 à 412 de pyrine constituent le domaine B-Box qui participe à l'oligomérisation de pyrine. Le domaine B-Box est suivi par une série d'hélices alpha (CHS) qui constitue un support pour le domaine à l'extrémité C-terminale – le B30.2.

Le B30.2 de pyrine comporte une cavité dont la surface est recouverte de résidus hydrophobes. Cette poche est un site potentiel d'interaction avec un ligand inconnu. La nature de ce ligand fait objet de nombreuses études et plusieurs candidats ont été identifiés. Néanmoins, il reste à confirmer quel est le ligand du B30.2 de pyrine – protéine ou petite molécule non-protéique – et quel est son rôle dans la régulation de l'inflammasome pyrine.

Pyrine est un senseur de l'inhibition de RhoA – une GTPase qui est ciblée par des effecteurs et toxines bactériennes tels que TcdA et TcdB de *C. difficile* ou YopE et YopT de *Y. pestis*. L'inhibition de pyrine à l'état basal est maintenue par la phosphorylation réalisée par les kinases PKN1/2 qui sont des effecteurs de RhoA. Plus récemment, une phosphatase responsable de la déphosphorylation de pyrine - PP2A - a été identifiée. Quand RhoA est inhibée, PKN1/2 sont également inhibées et la pyrine est déphosphorylée. Ceci constitue la première étape de son activation. Il existe un deuxième point de régulation de l'activation de l'inflammasome pyrine probablement lié à la dynamique des microtubules mais qui est mal connu.

Les mutations du gène *MEFV* sont à l'origine de la maladie auto-inflammatoire monogénique la plus répandue dans le monde – la fièvre Méditerranéenne familiale (FMF). La FMF touche en particulier les populations du bassin Méditerranéen. La prévalence de FMF est la plus élevée en Turquie (comprise entre 1 : 400 et 1 : 1000 selon différentes estimations), suivie par l'Arménie (1 : 500). La FMF est caractérisée par des attaques de fièvre stériles récurrentes accompagnées de douleurs abdominales, musculaires ou encore articulaires. Les poussées de FMF peuvent durer entre 12 heures et 3 jours. D'un point de vue moléculaire, les mutations de *MEFV* associées à la FMF diminuent de manière significative le seuil d'activation de l'inflammasome pyrine. *In vitro* la simple déphosphorylation des variants de pyrine associés à la FMF suffit pour déclencher l'activation de l'inflammasome. Le diagnostic de FMF est fait sur la base de critères cliniques et dans certains cas nécessite une confirmation génétique. La FMF est traitée par la colchicine dont la prise débute dès le diagnostic et est poursuivie à vie.

D'autres maladies auto-inflammatoires sont également associées aux mutations dans le gène *MEFV* ou à l'activation anormale de l'inflammasome pyrine. Notamment, l'auto-inflammation associée à la pyrine et dermatose neutrophilique (PAAND) est provoquée par des mutations du gène *MEFV* qui impactent les sites de phosphorylation de pyrine. D'autres, comme le déficit en mévalonate kinase (MKD), ou encore le syndrome PAPA sont liées à des mutations dans d'autres gènes mais qui amènent indirectement à une activation anormale de l'inflammasome pyrine.

Le déclenchement de poussées de FMF est lié aux plusieurs facteurs : la fatigue physique et mentale, le stress, l'exposition au froid. Chez 30-50% des femmes atteintes de FMF, les attaques de fièvre sont associées au cycle menstruel et à la menstruation. Dans la population saine la phase lutéale du cycle menstruel est accompagnée d'une augmentation de la température corporelle. De plus, l'accouchement spontané est reconnu comme un état de l'inflammation stérile. En même temps, les hormones sexuelles stéroïdes telle que la progestérone ou la testostérone ont des propriétés anti-inflammatoires : les macrophages activés traités à la testostérone secrètent moins d'IL-1 β . Cependant, le rôle des molécules stéroïdes dans la régulation de l'inflammasome pyrine n'est pas connu.

Résultats

L'activation non-canonique de l'inflammasome pyrine par les catabolites des hormones stéroïdes.

Afin d'étudier la deuxième étape dans l'activation de pyrine nous avons utilisé une lignée cellulaire de monocytes humains (U937) qui expriment un variant de pyrine dont la première étape est constitutivement activée grâce à la mutation d'un des deux sites de phosphorylation – p.S242R. Nous avons effectué un crible chimique dans le cadre duquel les monocytes exprimant p.S242R ont été traités avec une banque de molécules chimiques, puis la mort cellulaire a été mesurée 90 minutes après le traitement. Le crible a permis d'identifier l'étiocolanolone (3 α -hydroxy-5 β -androstane-17-one) et la prégnanolone (3 α -hydroxy-5 β -pregnan-20-one), des catabolites de testostérone et de progestérone, en tant qu'activateur de l'inflammasome pyrine. Ni la testostérone, ni la progestérone n'ont induit de mort cellulaire pyrine-dépendante dans les monocytes U937. L'activation de pyrine par l'étiocolanolone et la prégnanolone a été confirmée dans des monocytes primaires préalablement traités avec UCN-01, un inhibiteur de PKN1/2, afin de déphosphoryler pyrine et de répliquer les conditions du crible. Le traitement avec uniquement l'étiocolanolone ou la prégnanolone n'ont pas induit de mort cellulaire dans les monocytes primaires.

Les concentrations peu élevées de étiocolanolone (12 μ M) et prégnanolone (6 μ M) ne suffisent pas pour activer l'inflammasome pyrine sans une déphosphorylation préalable. En revanche, nous avons constaté qu'à forte concentration l'étiocolanolone (100 μ M) et la prégnanolone (50 μ M) seuls activent l'inflammasome pyrine. Cette activation s'accompagne de l'oligomérisation d'ASC pour former une structure dite "speck", du clivage et de l'activation de la caspase-1 ainsi que du clivage et de la sécrétion d'IL-1 β et IL-18. La mort cellulaire induite par l'étiocolanolone et la prégnanolone a été complètement abolie dans les monocytes déficients pour la caspase-1 ou la gasdermine D (GSDMD).

Puisque l'activation de pyrine est dépendante des microtubules, elle est inhibée par la colchicine grâce à son effet inhibiteur sur la dynamique des microtubules. La mort cellulaire pyrine-dépendante induite par les molécules stéroïdes a été également inhibée par la colchicine ce qui suggère que la dynamique des microtubules est indispensable à l'activation de l'inflammasome par ces molécules. En revanche, tandis que l'activation canonique de pyrine est déclenchée par l'inhibition de RhoA, nous avons observé que le traitement avec l'étiocolanolone ou la prégnanolone n'inhibe pas l'activité de RhoA. Par conséquent, l'activation de pyrine par les catabolites d'hormones stéroïdes passe par une voie non-canonique. De plus, nous nous sommes intéressés aux domaines de la protéine pyrine nécessaire à son activation par les molécules dérivées des hormones stéroïdes. Nos

résultats nous ont permis de conclure que le domaine B30.2 est indispensable à l'activation de pyrine par l'étiocolanolone et la prégnanolone.

Nous avons démontré que l'activation non-canonique de l'inflammasome pyrine par les dérivées d'hormones stéroïdes est spécifique de pyrine humaine puisque les cellules exprimant la pyrine murine ou simienne n'ont pas répondu au traitement avec les dérivés de stéroïdes.

Les monocytes primaires humains isolés à partir du sang de patients atteints de la FMF ont démontré une activation légèrement plus élevée que les monocytes isolés du sang de donneurs sains en réponse aux dérivés d'hormones stéroïdes. En revanche, les monocytes isolés du sang des patients PAAND ont été fortement activés par les dérivés d'hormones stéroïdes ce qui récapitule le phénotype observé dans les monocytes U937 avec un site de phosphorylation muté. Cette dernière observation suggère que les dérivés d'hormones stéroïdes pourraient contribuer au phénotype autoinflammatoire des patients PAAND.

Les mutations dans les domaines B30.2 et CHS altèrent de manière différentielle l'activation de l'inflammasome pyrine

Nous nous sommes intéressés au rôle des différents domaines dans la régulation de l'inflammasome pyrine. Afin de pouvoir l'étudier nous avons créé des lignées cellulaires de monocytes U937 qui expriment pyrine délétée pour chacun des domaines. Nous avons examiné la réponse de ces monocytes face à un stimulus physiologique qui active l'inflammasome pyrine – la toxine bactérienne TcdA. Nous avons constaté que le domaine B30.2 n'est pas nécessaire à l'activation de pyrine par TcdA.

Etant donné que la majorité des mutations associées à la FMF se trouvent au sein du domaine B30.2, et que la mort cellulaire des monocytes isolés à partir du sang de patient atteint de FMF est déclenchée par la simple déphosphorylation de pyrine, nous avons étudié l'impact de la délétion du B30.2 sur l'activation de pyrine suite à la déphosphorylation. L'activation de l'inflammasome pyrine dans les monocytes qui expriment la pyrine Δ B30.2 est induite par l'inhibition de la kinase responsable de sa phosphorylation. Ce résultat démontre que le domaine B30.2 est responsable de la deuxième étape d'activation de l'inflammasome pyrine. De plus, nous avons démontré que la délétion du B30.2 n'impacte pas la phosphorylation de pyrine à l'état basal. L'activation de l'inflammasome pyrine délétée du domaine B30.2 suivie grâce à la formation des specks d'ASC n'est pas été impactée dans les cellules déficientes pour la caspase-1.

La FMF classique est caractérisée par une transmission récessive mais il existe également des mutations capables de provoquer la FMF de manière dominante. Notamment, p.H478Y et p.Q436R

sont localisées dans le domaine CHS. D'autres mutations pathogéniques mais récessives se trouvent dans ce domaine telles que p.F479L, p.E552D et p.L559F. Afin de mieux comprendre le rôle du domaine CHS dans la régulation de pyrine, nous avons créés des lignées U937 qui expriment les variants de pyrine de CHS mentionnés ci-dessus. Nous avons étudié leurs réponses aux stimuli divers qui ciblent l'inflammasome pyrine en terme de mort cellulaire et de sécrétion des cytokines pro-inflammatoires, IL-1 β et IL-18.

Nous avons constaté des phénotypes variables en réponse à TcdA. Le variant p.H478Y est activé comme le variant typique de FMF – p.M694V, tandis que les variants p.Q426R, p.F479L et p.E552D ont des phénotypes intermédiaires entre le WT et le p.M694V, et le variant p.L559F est activé par TcdA comme la pyrine WT. La déphosphorylation de pyrine par un inhibiteur de kinases PKN1/2 a déclenché la pyroptose dans les cellules qui expriment les variants p.Q426R, p.H478Y et p.F479L de manière comparable au variant de la FMF, p.M694V. Nous avons donc constaté que les mutations du domaines CHS impactent la deuxième étape de régulation de pyrine.

Les mutations dans le domaine CHS impactent différenciellement l'activation de l'inflammasome pyrine par les dérivés d'hormones stéroïdes. Notamment, la dose de prégnanolone nécessaire à l'induction de 50 % de mort cellulaire (EC50) dans les monocytes U937 qui expriment les variants p.Q426R et p.F479L est 50 fois inférieure à la dose nécessaire à l'induction de 50 % de mort cellulaire dans les cellules qui expriment la pyrine WT. Pour l'étiocolanolone, la différence entre les EC50 est moins importante mais les variants p.Q426R et p.F479L sont également plus sensibles. En revanche, les monocytes exprimant la pyrine p.H478Y sont moins sensibles à l'activation par la prégnanolone et l'étiocolanolone que les monocytes exprimant pyrine WT. En accord avec ces observations, nous avons démontré que les variants p.Q426R et p.F479L sont déphosphorylés par des faibles doses de prégnanolone (6 μ M) alors que la pyrine WT et le variant p.H478Y ne le sont pas.

Les mutations sont des mutations très rares mais nous avons réussi à obtenir des échantillons du sang de 6 patients portant la mutation p.F479L. Nous avons isolé les monocytes primaires de l'échantillon, et nous avons analysé la mort cellulaire et la sécrétion d'IL-1 β par ces monocytes en réponse à TcdB, UCN-01 et les dérivés d'hormones stéroïdes : étiocolanolone et pregnanolone, en comparaison avec les monocytes primaires isolés du sang de donneurs sains. Nous avons observé une mort cellulaire et une sécrétion d'IL-1 β comparable au donneur en réponse au traitement avec TcdB. Cependant, en accord avec nos observations dans le modèle U937, les monocytes de patients atteints de FMF avec la mutation p.F479L sont plus sensible à UCN-01, avec un phénotype qui ressemble à celui des monocytes issus des patients FMF avec des mutations classiques telles que p.M694V. Contrairement aux monocytes des donneurs sains, les monocytes primaires avec la

mutation de pyrine p.F479L sont activés par les faibles doses d'étiocolanolone (12 μ M) et de prégnanolone (6 μ M). Ces observations confirment les phénotypes que nous avons observé dans notre modèle de monocytes U937 et valident que des mutations spécifiques du CHS observées chez certains patients FMF rendent l'inflammasome pyrine hautement réactifs aux catabolites des hormones sexuelles.

Résultats supplémentaires

Des expériences supplémentaires nous ont permis de démontrer que les mutations de pyrine au sein du domaine CHS qui abaissent de manière significative le seuil d'activation de pyrine par les dérivés d'hormones stéroïdes - p.Q426R et p.F479L – élargissent également le spectre de stéroïdes capables d'activer l'inflammasome pyrine. Notamment, les cellules qui expriment les variants p.Q426R et p.F479L mais pas celles qui expriment p.H478Y, subissent une mort cellulaire rapide en réponse au traitement avec la testostérone, la progestérone et l'androstérone. De plus, nous avons découvert que le prétraitement avec la progestérone inhibe l'activation de pyrine WT par la prégnanolone. Cette inhibition est dose-dépendante : elle a lieu si la concentration de progestérone est supérieure à celle de prégnanolone.

La simvastatine est un inhibiteur de l'HMG-CoA réductase, une enzyme impliquée dans la voie de mévalonate kinase. L'inhibition de cette voie inhibe à la fois RhoA et la synthèse de cholestérol. D'autre part la simvastatine est un activateur de l'inflammasome pyrine. Les variants de pyrine avec des mutations dans le domaine CHS répondent différemment au traitement avec la simvastatine. D'une manière qui mime la réponse différentielle de ces variants aux dérivés d'hormones stéroïdes, le seuil d'activation par la simvastatine est plus bas pour les monocytes qui expriment pyrine p.Q426R et p.F479L. Les monocytes exprimant le variant p.H478Y ne subissent pas d'activation de l'inflammasome pyrine.

Discussion

L'activation de pyrine par les dérivés d'hormones stéroïdes est dépendante du domaine B30.2 et à la fois modulée par les mutations au sein du domaine CHS. Les domaines B30.2 et CHS coopèrent pour la transduction de signal perçu par le domaine B30.2, et transmis le long de la protéine grâce à des changements de conformation au niveau du domaine CHS. Le signal est ainsi conduit jusqu'aux sites de phosphorylation de pyrine, la protéine est ainsi déphosphorylée et activée. Un mécanisme de coopération semblable entre un domaine B30.2 et un domaine CHS est décrit dans le cas de la protéine BTN3A1 exprimée par les cellules présentatrices de l'antigène dans le cadre de l'activation des lymphocytes gamma delta.

La diversité de phénotypes associés aux variants de pyrine avec des mutations dans le domaine CHS met en évidence l'importance et la complexité du rôle de ce domaine dans la régulation de pyrine. Les travaux présentés dans ce manuscrit éclairent un nouveau mécanisme d'activation de l'inflammasome pyrine. Nos observations accordent un nouveau rôle à la pyrine : celui de la surveillance du métabolisme de cholestérol et de l'équilibre des hormones stéroïdes et de leurs dérivés dans la cellule.

Nous proposons un modèle de fonctionnement de pyrine selon lequel le domaine B30.2 sert de site de fixation pour une molécule d'origine stéroïde. Nous ne savons pas si cette interaction a un effet inhibiteur ou activateur sur l'inflammasome à l'état basal, il est en effet possible qu'il existe à la fois des ligands inhibiteurs (comme progestérone) et des ligands activateurs (comme prégnanolone), et qu'il y ait une compétition entre les deux types de ligands dont l'affinité au B30.2 de pyrine ne serait pas égale. Pyrine serait activée par la fixation d'un ligand activateur au B30.2 ou par la perte d'interaction du B30.2 avec un ligand inhibiteur, ce qui provoquerait une cascade de changements de conformations transmise par le CHS. La concentration des dérivés d'hormones stéroïdes utilisée dans nos expériences est supérieure à la concentration physiologique à laquelle sont exposés les monocytes humains circulants. Nous pensons que dans les conditions physiologiques la pyrine est seulement amorcée par des petites quantités de molécules telles que la prégnanolone et l'étiocolanolone, ce qui baisserait le seuil d'activation de l'inflammasome pyrine par d'autres signaux. Il reste à démontrer si l'activation de pyrine par les dérivés d'hormones stéroïdes est médiée par une interaction directe entre le domaine B30.2 et les molécules en question.